

**CHARACTERIZING HYDROXYPROPYL  
GUAR - BORATE INTERACTIONS WITH  
MODEL TEAR FILM COMPONENTS**

**CHARACTERIZING HYDROXYPROPYL  
GUAR - BORATE INTERACTIONS WITH  
MODEL TEAR FILM COMPONENTS**

By

YUGUO CUI, B. ENG., M. ENG.

A Thesis

Submitted to the School of Graduate Studies

in Partial Fulfillment of the Requirements

for the Degree

Doctor of Philosophy

McMaster University

© Copyright by Yuguo Cui, July 2010

DOCTOR OF PHILOSOPHY (2010)      McMaster University  
(Chemical Engineering)              Hamilton, Ontario

TITLE:                      Characterizing Hydroxypropyl Guar - Borate  
   Interactions with Model Tear Film Components

AUTHOR:                  Yuguo Cui  
   B.ENG. (Tianjin University)  
   M.ENG. (China Institute of Atomic Energy)

SUPERVISOR: Professor Robert H. Pelton

NUMBER OF PAGES: xi, 200

## Abstract

Hydroxypropyl guar (HPG) is an effective ingredient in lubricant eye drops used by patients with dry eye disease. The overall goal of the work described in this thesis is to understand the physical-chemical properties of HPG in the presence of model surfaces and solutes with view to understanding the behavior of HPG in the tear film.

HPG behaviors are complex because borate ions bind to HPG, which converts nonionic HPG into anionic polyelectrolyte, HPG-borate. The borate binding constants are very low, meaning the charges on HPG-borate are labile. Another consequence of weak binding is that the equilibrium electrolyte concentration with HPG-borate is relatively high. Mathematical models were developed to predict the structure of HPG-borate as functions of pH.

This thesis probes the question “When does HPG-borate behave as an anionic polyelectrolyte?” This work shows that HPG-borate exhibits deviant behaviors of an anionic polyelectrolyte: does not interact with cationic surfactants below the CMC; does not interact with lysozyme (cationic protein), and does not adsorb onto cationic liposomes. By contrast, anionic polyelectrolytes such as carboxymethyl guar display generic behaviors. On the other hand, HPG-borate forms polyelectrolyte complexes with cationic polyelectrolytes at low ionic strength and other work from our laboratory has shown that HPG-borate flocculates cationic polystyrene latex.

This complex range of HPG-borate behaviors was rationalized by proposing that the labile nature of the charge groups means that the charge density on HPG-borate is regulated by the local electrostatic environment. Near a cationic surface HPG-borate charge density increases whereas near an anionic surface the charge density is lower.

Anionic liposome interactions with HPG-borate were characterized. HPG concentrations close to clinical levels induced depletion flocculation of the anionic liposomes. This is the first example we have found depletion interactions were proposed for the tear film.

To summarize the main implications for the ophthalmic application of HPG are:  
1) under ophthalmic conditions HPG-borate behaves as a nonionic water soluble polymer;  
2) HPG-borate will adsorb onto hydrophobic domains but will not interact with lysozyme;  
3) depletion interactions are important and have the potential to stabilize the lipid layer and destabilize emulsion droplets and other dispersed species in the tear film.

## Acknowledgements

First, I would like to give my sincere gratitude to my supervisor, Professor Robert Pelton, for supervising me during this thesis, for teaching me all the knowledge of colloid and polymer science and teaching me skills of writing papers, conducting presentations and doing modeling. I also would like to thank my supervisory committee members, Professor Heather Sheardown and Professor Harald Stöver for their suggestions and help on my research work. Many thanks are to be given to Professor Shiping Zhu for teaching me fundamental knowledge of polymer.

I wish to thank Alcon Laboratories and Natural Sciences and Engineering Research Council of Canada (NSERC) for their financial support of my research work. Especially, I am grateful to Dr Howard Ketelson and Dr Davis James of Alcon Laboratories for their support. I would like to thank Alcon project group members, Dr Sheng Dai, Justin Hu, Liang Zhang, and Dr Anil Khanal for their useful discussions and suggestions.

I would like to thank Professor Harald Stöver again for access to his pH and conductivity titration instrument and GPC instrument and Nicholas A. Burke for his help in GPC measurement, Professor Richard Epanand Professor Raquel Epanand for access to ITC instrument and refractometer, Professor Jeffrey Weitz for access to SPR instrument and Alan R. Stafford for his kind help in SPR experiments, Professor Terence Cosgrove, Professor Robert Richardson and Dr Isabelle Grillo for their help and support in SANS experiments, ILL for access to SANS instrument, Dr Steve Kornic and Donald Hughes for their help in NMR, FT-IR and elemental analysis measurements.

I also wish to give my special thanks to the staffs in Department of Chemical Engineering, Ms Kathy Goodram, Ms Lynn Falkiner, Ms Nanci Cole, and Ms Andrea Vickers for their administrative assistance, and Dr James Lei, Mr. Paul Gatt, Ms Justyna Derkach and Mr. Dan Wright for their technical support.

I would like to thank all the people in McMaster Interfacial Technologies Group, especially laboratory manager Mr. Doug Keller for all kind of support and assistance. I also thank SENTINEL network secretary Francis Lima and Sally Watson for their help in administration. I would like to thank Dr Chengming Li for his advice on synthesis, Dr Xinglian Geng for her technical support, Dr Xianhua Feng, Dr Wei Chen and Dr Hiroo Tanaka for their useful discussions, summer student Jacob Rohan and Yuanyuan Ren for their help in experimental works and all current and previous members for their encouragement.

Finally, I wish to thank my wife, Lan Li, and my son, Fengqi Cui for their love and support.

# TABLE OF CONTENTS

<b>Abstract.....</b>	<b>iii</b>
<b>Acknowledgements .....</b>	<b>iv</b>
<b>Chapter 1 Introduction.....</b>	<b>1</b>
1.1 Tear film.....	1
1.1.1 Tear Film Functions .....	1
1.1.2 Tear Film Structure and Components .....	1
1.1.3 The Break-up of the Tear Film .....	3
1.2 Artificial Tears .....	5
1.3 Guar, HPG and HPG-borate .....	8
1.4 HPG-borate Interaction with Tear Film Components.....	11
1.4.1 Fundamentals .....	11
1.4.2 Literature Review.....	13
1.5 Objectives .....	14
1.6 Thesis Outline .....	14
1.7 References.....	16
<b>Chapter 2 Synthesis and Characterization of Carboxymethyl Guar, Cationic Guar and Hydrophobically Modified Guar.....</b>	<b>21</b>
Abstract .....	21
2.1 Introduction.....	22
2.2 Experimental .....	23
2.2.1 Materials .....	23
2.2.2 Methods.....	23
2.3 Results and Discussion .....	25
2.4 Conclusions.....	28
2.5 Tables.....	29
2.6 Schemes .....	30
2.7 Figures.....	34
2.8 References.....	43
<b>Chapter 3 Characterization and modeling of HPG-borate, a labile polyelectrolyte, by polyelectrolyte titration and interaction of HPG-borate with oppositely charged polyelectrolyte .....</b>	<b>45</b>
Abstract .....	45
3.1 Introduction.....	46
3.2 Experimental .....	47
3.3 Modeling Polyelectrolyte Titrations .....	48
3.4 Results.....	51
3.4.1 Polyelectrolyte Type .....	51
3.4.2 Borate Concentration and pH.....	52
3.4.3 Borate Type.....	53
3.4.4 Key Model Parameters.....	53
3.5 Discussion .....	54
3.6 Conclusions.....	55

3.7 Figures.....	56
3.8 References.....	67
<b>Chapter 4 Interaction of HPG-Borate with Cationic Surfactant Dodecyltrimethyl Ammonium Bromide (DTAB) .....</b>	<b>69</b>
Abstract.....	69
4.1 Introduction.....	70
4.2 Experimental.....	72
4.2.1 Materials .....	72
4.2.2 Methods.....	73
4.3 Results.....	74
4.4 Discussion.....	77
4.5 Conclusions.....	78
4.6 Tables.....	79
4.7 Figures.....	80
4.8 References.....	89
<b>Chapter 5 HPG-Borate and Modified Guar Interactions with Lysozyme .....</b>	<b>94</b>
Abstract.....	94
5.1. Introduction.....	95
5.2. Experimental.....	97
5.2.1 Materials .....	97
5.2.2 Methods.....	97
5.3 Results.....	99
5.3.1 CMG Interaction with Lysozyme .....	99
5.3.1.1 CMG Interaction with Lysozyme at Low Ionic Strength .....	99
5.3.1.2 Salt Effect on CMG Interaction with Lysozyme .....	100
5.3.2 Hydrophobically Modified Guar Interaction with Lysozyme .....	101
5.3.3 HPG-Borate Interaction with Lysozyme .....	101
5.3.3.1 Determination of Charge Content on HPG Polymer Chain.....	101
5.3.3.2 Experimental Results of HPG-Borate Interaction with Lysozyme.....	103
5.4 Discussion.....	104
5.5 Conclusions.....	106
5.6 Tables.....	107
5.7 Figures.....	108
5.8 References.....	122
<b>Chapter 6 HPG-Borate and Modified Guar Interactions with Phosphatidic Acid Liposomes .....</b>	<b>126</b>
Abstract.....	126
6.1 Introduction.....	127
6.2 Experimental.....	128
6.2.1 Materials .....	128
6.2.2 Methods.....	129
6.3 Results.....	130
6.3.1 Cationic Guar Interaction with PA Liposomes.....	130
6.3.2 Hydrophobically Modified Guar (HMG) Interaction with PA Liposome .....	131

6.3.3 HPG-Borate Interaction with PA Liposome .....	131
6.3.4 Guar and Partially Hydrolyzed Guar Interaction with PA Liposome .....	132
6.4 Discussion .....	132
6.5 Conclusions .....	135
6.6 Figures .....	137
6.7 References .....	154
<b>Chapter 7 Concluding Remarks .....</b>	<b>157</b>
7.1 Key Findings and Contributions .....	157
7.2 Future Work .....	158
7.3 References .....	159
<b>Appendices .....</b>	<b>160</b>
Appendix A Modeling of polyelectrolyte titration of HPG/borate with PDADMAC .....	160
Appendix B .....	176
Appendix B.1 Determination of Charge Density on Lysozyme by Polyelectrolyte Titration .....	176
Appendix B.2 One site binding model for isothermal titration calorimetry (ITC) .....	177
Appendix B.3 Calculation of charge ratio of CMG or HPG-borate to lysozyme and molar ratio of HMG to lysozyme .....	179
Appendix B.4 Example calculation of Gibbs free energy and entropy in ITC .....	186
Appendix B.5 Example calculation of borate content on HPG polymer chain .....	187
Appendix B.6 Calculation of critical salt concentrations on HPG/borate or CMG interaction with lysozyme .....	192
Appendix C .....	195
Appendix C.1 Example calculation of HPG viscosity effect on PA liposome mobility .....	195
Appendix C.2 Modeling of depletion flocculation of PA liposomes induced by HPG .....	196
Appendix C.3 Estimation of the radius of gyration of HPG, native guar and PHG .....	199

## LIST OF FIGURES

Figure 1.1	Schematic representation of the tear film (adapted from <a href="http://www.systane.com/Eye-Moisture.aspx">http://www.systane.com/Eye-Moisture.aspx</a> ).....	2
Figure 1.2	Rupture of tear film induced by lipid (Adapted from Holly 1973).....	4
Figure 1.3	(A) Normal tear film (B) Tear film rupture initiated from menisci (black lines near the upper and lower eyelids) (Adapted from Bruce 2001). ....	5
Figure 1.4	Synthetic polymers commonly used in artificial tears.....	6
Figure 1.5	Polysaccharides commonly used in artificial tears. ....	7
Figure 1.6	Structure of guar and HPG.....	9
Figure 1.7	The structure of borate bound HPG. ....	10
Figure 1.8	Borate binds with HPG and cross-links HPG. ....	11
Figure 2.1	The structure of carboxymethyl guar (CMG). ....	34
Figure 2.2	The structure of cationic guar. ....	35
Figure 2.3	The structure of hydrophobically modified guar (HMG). ....	36
Figure 2.4	Infra-red spectra of guar and carboxymethyl guar (CMG). ....	37
Figure 2.5	Conductometric and potentiometric titration to determine degree of substitution of carboxymethyl guar (DS 0.39).....	38
Figure 2.6	Nuclear magnetic resonance (NMR) characterization of degree of substitution of cationic guar (DS 0.09). ....	39
Figure 2.7	Polyelectrolyte titration characterization of degree of substitution of cationic guar (DS 0.09). ....	40
Figure 2.8	Nuclear magnetic resonance (NMR) characterization of degree of substitution of hydrophobically modified guar (N-hexylamide substitution) (DS 0.12) synthesized from carboxymethyl guar (DS 0.13). ....	41
Figure 2.9	Characterization of carboxyl residue on hydrophobically modified guar (N-hexylamide substitution) (DS 0.13) by conductometric and potentiometric titration.....	42
Figure 3.1	Schematic illustration of a streaming current detector.....	56
Figure 3.2	Comparison of polyelectrolyte titration curves for PVSK, a strong polyelectrolyte, PAA, a weak polyelectrolyte, and HPG-borate, a labile polyelectrolyte.....	57
Figure 3.3	The structure of HPG-borate.....	58
Figure 3.4	Comparing model and experimental polyelectrolyte titrations. The model parameters are: $\gamma = 3$ , $\sigma_0 = -0.06 \text{ C/m}^2$ , $[\text{NaCl}] = 10 \text{ mM}$ , $[\text{P}_T] = 0.15 \text{ mM}$ , $[\text{B}_T] = 19 \text{ mM}$ , $\Gamma_{\text{HPG}} = 2 \text{ mg/m}^2$ and $\alpha = 4$ . ....	59
Figure 3.5	Influence of borate concentration on the titration of HPG-borate with PDADMAC.....	60
Figure 3.6	Simulating the influence of borate concentration. $K_1 = 100 \text{ L/mol}$ , remaining parameters given in caption of Figure 3.4. ....	61
Figure 3.7	Evolution of pH during the titration of HPG-borate with PDADMAC.....	62

Figure 3.8	Simulating the influence of borate concentration on the evolution of pH during the titration of HPG-borate with PDADMAC. $K_1 = 100$ L/mol, remaining parameters given in caption of Figure 3.4. ....	63
Figure 3.9	PDADMAC addition to HPG-methylborate and to HPG-borate. The methylborate can only add once whereas borate can bind twice to give a cross-link. ....	64
Figure 3.10	Influence of $\gamma$ on the shape of the simulated polyelectrolyte titrations. $K_1 = 100$ L/mol, remaining parameters given in caption of Figure 3.4. ....	65
Figure 3.11	Influence of the assumed amount of adsorbed HPG on the shape of the simulated titrations. $K_1 = 100$ L/mol, remaining parameters given in caption of Figure 3.4. ....	66
Figure 4.1	Cross-linking of water-soluble polymers containing cis-diol groups with the borate ion. ....	80
Figure 4.2	The condensation of borate with HPG to form HPG-borate. ....	81
Figure 4.3	Structure of carboxymethyl guar (CMG). ....	82
Figure 4.4	Surface tension as a function of DTAB concentration. The HPG concentrations were 0.05% (w/w) and the total boron concentrations in the borax (open circles) and methylboronate (red triangles) experiments were 0.02M. ....	83
Figure 4.5	Influence of 0.05% carboxymethyl guar (CMG) on the DTAB surface tension. The degree of carboxymethyl substitution was 0.39. The total boron concentration for the borax experiments was 0.02M. ....	84
Figure 4.6	Isothermal calorimetric titration with concentrated (0.2 M) DTAB. The pH of the borate solutions was 9.2. ....	85
Figure 4.7	Small-angle neutron scattering results for D-DTAB in $H_2O$ . Surfactant concentrations are expressed as functions of the cmc (15 mM). The solid red line was fitted using parameters in Table 4.1. ....	86
Figure 4.8	Influence of HPG (0.05% w/w) on the scattering behavior D-DTAB above and below the cmc in 20 $D_2O$ : 80 $H_2O$ (vol%). ....	87
Figure 4.9	D-DTAB and HPG (0.05%) in 20% $D_2O$ 80% $H_2O$ (which is contrast matched to guar) with added borax (10 mM, pH 9.2). ....	88
Figure 5.1	Structure of hen egg white lysozyme (Adapted from Rothwarf 1996, see reference 12). The right white part and left black part represents $\alpha$ domain and $\beta$ domain respectively. The hydrophobic tryptophan side chains are shown. The double balls represent disulfide bonds. ....	108
Figure 5.2	Turbidity measurement of CMG and lysozyme as a function of CMG concentration. ....	109
Figure 5.3	Electrophoretic mobility measurement of CMG and lysozyme as a function of CMG concentration. ....	110
Figure 5.4	Particle Size Distribution and Correlation Function (Inlet) of Dynamic Light Scattering of 0.125 g/L CMG with 0.3 g/L Lysozyme at pH 7.4, NaCl Concentration of 0.01mol/L in 0.05mol/L HEPES Buffer, poly 0.113, intensity 235.7 kcps, average particle size 216.8 nm. ....	111
Figure 5.5	Salt effect on turbidity of CMG and lysozyme. ....	112

Figure 5.6	Salt effect on electrophoretic mobility of CMG and lysozyme. ....	113
Figure 5.7	ITC measurement of CMG interaction with lysozyme. ....	114
Figure 5.8	SPR measurement of CMG interaction with lysozyme. ....	115
Figure 5.9	ITC measurement of hydrophobically modified guar interaction with lysozyme. ....	116
Figure 5.10	Turbidity measurement of HPG with lysozyme in the presence of borate as a function of HPG concentration. ....	117
Figure 5.11	Electrophoretic mobility of HPG with lysozyme in the presence of borate as a function of HPG concentration. ....	118
Figure 5.12	ITC measurement of HPG-borate interaction with lysozyme. ....	119
Figure 5.13	SPR measurement of HPG interaction with lysozyme in the presence of HEPES buffer and borate buffer. ....	120
Figure 5.14	(a) Ionic strength effects on HPG-borate interaction with lysozyme. (b) Ionic strength effects on CMG interaction with lysozyme. ....	121
Figure 6.1	Phosphatidic acid sodium salt. ....	137
Figure 6.2	Schematic representation of a cross-section of a unilamellar liposome structure. ....	138
Figure 6.3	Turbidity and mobility measurement of PA liposomes interaction with cationic guar in HEPES buffer (The degree of substitution (DS) of cationic guar is 0.09 (0.09 cationic group per sugar unit) and molecular weight of cationic guar is about $3 \times 10^6$ Da.) ....	139
Figure 6.4	DLS measurement of PA liposomes sizes in the presence of cationic guar in HEPES buffer (The degree of substitution (DS) of cationic guar is 0.09 (0.09 cationic group per sugar unit) and molecular weight of cationic guar is about $3 \times 10^6$ Da.) ....	140
Figure 6.5	Turbidity and mobility measurement of PA liposomes interaction with hydrophobically modified guar in HEPES buffer (The degree of substitution (DS) of HMG is 0.13 (0.13 hydrophobic group per sugar unit) and molecular weight of HMG is about $3 \times 10^6$ Da.) ....	141
Figure 6.6	DLS measurement of PA liposomes sizes in the presence of hydrophobically modified guar in HEPES buffer (The degree of substitution (DS) of HMG is 0.13 (0.13 hydrophobic group per sugar unit) and molecular weight of HMG is about $3 \times 10^6$ Da.) ....	142
Figure 6.7	Turbidity measurement of HPG interaction with PA liposome in HEPES buffer and borate buffer. ....	143
Figure 6.8	Mobility measurement of PA liposomes in the presence of HPG in HEPES buffer and borate buffer. ....	144
Figure 6.9	DLS measurement of PA liposomes sizes in the presence of HPG in HEPES buffer and borate buffer. ....	145
Figure 6.10	DLS measurement of PA liposomes sizes in the presence of guar with different molecular weights in HEPES buffer at pH 7.4. ....	146
Figure 6.11	DLS measurement of PA liposomes sizes in the presence of guar with different molecular weights in boric acid at pH 7.4. ....	147

Figure 6.12	DLS measurement of PA liposomes particle sizes in the presence of guar with different molecular weights in borax buffer at pH 9.2.....	148
Figure 6.13	Mobility measurement of PA liposomes in the presence of native guar in HEPES buffer and borate buffer. ....	149
Figure 6.14	Mobility measurement of PA liposomes in the presence of PHG in HEPES buffer and borate buffer. ....	150
Figure 6.15	Potential energy as a function of PA liposomes separation distance. The calculation of above potentials is based on the conditions: HPG volume fraction 0.05%, radius of gyration of HPG 128 nm, HPG molecular weight 1750000 Da, HPG second virial coefficient $0.00003 \text{ cm}^3 \text{ mol/g}^2$ ; radius of PA liposome 40 nm, surface potential of PA liposome 38 mV, Hamaker constant of PA liposome $7 \times 10^{-21} \text{ J}$ ; NaCl concentration 0.1 mol/L.....	151
Figure 6.16	Secondary minimums of the sum of the potentials between PA liposomes as a function of HPG concentration. ....	152
Figure 6.17	Molecular weight dependence of onset concentration for guar to aggregate PA liposomes. ....	153

## LIST OF TABLES

Table 2.1	Properties of modified guar. ....	29
Table 4.1	Parameter values used to fit the neutron scattering data.....	79
Table 5.1	DLS measurement of hydrodynamic diameter of CMG and lysozyme (0.3g/L) at pH 7.4, 0.01mol/L NaCl in 0.05mol/L HEPES buffer.....	107

## LIST OF SCHEMES

Scheme 2.1	Synthesis of carboxymethyl guar.....	30
Scheme 2.2	Synthesis of cationic guar. ....	31
Scheme 2.3	Synthesis of hydrophobically modified guar. ....	32
Scheme 2.4	Reaction of carboxylic acid with primary amines in the presence of EDC (Adapted from Hermanson, G. T., 2008, also see reference 14). ....	33

## Chapter 1 Introduction

Millions of people in North America suffer from dry eye syndrome.<sup>1,2</sup> The chances of dry eye disease increase with age, and women are more susceptible.<sup>1-4</sup> Patients with dry eye syndrome usually complain of eye dryness, eye inflammation, itch and foreign body sensation.<sup>5</sup> Other symptoms include blurry vision, tired eyes, and photophobia, etc.<sup>1,3</sup> It has been defined as “a disorder of the tear film due to tear deficiency or excessive evaporation that causes damage to the interpalpebral ocular surface and is associated with symptoms of discomfort.”<sup>6,7</sup>

Many artificial tears have been developed to treat dry eye syndrome.<sup>8</sup> Artificial tears are inserted in tear film to relieve the symptoms such as eye dryness. Recently, an artificial tear with hydroxypropyl guar-borate (HPG-borate) as a component has been proven in clinical tests to be very efficient to treat dry eye syndrome, especially in relieving eye dryness.<sup>9,10</sup> In order to justify the application of HPG-borate in artificial tears, the interaction of HPG-borate and tear film components must be studied to clarify possible side effects.

### 1.1 Tear film

The (precorneal) tear film is secreted by the conjunctiva to cover and protect the corneal surface.<sup>11</sup> The thickness of the tear film is of the order of tens of  $\mu\text{m}$ .<sup>11-16</sup>

#### 1.1.1 Tear Film Functions

In the eye, the tear film mainly serves three functions<sup>17</sup>:

- It lubricates the cornea and provides a smooth surface for light refraction;
- It maintains the metabolism of the cornea and provides nutrients to it;
- It protects the cornea from foreign contaminants and bacterial attack.

#### 1.1.2 Tear Film Structure and Components

Conventionally, tear film has been divided into three layers: the inner layer, closest to the corneal surface, is the mucus layer; the middle layer is the aqueous layer; and the outer layer, at the air-water interface is the lipid layer.<sup>17-20</sup> Recently, a new tear film model has been proposed, in which there is no boundary between the mucus and aqueous layers. Mucin diffuses into the aqueous layer so that a mucin gradient is set up from the mucus layer to the aqueous layer. In addition, the lipid layer can also take up proteins. This suggests the tear film model shown in Figure 1.1.

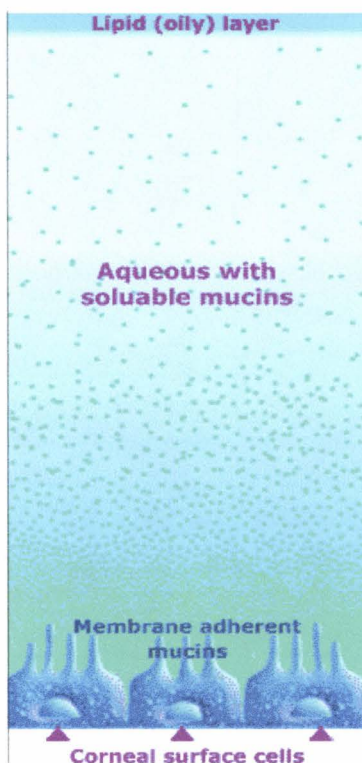


**Figure 1.1** Schematic representation of the tear film (adapted from <http://www.systane.com/Eye-Moisture.aspx>).

The mucus layer is mostly composed of mucin. Secreted by conjunctival goblet cells, the mucus layer provides the corneal surface with a hydrophilic layer as the corneal surface is hydrophobic.<sup>17, 21</sup> The hydrophilic layer facilitates the spread of the aqueous layer, lubricates the corneal surface and protects it from bacterial contamination. Mucins are glycoproteins consisting of both protein and sugar with molecular weight as high as  $10^6$  Da. Although fifteen types of mucins have been found, only seven of them are related to tear film which can be divided into membrane bound mucins, gel forming mucins and soluble mucins.<sup>22</sup> Membrane bound mucins mainly exist in the mucus layer, having hydrophobic amino acid groups which attach to the corneal surface. Membrane bound mucins have a thickness of 200-500 nm, and protect the corneal surface from bacterial attack. Gel forming mucins form gels to lubricate the corneal surface and prevent it from shear force. The total thickness of the mucus layer has been estimated to be up to be about  $1\ \mu\text{m}$ .<sup>18</sup>

The thickness of the aqueous layer is about  $10\ \mu\text{m}$ . It provides nutrients such as proteins, inorganic salts and oxygen, removes foreign contaminants and lubricates the corneal surface.<sup>23</sup> The aqueous layer is composed mainly of water (95-98%), with the important components: proteins and inorganic salts. The diffusing mucins in the aqueous layer decrease the surface tension between the mucus and aqueous layers and ease the spread of the aqueous layer on the mucus layer. The proteins, with a total concentration of

6-20 g/L, include lysozyme, albumin, lactoferrin, transferrin and immunoglobulins such as immunoglobulin A (IgA), immunoglobulin G (IgG) and immunoglobulin E (IgE).<sup>24</sup> Among these proteins, lysozyme is an antibacterial protein. Its concentration is difficult to measure, but ranges approximately from 0.1g/L to 1g/L in human tear film. The inorganic salts include sodium chloride, potassium chloride, calcium chloride and magnesium chloride. Among these salts, sodium chloride is the most abundant (above 0.1mol/L), followed by potassium chloride (above 0.06mol/L), calcium chloride and magnesium chloride. The pH of the aqueous layer is rather neutral, about 7.4 in the normal population.<sup>23</sup>

The thickness of the lipid layer in the human tear film is less than 100 nm, which is much thinner than the other two layers.<sup>18</sup> The lipid layer contributes to the lubrication of eyelids, the prevention of water evaporation, the stabilization of the tear film, the reduction of the air-water surface tension, and the protection against bacteria and foreign bodies.<sup>18, 25-28</sup> The lipid layer is excreted from the meibomian gland<sup>29</sup>, and made up mainly of non-polar lipids such as wax esters, cholesterol and its esters (60-70%), and polar lipids such as phospholipids and glycolipids. In addition, small amounts of fatty acids, alcohols, glycerides and hydrocarbons are present in the lipid layer.<sup>18</sup> An early lipid layer model proposed that polar lipids, mainly phospholipids, first spread onto the aqueous layer followed by non-polar lipids interacting with the hydrophobic tail of the polar lipid.<sup>30</sup> A more recent model proposes that the lipid also interacts with proteins in the aqueous layer.<sup>27</sup>

### 1.1.3 The Break-up of the Tear Film

Dynamically, a stable tear film can be formed within seconds following the eye's blink. Before its rupture, the tear film can survive up to 10-40 seconds, which is longer than the interval between blinks (5 seconds). For the dry eye patient, the tear film can only survive for less than 10 seconds. Conventionally, it has been assumed that the rupture of the tear film is induced by evaporation<sup>31</sup>, but the thick tear film upon rupture reduces the possibility of this mechanism. However, Holly<sup>30</sup> has proposed a tear film break-up mechanism involving tear receding, in which the lipid nucleates dry spots on the corneal surface, causing the tear film to rupture instantly, as shown in Figure 1.2.

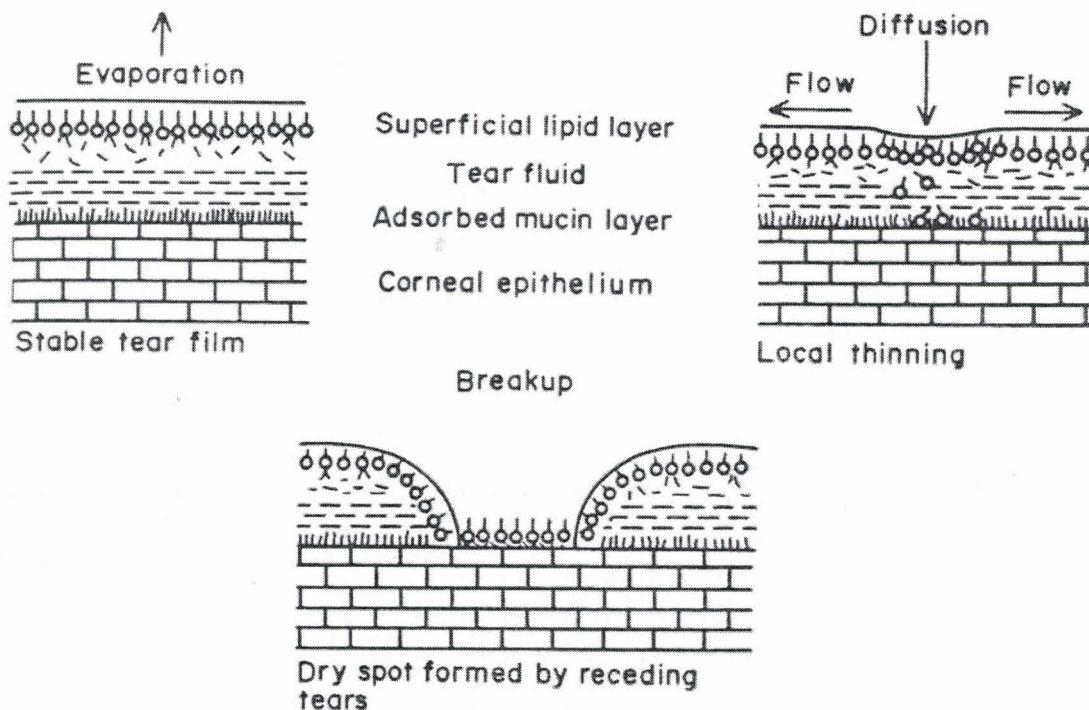


**Figure 1.2 Rupture of tear film induced by lipid (Adapted from Holly 1973).**

In addition, a meniscus forced thinning mechanism has been proposed by McDonald et al.<sup>32</sup> They propose that the thin black lines near the edge of the eyelids initiate the rupture of the tear film. This mechanism has been supported by experiment, as shown in Figure 1.3.<sup>33</sup>

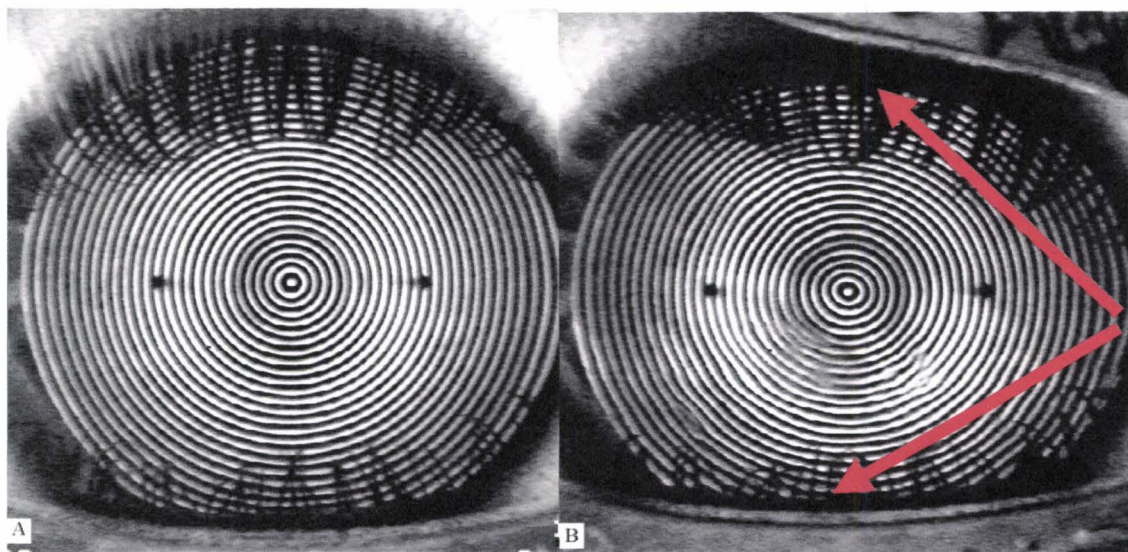


**Figure 1.3 (A) Normal tear film (B) Tear film rupture initiated from menisci (black lines near the upper and lower eyelids) (Adapted from Bruce 2001).**

In summary, the mechanisms of tear film rupture are not fully understood. Further study on the mechanism is needed. Understanding this mechanism will help in developing appropriate artificial tears to treat dry eye syndrome.

## 1.2 Artificial Tears

To treat the dry eye syndrome, many types of artificial tears have been developed. Artificial tears are designed to mimic the properties of natural tears. But they cannot replicate natural tears exactly. Although the structure of tear films can only survive for tens of seconds and the active components decompose quickly, eyelid blinking ensures the delivery within seconds of active components and nutrients, and the continuous protection provided by the tear film. However, artificial tears can only be applied to the eyes intermittently.<sup>8</sup> Since artificial tears should serve the same functions as natural tears, they should have similar properties.

Natural tears are composed of 98% water.<sup>23</sup> Commercial artificial tears usually consist of 97-99% of water.<sup>8</sup>

Salts or electrolytes are usually used in artificial tears. As in natural tears, electrolytes in artificial tears have three functions: (1) Electrolytes such as sodium chloride, potassium chloride, calcium chloride and magnesium chloride are used in artificial tears to lower osmotic pressure difference between natural tear and artificial tear.<sup>34</sup> When artificial tears with electrolytes contact with the cells, it prevents the cells from swelling or shrinking. (2) Salts such as sodium bicarbonate, sodium phosphate,

sodium phosphate monobasic, sodium phosphate dibasic and sodium borate are also added to artificial tears as buffers to maintain the pH in the tear film solution.<sup>35</sup>

(3) Some salts, such as borates and benzalkonium chloride, are added as preservatives, to prevent the decomposition of the components of artificial tears from bacterial attack although they may be cytotoxic to the ocular surface to some extent.<sup>36</sup>

In addition to inorganic salts, small organic molecules are used in artificial tears. For example, dextrose can be used to adjust osmotic pressures, sucrose can be used as a surfactant, and glycerol, sorbitol and mannitol can be used as lubricants.<sup>8</sup>

Proteins have also been used in artificial tears. For example, gelatins have been used as artificial tears because they are good surfactants and gelling agents. They can function at both the air-water interface and the water-cornea interface to stabilize the tear film. However, they have to be extracted from animal collagen<sup>8</sup>, and are therefore more expensive than other artificial tear formulations.

Mucins which exist in natural tears can also be added to artificial tears. The mucus layer in the tear film functions to facilitate the spread of the aqueous layer and to lubricate the corneal surface. Therefore, the deficiency of mucins reduces the spread of the aqueous layer and induces the early break-up of the tear film. The addition of mucins supplements the mucin deficiency of dry eye syndrome.<sup>17,21</sup> Similar to proteins, they are expensive.

Lipids are another important component of tear film. They prevent water evaporation, lubricate the eyelids, and stabilize the tear film.<sup>18,25-28</sup> Because of the insolubility of the lipid components, they are used only in ointments and not in artificial tears. Experimentally, paraffin, lecithin and cholesterol have been used in artificial tears to mimic the lipid components in natural tears.<sup>37</sup>

Polymers are frequently used as active components in artificial tears because they are relatively cheap compared to other components of natural tears such as mucins, proteins and lipids, and can mimic the properties of these components.

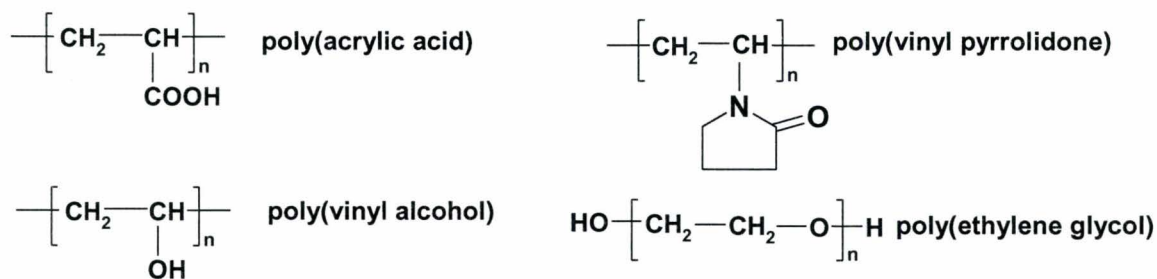


**Figure 1.4 Synthetic polymers commonly used in artificial tears.**

Synthetic polymers (Figure 1.4) such as polyethylene glycol (PEG), polyvinyl pyrrolidone and polysorbate are used as surfactants and serve at both the solid liquid interface and the air-liquid interface. At the water-cornea interface, they mimic the function of mucins in reducing the surface tension and improve the spread of the aqueous phase on the corneal surface. At the air-water interface, they mimic the function of lipids in stabilizing the tear film, and preventing the evaporation of water. Polyvinyl alcohol (PVA) was found to be very adsorptive at the corneal surface and has therefore been used as a lubricant that mimics the function of mucins.<sup>38</sup> Poly(acrylic acid) (PAA) can cross-link with polyalcohols or divinyl glycol, and form gels which are highly mucoadhesive, and so it is usually used to increase solution viscosity and mimic the function of mucins.<sup>39, 40</sup> Although synthetic polymers have the advantages of high stability and homogeneous molecular weight, they all have various drawbacks. PVA is incompatible with some components used in artificial tears. PAA may cause an inflammatory response and even damage the corneal surface.<sup>41</sup> Surfactants may dissolve lipids and induce instability in tear films.<sup>42</sup> In addition, synthetic polymers have the potential to be toxic.

Therefore, natural polymers have received more attention in recent years. The most commonly used natural polymers in artificial tears are polysaccharides (Figure 1.5). They are suitable for application to artificial tears since they can mimic mucins due to their similar structures and high molecular weight. They can be divided into three categories: mucopolysaccharides, dextrans and mucilages.<sup>8</sup>

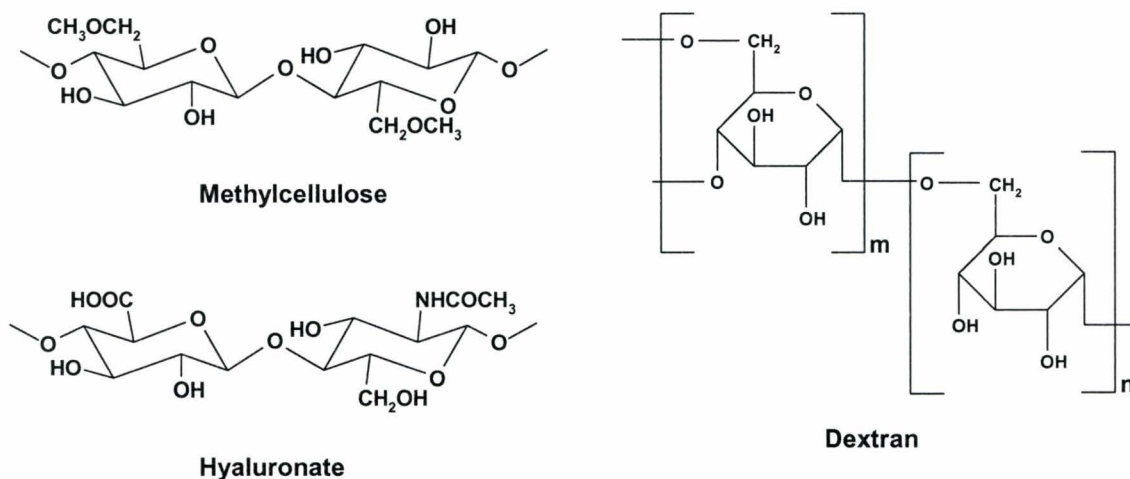


**Figure 1.5 Polysaccharides commonly used in artificial tears.**

A typical mucopolysaccharide is sodium hyaluronate (HA) as shown in Figure 1.5. HA is the polysaccharide most similar in structure (sugar units with amido groups) to mucins which are glycoproteins. Therefore, it is very mucoadhesive and can have similar function like mucins in tear film. Clinical studies have shown that HA is effective in treating dry eye syndrome.<sup>43, 44</sup> But the viscosity induced by HA addition is too high for the HA to be removed from corneal surface in as a short time with mucins.<sup>45</sup> The

retention of HA on the corneal surface tampers vision and reduces the removal of contaminants.

Dextrans are polysaccharides with a glucose main chain and glucose branch chains, with a lower molecular weight than HA. Dextrans provide mechanical strength to tear film and induce high onconic pressure.<sup>46</sup> But they are poorly mucoadhesive, and most importantly, they are highly allergenic.<sup>8</sup>

Mucilages are made of cellulose or gums. Because of the poor solubility of cellulose, its derivatives are used instead in artificial tears. These cellulose derivatives are methylcellulose, hydroxyethyl cellulose, hydroxypropyl cellulose and carboxymethyl cellulose. These increase the viscosity of tears.<sup>41, 43, 44, 47</sup> Most importantly, they provide mild adsorption properties to the corneal surface.<sup>8</sup> Therefore, they properly mimic the properties of mucins. However, some cellulose derivatives such as carboxymethyl cellulose can interact with proteins, such as lysozyme in tear film.

In recent years, other mucilages such as alginate<sup>48</sup> and guar gum have been investigated for use in artificial tears. Hydroxypropyl guar (HPG, a hydroxypropyl derivative of guar) has been found to be very efficient in treating dry eye syndrome, by increasing the retention time of tears.<sup>9, 10, 49-51</sup>

### 1.3 Guar, HPG and HPG-borate

Extracted from seeds of *Cyamopsis tetragonaloba*, guar is a polysaccharide composed of a  $\beta$ -1,4 linked mannose backbone and an  $\alpha$ -1,6 linked galactose pendant group with a galactose to mannose ratio of 1:1.6 to 1:2, depending on the source of the guar.<sup>52</sup> The structure of guar is shown in Figure 1.6. Because of its high molecular weight (over  $10^6$  Da), guar is widely used in food, cosmetics, and oil industry as a thickener or fracturing agent.<sup>53</sup> Guar has a radius of gyration of about 133 nm at a molecular weight of  $1.87 \times 10^6$  Da and has a characteristic ratio of 11.87, indicating that guar is a rather stiff polymer.<sup>53, 54</sup> Polymannose is water insoluble, and galactose is critical for water solubility. But due to the intermolecular hydrogen bonding, guar always has some aggregates in aqueous solution.<sup>54</sup>

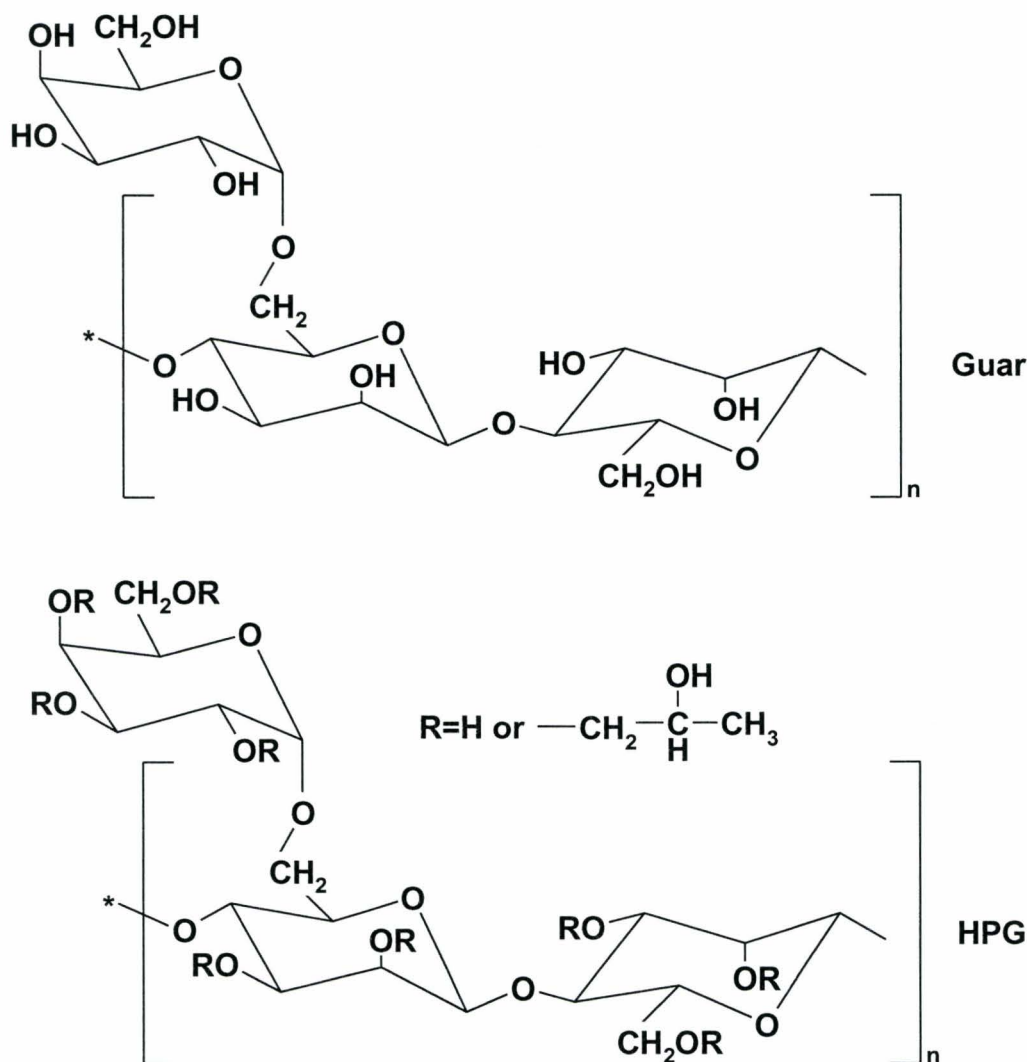


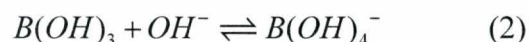
**Figure 1.6** Structure of guar and HPG.

HPG (structure shown in Figure 1.6) is a hydroxypropyl derivative of guar which is a product of guar reaction with propylene oxide. The hydroxypropyl groups block the intermolecular hydrogen bonding so that the solubility of guar is increased. The Flory-Huggins parameter of HPG is 0.39, comparing to 0.7 for guar, indicating that HPG is more water soluble than guar. And HPG has a characteristic ratio of 13.02 which makes it stiffer than guar because the steric hindrance from hydroxypropyl groups limits the bending of the backbone bonds.<sup>53</sup> The distribution of the hydroxypropyl groups is nearly random, slightly favoring primary hydroxyl groups.<sup>55</sup> The hydroxypropyl content is described as degree of substitution (DS), which is the average number of hydroxypropyl groups per sugar ring. The typical HPG used in our research has a DS of 0.36.

In artificial tears, sodium borate ( $\text{Na}_2\text{B}_4\text{O}_7 \cdot 10\text{H}_2\text{O}$ ) is usually used as buffer. In the aqueous phase, sodium borate can dissociate into equal numbers of molecules of boric acid and borate ion, as shown in equation (1):



And boric acid-borate ions are in equilibrium in the aqueous phase as shown in equation (2):



The pKa of boric acid is about 9.2 meaning that boric acid and borate ions have an equal numbers of molecules at pH 9.2 in the aqueous phase.

It is well accepted that borate ions can bind with cis-diols to form covalent bonds. Pezron et al.<sup>56</sup> confirmed that borate ions could also bind with cis-diols on HPG (structure as shown in Figure 1.7 and Figure 1.8), and borate ions cross-link with HPG by binding with two molecules of HPG as shown in Figure 1.8. Borate binding converts HPG into a negatively charged polyelectrolyte, HPG-borate.

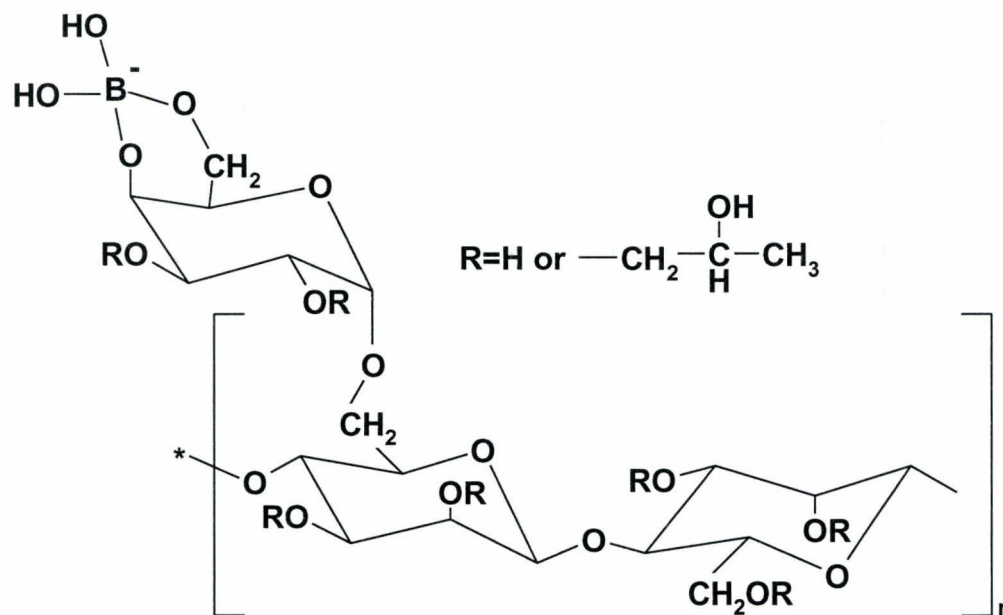


**Figure 1.7** The structure of borate bound HPG.

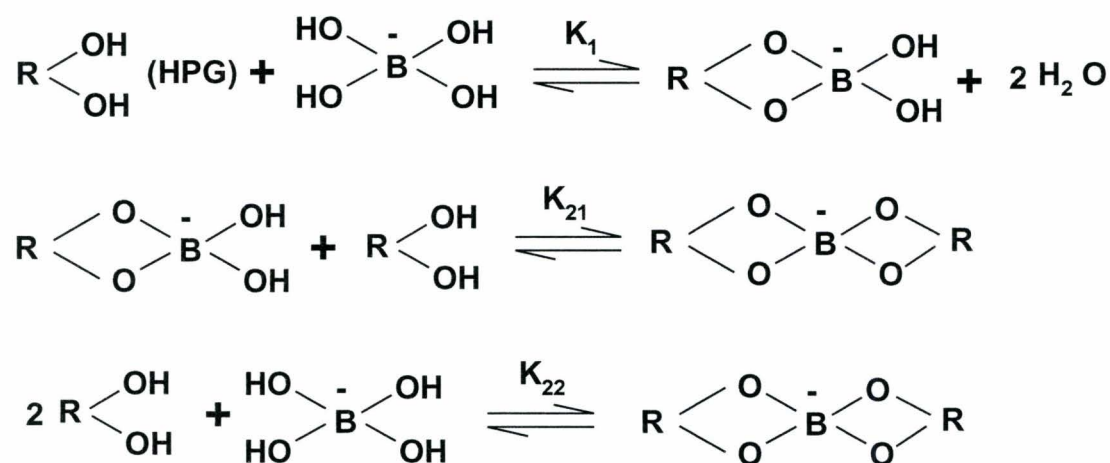


**Figure 1.8 Borate binds with HPG and cross-links HPG.**

Pezron et al.<sup>56</sup> determined the binding constant  $K_1$  of borate with HPG to be about 11 L/mol using dialysis and NMR experiments. Jasinski<sup>57</sup> reported a binding constant of about 100 L/mol using NMR experiments. Although they disagree with each other, all the reported binding constants are lower than expected for covalent bonds. The binding energy between borate ion and HPG corresponds to a binding constant of 11 L/mol, which is only about -5.9 kJ/mol when calculated using  $\Delta G = -RT \ln K_1$ , even lower than that of the hydrogen bond which is about 18 kJ/mol. This low binding energy leads to the question whether HPG and borate binding is a covalent bond. Hence, the binding constant of HPG-borate needs to be clarified.

## 1.4 HPG-borate Interaction with Tear Film Components

### 1.4.1 Fundamentals

As a component in artificial tears, HPG-borate may interact with both tear film and artificial tear components. The possible components that HPG-borate may interact with are proteins, lipids, mucins, polymers, surfactants, particles and surfaces including the air-water interface and the liquid-solid interface.

Although the components of tear film and artificial tears are complicated, all the interactions of HPG-borate with these components fall into the following categories: van der Waals interaction, electrostatic interaction, hydrophobic interaction, hydrodynamic effect, depletion, steric effect and hydrogen bonding.

The attractive interactions mainly come from the van der Waals attraction, electrostatic attraction, hydrophobic attraction, hydrogen bonding, and depletion.

Electrostatic repulsion, steric effect and hydrodynamic effect contribute to the repulsive interactions.<sup>58</sup>

The van der Waals force is one of the major attractive forces in intermolecular interaction due to the attraction force between two instantaneously induced dipoles. The van der Waals energy depends on the inverse 6<sup>th</sup> power of the separation between two molecules, which can be expressed as equation (3)<sup>59</sup>:

$$V_A = -\beta\delta^{-6} \quad (3)$$

where  $V_A$  is van der Waals attraction energy,  $\beta$  is a constant, and  $\delta$  is the separation distance between two molecules. However, the van der Waals attraction between colloids can be described by the Hamaker theory. For example, the attraction between two similar spheres is shown in equation (4)<sup>59</sup>:

$$V_A = -\frac{AR}{12\delta} \quad (4)$$

where  $A$  is the Hamaker constant and  $R$  is the radius of sphere.

Electrostatic attraction occurs when two molecules have opposite charges. Hydrogen bonding is an attractive force between a hydrogen atom and atom which is an electron donor such as oxygen, for example, hydrogen atom and oxygen atom in water molecule. Hydrophobic attraction is the attractive force between two molecules with hydrophobic groups.<sup>58</sup> An example of a depletion force is the attraction between two surfaces driven by non-adsorbed polymers, so that the osmotic pressure between them is reduced.<sup>60</sup>

The fundamental theory describing the electrostatic repulsion between surfaces is the electrical double layer theory. For an independent particle surface, the Stern-Gouy-Chapman (SGC) model is a classical model which describes the electrical double layer theory. In this model, close to the surface there is a layer whose potential and charge density decay linearly from the surface. The potential at the double layer is called the zeta potential. It can be calculated by equation (5) for spherical particles<sup>61</sup>:

$$\psi_d = \psi_0(R/r) \exp(-\kappa(r-R)) \quad (5)$$

In equation (5),  $\psi_d$  is zeta potential,  $\psi_0$  is surface potential,  $R$  is the radius of the particle,  $r$  is the sum of the particle radius and the double layer thickness,  $1/\kappa$  is the Debye length, where  $\kappa$  can be calculated by equation (6)<sup>61</sup>:

$$\kappa = \sqrt{\frac{e_0^2 N_A}{\epsilon_0 \epsilon_r k_b T} 2c} \quad (6)$$

In equation (6),  $e_0$  is elementary charge,  $N_A$  is Avagadro constant,  $\epsilon_0$  is the permittivity in vacuum,  $\epsilon_r$  is relative permittivity,  $k_b$  is Boltzmann constant, and  $c$  is salt concentration.

For two spheres with constant surface potential, the repulsion potential between them can be calculated as in equation (7)<sup>61</sup>:

$$V_r = 2\pi\epsilon_0\epsilon_r R\psi_o^2 \ln(1 + \exp(-\kappa h)) \quad (7)$$

where  $h$  is the separation distance between the spheres, and  $V_r$  is the electrostatic repulsion potential.

Hydrodynamic effects inhibit the attraction of particles by the hydration layer, while steric effects prevent surfaces from coming together by space inhibition, usually resulting from the surface bound polymers on the colloid surface.<sup>58</sup>

## 1.4.2 Literature Review

HPG-borate interactions with tear film and artificial tear components have not been studied before.

Anthony et al.<sup>62</sup> reported the interactions between cationic guar and oppositely charged surfactants. Cationic guar and surfactant mixtures have similar behaviors to the usual oppositely charged polyelectrolyte/surfactant mixtures. The mixtures phase separated at a surfactant concentration below the critical micelle concentration (cmc) of the surfactant, and redissolved at a surfactant concentration of a few times the cmc. Kastner et al.<sup>63</sup> reported the interactions of HPG and hydrophobically modified HPG with cationic surfactant dodecyltrimethylammonium bromide (DTAB). No significant interactions between HPG and DTAB were observed, whereas hydrophobic interaction was found between the hydrophobically modified HPG and the surfactant, via non-cooperative binding below the cmc of DTAB, which is common behavior between the hydrophobic polymer and the surfactant.

There are few reports of guar or HPG interactions with proteins. Bourriot et al.<sup>64</sup> studied casein (a protein) and guar mixtures which are often used in the food industry. They suggested that casein and guar mixtures form two phases in aqueous solution. There are no reports on guar-borate or HPG-borate interactions with proteins.

There are also no reports on the interactions of HPG-borate with lipids, or even HPG or guar interaction with lipids.

As for guar or HPG interaction with surfaces, the adsorption behavior of guar on mineral surfaces has been well studied because of its applications in mineral processing. Hydrogen bonding is possibly the driving force for the adsorption of guar on mineral

surfaces.<sup>65-68</sup> But none of these reports involve the behaviors of guar-borate or HPG-borate interaction with mineral surfaces.

Lu et al.<sup>69</sup> have studied the interaction between mucin microgel particles and HPG in the presence of borate using dynamic light scattering, viscosity measurements and electrophoretic mobility. They suggested that HPG does not bind with mucin, even in the presence of borate. Although they also tried to study the electrostatic interaction between lysozyme and HPG in the presence of borate using dynamic light scattering, more appropriate techniques need to be employed to investigate the interaction between lysozyme and HPG-borate. Hydrophobic interaction between them also needs to be investigated.

## 1.5 Objectives

The overall objective of the work summarized in this thesis is to investigate the possible interactions of HPG-borate with tear film components and artificial tear components at physiological conditions, and assess the application of HPG-borate to artificial tears. The specific objectives are as follows.

1. To prepare modified guar with charged groups and hydrophobic groups, so as to magnify electrostatic and hydrophobic interactions with tear film or artificial tear components.
2. To study the properties of HPG-borate as a polyelectrolyte, including the interaction with oppositely charged polyelectrolytes.
3. To investigate the interaction of HPG-borate with oppositely charged small molecules (surfactants).
4. To study the interaction mechanism of HPG-borate with oppositely charged protein-lysozymes under physiological conditions.
5. To examine the effect of HPG-borate on similarly charged lipids under physiological conditions.

## 1.6 Thesis Outline

Chapter 1. *Introduction*. This chapter introduces the background to this thesis including dry eye syndrome, tear film, artificial tears, guar, HPG, HPG-borate and the interaction of guar or HPG with tear film components. The objective of the thesis, and the thesis outline, are provided.

Chapter 2. *Synthesis and characterization of carboxymethyl guar, cationic guar and hydrophobically modified guar*. This chapter described methods of synthesis of carboxymethyl guar, cationic guar and hydrophobically modified guar. The degrees of substitution of carboxymethyl, cationic and hydrophobic groups per sugar ring are also investigated.

Chapter 3. *Characterization and modeling of HPG-borate, a labile polyelectrolyte, by polyelectrolyte titration and interaction of HPG-borate with oppositely charged polyelectrolyte.* In this chapter, HPG-borate, a polyelectrolyte that different from conventionally defined polyelectrolyte, was characterized by polyelectrolyte titration with cationic poly(diallyldimethyl ammonium chloride) (PDADMAC). The total binding sites of borate ion on HPG were measured by polyelectrolyte titration. A model was developed to describe the process of polyelectrolyte titration of HPG-borate with PDADMAC. The experiments were all done by me. Both Dr Pelton and I contributed to the modeling. I wrote the draft and Dr Pelton helped me revise it. This chapter has been published in *Macromolecules*.<sup>70</sup> The modeling paper to describe the polyelectrolyte titration of conventionally defined polyelectrolyte has been published in *Analytical Chemistry* and Dr. Pelton contributed the most to the modeling and writing.<sup>71</sup>

Chapter 4. *Interaction of HPG-borate with cationic surfactant dodecyltrimethyl ammonium bromide (DTAB).* In this chapter, a deviant behavior of HPG-borate as a polyelectrolyte was described by investigating the interaction between HPG-borate and cationic surfactant dodecyltrimethyl ammonium bromide (DTAB). Carboxymethyl guar (CMG) interaction with DTAB was also studied to emphasize the deviant behavior of HPG-borate. Dr. Pelton, Dr. Cosgrove, Dr. Richardson, Dr. Prescott and I cooperated in SANS experiments. Isothermal titration calorimetric (ITC) experiments were conducted by Dr. Dai. Surface tension experiments were performed by me. I prepared the draft and Dr. Pelton helped me revise it. This chapter has been published in *Langmuir*.<sup>72</sup>

Chapter 5. *HPG-borate and modified guar interactions with lysozyme.* HPG-borate interactions with lysozyme are investigated. CMG and hydrophobically modified guar interactions with lysozyme are also compared. Ionic strength and pH effects are studied. A model is developed to describe the effects of ionic strength on the interactions. This chapter is being prepared for publication.

Chapter 6. *HPG-borate and modified guar interactions with phosphatidic acid liposomes.* The experimental investigation of interactions between phosphatidic acid liposomes and HPG-borate are described. Cationic guar and hydrophobically modified guar were also employed to compare the interactions with phosphatidic acid liposomes. Molecular weight and pH effects on the interactions are studied. A depletion model is used to describe the interactions of HPG with phosphatidic acid liposomes. Liang Zhang contributed most to find a proper depletion model. This paper is in preparation for publication. HPG-borate and modified guar interaction with a cationic lipid 1,2-dioleoyl-3-trimethylammonium-propane(DOTAP) are also investigated. I contributed to the experiment of carboxymethyl guar (CMG) interaction with DOTAP and salt effect model. This paper is being prepared for publication.

Chapter 7. *Concluding remarks.* This chapter presents the conclusions, major contributions and future work.

## 1.7 References

1. Schaumberg, D. A.; Dana, R.; Buring, J. E.; Sullivan, D. A., Prevalence of dry eye disease among us men estimates from the physicians' health studies. *Archives of Ophthalmology* 2009, 127, (6), 763-768.
2. Schaumberg, D. A.; Sullivan, D. A.; Buring, J. E.; Dana, M. R., Prevalence of dry eye syndrome among us women. *American Journal of Ophthalmology* 2003, 136, (2), 318-326.
3. Jackson, W. B., Management of dysfunctional tear syndrome: A canadian consensus. *Canadian Journal of Ophthalmology-Journal Canadien D Ophtalmologie* 2009, 44, (4), 385-394.
4. Moss, S. E.; Klein, R.; Klein, B. E. K., Incidence of dry eye in an older population. *Archives of Ophthalmology* 2004, 122, (3), 369-373.
5. Wolkoff, P.; Nojgaard, J. K.; Troiano, P.; Piccoli, B., Eye complaints in the office environment: Precorneal tear film integrity influenced by eye blinking efficiency. *Occupational and Environmental Medicine* 2005, 62, (1), 4-12.
6. A. Lemp, C. M., Report of the national eye institute/industry workshop on clinical trials in dry eyes. *Eye & Contact Lens* 1995, 21, (4), 221-232.
7. Pflugfelder, S. C.; Solomon, A.; Stern, M. E., The diagnosis and management of dry eye - a twenty-five-year review. *Cornea* 2000, 19, (5), 644-649.
8. Murube, J.; Paterson, A.; Murube, E., Classification of artificial tears. I: Composition and properties. *Advances in experimental medicine and biology* 1998, 438, 693-704.
9. Christensen, M. T.; Cohen, S.; Rinehart, J.; Akers, F.; Pemberton, B.; Bloomenstein, M.; Leshner, M.; Kaplan, D.; Meadows, D.; Meuse, P.; Hearn, C.; Stein, J. M., Clinical evaluation of an HP-guar gellable lubricant eye drop for the relief of dryness of the eye. *Current Eye Research* 2004, 28, (1), 55-62.
10. Ubels, J. L.; Clousing, D. P.; Van Haitsma, T. A.; Hong, B. S.; Stauffer, P.; Asgharian, B.; Meadows, D., Pre-clinical investigation of the efficacy of an artificial tear solution containing hydroxypropyl-guar as a gelling agent. *Current Eye Research* 2004, 28, (6), 437-444.
11. King-Smith, P. E.; Fink, B. A.; Hill, R. M.; Koelling, K. W.; Tiffany, J. M., The thickness of the tear film. *Current Eye Research* 2004, 29, (4-5), 357-368.
12. King-Smith, P. E.; Fink, B. A.; Fogt, N., Three interferometric methods for measuring the thickness of layers of the tear film. *Optometry and Vision Science* 1999, 76, (1), 19-32.
13. King-Smith, P. E.; Fink, B. A.; Fogt, N.; Kinney, K. A.; Hill, R. M., Is the thickness of the tear film about 40  $\mu\text{m}$  or about 3  $\mu\text{m}$ ? *Investigative Ophthalmology & Visual Science* 1999, 40, (4), 2876B751.
14. King-Smith, P. E.; Fink, B. A.; Hill, R. M.; Koelling, K. W.; Tiffany, J. M., Reply to letter by Dr. C.J. Radke. *Current Eye Research* 2005, 30, (12), 1133-1134.

15. King-Smith, P. E.; Fink, B. A.; Nichols, J. J.; Nichols, K. K.; Hill, R. M., Interferometric imaging of the full thickness of the precorneal tear film. *Journal of the Optical Society of America a-Optics Image Science and Vision* 2006, 23, (9), 2097-2104.
16. Nichols, J. J.; King-Smith, P. E., Thickness of the pre- and post-contact lens tear film measured in vivo by interferometry. *Investigative Ophthalmology & Visual Science* 2003, 44, (1), 68-77.
17. Davidson, H. J.; Kuonen, V. J., The tear film and ocular mucins. *Veterinary Ophthalmology* 2004, 7, (2), 71-77.
18. Bron, A. J.; Tiffany, J. M.; Gouveia, S. M.; Yokoi, N.; Voon, L. W., Functional aspects of the tear film lipid layer. *Experimental Eye Research* 2004, 78, (3), 347-360.
19. Sharma, A., Surface properties of damaged and normal corneal epithelia. *J Dispersion Sci Tech* 1992, 13, 459-478.
20. Sharma, A.; Khanna, R.; Reiter, G., A thin film analog of the corneal mucus layer of the tear film: An enigmatic long range non-classical DLVO interaction in the breakup of thin polymer films. *Colloids and Surfaces B: Biointerfaces* 1999, 14, (1-4), 223-235.
21. Corfield, A. P.; Carrington, S. D.; Hicks, S. J.; Berry, M.; Ellingham, R., Ocular mucins: Purification, metabolism and functions. *Progress in Retinal and Eye Research* 1997, 16, (4), 627-656.
22. Argueso, P.; Gipson, I. K., Epithelial mucins of the ocular surface: Structure, biosynthesis and function. *Experimental Eye Research* 2001, 73, (3), 281-289.
23. Van Haeringen, N. J., Clinical biochemistry of tears. *Survey of Ophthalmology* 1981, 26, (2), 84-96.
24. Johnson, M. E.; Murphy, P. J., Changes in the tear film and ocular surface from dry eye syndrome. *Progress in Retinal and Eye Research* 2004, 23, (4), 449-474.
25. Foulks, G. N., The correlation between the tear film lipid layer and dry eye disease. *Survey of Ophthalmology* 2007, 52, (4), 369-374.
26. Jones, M. B.; McElwain, D. L. S.; Fulford, G. R.; Collins, M. J.; Roberts, A. P., The effect of the lipid layer on tear film behaviour. *Bulletin of Mathematical Biology* 2006, 68, (6), 1355-1381.
27. McCulley, J. P.; Shine, W. E., Meibomian gland and tear film lipids: Structure, function and control. *Lacrimal gland, tear film, and dry eye syndromes 3: basic science and clinical relevance* 2002, 373.
28. McCulley, J. P.; Shine, W. E., The lipid layer of tears: Dependent on meibomian gland function. *Experimental Eye Research* 2004, 78, (3), 361-365.
29. Tiffany, J. M., Physiological functions of the meibomian glands. *Progress in Retinal and Eye Research* 1995, 14, (1), 47-74.
30. Holly, F. J., Formation and rupture of the tear film. *Experimental Eye Research* 1973, 15, (5), 515-525.
31. Mathers, W., Evaporation from the ocular surface. *Experimental Eye Research* 2004, 78, (3), 389-394.
32. McDonald, J. E.; Brubaker, S., Meniscus-induced thinning of tear films. *American Journal of Ophthalmology* 1971, 72, (1), 139.
33. Bruce, A. S.; Mainstone, J. C.; Golding, T. R., Analysis of tear film breakup on etafilcon a hydrogel lenses. *Biomaterials* 2001, 22, (24), 3249-3256.

34. Green, K.; Mackeen, D. L.; Slagle, T.; Cheeks, L., Tear potassium contributes to maintenance of corneal thickness. *Ophthalmic Research* 1992, 24, (2), 99-102.
35. Bernal, D. L.; Ubels, J. L., Artificial tear composition and promotion of recovery of the damaged corneal epithelium. *Cornea* 1993, 12, (2), 115-120.
36. Baudouin, C., The pathology of dry eye. *Survey of Ophthalmology* 2001, 45, S211-S220.
37. Guomundsson, O. G.; Thorisdottir, S.; Loftsson, T.; Frioriksdottir, H.; Guomundsson, O.; Sigthorsson, T.; Stefansson, E., 2-hydroxypropyl-beta-cyclodextrin (hp-beta-cd) and cholesterol tear substitute. *Investigative Ophthalmology & Visual Science* 1994, 35, (4), 1694-1694.
38. Holly, F. J., Ophthalmic solution for treatment of dry-eye syndrome. In Google Patents: 1989.
39. Bron, A. J.; Mangat, H.; Quinlan, M.; Foley-Nolan, A.; Eustace, P.; Fsadni, M.; Raj, P. S., Polyacrylic acid gel in patients with dry eyes: A randomised comparison with polyvinyl alcohol. *European Journal of Ophthalmology* 1998, 8, (2), 81-89.
40. Oechsner, M.; Keipert, S., Polyacrylic acid polyvinylpyrrolidone bipolymeric systems. I. Rheological and mucoadhesive properties of formulations potentially useful for the treatment of dry-eye-syndrome. *European Journal of Pharmaceutics and Biopharmaceutics* 1999, 47, (2), 113-118.
41. Diebold, Y.; Herreras, J. M.; Callejo, S.; Argueso, P.; Calonge, M., Carbomer-versus cellulose-based artificial-tear formulations: Morphologic and toxicologic effects on a corneal cell line. *Cornea* 1998, 17, (4), 433-440.
42. Smith, S. G., Ophthalmic compositions and process of using. In Google Patents: 1999.
43. Doughty, M. J.; Glavin, S., Efficacy of different dry eye treatments with artificial tears or ocular lubricants: A systematic review. *Ophthalmic and Physiological Optics* 2009, 29, (6), 573-583.
44. Liu, L.; Tiffany, J.; Dang, Z. X.; Dart, J. K. G.; Watson, S. L.; Daniels, J. T.; Geerling, G., Nourish and nurture: Development of a nutrient ocular lubricant. *Investigative Ophthalmology & Visual Science* 2009, 50, (6), 2932-2939.
45. Snibson, G. R.; Greaves, J. L.; Soper, N. D. W.; Prydals, J. I.; Wilson, C. G.; Bron, A. J., Precorneal residence times of sodium hyaluronate solutions studied by quantitative gamma scintigraphy. *Eye* 1990, 4, 594-602.
46. Redkar, M.; Srividya, B.; Ushasree, P.; Amin, P. D., Dextran - hpmc eye drops as artificial tears. *Journal of Scientific & Industrial Research* 2000, 59, (12), 1027-1031.
47. Wander, A. H.; Koffler, B. H., Extending the duration of tear film protection in dry eye syndrome: Review and retrospective case series study of the hydroxypropyl cellulose ophthalmic insert. *Ocular Surface* 2009, 7, (3), 154-162.
48. Hartmann, V.; Keipert, S., Physico-chemical, in vitro and in vivo characterisation of polymers for ocular use. *Pharmazie* 2000, 55, (6), 440-443.
49. Christensen, M. T.; Hearn, C. J.; Meadows, D. L.; Stein, J. M., Results of a clinical evaluation with a new artificial tear solution containing HP-guar. *Investigative Ophthalmology & Visual Science* 2003, 44, 2483.

50. Hartstein, I.; Khwarg, S.; Przydryga, J., An open-label evaluation of HP-guar gellable lubricant eye drops for the improvement of dry eye signs and symptoms in a moderate dry eye adult population. *Current Medical Research and Opinion* 2005, 21, (2), 255-260.
51. Gifford, P.; Evans, B. J. W.; Morris, J., A clinical evaluation of systane. *Contact Lens and Anterior Eye* 2006, 29, (1), 31-40.
52. Srivastava, M.; Kapoor, V. P., Seed gallactomannans: An overview. *Chemistry & Biodiversity* 2005, 2, (3), 295-317.
53. Cheng, Y.; Brown, K. M.; Prud'homme, R. K., Characterization and intermolecular interactions of hydroxypropyl guar solutions. *Biomacromolecules* 2002, 3, (3), 456-461.
54. Picout, D. R.; Ross-Murphy, S. B.; Errington, N.; Harding, S. E., Pressure cell assisted solution characterization of polysaccharides. 1. Guar gum. *Biomacromolecules* 2001, 2, (4), 1301-1309.
55. McNeil, M.; Albersheim, P., A quantitative method to determine the points of ortho-(2-hydroxypropyl) substitution in ortho-(2-hydroxypropyl)-guar. *Carbohydrate Research* 1984, 131, (1), 131-137.
56. Pezron, E.; Ricard, A.; Lafuma, F.; Audebert, R., Reversible gel formation induced by ion complexation .1. Borax galactomannan interactions. *Macromolecules* 1988, 21, (4), 1121-1125.
57. Jasinski, R.; Redwine, D.; Rose, G., Boron equilibria with high molecular weight guar: An NMR study. *Journal of Polymer Science, Part B: Polymer Physics* 1996, 34, (8), 1477-1488.
58. Evans, D. F.; Wennerstrom, H., The colloidal domain: Where physics. *Chemistry, Biology, and Technology Meet* 1994.
59. Goodwin, J. W., *Colloids and interfaces with surfactants and polymers: An introduction*. Wiley: 2004.
60. Asakura, S.; Oosawa, F., Interaction between particles suspended in solutions of macromolecules. *Journal of Polymer Science* 1958, 33, (126), 183-192.
61. Hunter, R. J.; White, L. R.; Chan, D. Y. C., *Foundations of colloid science*. Clarendon Press Oxford: 1987, 415.
62. Anthony, O.; Marques, C. M.; Richetti, P., Bulk and surface behavior of cationic guar in solutions of oppositely charged surfactants. *Langmuir* 1998, 14, (21), 6086-6095.
63. Kastner, U.; Zana, R., Interactions between quaternary ammonium surfactant oligomers and water-soluble modified guar. *Journal of Colloid and Interface Science* 1999, 218, (2), 468-479.
64. Bourriot, S.; Garnier, C.; Doublier, J. L., Phase separation, rheology and microstructure of micellar casein-guar gum mixtures. *Food Hydrocolloids* 1999, 13, (1), 43-49.
65. Liu, Q.; Zhang, Y. H.; Laskowski, J. S., The adsorption of polysaccharides onto mineral surfaces: An acid/base interaction. *International Journal of Mineral Processing* 2000, 60, (3-4), 229-245.
66. Rath, R. K.; Subramanian, S., Studies on adsorption of guar gum onto biotite mica. *Minerals Engineering* 1997, 10, (12), 1405-1420.

67. Wang, J.; Somasundaran, P., Study of galactomannose interaction with solids using AFM, IR and allied techniques. *Journal of Colloid and Interface Science* 2007, 309, (2), 373-383.
68. Wang, J.; Somasundaran, P.; Nagaraj, D. R., Adsorption mechanism of guar gum at solid-liquid interfaces. *Minerals Engineering* 2005, 18, (1), 77-81.
69. Lu, C.; Kostanski, L.; Ketelson, H.; Meadows, D.; Pelton, R., Hydroxypropyl guar-borate interactions with tear film mucin and lysozyme. *Langmuir* 2005, 21, (22), 10032-10037.
70. Cui, Y. G.; Pelton, R.; Ketelson, H., Shapes of polyelectrolyte titration curves. 2. The deviant behavior of labile polyelectrolytes. *Macromolecules* 2008, 41, (21), 8198-8203.
71. Pelton, R.; Cabane, B.; Cui, Y.; Ketelson, H., Shapes of polyelectrolyte titration curves. 1. Well-behaved strong polyelectrolytes. *Analytical Chemistry* 2007, 79, (21), 8114-8117.
72. Cui, Y. G.; Pelton, R.; Cosgrove, T.; Richardson, R.; Dai, S.; Prescott, S.; Grillo, I.; Ketelson, H.; Meadows, D., Not all anionic polyelectrolytes complex with DTAB. *Langmuir* 2009, 25, (24), 13712-13717.

## Chapter 2 Synthesis and Characterization of Carboxymethyl Guar, Cationic Guar and Hydrophobically Modified Guar

### Abstract

Carboxymethyl guar, cationic guar and hydrophobically modified guar were synthesized by reacting guar with chloroacetic acid, and glycidyltrimethyl ammonium chloride, and by reacting carboxymethyl guar with alkyl amines or aromatic amine in the presence of N-(3-Dimethylaminopropyl)-N'-ethylcarbodiimide hydrochloride (EDC). Carboxymethyl guar was characterized by FT-IR qualitatively, and degree of substitution of the carboxymethyl group was determined by conductometric titration. Cationic guar and hydrophobically modified guar were characterized by NMR, and the degree of substitution of cationic group in cationic guar, and of hydrophobic groups in hydrophobically modified guar, were calculated from NMR spectra. The degree of substitution of cationic guar was also determined by polyelectrolyte titration and found to be in accordance with the NMR result. The carboxyl residues on hydrophobically modified guar were characterized by conductometric titration. Results show that carboxymethyl guar with degrees of substitution (DS) of 0.39 and 0.13, cationic guar with a DS of 0.09, and hydrophobically modified guar with a DS of 0.13, were all successfully synthesized.

## 2.1 Introduction

Guar is a polysaccharide with polymannose as the main chain and pendant galactose as side chains. Because of its poor solubility<sup>1</sup>, hydroxypropyl groups have been added to guar molecules. Hydroxypropyl groups block the hydrogen bonding between guar molecules so that the solubility of guar is dramatically increased.<sup>2</sup>

Guar and hydroxypropyl guar (HPG) have been used as a fracturing agent in oil industry, and as a thickener in food industry. Recently HPG has been applied in the drug industry, and was found very efficient in the treatment of dry eye syndrome.<sup>3-6</sup> But the interaction mechanism of HPG with these components in the tear film was not well understood.

HPG and borate are among the most efficient components to treat dry eye syndrome. It was well known that HPG can be converted from a non-ionic polymer into a negatively charged polyelectrolyte when bound with borate.<sup>7</sup> And the hydroxypropyl groups in HPG are slightly hydrophobic.

We propose that electrostatic and hydrophobic interaction dominate the interaction between HPG-borate and tear film components. Therefore, modified guar with charged groups such as carboxymethyl guar, cationic guar and hydrophobically modified guar must be synthesized so as to explore the significance of electrostatic and hydrophobic interactions.

Carboxymethylation of polysaccharide has usually been achieved by reacting polysaccharide with chloroacetate catalyzed by a base; a typical example is carboxymethyl cellulose (CMC) which results from cellulose reacting with chloroacetate in the presence of sodium hydroxide.<sup>8</sup> Recently, this method has also been used in the carboxymethylation of guar.<sup>9</sup>

Cationic guar can be prepared using the same method as in the preparation of hydroxypropyl guar (HPG), which is a product of guar reacting with propylene oxide<sup>10</sup>. In the case of the preparation of cationic guar, guar can react with a compound with an epoxy group at one end and a cationic group at the other end. Quaternary ammonium is a good candidate for the cationic group because the charge density of quaternary ammonium does not change with pH.

Primary alkyl halides have frequently been used to synthesize hydrophobically modified compounds with hydroxyl groups, such as polysaccharides.<sup>11</sup> Although long alkyl chains derivatives have been reported to be synthesized by this method,<sup>12</sup> only short chain modification such as methylation has been attained efficiently.<sup>13</sup> In addition to taking guar molecules as a reactant, carboxymethyl guar can be employed as the starting material for the hydrophobic modification of guar so as to react with primary amines in

the presence of N-(3-Dimethylaminopropyl)-N'-ethylcarbodiimide hydrochloride (EDC). Thus, hydrophobic groups will be attached to guar molecules with amide bond formation.<sup>14</sup>

## 2.2 Experimental

### 2.2.1 Materials

Guar with molecular weight  $3 \times 10^6$  Dalton was provided by Alcon Laboratories (Fort Worth, Texas). Chloroacetic acid, 2-(N-morpholino) ethanesulfonic acid (MES) hydrate, N-(3-dimethylaminopropyl)-N'-ethylcarbodiimide hydrochloride (EDC), hexyl amine, octyl amine, dodecyl amine, octadecyl amine and benzyl amine were purchased from Sigma-Aldrich. Glycidyltrimethylammonium chloride was purchased from Fluka. Polyvinyl sulphate potassium (PVSK) solution of 1mM was purchased from BTG America. Sodium hydroxide and hydrochloric acid were purchased from Anachemia. Isopropanol (2-propanol) was purchased from Caledon Laboratories Ltd. All reagents were used without purification.

### 2.2.2 Methods

#### Preparation of Carboxymethyl Guar (CMG)

Carboxymethyl guar (CMG) was prepared by reacting guar with chloroacetic acid as shown in Scheme 2.1. In a typical experiment, 10 grams of guar was dispersed in 100 mL of 2-propanol in a three-neck glass flask reactor fitted with a mechanical stirrer. Sodium hydroxide (5.6 grams) was added with stirring at room temperature, followed by chloroacetic acid. The mixture was stirred for four hours at 70°C. After cooling, the dispersed product was collected on a Whatman No.1 medium fast paper filter and washed with 300 mL 2-propanol. Then the products were dissolved in water and the solution was centrifuged and decanted to isolate the solids. The pH of the solution was adjusted to 7.0 using hydrochloric acid. Finally, the solution was precipitated with 2-propanol. The precipitation product was collected, freeze-dried and then ground into powder.

The content of carboxymethyl groups was determined by conductometric titration (the procedure will be described below). CMG samples with a degree of substitution (DS) of 0.13 and 0.39 were synthesized, where the DS is defined as the number of carboxyl group per sugar ring. The structure of CMG is shown in Figure 2.1.

#### Preparation of Cationic Guar

Cationic guar was prepared by reacting guar with glycidyltrimethylammonium chloride as shown in Scheme 2.2. In a typical synthesis process, 10 grams of guar was

dispersed in 200mL of 2-propanol in a 500 mL three necked round flask. Then 50mL of 30% (w/w) NaOH was added drop by drop. After stirring for 30 min, 80 mL of glycidyltrimethylammonium chloride was added and reacted with guar for 4 hours at 70°C. The dispersed products were collected on a Whatman No.1 medium fast paper filter and washed with 300 mL 2-propanol. Then the products were dissolved in water and the solution was centrifuged and decanted to isolate the solids. The pH of the solution was adjusted to 7.0 using hydrochloric acid. Finally, the solution was precipitated with 2-propanol. The precipitation product was collected, freeze-dried and then ground into powder.

The contents of the cationic group were determined by NMR and polyelectrolyte titration (details of the experiments will be described below). Cationic samples with degrees of substitution (DS) of 0.09 were prepared, where the DS is now defined as the number of cationic groups per sugar ring. The structure of cationic guar is shown in Figure 2.2.

### **Preparation of Hydrophobically Modified Guar (HMG)**

Hydrophobically modified guar were prepared by reacting carboxymethyl guar with alkyl or aromatic amines in the presence of EDC, as shown in Scheme 2.3. In a typical experiment, 1 gram of carboxymethyl guar (DS 0.13) was dissolved in 0.1 mol/L MES buffer solution (pH adjusted to 4.7-4.8) in a 250 mL three-necked round flask under stirring. A ten fold excess of amine (amine group to carboxyl group) was added to the flask under stirring. After mixing for about 30 min, a ten fold excess of EDC was added to the flask under stirring. Reaction was allowed to proceed overnight at room temperature. After that, the products were loaded into a dialysis membrane and dialyzed for two weeks to remove the small molecules. Finally the products were freeze-dried.

The contents of the cationic group were determined by NMR and conductometric titration (details of experiments will be described below). Hydrophobically modified guar samples with a degree of substitution (DS) of 0.13 were prepared, where the DS is now defined as the number of hydrophobic groups per sugar ring. The structure of hydrophobically modified guar is shown in Figure 2.3.

## **Titration**

### **Potentiometric and Conductometric Titration**

Both potentiometric and conductometric titration were performed with a PC-Titrator (Man-Tech Associates) equipped with a Burivar-I/2 buret controlled by PC-Titrator software. The pH and conductivity were measured with a pH electrode (Man-Tech Associates) and a conductivity electrode connected with a 4010 conductivity meter. A 100 mL titration cell that was thermostated with an mgw Lauda RM6 pump controlled by an mgw Lauda RMS system was employed. Samples were usually dissolved in 5

mmol/L of KCl. The pH of samples was initially adjusted to about 3.0 using hydrochloric acid. Then, either 0.1 mol/L or 1 mol/L of NaOH was used as titrant with an injection rate of 60 mV/pH by the base into acid titration method.

### **Polyelectrolyte Titration**

Polyelectrolyte titrations were performed using a Mütek PCD T3 titrator fitted with a Mütek PCD 03 streaming current detector (SCD), composed of a reciprocating piston fitted in a fluoropolymer cylinder. A 10mL cationic guar sample with pH 7.4 and NaCl concentration 0.01mol/L was loaded into the cylinder and allowed to equilibrate for 30 min before starting the titration. The mixture was titrated with 1 mol/L of PVSK. The apparatus automatically added 0.001-0.01mL of PVSK when the drift rate was below 8mV in 10 seconds. All experiments were performed at room temperature.

### **Nuclear Magnetic Resonance (NMR)**

Modified guar samples were prepared by dissolving in D<sub>2</sub>O. Then <sup>1</sup>H NMR was performed using a Bruker 200MHz spectrometer. The chemical shifts of <sup>1</sup>H spectra are reported in ppm.

## **2.3 Results and Discussion**

### **Synthesis of Carboxymethyl Guar (CMG)**

As shown in Scheme 2.1, carboxymethyl guar was synthesized by reacting guar with chloroacetic acid. FT-IR spectra can qualitatively analyze the change from alcohol to carboxylic acid. From FT-IR spectra of both native guar and the product shown in Figure 2.4, the broad peak in the guar spectrum at about 3200-3600 cm<sup>-1</sup> represents O-H stretching absorption, while from the carboxymethyl guar spectrum, the O-H stretching absorption covers much broader region at about 2400-3600 cm<sup>-1</sup>, indicating the existence of carboxymethyl groups.

To quantitatively analyze the carboxymethyl group attached to guar molecules so as to determine the degree of substitution, conductometric titrations were performed. From a typical conductometric titration, as shown in Figure 2.5, we can calculate the volume of titrant (1mol/L NaOH) consumed. The volume between the two inflection points represents the volume of titrant used to titrate carboxymethyl groups and can be calculated using three linear equations each representing a linear curve as shown in Figure 2.5.

The calculation for the degree of substitution (DS) of carboxymethyl groups is shown in equation (1):

$$DS = \frac{162 \times C_{NaOH} \times V_{NaOH}}{(m - 58 \times C_{NaOH} \times V_{NaOH})} \quad (1)$$

Where  $DS$  is degree of substitution;  $C_{NaOH}$  is added NaOH concentration;  $V_{NaOH}$  is added NaOH volume;  $m$  is mass of added carboxymethyl guar, and 162 and 58 represent molecular weight of one sugar unit and carboxymethyl group respectively.

Carboxymethyl guar with  $DS$  0.39 and 0.13 were synthesized according to FT-IR and conductometric titration.

### Synthesis of Cationic Guar

As shown in Scheme 2.2, cationic guar was synthesized by reacting guar with glycidyltrimethylammonium chloride which has an epoxy at one end and quaternary ammonium at the other end.

The product was characterized by NMR; an example of cationic guar with  $DS$  0.09 is shown in Figure 2.6. Here, peak No. 4 at about 3.1 ppm represents protons in the three methyl groups attached to nitrogen in glycidyltrimethylammonium chloride. Protons attached to the carbon bearing hydroxyl group should have a peak at about 3.2 ppm. The protons in the methylene group attached to nitrogen should have a peak at about 3.3 ppm, while the protons in the methylene group attached to the guar molecule should have a peak at about 3.4 ppm. In the NMR spectrum, those peaks were masked by resonance due to the protons in the sugar unit with peaks ranging from 3.5 ppm to 4.4 ppm, representing every proton in the sugar unit except the proton attached to carbon No.1 in the sugar unit whose peak is at about 4.9 ppm.<sup>15</sup> The degree of substitution of cationic guar represents the number of cationic groups per sugar ring, and was determined by comparison of integration of those peaks representing protons in the three methyl groups attached to nitrogen in glycidyltrimethylammonium chloride and integration of those peaks representing protons in the guar sugar unit and other protons (except protons in the three methyl groups) in glycidyltrimethylammonium chloride. The degree of substitution of the cationic group in cationic guar was determined to be about 0.09, using NMR.

To confirm the degree of substitution results of NMR, the degree of substitution of cationic guar was also estimated by polyelectrolyte titration using 1mmol/L PVSK as titrant. The titration curve is shown in Figure 2.7. Molar concentration of the cationic group in cationic guar was calculated in equation (2):

$$C_{CaG} = \frac{C_{PVSK} \times V_{PVSK}}{V_{CaG}} \quad (2)$$

where  $C_{CaG}$  is molar concentration of the cationic group in cationic guar;  $V_{CaG}$  is the volume of cationic guar which is 10mL,  $C_{PVSK}$  and  $V_{PVSK}$  are respective molar

concentration of PVSK and volume of PVSK, namely 1mmol/L and 2.6mL. So  $C_{CaG}$  was calculated to be 0.26mmol/L. Degree of substitution of the cationic group in cationic guar was calculated in equation (3):

$$DS = \frac{C_{CaG}}{\frac{M_{CaG}}{(Mw_s + Mw_g \times DS)}} \quad (3)$$

where  $M_{CaG}$  is mass concentration of cationic guar which is 0.5g/L,  $Mw_s$  is the molecular weight of one sugar unit, which is 162 g/mol,  $Mw_g$  is the molecular weight of glycidyltrimethylammonium chloride, which is 151.5 g/mol. So the degree of substitution of the cationic group in cationic guar was calculated to be 0.09.

### Synthesis of Hydrophobically Modified Guar

Hydrophobically modified guar was synthesized by reacting carboxymethyl guar (CMG) with primary alkyl amines or aromatic amines such as benzyl amine in the presence of EDC. As shown in Scheme 2.3 and Scheme 2.4, EDC first reacts with the carboxymethyl group and creates an intermediate that can then react with primary amine to form an amide bond, releasing an isourea by-product simultaneously.

Products of synthesis were characterized by NMR. Figure 2.8 shows an NMR spectrum of hydrophobically modified guar derived from the reaction of CMG with hexylamine. In this spectrum, peak No.1 at about 0.8 ppm represents protons of the methyl group in an alkyl chain of hexylamine. Peak No. 2 at about 1.2 ppm represents protons of methylene groups in an alkyl chain of hexylamine. Peak No. 3 at about 2.8 ppm represents protons of methylene groups attached to amine group. Comparison of those peaks representing protons of alkyl chains with those peaks representing protons of a sugar unit give a degree of substitution of 0.12.

In addition to NMR, conductometric titration was conducted to determine whether all carboxylic groups in CMG react with primary amines to form amide bonds. Figure 2.9 shows conductometric titration results for hydrophobically modified guar derived from hexylamine. We can see that very little NaOH (0.1mol/L, the volume between the two inflection points close to zero) was consumed to neutralize the carboxylic group in CMG. We conclude that nearly all carboxylic groups were converted to amide.

The properties of modified guar were generalized in Table 2.1.

## 2.4 Conclusions

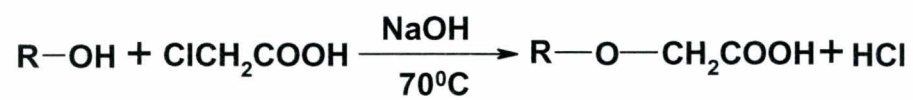
1. Carboxymethyl guar with degree of substitution (DS) of 0.39 and 0.13 was successfully synthesized by reacting guar with chloroacetic acid. The DS was characterized by conductometric titration.
2. Cationic guar with a DS of 0.09 was synthesized by reacting guar with glycidyltrimethyl ammonium chloride. The DS of cationic groups was characterized by NMR and polyelectrolyte titration.
3. Hydrophobically modified guars with DS of 0.13 were synthesized by reacting carboxymethyl guar with primary amines in the presence of EDC. The characterization of hydrophobically modified guar was conducted using NMR. Conductometric titration was employed to determine the residue of carboxy groups in hydrophobically modified guar. This showed that there was nearly no carboxy residue in hydrophobically modified guar.

## 2.5 Tables

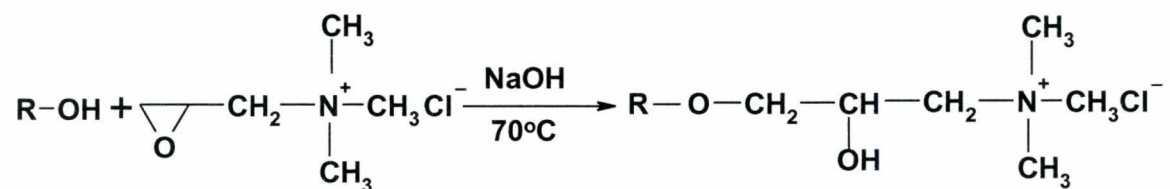
**Table 2.1 Properties of modified guar.**

Modified guar		Functional group	Degree of substitution (DS)	Starting material	Water solubility
Carboxymethyl guar (CMG)		$-\text{CH}_2\text{COOH}$	0.39	Native guar (MW 3MDa)	good
Cationic guar		$  \begin{array}{c}  \text{CH}_3 \\    \\  -\text{CH}_2-\text{CH}-\text{CH}_2-\text{N}^+-\text{CH}_3 \text{Cl}^- \\    \quad   \\  \text{OH} \quad \text{CH}_3  \end{array}  $	0.09	Native guar (MW 3MDa)	good
Hydrophobically modified guar (HMG)	HMG-6	$  \begin{array}{c}  \text{O} \quad \text{H} \\     \quad   \\  -\text{CH}_2-\text{C}-\text{N}-\text{CH}_2-\text{R}' \\  \text{R}'=(\text{CH}_2)_4\text{CH}_3  \end{array}  $	0.13	Native guar (MW 3MDa)	<0.1g/L
	HMG-benzyl	$  \begin{array}{c}  \text{O} \quad \text{H} \\     \quad   \\  -\text{CH}_2-\text{C}-\text{N}-\text{CH}_2-\text{R}' \\  \text{R}'=\text{C}_6\text{H}_5  \end{array}  $	0.13	Native guar (MW 3MDa)	<0.1g/L

## 2.6 Schemes



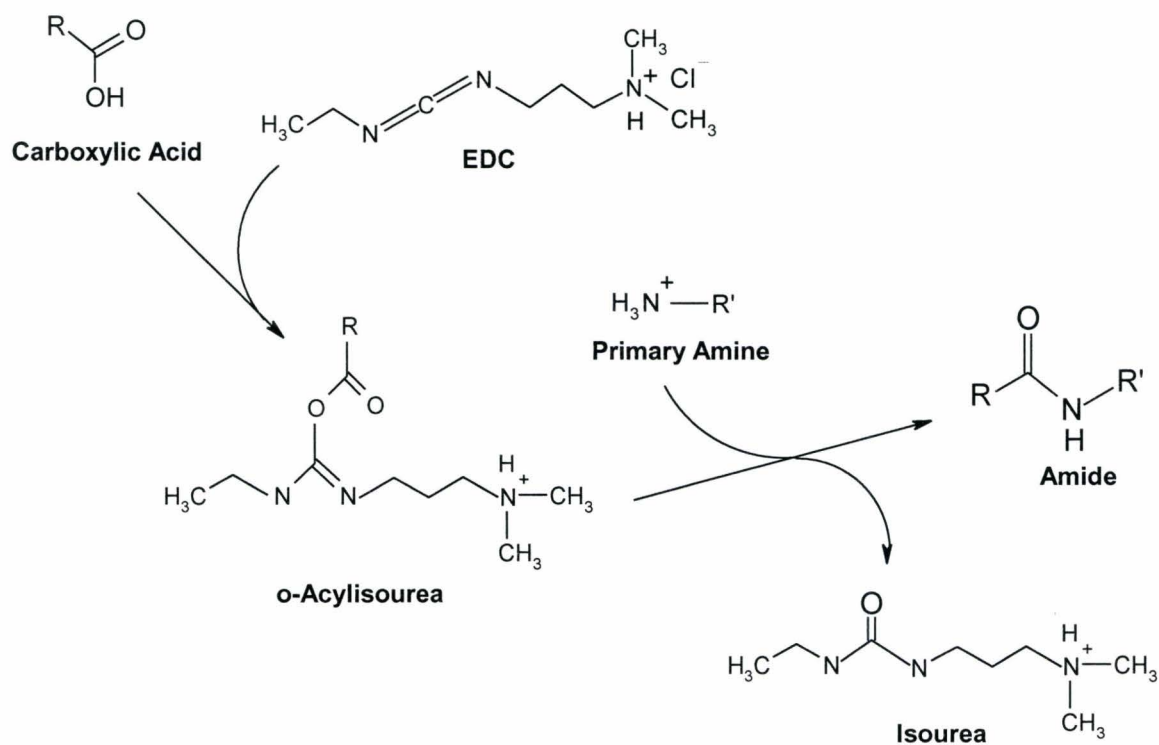
Scheme 2.1 Synthesis of carboxymethyl guar.



Scheme 2.2 Synthesis of cationic guar.



Scheme 2.3 Synthesis of hydrophobically modified guar.



**Scheme 2.4** Reaction of carboxylic acid with primary amines in the presence of EDC (Adapted from Hermanson, G. T., 2008, also see reference 14).

## 2.7 Figures

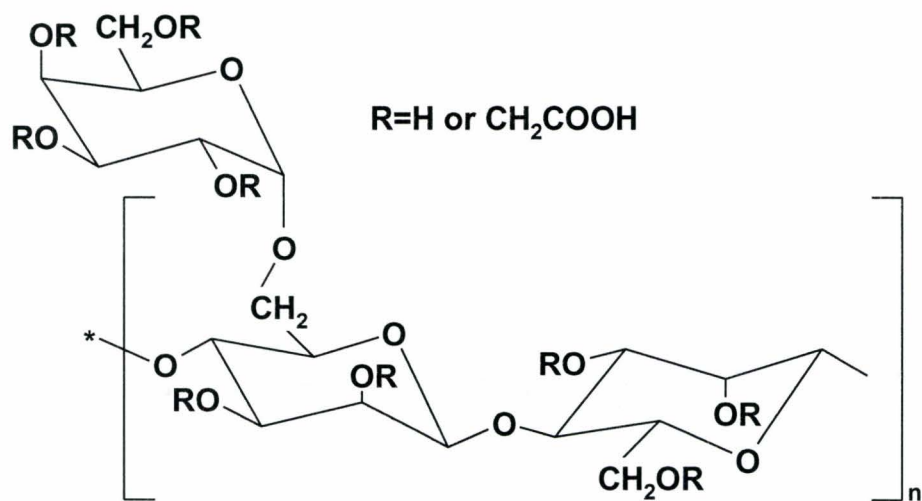


Figure 2.1 The structure of carboxymethyl guar (CMG).

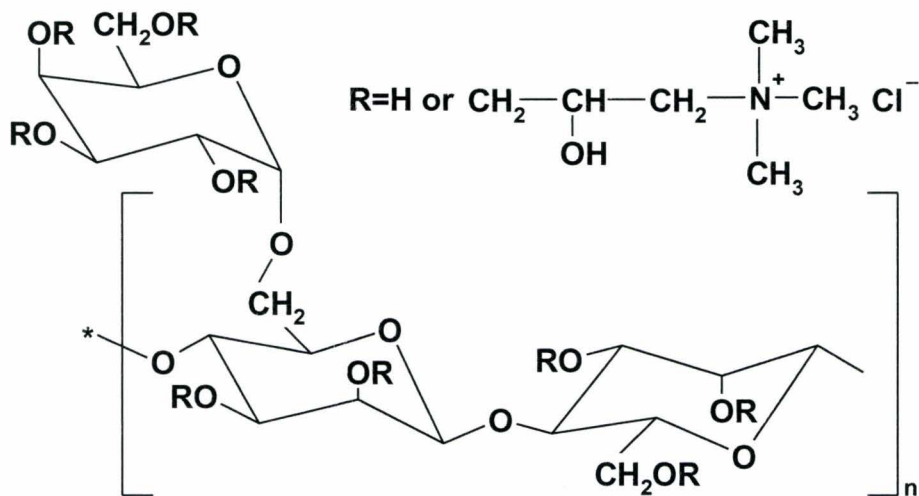


Figure 2.2 The structure of cationic guar.

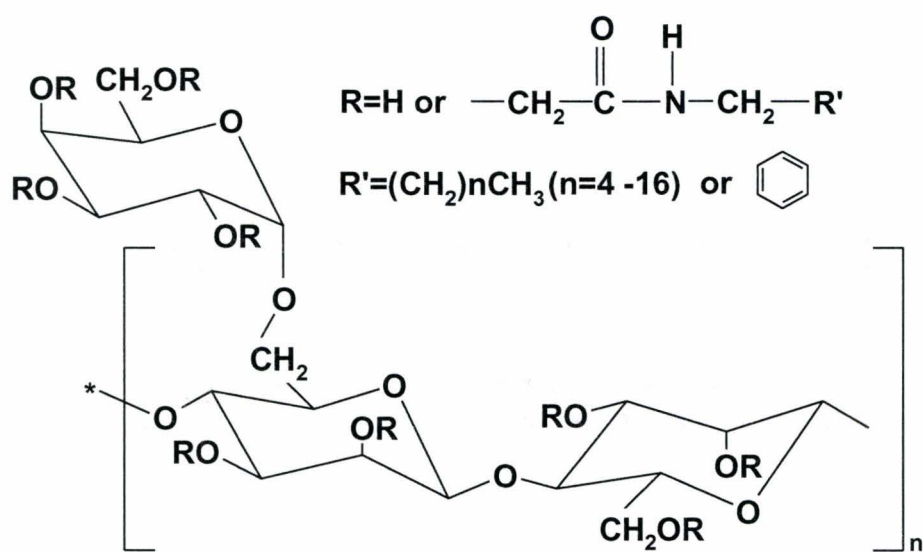


Figure 2.3 The structure of hydrophobically modified guar (HMG).

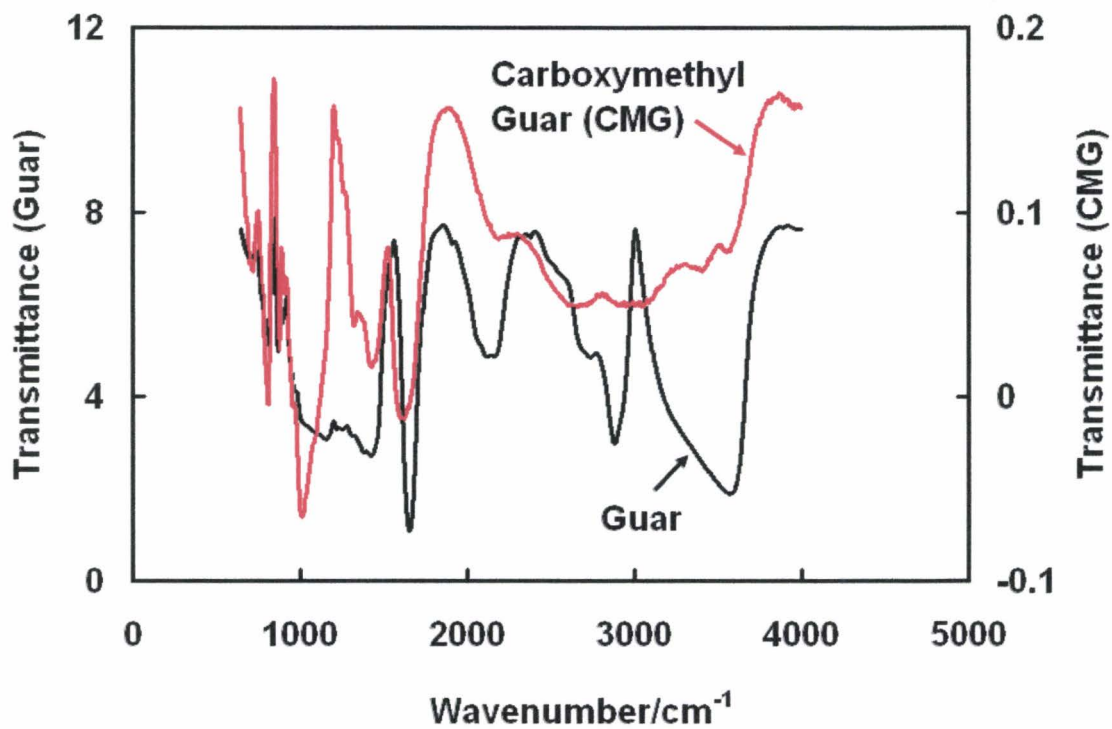


Figure 2.4 Infra-red spectra of guar and carboxymethyl guar (CMG).

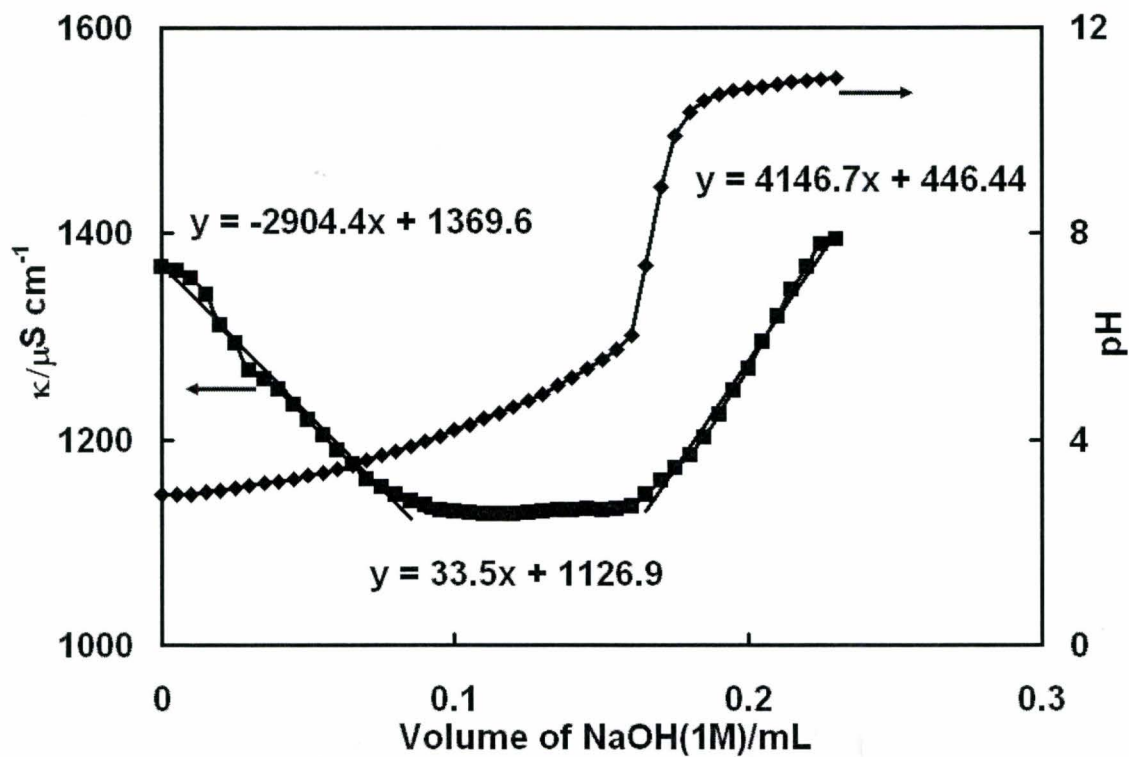


Figure 2.5 Conductometric and potentiometric titration to determine degree of substitution of carboxymethyl guar (DS 0.39).

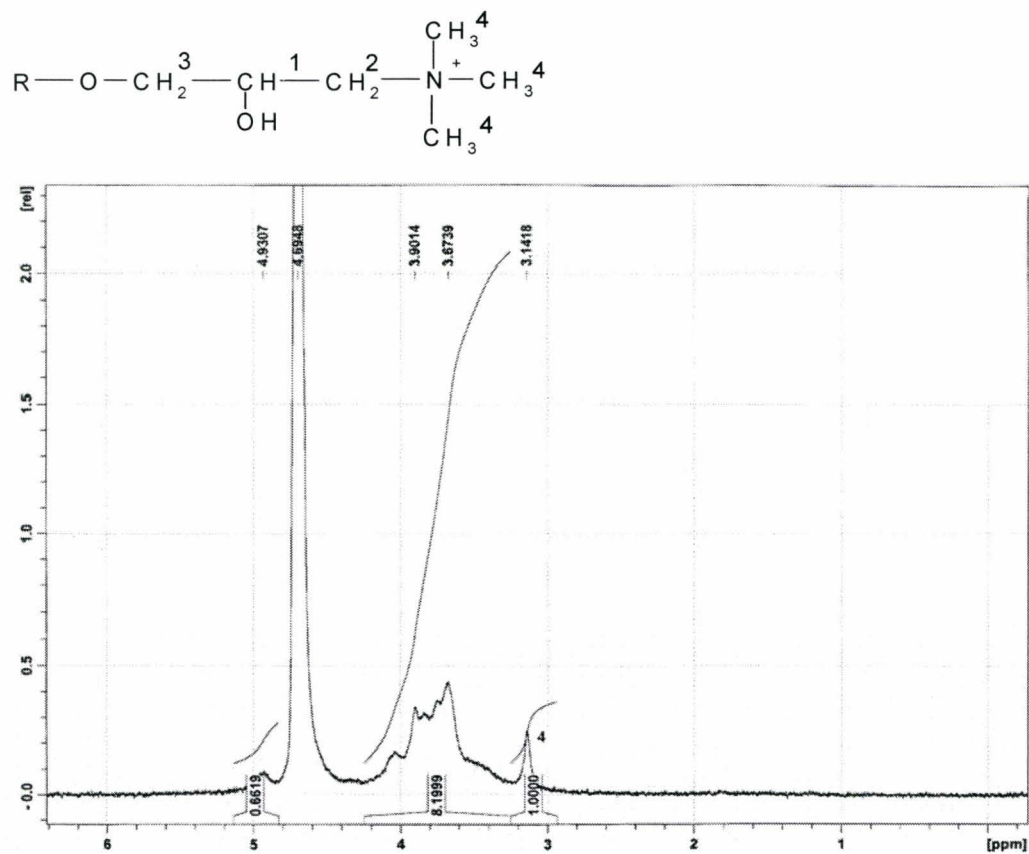


Figure 2.6 Nuclear magnetic resonance (NMR) characterization of degree of substitution of cationic guar (DS 0.09).

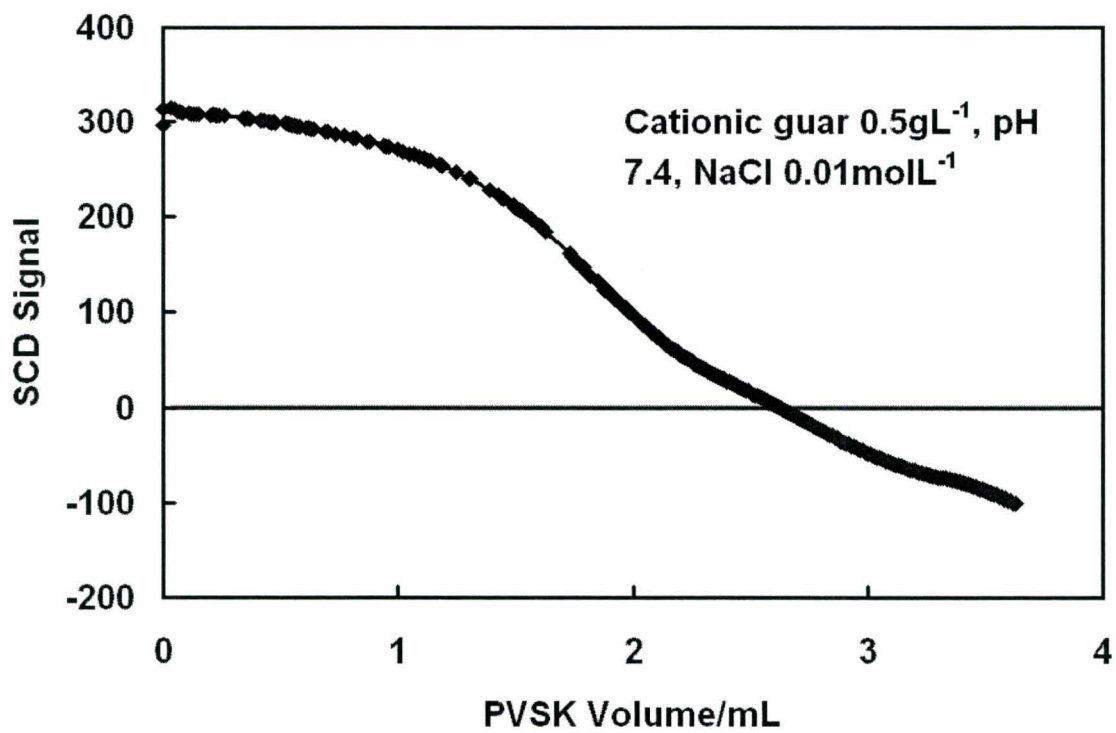
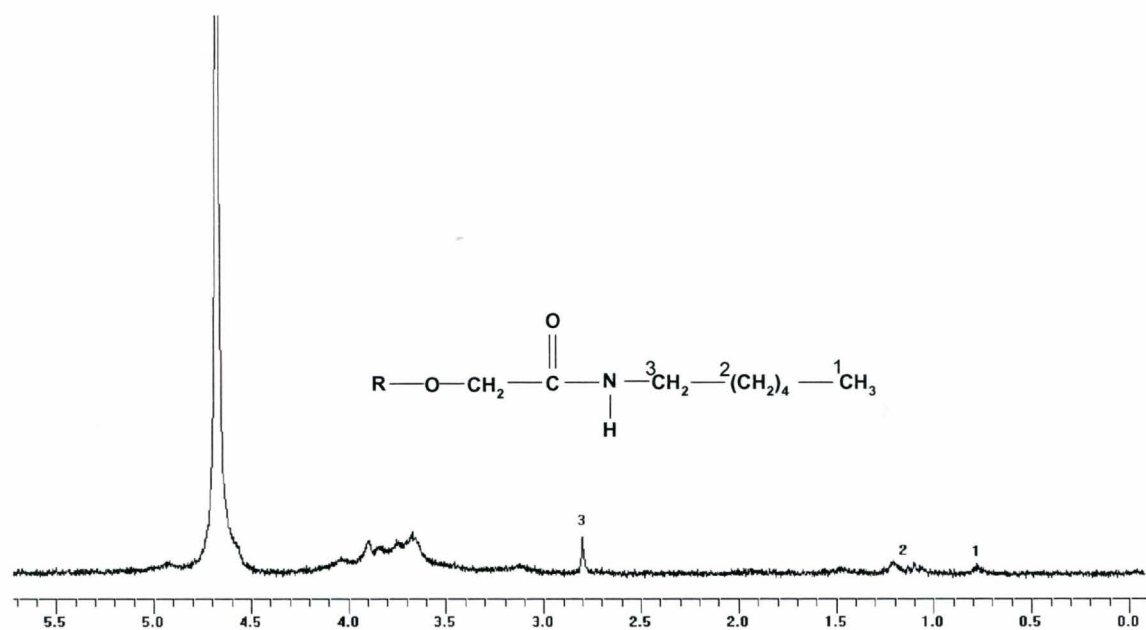


Figure 2.7 Polyelectrolyte titration characterization of degree of substitution of cationic guar (DS 0.09).



**Figure 2.8** Nuclear magnetic resonance (NMR) characterization of degree of substitution of hydrophobically modified guar (N-hexylamide substitution) (DS 0.12) synthesized from carboxymethyl guar (DS 0.13).

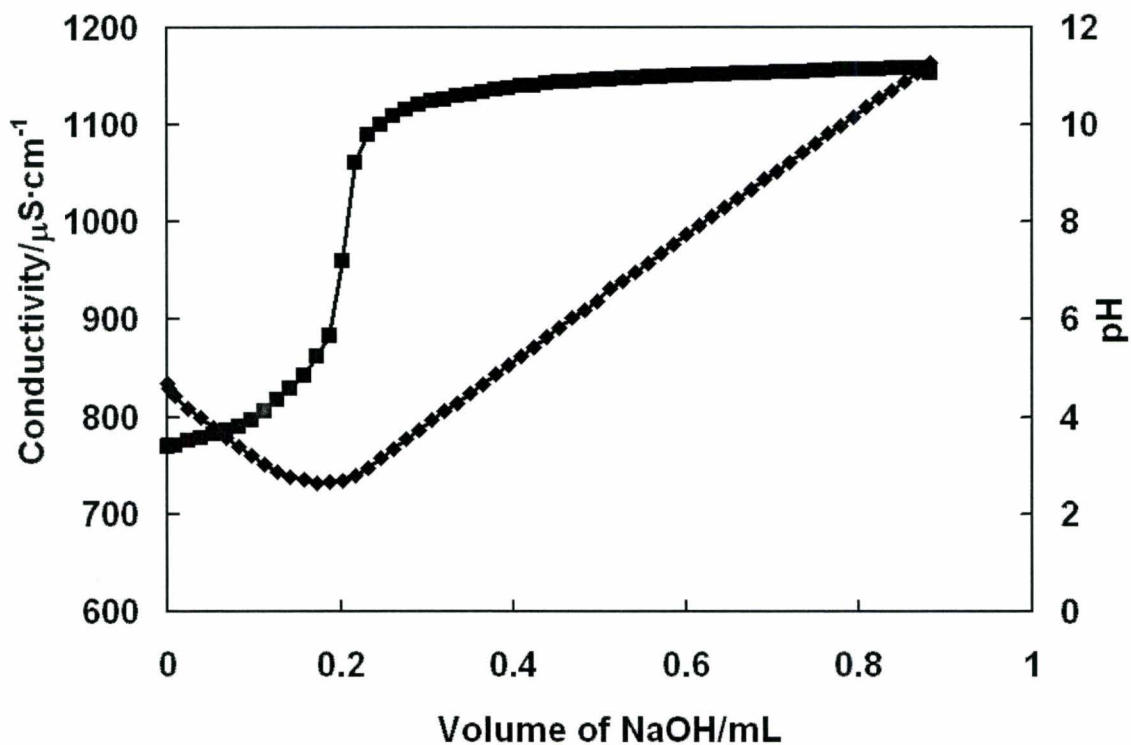


Figure 2.9 Characterization of carboxyl residue on hydrophobically modified guar (N-hexylamide substitution) (DS 0.13) by conductometric and potentiometric titration.

## 2.8 References

1. Picout, D. R.; Ross-Murphy, S. B.; Errington, N.; Harding, S. E., Pressure cell assisted solution characterization of polysaccharides. 1. Guar gum. *Biomacromolecules* 2001, 2, (4), 1301-1309.
2. Cheng, Y.; Brown, K. M.; Prud'homme, R. K., Characterization and intermolecular interactions of hydroxypropyl guar solutions. *Biomacromolecules* 2002, 3, (3), 456-461.
3. Christensen, M. T.; Cohen, S.; Rinehart, J.; Akers, F.; Pemberton, B.; Bloomenstein, M.; Leshner, M.; Kaplan, D.; Meadows, D.; Meuse, P.; Hearn, C.; Stein, J. M., Clinical evaluation of an HP-guar gellable lubricant eye drop for the relief of dryness of the eye. *Current Eye Research* 2004, 28, (1), 55-62.
4. Ubels, J. L.; Aupperlee, M. D.; Meadows, D. L., Artificial tear solutions and protection of the corneal epithelium from desiccation. *Journal of Toxicology-Cutaneous and Ocular Toxicology* 2002, 21, (4), 273-281.
5. Ubels, J. L.; Clousing, D. P.; Van Haitsma, T. A.; Hong, B. S.; Stauffer, P.; Asgharian, B.; Meadows, D., Pre-clinical investigation of the efficacy of an artificial tear solution containing hydroxypropyl-guar as a gelling agent. *Current Eye Research* 2004, 28, (6), 437-444.
6. Young, N. W. G.; Williams, P. A.; Meadows, J.; Allen, E., A promising hydrophobically-modified guar for completion applications. *Proceedings - SPE/DOE Symposium on Improved Oil Recovery, 11th, Tulsa, Okla., Apr. 19-22, 1998* 1998, 2, 463-470.
7. Pezron, E.; Ricard, A.; Lafuma, F.; Audebert, R., Reversible gel formation induced by ion complexation .1. Borax galactomannan interactions. *Macromolecules* 1988, 21, (4), 1121-1125.
8. Ramos, L. A.; Frollini, E.; Heinze, T., Carboxymethylation of cellulose in the new solvent dimethyl sulfoxide/tetrabutylammonium fluoride. *Carbohydrate Polymers* 2005, 60, (2), 259-267.
9. Bahamdan, A.; Daly, W. H., Poly(oxyalkylene) grafts to guar gum with applications in hydraulic fracturing fluids. *Polymers for Advanced Technologies* 2006, 17, (9-10), 679-681.
10. Molteni, G.; Nicora, C.; Cesaro, A.; Pricl, S., Modified galactomannans and process for their preparation. In Google Patents: 1990.
11. Wang, Y.; Chen, X. N.; Pelton, R., Interactions of hydrophobically modified polyvinylamine with pluronic triblock copolymer micelles. *Langmuir* 2006, 22, (11), 4952-4958.
12. DeGuia, A. A.; Stackman, R. W.; Conciatori, A. B., Process for production of polygalactomannan ethers. In Google Patents: 1979.
13. Risica, D.; Dentini, M.; Crescenzi, V., Guar gum methyl ethers. Part I. Synthesis and macromolecular characterization. *Polymer* 2005, 46, (26), 12247-12255.
14. Hermanson, G. T., *Bioconjugate techniques*. Academic Press: 2008.

15. Crescenzi, V.; Dentini, M.; Risica, D.; Spadoni, S.; Skjak-Braek, G.; Capitani, D.; Mannina, L.; Viel, S., C(6)-oxidation followed by c(5)-epimerization of guar gum studied by high field nmr. *Biomacromolecules* 2004, 5, (2), 537-546.

## **Chapter 3 Characterization and modeling of HPG-borate, a labile polyelectrolyte, by polyelectrolyte titration and interaction of HPG-borate with oppositely charged polyelectrolyte**

### **Abstract**

Hydroxypropyl guar (HPG), a nonionic water soluble polymer, becomes an anionic polyelectrolyte in the presence of borate or boronate ions which bind to HPG. However, the charge groups on the HPG-borate are labile which complicates the interpretation of polyelectrolyte titration behavior. Specifically, polyelectrolyte complex formation between HPG-borate and cationic poly(diallyldimethyl ammonium chloride), PDADMAC, stimulates further borate binding to HPG. We propose that labile polyelectrolytes such as HPG-borate are new class of polyelectrolytes that fall outside conventional “strong” or “weak” polyelectrolyte behavior.

### 3.1 Introduction

Polyelectrolyte titrations, originally called the colloid titration<sup>1</sup>, are widely used to measure the concentration of charged groups bound to polymer chains and solid surfaces in water. This technique is based on the quantitative, irreversible complex formation between oppositely charged polyelectrolytes<sup>2</sup>. Originally, polyelectrolyte titration endpoints were detected with an indicator dye. However, the streaming current detector (SCD) is widely used for endpoint detection. The SCD consists of a loosely fitting fluorocarbon coated piston that reciprocates in a cylinder with a closed end (see Figure 3.1). Electrodes measure the streaming current induced by the flow of liquid over the cylinder walls. It is assumed that polyelectrolyte complex species in solution are identical to those adsorbed on the SCD cylinder wall so that the SCD signal gives a measure of the electrostatic potential of the polyelectrolyte complex species in solution. For example, the curve labeled PVSK, potassium poly(vinyl sulfate), in Figure 3.2 shows the evolution of SCD signal with addition of PDADMAC, poly(diallyldimethyl ammonium chloride), to a PVSK solution. This is the behavior of classic, well-behaved polyelectrolytes; there are similar examples in the literature<sup>3-6</sup>. Because of the dramatic change in signal near the equivalence point, most practitioners simply assign an endpoint corresponding to a SCD signal of 0 mV and do not report the entire titration curve.

In this chapter we present and interpret the colloid titration curves of deviant systems we call “labile polyelectrolytes”; the curve labeled HPG-borate in Figure 3.2 is an example. The HPG-borate curve in Figure 3.2 refers to titration of a mixture of hydroxypropyl guar (HPG) and sodium borate. HPG is a water-soluble, nonionic polymer that binds borate ions giving the structure of HPG shown in Figure 3.3. The hydroxypropyl groups are added to guar to inhibit intermolecular interactions and thus improve water solubility<sup>7</sup>. The distribution of hydroxypropyl groups is approximately random<sup>8</sup>. A single borate ion can condense onto two HPG segments to give a cross-link, increasing viscosity and giving gels<sup>9</sup>. Audebert emphasized that, in addition to cross-linking, borate addition converts nonionic guar (or HPG) into an anionic polyelectrolyte<sup>10</sup>. The goal of this chapter is to explain the shape of the HPG-borate curve, including identifying the location and meaning of the endpoint. From an analytical chemistry perspective, the unusual behavior of HPG-borate titration is important because we will show that the endpoint does not correspond to zero SCD signal and that the endpoint is not a measure of the initial charge content of HPG-borate. From a polyelectrolyte physical chemistry perspective, this work is also significant because it suggests a new class of polyelectrolytes - “labile polyelectrolytes”, which display more complicated behaviors. The properties of HPG-borate are now described in context with classic “strong” and “weak” polyelectrolytes.

It is common practice to divide polyelectrolytes into “strong” and “weak”. Strong polyelectrolytes bear charge groups such as sulfate, sulfonate and quaternary ammonium whose degrees of ionization are not sensitive to pH and ionic strength. By contrast, with

weak polyelectrolytes such as polyvinylamine<sup>11</sup> and poly(acrylic acid), the degree of ionization is very sensitive to pH and ionic strength. It is generally accepted that borate  $B(OH)_4^-$ , and not  $B(OH)_3$ , binds to HPG because alkaline pH is required to observe viscosity increases and other measures of borate binding. This pH sensitivity suggests HPG-borate is another “weak polyelectrolyte”, however, such a conclusion is misleading. Borate-guar binding constants in the literature are 11 L/mol<sup>10</sup> and 100 L/mol<sup>12</sup>. By contrast, the free energy associated with the protonation of poly(acrylic acid) is about 5 times greater than the borate binding energy<sup>13</sup>.

In this chapter we explain the unusual polyelectrolyte titration behavior of HPG-borate, and related systems, as a manifestation of the low borate binding constant to HPG. Future work will show that this labile polyelectrolyte characteristic also impacts interactions with cationic surfactants.

## 3.2 Experimental

Hydroxypropyl guar (HPG) with 0.36 hydroxypropyl groups per sugar ring and molecular weight of  $1.0 \times 10^6$  Da was a gift from Alcon Laboratories, Fort Worth Texas. Poly(diallyldimethylammonium chloride), (PDADMAC) solutions (1 meq/L) with molecular weight of 10,700 Da and potassium polyvinyl sulfate (PVSK) (1 meq/L) with molecular weight of 19,100 Da were purchased from BTG Americas Inc. Poly(acrylic acid) with molecular weight of  $1.0 \times 10^6$  Da was purchased from Polysciences Inc. Methylboronic acid was purchased from Sigma-Aldrich. Sodium borate (borax), sodium hydroxide and hydrochloric acid were purchased from Anachemia. Sodium chloride was purchased from Caledon Laboratories Inc. All experiments were performed with MilliQ water from a Millipore system.

Polyelectrolyte titrations were performed using a Mutek PCD T3 titrator fitted with Mutek PCD 03 streaming current detector (SCD). The heart of the detector is a reciprocating piston fitted in a fluoropolymer cylinder (see Figure 3.1). In a typical experiment, 42 mL 0.01% HPG and 2.1 mL of 0.1 M borax solutions were mixed and the pH was adjusted with sodium hydroxide or hydrochloric acid solution. Ionic strengths of the solutions were adjusted with sodium chloride. A 10 mL sample was loaded into the cell, and was allowed to equilibrate for 30 min before starting the titration. The mixture was titrated with 1 meq/L PDADMAC. The apparatus automatically added 0.02-0.2 mL increments of PDADMAC when the drift rate was below 8 mV in 10 seconds, and SCD signal was recorded. All experiments were performed at room temperature.

The pH change during addition of PDADMAC to HPG-borate solutions was measured with a Thermo pH electrode connected to a Beckman  $\Phi 390$  pH/Temp/mV/ISE Meter. In a typical experiment, 42 mL of 0.01% HPG and 0.01-0.05 mL 0.1M sodium borate were added to a 100 mL beaker. PDADMAC (1 meq/L) was manually titrated to HPG and borax solutions under stirring and pH was recorded after each addition.

### 3.3 Modeling Polyelectrolyte Titrations

The goal of this section is to present a model that simulates the range of titration curves shown in Figure 3.2. Because SCD detectors are commercial devices, we do not know the detailed nature of the SCD signal. Following Walker's approach we assume that the SCD signal is proportional to the zeta potential ( $\zeta$ ) of the SCD wall<sup>14</sup>. Furthermore, we assume that the proportionality factor  $\alpha$  is a constant for a titration.

$$\text{SCD signal} = \alpha\zeta \quad (1)$$

Initially in a titration, the SCD cell contains a dilute solution of anionic polyelectrolyte that adsorbs onto the SCD fluorocarbon wall, influencing the zeta potential,  $\zeta$ , and the net surface charge density,  $\sigma_d$ . For the case of strong polyelectrolyte pairs, such as PVSK titrated with PDADMAC, we assumed that the net charge density changed linearly with the volume of added PDADMAC,  $V_T$  - see equation (2), where  $\beta$  is a constant:

$$\sigma_d = \sigma_{dl} + \beta V_T \quad (2)$$

Our previous publication focused only on the strong polyelectrolyte titration case and we showed that classical diffuse double layer theory could be used to simulate the evolution of the SCD signal during a colloid titration<sup>2</sup>. According to standard diffuse double layer theory, the corresponding net charge density,  $\sigma_d$ , on SCD cell wall is given by equation (3), where  $N_A$  is Avogadro's number,  $k_b$  is the Boltzmann constant,  $T$  is temperature,  $\varepsilon$  is the combined dielectric constant and  $c$  is the sodium chloride molarity. Equations (2) and (3) can simulate the shapes of polyelectrolyte titrations with strong polyelectrolytes, including the effects of sodium chloride addition<sup>2</sup>.

$$\sigma_d = \frac{\varepsilon k_b T \kappa}{e_o} \sinh\left(\frac{e_o \zeta}{2k_b T}\right) \quad \text{where } \kappa = \sqrt{\frac{e_o N_A}{\varepsilon k_b T}} 2c \quad (3)$$

A more complex model is required to explain the titration curves when PDADMAC is added to HPG-borate mixtures. Borate binding to HPG is expressed as the following equilibrium where  $[B_c^-]$  is the concentration of free borate ions near the HPG,  $[P]$  is the concentration of unoccupied borate binding sites on HPG, and  $[BP^-]$  is the concentration of bound borate ions. For dilute mixtures of HPG and borate in the absence of other chemicals,  $[B_c^-]$  approximately equals average borate concentration in solution. The binding of borate to HPG has been described by equation (4) and the binding constants reported in the literature are 11 L/mol<sup>10</sup> and 100 L/mol<sup>12</sup>.

$$K_1 = \frac{[BP^-]}{[B_c^-][P]} \quad (4)$$

The most important assumption in our model accounts for the depletion of free borate ions near a negatively charged interface and the corresponding enrichment of borate ions near a positive surface. This was accomplished through equation (5) which shows that when the local electrical potential of the HPG chain,  $\zeta$ , is negative, the effective concentration of borate ions  $[B_c^-]$  will be less than the average concentration in solution,  $[B^-]$ . The term  $\gamma$  is an adjustable parameter which was normally set as 3 – the sensitivity of model results to  $\gamma$  will be presented. We acknowledge similarities between equation (5) and the work of Leibler et al. who modeled the electrostatic retardation of borate binding by existing charges on the guar chain<sup>15</sup>.

$$[B_c^-] = [B^-] \exp\left(\frac{e_o \zeta \gamma}{k_b T}\right) \quad (5)$$

There are three contributions to net charge density on the SCD wall:  $\sigma_o$  the charge on clean cell wall;  $\sigma_{HPG}$  the contribution of the borate groups bound to HPG; and,  $\sigma_{DAD}$  the charge associated with added cationic titrant (see equation (6)). For a strong polyelectrolyte, the contributions of clean cell charge density and the adsorbed anionic polymer are constant; thus  $\sigma_{dl}$  in equation (2) was treated as a constant. By contrast, in HPG-borate titrations,  $\sigma_{HPG}$  may increase during the titration due to increased borate binding.

$$\sigma_d = \sigma_o + \sigma_{HPG} + \sigma_{DAD} \quad (6)$$

Equation (6) illustrates the three contributions to the net surface charge density of the surfaces of the SCD cell, The SCD reading for a clean cell is negative so  $\sigma_o$ , the initial cell charge density, was assumed to be constant and negative.

The contribution of the adsorbed HPG to charge density,  $\sigma_{HPG}$ , is given by equation (7) where  $\Gamma_{HPG}$  (mg/m<sup>2</sup>) is the coverage of adsorbed HPG,  $EW_{HPG}$  is the equivalent weight of HPG fully saturated with bound borate,  $[P_T]$  is the total concentration of borate binding sites in the cell and F is the Faraday constant. We assume that  $\Gamma_{HPG}$  is constant, meaning that HPG does not desorb or adsorb during the titration. The term  $[BP^-]/[P_T]$  is the fraction of occupied borate binding sites on HPG- thus we assume that the extent of borate binding in solution is the same of the HPG adsorbed on the cell wall. This is a serious approximation since  $\zeta$  (see equation (5)) near a borate binding site on HPG in solution will differ from  $\zeta$  near the charged SCD cell surface.

$$\sigma_{HPG} = \frac{-\Gamma_{HPG} [BP^-] F}{EW_{HPG} [P_T]} \quad (7)$$

In the course of a titration, the cationic titrant (PDADMAC) binds to the HPG adsorbed on the SCD cell wall. It is unlikely that the amount of adsorbed HPG is constant during the titration. In the extreme as HPG-borate/PDADMAC approach neutrality, deposition of large complexes may occur. However, we are modeling the streaming potential which is sensitive to the composition at the shear plane. Thus, we are really assuming that HPG concentration at the shear plane is constant which is not too restrictive.

We assumed that all of the added PDADMAC is associated with HPG-borate so that the coverage of adsorbed PDADMAC,  $\Gamma_{DAD}$ , is given by equation (8) and the corresponding contribution to cell surface charge density is give by equation (9), where  $EW_{DAD}$  is the equivalent weight of PDADMAC (161 Da), and  $C_{DAD}/C_{HPG}$  is the ratio of the total mass concentrations of PDADMAC to HPG in the cell. Note that during a titration,  $C_{DAD}$  increases from an initial value of 0 whereas  $C_{HPG}$  is constant.

$$\Gamma_{DAD} = \frac{C_{DAD}}{C_{HPG}} \Gamma_{HPG} \quad (8)$$

$$\sigma_{DAD} = \frac{\Gamma_{DAD} F}{EW_{DAD}} \quad (9)$$

The boric acid equilibrium is required to account for the influence of pH. Boric acid is a Lewis acid, forming the borate ion by reaction with hydroxyl. The borate formation constant (see equation (10) where  $[B_T]$  is the total boron molarity),  $K_o = 6.3 \times 10^4$  L/mol which corresponds to a pKa of 9.2.

$$K_o = \frac{[B^-]}{([B_T] - [B^-])[OH^-]} \quad (10)$$

We employed borax ( $Na_2B_4O_7 \cdot 10H_2O$ ) that adds two sodium ions for every four boron atoms. Thus, the following charge balance holds.

$$\frac{[B_T]}{2} + [H^+] = [OH^-] + [B^-] + [BP^-] \quad (11)$$

Equations (3)-(11) were solved numerically to give  $\zeta$  as a function of the amount of added PDADMAC ( $C_{DAD}$ ) using MathCAD 14. An example calculation is provided in the appendix A. Most of the parameters have known values. The unknown parameters were the amount of adsorbed HPG,  $\Gamma_{HPG}$ , the electrostatic multiplier,  $\gamma$ , and  $\alpha$ , the proportionality constant relating SCD signal to zeta potential.

## 3.4 Results

### 3.4.1 Polyelectrolyte Type

Figure 3.2 shows polyelectrolyte titration curves for three types of anionic polyelectrolytes titrated with PDADMAC. The x-axis shows the volumes of PDADMAC added divided by the volume corresponding to 0 SCD signal. Potassium poly(vinyl sulfate), PVSK, is a strong polyelectrolyte which gives classic behavior. The SCD signal maintained a constant negative value to very near the endpoint.

The curve labeled PAA denotes the titration of poly(acrylic acid) at neutral pH where the degree of ionization is  $\sim 0.65$ <sup>16</sup>. The shape of PAA titration is similar to PVSK and it has been long known that the polyelectrolyte titration gives good estimates of the degree of ionization of weak polyelectrolytes<sup>16,17</sup>. For example, Phipps showed that potentiometric titration and polyelectrolyte titration gave the degree of ionization of polyethyleneimine as a function of pH<sup>6</sup>. Thus, PAA and other standard weak polyelectrolytes do not undergo a significant change in the degree of ionization during the polyelectrolyte titration.

Finally, the non-ideal HPG-borate titration curve in Figure 3.2 is the focus of this chapter. The structure of HPG-borate is shown in Figure 3.3. This curve, and other examples to follow, shows unusual features. Initially there is a rapid decrease in SCD signal followed by long near constant section. Our explanation of the shape is that initially the HPG chain was not saturated with bound borate; however, the presence of cationic PDADMAC during the titration facilitates further borate binding. This hypothesis is built into our model described in the previous section.

Figure 3.4 compares the HPG-borate experimental curve with two simulated curves. The experimental SCD signals were divided by 4 to give values more typical of zeta potential measurements. In other words,  $\alpha$  in equation (1) was assumed to be equal to 4. The x-axis for the experimental curve is the same as in Figure 3.2, whereas for simulated curves the x-axis is the equivalents of added PDADMAC divided by the total number of equivalents of borate binding sites on HPG.

The two simulated titrations differ in the borate binding constant,  $K_I$  in equation (4). The  $K_I = 100$  L/mol curve shows the same features as the HPG-borate data. This is Jasinski's value for the binding constant<sup>12</sup>. By contrast the simulated curve for the high binding constant closely resembles the PAA and PVSK curves in Figure 3.2. In this case the HPG is initially saturated with bound borate. The caption in Figure 3.4 gives the other model parameters. Of these, only  $\gamma$  and  $\Gamma_{HPG}$  were arbitrary – the sensitivity of the simulated curves to these arbitrary parameters will be shown at the end of this section.

Finally, we defined the endpoints of the simulated curves as the inflection points where the second derivative equals zero- see the Discussion section for justification. Thus the endpoints for the simulated curves in Figure 3.4 correspond to the total amount of added titrant, being about 1.2 times the concentration of borate binding sites. The extra 20% reflects the initial charge on the cell wall ( $\sigma_o$  in the model). We will show in the following sections that the computed endpoints shift to the expected value of 1 when the concentration of adsorbed HPG ( $\Gamma_{HPG}$ ) is increased.

### 3.4.2 Borate Concentration and pH

Borate serves two roles – when bound to HPG, borate is a source of charge and borate is a pH buffer. Figure 3.5 shows a series of titrations where the initial concentration of borax was varied. Note that we give the total concentration of boron species, which include boric acid, free borate ion and borate bound to HPG. For high boron concentrations, the titrations were not sensitive to boron concentration whereas with lower borate concentrations influence the titrations. With very low borate in the cell, there is not enough to saturate the HPG chain and to keep the pH constant.

Figure 3.6 shows simulated titrations with varying borate concentrations. In this figure we express the total boron concentration,  $[B_T]$ , as a ratio to the total concentration of borate binding sites on HPG,  $[P_T]$ . Comparing the  $B_T=10 P_T$  and  $B_T=100 P_T$  curves showed that the endpoint was constant, whereas the higher borate concentration gave a small vertical shift toward more negative potentials. By contrast, when there was insufficient borate to saturate the HPG, the curves changed shape. The trends in Figure 3.6 show the main features of the experimental curves in Figure 3.5.

One might predict that at high total borate concentration, that the initial bound borate concentration should be high and that the shape of the polyelectrolyte titration should approach those of PAA or PVSK. However, the negative surface potential near the clean cell lowers the amount of bound borate. The model accounts for this effect with equation (5). Consider, for example, the  $B_T=100 P_T$  curve in Figure 3.6. The fraction of occupied borate binding sites on HPG is  $6 \times 10^{-7} \sim 0$  before any PDADMAC is added. However, if we turn off the electrostatic influence on borate binding by setting  $\gamma=0$  in equation (5), the occupied fraction of borate binding sites is 0.43.

Borate binding lowers the pH because the bound ion can no longer participate as a buffer. Indeed, pH change measurement is one of the methods used estimate borate binding constants<sup>18</sup>. It was not possible to measure pH during a SCD titration; however, in independent experiments we monitored pH as a function of the quantity of PDADMAC added to HPG-borate mixtures. The results are summarized in Figure 3.7. The initial solutions were prepared with borax so that the initial pH approximately equaled the pKa of 9.2. The boron concentrations are expressed as a fraction of the total concentration of borate binding sites on HPG. There was no pH change when very high boron concentrations were used (data not shown). The highest borate concentration in Figure 3.7

was 240% higher than the concentration of binding sites, so there was little pH change during the titration. By contrast, when the total boron concentrations were less than the concentration of binding sites, there was a substantial pH drop during the titration because PDADMAC addition induced most of the borate to bind to the HPG.

Our model was also capable of simulating the pH lowering during a titration. Figure 3.8 shows simulations at four initial boron concentrations. The model predicts the general features of the data in Figure 3.7. However, the detailed shapes of the pH evolution curves were sensitive to the assumed  $\gamma$  value – this will be shown in a later section.

### 3.4.3 Borate Type

One of the complications of the HPG borate system is that a borate ion can bind twice to HPG giving a cross-link. We were concerned that the unusual SCD titration curves were some artifact of cross-linking. Several titrations were conducted in which boric acid was replaced by methylboronic acid. The alkyl boronate can only bind once, thus adding a charge to HPG without cross-linking. The two types of boric acids are compared in Figure 3.9. The most important conclusion is that the shapes of both curves are the same, showing that cross-link formation is not an important issue. A secondary point is that slightly more PDADMAC was required for the methylboronic solution. This suggests that with HPG-borate there were some cross-links because the HPG bound less borate than methylborate.

### 3.4.4 Key Model Parameters

The major assumption in our model is that positive potential induced by PDADMAC increases the local borate concentration near the HPG which gives more binding. This assumption is implemented through equation (5) that contains the adjustable parameter  $\gamma$ . Figure 3.10 shows the influence of  $\gamma$  on the simulated titration curves. For  $\gamma$  values of 3 and greater the curves are not sensitive to  $\gamma$  and look similar to experimental curves. By contrast, the simulated curves for  $\gamma = 1$  and  $\gamma = 0.5$  were elongated showing little structure.

We also assumed that the amount of HPG adsorbed on the SCD detector wall,  $\Gamma_{HPG}$ , was constant throughout the titration. Figure 3.11 shows the influence of amount of adsorbed HPG on the simulated titrations. For very high  $\Gamma_{HPG}$  values (10 and 200 mg/m<sup>2</sup>), the titration curves were independent of  $\Gamma_{HPG}$  and the endpoints corresponded to dimensionless PDADMAC concentration equal to 1. This means the apparent endpoint was a measure of the total concentration of binding sites on HPG. However, the titration curves for the lower  $\Gamma_{HPG}$  values of 1 and 2 mg/m<sup>2</sup> were shifted to right along the dimensionless PDADMAC axis. The shift in the endpoint to higher dimensionless PDADMAC concentrations reflects the larger contribution of initial charge density (clean

cell before HPG is added,  $\sigma_o$  in equation (6)) to the consumption of cationic polymer. We propose that this sensitivity to clean cell charge density is exaggerated in the model because as HPG and PDADMAC adsorb, the shear plane will move out from the SCD wall, lowering the influence of  $\sigma_o$ .

### 3.5 Discussion

Originally we performed polyelectrolyte titrations on HPG-borate mixtures to measure the quantity of borate ions attached to HPG. Although the titrations were reproducible, their shapes were unusual and the endpoints corresponding to zero SCD signal seemed incorrect. The work herein was aimed at clarifying the criterion for choosing endpoints and to identify the meaning of the endpoint.

Examination of the experimental HPG-borate titration curves reveals that the PDADMAC volume corresponding to the endpoint is not distinct and does not correspond to zero SCD signal. A better endpoint criterion is titrant volume where the second derivative of the curve is zero, although this was also indistinct in many cases with HPG-borate.

With the simulated titration curves, the zeta potential corresponding to the endpoint could be positive or negative. If the binding constant,  $K_I$  was high, the endpoint occurred when the SCD surface was still negatively charged whereas low  $K_I$  values required a positively charged surface to saturate the HPG chain with bound borate.

The modeling suggests that the endpoint in our polyelectrolyte titrations gives a measure of the maximum number of borate binding sites on HPG. There is no consensus in the literature as to the identity of the binding sites on HPG ( $[P_7]$  in the model). The three structural units on HPG (Figure 3.2) are galactose, bare mannose and mannose units supporting a galactose. The presence of the hydroxypropyl groups is another complication. The endpoints in our titrations correspond closely to the number of galactose units causing us to believe that most of the guar binding sites are on the galactose units.

Our interest in HPG-borate behavior arises from its efficacy as a component of artificial tears<sup>19</sup>. Previously, we showed that HPG-borate forms complexes with lysozyme, a cationic protein present in tear fluid<sup>20</sup>. The present work suggests that the HPG-borate/PDADMAC interaction is cooperative in that complexation may stimulate additional borate binding to HPG.

Finally, we propose that the polyelectrolyte titration of HPG-borate and HPG-methylborate illustrates polyelectrolyte behaviors that fall outside the conventional landscape of strong and weak polyelectrolytes. Specifically, the labile nature of the boronate binding causes the anionic charge density of HPG-borate to respond to small changes in local environment. Work in our group shows that HPG-borate behaves like a

conventional polyelectrolyte in that it can induce bridging flocculation. On the other hand, we will also show that unlike conventional strong and weak anionic polyelectrolytes, HPG-borate does not complex with cationic surfactants. Therefore a picture is developing that is consistent with the interactions of labile HPG-borate with macromolecules and surfaces being more complicated than with conventional polyelectrolytes.

### 3.6 Conclusions

1. The polyelectrolyte titration does not measure the initial charge content of labile polyelectrolytes such as HPG-borate because the presence of cationic titrant facilitates further borate binding to HPG.
2. The polyelectrolyte titration can give a measure of the total concentration of borate binding sites on HPG.
3. Endpoints for the HPG-borate polyelectrolyte titrations are not distinct and do not correspond to zero streaming current potential.
4. HPG binds slightly more methylboronic acid than borate ion because some of the borate ions occupy two sites on HPG, whereas methylborate can bind only to one site.
5. The shapes of the polyelectrolyte titration curves and the pH changes during a titration were simulated by a model that accounts for electrostatic enhancement of borate binding to HPG in the presence of cationic PDADMAC.

## 3.7 Figures

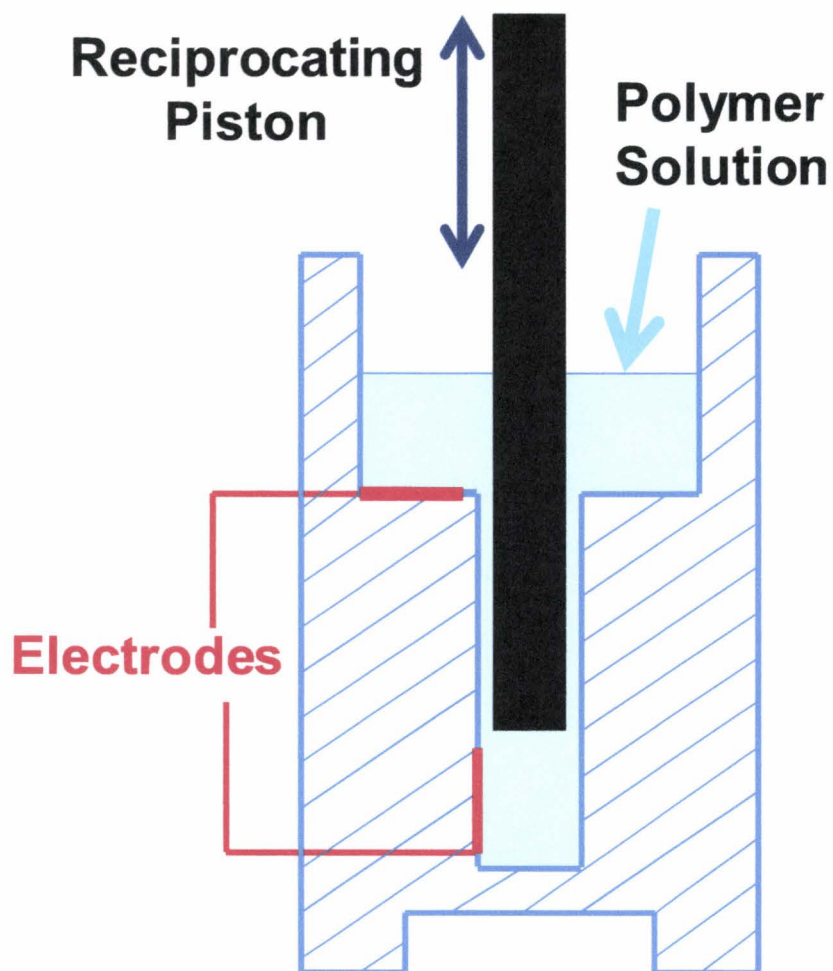


**Figure 3.1** Schematic illustration of a streaming current detector.

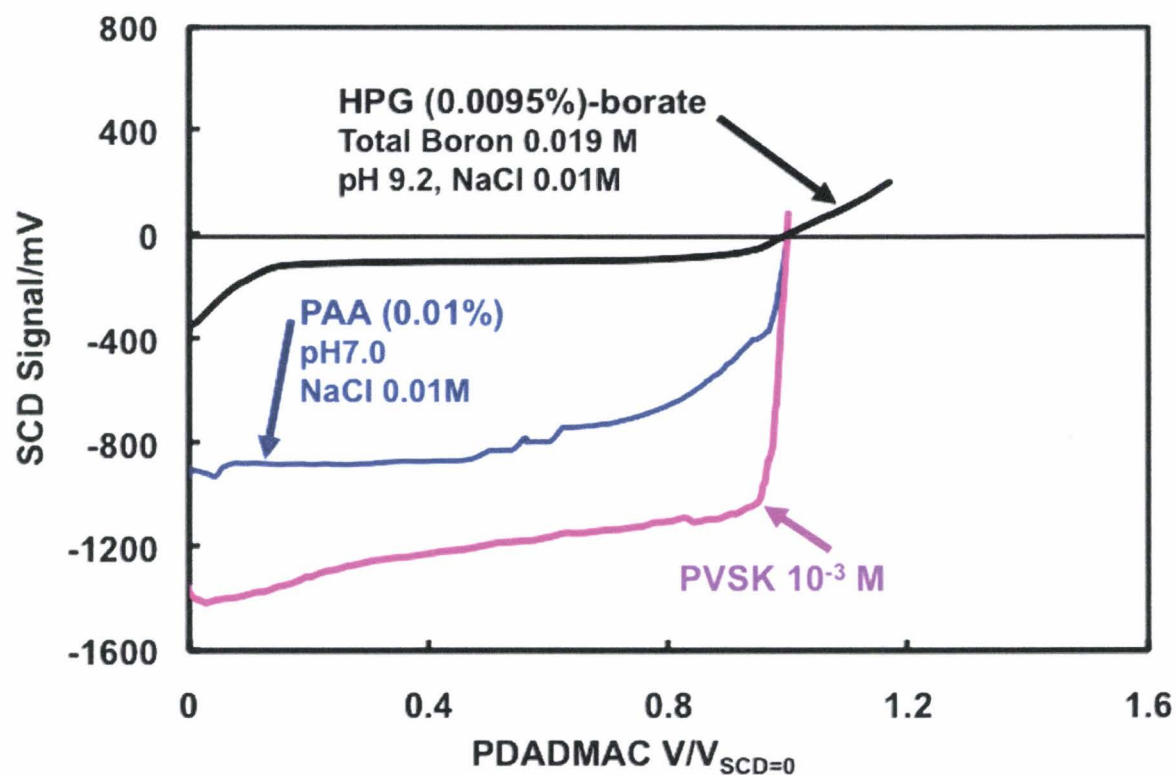


**Figure 3.2** Comparison of polyelectrolyte titration curves for PVSK, a strong polyelectrolyte, PAA, a weak polyelectrolyte, and HPG-borate, a labile polyelectrolyte.

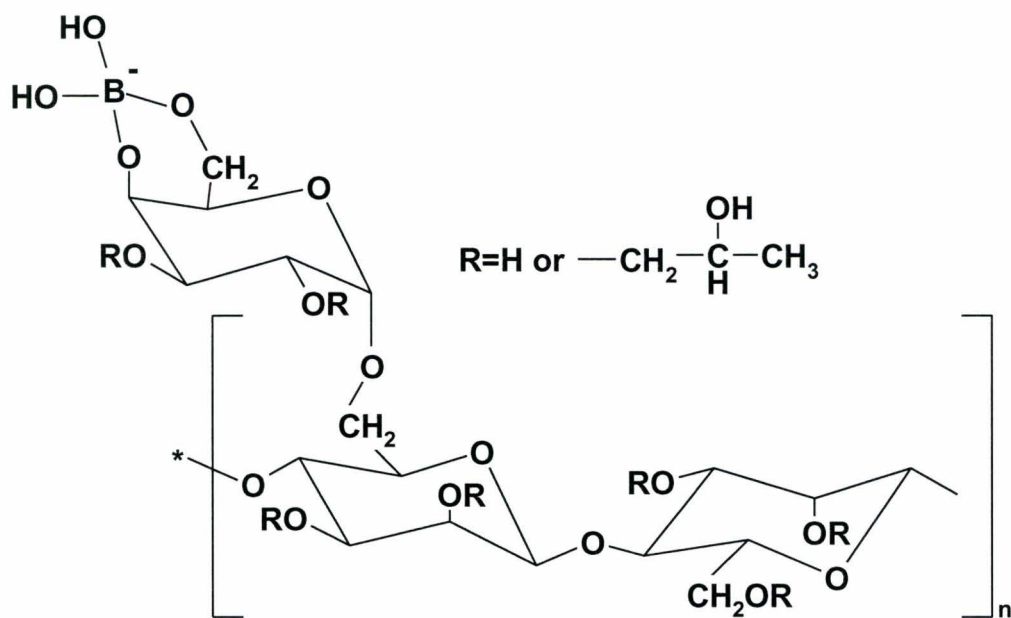


Figure 3.3 The structure of HPG-borate.

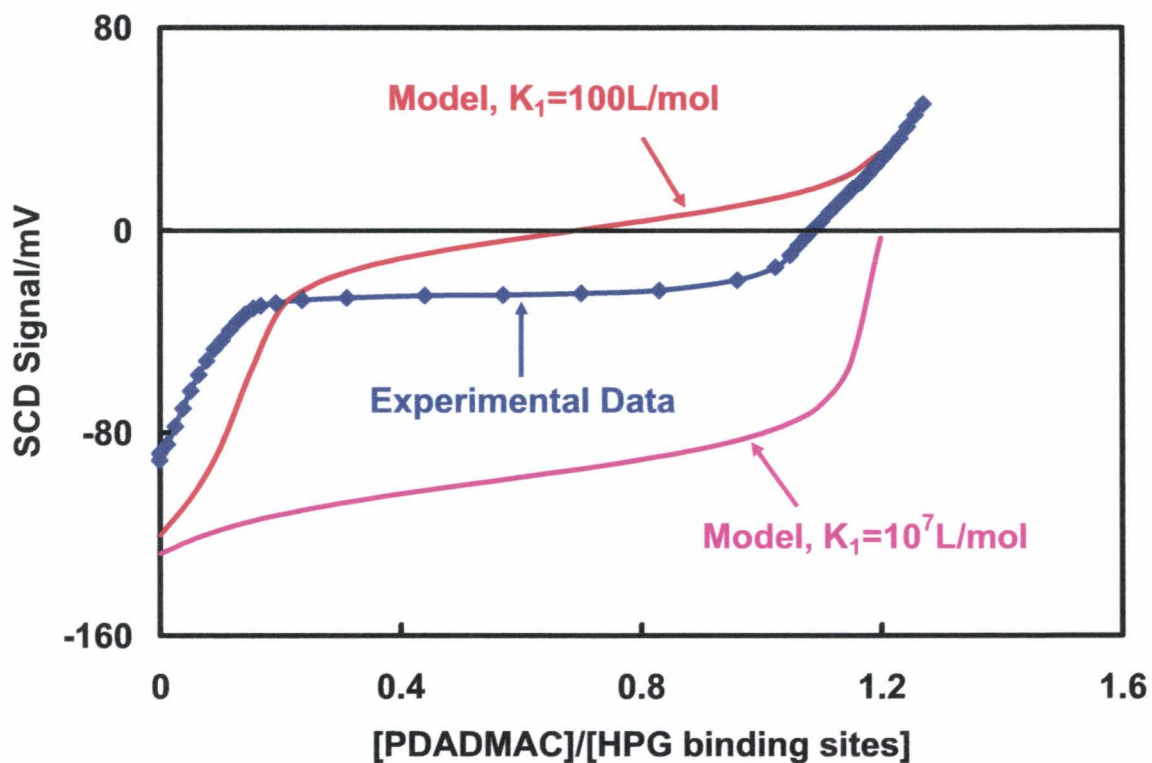


Figure 3.4 Comparing model and experimental polyelectrolyte titrations. The model parameters are:  $\gamma = 3$ ,  $\sigma_0 = -0.06\text{ C/m}^2$ ,  $[\text{NaCl}] = 10\text{ mM}$ ,  $[\text{P}_T] = 0.15\text{ mM}$ ,  $[\text{B}_T] = 19\text{ mM}$ ,  $\Gamma_{\text{HPG}} = 2\text{ mg/m}^2$  and  $\alpha = 4$ .

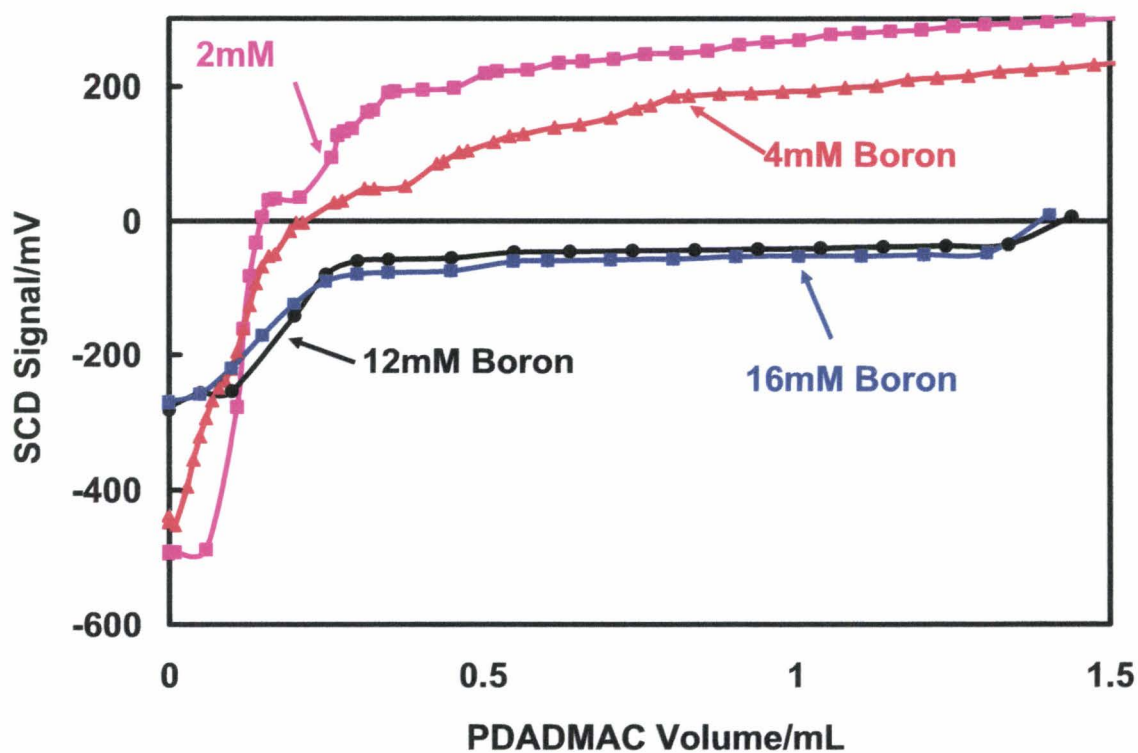


Figure 3.5 Influence of borate concentration on the titration of HPG-borate with PDADMAC.

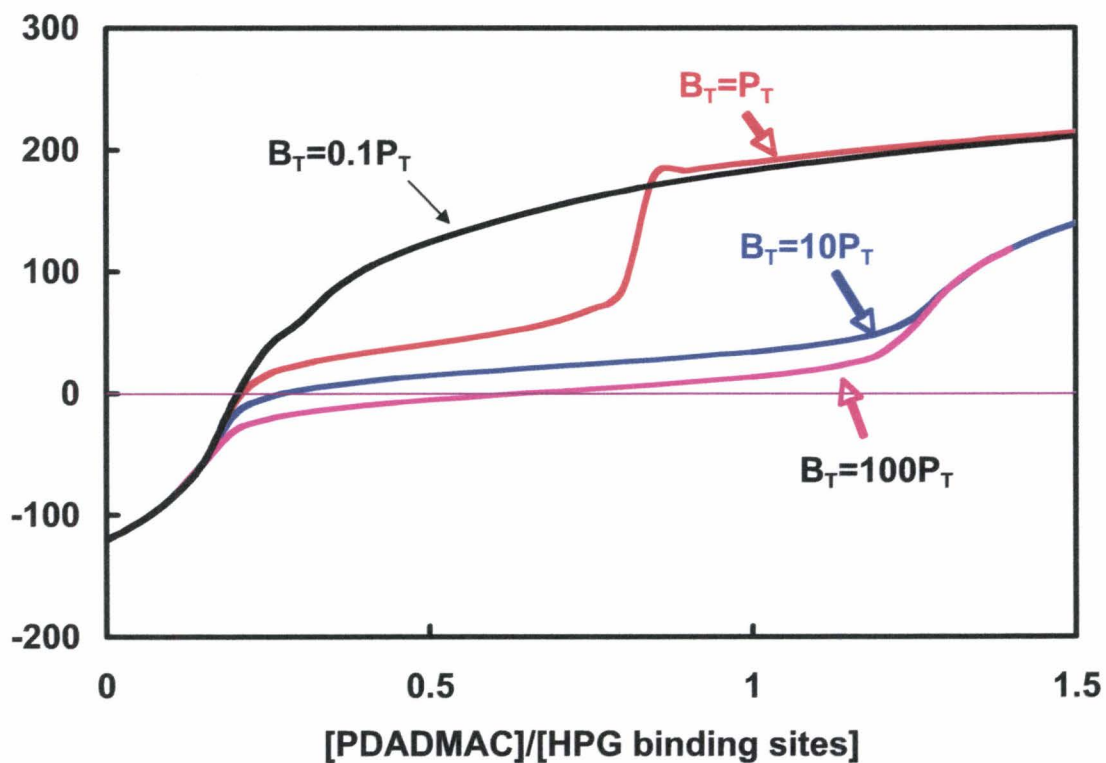


Figure 3.6 Simulating the influence of borate concentration.  $K_1 = 100 \text{ L/mol}$ , remaining parameters given in caption of Figure 3.4.

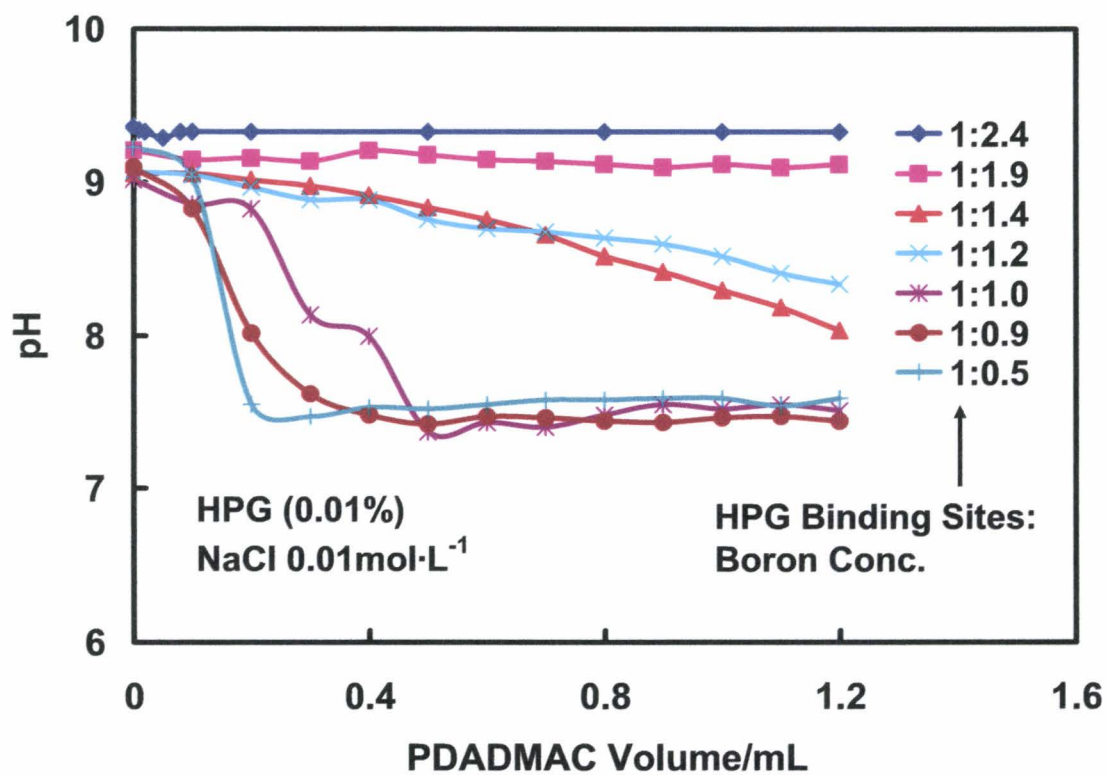


Figure 3.7 Evolution of pH during the titration of HPG-borate with PDADMAC.

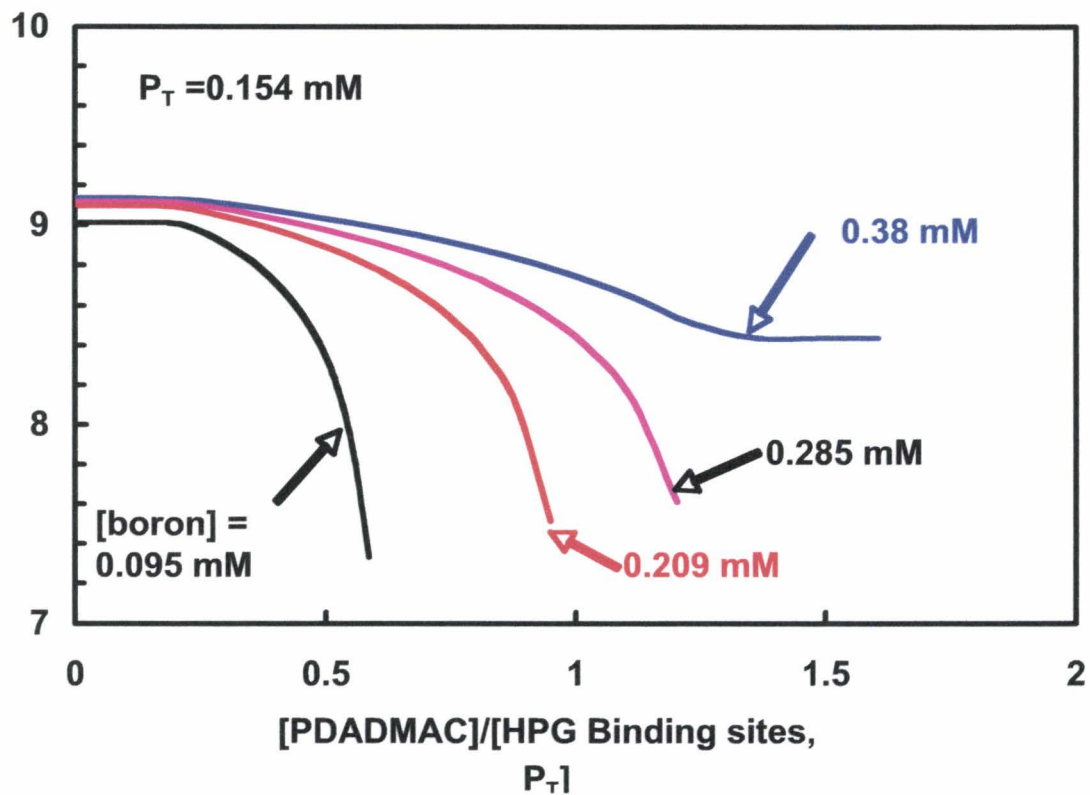


Figure 3.8 Simulating the influence of borate concentration on the evolution of pH during the titration of HPG-borate with PDADMAC.  $K_1 = 100 \text{ L/mol}$ , remaining parameters given in caption of Figure 3.4.

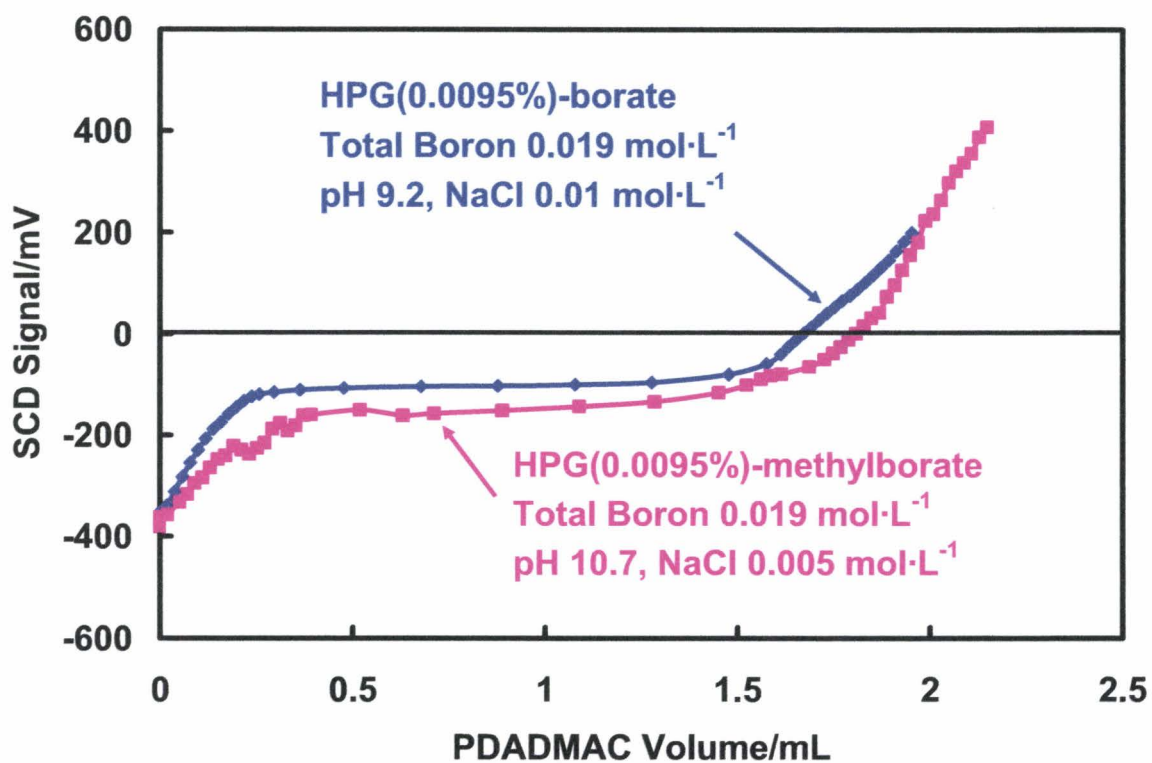


Figure 3.9 PDADMAC addition to HPG-methylborate and to HPG-borate. The methylborate can only add once whereas borate can bind twice to give a cross-link.

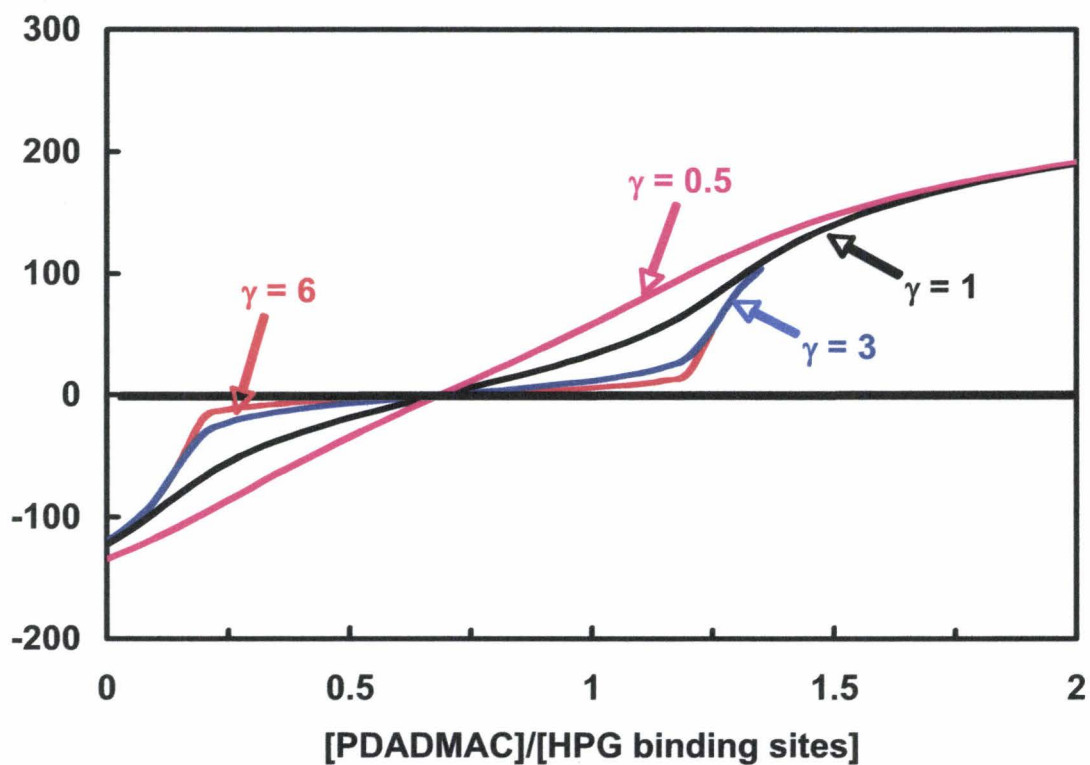


Figure 3.10 Influence of  $\gamma$  on the shape of the simulated polyelectrolyte titrations.  $K_1 = 100$  L/mol, remaining parameters given in caption of Figure 3.4.

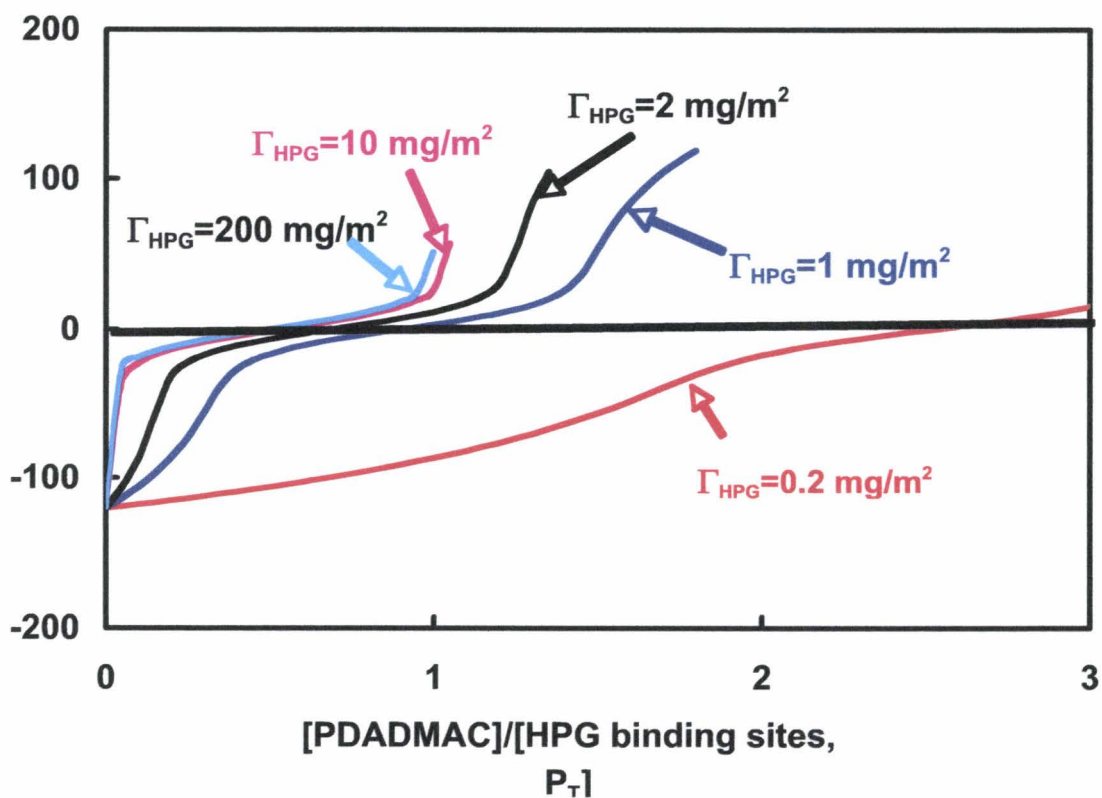


Figure 3.11 Influence of the assumed amount of adsorbed HPG on the shape of the simulated titrations.  $K_1 = 100 \text{ L/mol}$ , remaining parameters given in caption of Figure 3.4.

### 3.8 References

1. Terayama, H., Method of colloid titration (a new titration between polymer ions). *Journal of Polymer Science* 1952, 8, (2), 243-253.
2. Pelton, R.; Cabane, B.; Cui, Y.; Ketelson, H., Shapes of polyelectrolyte titration curves. 1. Well-behaved strong polyelectrolytes. *Analytical Chemistry* 2007, 79, (21), 8114-8117.
3. Kam, S. K.; Gregory, J., Charge determination of synthetic cationic polyelectrolytes by colloid titration. *Colloids and Surfaces, A: Physicochemical and Engineering Aspects* 1999, 159, (1), 165-179.
4. Chen, J. H.; Heitmann, J. A.; Hubbe, M. A., Dependency of polyelectrolyte complex stoichiometry on the order of addition. 1. Effect of salt concentration during streaming current titrations with strong poly-acid and polybase. *Colloids and Surfaces, A: Physicochemical and Engineering Aspects* 2003, 223, (1-3), 215-230.
5. Bockenhoff, K.; Fischer, W. R., Determination of electrokinetic charge with a particle-charge detector, and its relationship to the total charge. *Fresenius Journal of Analytical Chemistry* 2001, 371, (5), 670-674.
6. Phipps, J. S., Some mechanistic insights for using the streaming current detector to measure wet-end charge. *Tappi Journal* 1999, 82, (8), 157-165.
7. Cheng, Y.; Brown, K. M.; Prud'homme, R. K., Characterization and intermolecular interactions of hydroxypropyl guar solutions. *Biomacromolecules* 2002, 3, (3), 456-461.
8. McNeil, M.; Albersheim, P., A quantitative method to determine the points of ortho-(2-hydroxypropyl) substitution in ortho-(2-hydroxypropyl)-guar. *Carbohydrate Research* 1984, 131, (1), 131-137.
9. Noble, O.; Tavel, F. R., Rheological properties of galactomannan-based gels .2. Ion cross-linked galactomannan gels. *Carbohydrate Polymers* 1990, 12, (3), 279-293.
10. Pezron, E.; Ricard, A.; Lafuma, F.; Audebert, R., Reversible gel formation induced by ion complexation .1. Borax galactomannan interactions. *Macromolecules* 1988, 21, (4), 1121-1125.
11. Katchalsky, A.; Mazur, J.; Spitnik, P., Polybase properties of poly(vinylamine). *Journal of Polymer Science* 1957, 23, 513-30.
12. Jasinski, R.; Redwine, D.; Rose, G., Boron equilibria with high molecular weight guar: An NMR study. *Journal of Polymer Science, Part B: Polymer Physics* 1996, 34, (8), 1477-1488.
13. De Stefano, C.; Gianguzza, A.; Piazzese, D.; Sammartano, S., Polyacrylate protonation in various aqueous ionic media at different temperatures and ionic strengths. *Journal of Chemical and Engineering Data* 2000, 45, (5), 876-881.
14. Walker, C. A.; Kirby, J. T.; Dentel, S. K., The streaming current detector: A quantitative model. *Journal of Colloid and Interface Science* 1996, 182, (1), 71-81.
15. Leibler, L.; Pezron, E.; Pincus, P. A., Viscosity behavior of polymer-solutions in the presence of complexing ions. *Polymer* 1988, 29, (6), 1105-1109.

16. Nagasawa, M.; Murase, T.; Kondo, K., Potentiometric titration of stereoregular polyelectrolytes. *J. Phys. Chem.* 1965, 69, (11), 4005-12.
17. Wassmer, K. H.; Schroeder, U.; Horn, D., Characterization and detection of polyanions by direct polyelectrolyte titration. *Makromolekulare Chemie-Macromolecular Chemistry and Physics* 1991, 192, (3), 553-565.
18. Springsteen, G.; Wang, B. H., A detailed examination of boronic acid-diol complexation. *Tetrahedron* 2002, 58, (26), 5291-5300.
19. Christensen, M. T.; Cohen, S.; Rinehart, J.; Akers, F.; Pemberton, B.; Bloomenstein, M.; Leshner, M.; Kaplan, D.; Meadows, D.; Meuse, P.; Hearn, C.; Stein, J. M., Clinical evaluation of an HP-guar gellable lubricant eye drop for the relief of dryness of the eye. *Current Eye Research* 2004, 28, (1), 55-62.
20. Lu, C.; Kostanski, L.; Ketelson, H.; Meadows, D.; Pelton, R., Hydroxypropyl guar-borate interactions with tear film mucin and lysozyme. *Langmuir* 2005, 21, (22), 10032-10037.

## **Chapter 4 Interaction of HPG-Borate with Cationic Surfactant Dodecyltrimethyl Ammonium Bromide (DTAB)**

### **Abstract**

The influence of hydroxypropyl guar (HPG), with and without boric acid, on dodecyltrimethyl ammonium bromide (DTAB) micellization was characterized by surface tension measurements, isothermal titration calorimetry, and small angle neutron scattering. Although HPG is a nonionic water-soluble polymer, borate ions form weak bonds with HPG, transforming it into an anionic polyelectrolyte, HPG-borate. Surprisingly, the three independent measurements showed that HPG-borate does not promote DTAB micellization or phase separation normally seen when mixing oppositely charged polyelectrolytes and surfactants. However, the neutron scattering results suggested that HPG-borate binds to and flocculates existing DTAB micelles. The unusual behavior of HPG-borate with DTAB was underscored by showing that carboxymethyl guar (CMG) formed precipitates with DTAB.

## 4.1 Introduction

Polyelectrolytes strongly interact with oppositely charged water-soluble surfactants, giving phase separation or polymer bound micelles. In this chapter, we describe an anionic polyelectrolyte that does not interact with the cationic surfactant DTAB (dodecyltrimethyl ammonium bromide) at concentrations below the cmc (critical micelle concentration). The anionic polyelectrolyte is formed in situ by mixing boric acid with hydroxypropyl guar (HPG) and forms a new class of polyelectrolytes we call labile polyelectrolytes.<sup>1,2</sup>

Guar is a water soluble, linear natural carbohydrate with a polymannose backbone bearing pendant galactose rings roughly on every other mannose unit. Because aqueous guar has a tendency to phase separate with time, many applications employ HPG<sup>3</sup> where randomly distributed<sup>4</sup> hydroxypropyl groups improves long-term solubility. Our interests in HPG arise from it being an effective component of artificial tear solutions.<sup>5-8</sup> Specifically, we are interested in understanding how HPG, in the presence of boric acid, interacts with proteins,<sup>9</sup> polymers and surfaces with a view to understanding its efficacy in ophthalmic applications.

Under alkaline conditions, boric acid is present as borate ions that can condense onto polymer chains with cis diol groups. The generic reaction of boric acid with cis diols is shown in Figure 4.1 whereas Figure 4.2 shows the structure of the HPG chain with a bound borate anion. The ability of boric acid to cross-link HPG into pH-sensitive gels has led to the use of HPG-borate in tertiary oil recovery. Thus, there have been many publications describing the rheological properties of HPG-borate and guar-borate as functions of pH and boron concentration.<sup>10-20</sup> Prud'homme's work<sup>16</sup> is particularly comprehensive.

Twenty years ago, Pezron and co-workers published a series of papers describing the behavior of polymers and gels formed by mixing boric acid with guar, HPG, or poly(vinyl alcohol).<sup>17, 20-24</sup> They were the first to emphasize that the condensation of borate ions onto HPG or guar converts the nonionic carbohydrates into anionic polyelectrolytes.<sup>22</sup> They stated that “Two major differences distinguish this system from a classical polyelectrolyte. First, the number of charges on the chain is imposed by the chemical equilibria. Second, free ions always present in the solution partially screen out electrostatic interactions even in the absence of passive salt.”<sup>23</sup>

However, with binding constants of only 100 L/mol or less, the binding energies are low, suggesting that the bound borate ions are labile.<sup>25</sup> For example, Pezron argued that nearest-neighbor electrostatic repulsion caused a decrease in the apparent borate binding with increasing borate ion concentration in solution.<sup>23</sup> This electrostatic inhibition of borate binding was used to explain and model the complicated intrinsic viscosity of labile polyelectrolytes when plotted as a function of ionic strength.<sup>20</sup>

Given the labile nature of the bound borate ions, to what extent does HPG-borate behave as a polyelectrolyte? In our first publication in this series,<sup>1</sup> we reported that HPG-borate forms polyelectrolyte complexes with poly(diallyldimethylammonium bromide) (PDADMAC) much like other common anionic polyelectrolytes. However, there was one unusual feature in this work. The presence of PDADMAC near HPG chains promoted additional borate binding to the carbohydrate until the borate binding sites on HPG were saturated. By contrast, complex formation between PDADMAC and typical weak polyelectrolytes, such as poly(methacrylic acid), does not promote complete dissociation of the polyacid.

Subsequently, we reported that HPG-borate induced bridging flocculation of cationic polystyrene latex which is also typical anionic polyelectrolyte behavior.<sup>2</sup> In this work, we showed that the phenyl boronate adduct of HPG also was a good flocculant. Monofunctional organic boronates offer the advantage of having only one carbohydrate reactive site, so two-step reactions leading to cross-linking (Figure 4.1) are not possible. We also employed monoborates in the present work to convert HPG to anionic polyelectrolyte without any possibility of cross-linking.

In summary, HPG-borate displays two important features of polyelectrolyte behavior – polyelectrolyte complex formation with oppositely charged polymers and flocculation of oppositely charged colloidal particles. In this work, we explore a further feature of polyelectrolyte behaviors – strong interactions with oppositely charged surfactants. We will show that in this case HPG-borate does not behave like a typical anionic polyelectrolyte. Thus, it is pertinent to briefly review the literature describing the interactions of polyelectrolytes with oppositely charged surfactants.

The early work is summarized in Goddard's classic reviews of surfactant interactions with nonionic<sup>26</sup> and charged<sup>27</sup> water-soluble polymers; these have been followed by a number of more recent reviews of polymer-surfactant interactions.<sup>28-35</sup> There have been many studies of cationic surfactant interactions with anionic polymers, with much of the early focus on interactions below the cmc. Titration of a surfactant into aqueous anionic polyelectrolyte results in a lowering of surface tension and phase separation at surfactant concentrations far below the normal cmc. Further increasing the surfactant concentration can result in resolubilization of the mixture.

Below the cmc, surfactant monomers can interact with polyelectrolyte by electrostatic and by hydrophobic interactions, if the polyelectrolyte has hydrophobic domains. The surfactant-polyelectrolyte binding isotherms have been measured and modeled.<sup>36-38</sup> Binding often occurs far below the normal cmc and is cooperative. The structure of polymer bound surfactants has been probed by small angle neutron scattering and neutron reflectivity at the air-water interface.<sup>32, 35, 39-47</sup>

There have been a few studies of the role polyelectrolyte charge density on binding below the cmc. Generally, the higher the charge density, the lower is the critical

aggregation concentration (cac).<sup>29, 47-54</sup> However, there is no clear case where lowering the charge density below a specific value prevents surfactant binding. For example, Wang and Tam used isothermal titration calorimetry (ITC) to probe the interactions between poly(acrylic acid) (PAA) and DTAB and they showed that binding was due to hydrophobic interactions when the degree of ionization of the PAA was less than 0.3, whereas binding was driven by electrostatic interactions for more highly charged polymers.<sup>52</sup> However, for hydrophobically driven polymer-surfactant binding, the presence of charges on the polymer can inhibit binding.<sup>50</sup>

Dubin's group has systematically studied the interaction of polyelectrolytes with oppositely charged micelles, far above the cmc.<sup>28, 37, 48, 53, 55, 56</sup> Polyelectrolyte binding to a micelle depends on three electrostatic parameters, ( $\sigma$ , the micelle charge density;  $\zeta$ , the linear charge density on the polymer; and  $\kappa$ , the Debye-Huckel parameter), and polyelectrolyte stiffness – surfactant binding decreases with increasing persistence length. They employed a model to show that the critical micelle charge density for polyelectrolyte binding was related to the other electrostatic parameters by  $\sigma_c \approx \kappa^b \zeta^{-1}$  where  $b = 0.5-3$ .<sup>37</sup> An important point made in this work was that charges on weak polyelectrolytes such as PAA should rearrange in response to positively charged patches on proteins or micelles.<sup>37</sup>

There are no reports in the literature on the interactions of surfactants with guar or HPG in the presence of borate species. However, there have been a few studies involving surfactant interactions with guar and its derivatives. Of most relevance is the work of Kastner and Zana who showed that quaternary ammonium surfactants do not bind to guar unless it has been modified with hydrophobic substituents.<sup>57</sup> There is some evidence that nonionic surfactants based on polyethylene glycol can hydrogen bond to guar.<sup>58</sup> However, it seems that guar and HPG have little tendency to interact with ionic surfactants because the carbohydrate is very hydrophilic. Of course the situation changes once charge groups are introduced. For example, cationically modified guar strongly interacts with SDS and related anionic surfactants.<sup>59</sup>

## 4.2 Experimental

### 4.2.1 Materials

Guar and hydroxypropyl guar (HPG) with 0.36 hydroxypropyl groups per sugar ring, both with molecular weights of  $\sim 10^6$  Da, were gifts from Alcon Laboratories (Fort Worth, TX). Dodecyltrimethyl ammonium bromide (DTAB) and chloroacetic acid were purchased from Sigma-Aldrich. Dodecyltrimethylammonium-d<sub>34</sub> bromide was purchased from CDN Isotopes. D<sub>2</sub>O was purchased from Cambridge Isotope Laboratories. Sodium borate, sodium hydroxide and hydrochloric acid were purchased from Anachemia. Sodium chloride was purchased from Caledon Laboratories Inc. Methylboronic acid (97%) was purchased from Aldrich. All solutions were made in MilliQ water or D<sub>2</sub>O. All

surfactants and salts were used without further purification except DTAB which was recrystallized three times using 50v%v ethanol and 50v%v acetone as the solvent.

Sodium borate (also known as borax,  $\text{Na}_2\text{B}_4\text{O}_7 \cdot 10\text{H}_2\text{O}$ ) dissolves in dilute aqueous solution to give boric acid and borate ions. The actual distribution of boron species depends upon the pH and the other solution components. To minimize potential confusion, herein we express the total boron species concentrations as the molarity of boron atoms.

## 4.2.2 Methods

### Preparation of Carboxymethyl Guar

Carboxymethyl guar (structure as shown in Figure 4.3) was prepared by reaction guar with chloroacetic acid.<sup>60</sup> In a typical experiment, 10g of guar was dispersed in 100 mL of 2-propanol in a three-necked glass flask type of reactor fitted with a mechanical stirrer. Sodium hydroxide (5.6 g) was added with stirring at room temperature, followed by chloroacetic acid. The mixture was stirred for four hours at 70°C. After cooling, the dispersed products were collected on a Whatman No.1 medium fast paper filter and washed with 300 mL of 2-propanol. Then, the products were dissolved with water and the solution was centrifuged and decanted to isolate the solids. The pH of the solution was adjusted to 7.0 using hydrochloric acid. Finally, the solution was precipitated with 2-propanol. The precipitation products were collected, freeze-dried and then ground into powder.

The content of carboxymethyl groups was determined by conductometric titration – the procedure has been described elsewhere.<sup>61</sup> Two CMG samples were employed in this work. They had a degree of substitution (DS) of 0.15 and 0.39 where the DS is defined as the number of carboxyls per sugar ring.

### Surface Tension Measurements

Surface tensions were measured by a Krüss DSA10 pendant drop apparatus. The shape of the pendant drop was analyzed by DSA 1.80.0.2 shape analysis software. Pendant drops were formed by a Krüss stainless steel needle with outer diameter of about 1.5mm, connected with a 1mL Perfektum<sup>®</sup> glass syringe from Popper & Sons Inc. MilliQ water with surface tension of 72.8 mN/m was used to calibrate the effective needle diameter. All measurements were made in an closed cell at 22°C controlled by a NESLAB water bath. The results are the average of three measurements, and the maximum range of the replicates was 1mN/m.

### Isothermal Titration Calorimetry (ITC)

A Microcal VP-ITC microcalorimeter was used to measure the heat release or absorption resulting from the dilution of 200 mM DTAB solutions. Typically 274  $\mu\text{L}$  of

DTAB was loaded into the syringe and 1.431 mL of HPG and sodium borate (50 mM total boron with pH adjusted to 9.2) were loaded into the titration cell. The titration was controlled with VPViewer 2000 ITC software. The release or absorption heat per injection was calculated by integrating the raw data of injection heat versus time using Microcal ITC Data Analysis software (Origin 7.0). The reference cell was filled with MilliQ water. Both the titrant and sample were degassed before titration, using Microcal Thermovac sample degassing equipment.

### Small-Angle Neutron Scattering (SANS) Experiments

Small-angle neutron scattering (SANS) experiments were performed on the D22 instrument at the Institut Laue Langevin (ILL) (Grenoble, France). The scattering vector  $Q$  ranged from 0.006 to  $0.4\text{\AA}^{-1}$ , with sample-to-detector distance of 2, 5.6 and 8m at a neutron wavelength of 6 Å. The HPG contrast matching solvent was calculated to be 20vol% D<sub>2</sub>O and 80vol% H<sub>2</sub>O. The background was corrected by an ILL standard procedure with measurements of empty beam, empty cell, H<sub>2</sub>O and boron carbide. Quartz cells (Hellma) were used with path lengths of 2mm used for samples in D<sub>2</sub>O and 1mm for samples in 20vol% D<sub>2</sub>O and 80vol% H<sub>2</sub>O. All SANS experiments were performed at room temperature. Results were fitted using Insanity Version J21 (T. Cosgrove, Bristol University).

## 4.3 Results

### Surface Tension

Surface tension versus surfactant concentration plots are sensitive indicators of polymer surfactant interactions.<sup>27</sup> The onset of polymer–surfactant interactions at the critical aggregation concentration (cac) shifts to surface tension curves to the left corresponding to much lower surfactant concentration. Figure 4.4 shows measurements of surface tensions of DTAB alone and HPG and HPG-borate as functions of DTAB concentration. In dilute electrolyte, DTAB has a cmc of 15 mM.<sup>62</sup> Low concentrations of HPG with DTAB gave a slightly lower surface tension than DTAB alone; however, HPG did not promote DTAB micellization.

HPG-borate slightly shifted the DTAB micellization to lower concentrations. The pH for the HPG-borate experiments was 9.2, which is the effective pK<sub>a</sub> of boronic acid. Assuming that the borate binding constant to HPG is 100 L/mol,<sup>25</sup> these conditions correspond to approximately 0.18 bound borate ions per HPG sugar ring in equilibrium with 9.6 mM B(OH)<sub>4</sub><sup>-</sup> and 10 mM B(OH)<sub>3</sub> in solution.

The fourth curve in Figure 4.4 shows the DTAB surface tension in the presence of methylboronic acid and pH 10.7. This monofunctional borate adds to HPG as B(OH)<sub>4</sub><sup>-</sup>, converting the nonionic carbohydrate into an anionic polyelectrolyte. However, methylboronic acid is monofunctional, inducing no HPG cross-linking. Note that the pH

was adjusted to a higher value corresponding to the pKa of methylboronic acid. The HPG-methylboronate results were identical to the HPG-borate values both giving a minimum surface tension which occurred at about 0.5 times the cmc.

The results in Figure 4.4 suggest that neither HPG alone nor HPG with borate influenced DTAB micellization. Kastner and Zana had already shown HPG gives only a “weak interaction” with DTAB.<sup>57</sup> However, we expected strong interactions between HPG-borate and DTAB. For example, Figure 4.5 shows the influence of carboxymethyl guar (CMG, see Figure 4.3 for structure), with and without borate, on DTAB surface tension. In the CMG experiments, we observed the formation of turbid solutions at ~ 0.5 the normal cmc of DTAB. At DTAB concentrations above 2 cmc, the solution became clear again. Finally, the presence of borate had little additional influence on the CMG-DTAB mixtures.

### **Isothermal Titration Calorimetry**

A comparison of Figure 4.4 with Figure 4.5 suggests that HPG-borate does not behave as a typical anionic polyelectrolyte in that it does not strongly interact with DTAB. Isothermal titration calorimetry was employed to further probe HPG-borate interactions with DTAB. In these experiments, a concentrated DTAB solution was titrated into buffer and the heat effect associated with micelle dissolution was measured. These are sensitive measurements that can give the cmc and information about the thermodynamics of micellization.<sup>36, 63, 64</sup> In addition, ITC can show the interactions of micelles with polymers.<sup>65</sup> For example, we used ITC to characterize the interaction of nonionic micelles with hydrophobically modified polyvinylamine.<sup>66</sup>

Figure 4.6 shows the heat effects for the isothermal addition of concentrated DTAB into various solutions. The titration into water shows classical behavior – there is a near constant heat effect until the DTAB concentration in the cell approaches the cmc. Micelles added above the cmc do not dissolve, and the residual heat effect is associated with dilution.

The presence of HPG and/or borate clearly contributes to the observed total heat effects. The additional components give a new peak at ~ 4 mM DTAB. However, because borate alone or HPG-borate also displays the peak, it is not specifically due to HPG-borate interaction with DTAB. Furthermore, for all of the curves in Figure 4.6, a clear endpoint near the normal cmc of DTAB is observed, suggesting that HPG-borate does not significantly perturb the DTAB micellar dissolution. For the HPG-borate experiment, the calculated DS (degree of substitution which is the number of substituents per sugar ring) of the bound borate ion is 0.26 borate ion per sugar ring and the concentrations of B(OH)<sub>4</sub> and B(OH)<sub>3</sub> are 24.95 mM and 25 mM respectively.

## Small-Angle Neutron Scattering

Small-angle neutron scattering (SANS) has proven to be a powerful technique for characterizing surfactant behavior.<sup>67-69</sup> Micellar sizes fall within a convenient range of neutron distance scales, and the use of deuterated surfactants allows contrast matching experiments, maximizing the sensitivity to the species of interest.

We employed SANS to probe the influence of HPG-borate and CMG-borate on DTAB micellization. Figure 4.7 shows the scattering intensity versus  $Q$  plots for deuterated DTAB in water, above and below the cmc. The experimental data are plotted as error bars, which were small except at low  $Q$ . Above the cmc, there was a strong peak centered at scattering vector  $Q$  at about  $0.043 \text{ \AA}^{-1}$  whereas below the cmc there was little scattering. We fitted the scattering profile for the 2 cmc data with the Hayter and Penfold “hard sphere soft potential” model.<sup>70-72</sup> In this approach, the scattering intensity is given by the following function of the scattering vector,  $Q$ :

$$I(Q) = N_p V_p^2 \Delta\rho^2 P(Q) S(Q) \quad (1)$$

where  $N_p$  is the number of particles per unit volume in the sample,  $V_p$  is the volume of a particle,  $\Delta\rho^2$  is the contrast of the scattering length density between particle and solvent,  $P(Q)$  is form factor, and  $S(Q)$  is structure factor. We used the following form factor for spheres where  $R_s$  is the radius of the sphere.

$$P(Q) = \left[ \frac{3(\sin(QR_s) - QR_s \cos(QR_s))}{(QR_s)^3} \right]^2 \quad (2)$$

A log normal distribution was used to describe the size polydispersity. To calculate the structure factor  $S(Q)$ , which denotes interparticle interactions in equation (1), we used the rescaled mean spherical approximation model (RMSA) with a soft potential.<sup>72</sup>

The fitting parameters in Table 4.1 yielded the solid curves in Figure 4.7, Figure 4.8 and Figure 4.9. The micelle radius from fitting the SANS data was 1.78 nm which is in good agreement with published values.<sup>73</sup>

We estimated that the scattering length density of our HPG was  $1.02 \times 10^{14} \text{ m}^{-2}$  and the corresponding contrast matching mixture was 20% (v/v) D<sub>2</sub>O and 80% H<sub>2</sub>O. Figure 4.8 shows the scattering intensity versus  $Q$  plot for DTAB above and below the cmc in dilute HPG under contrast matching conditions. It is clear that HPG alone does not promote micelle formation even slightly below the normal cmc. Comparing Figure 4.7 with Figure 4.8 shows the micelle peak at the same  $Q$  value suggesting HPG displays no interactions with DTAB micelles.

The twice cmc data in Figure 4.8 were also fitted with the hard sphere soft potential model. The only changed fitting parameter was the volume fraction which was changed to  $2.90 \times 10^{-3}$ , a little higher than the value in Figure 4.7 as shown in Table 4.1, reflecting the change in solvent.<sup>74</sup>

DTAB + HPG + borate were also measured above and below the cmc and the results are shown in Figure 4.9. Again the lower DTAB concentration showed no evidence of micelle formation, giving yet more evidence for the conclusion that HPG-borate does not promote micellization. The higher DTAB concentration did give micelles with a maximum similar to that for DTAB alone. However, there is an upturn in the curve at low Q that is indicative of larger scattering species. We propose that anionic HPG-borate will induce some aggregation of the cationic DTAB micelles, similar to what we have recently reported for HPG-borate induced bridging flocculation of a cationic polystyrene latex.<sup>2</sup>

Finally, to illustrate the difference between HPG-borate and conventional anionic polyelectrolytes, we attempted to measure DTAB scattering in the presence of carboxymethyl guar. However, even below the cmc, macroscopic phase separation prevented reliable measurements and suggest strong interactions with the carboxylated guar in this case.

## 4.4 Discussion

Surface tension, ITC and neutron scattering results suggest that HPG-borate or HPG-methylboronate anionic polymers do not facilitate DTAB micellization. By contrast, carboxymethyl guar displays strong interactions with DTAB, resulting in macroscopic phase separation. One possible explanation may involve the charge distribution along the carbohydrate chain.

There are two published estimates of the borate binding constant to HPG – 11 L/mol<sup>22</sup> and 100 L/mol. Using the larger binding constant, we estimated the amount of bound borate on HPG in our experiments. For conditions corresponding to the neutron scattering studies in Figure 4.9, we estimate the concentration of bound borate ions to be 0.38 mM, which corresponds to a degree of borate substitution of 0.18. This corresponds to an average spacing between charge groups of about 1.9 nm.

We observed macroscopic phase separation when we mixed DTAB with both lower charge density CMG with a DS of 0.15 and a higher charge density of 0.39. Thus, the overall charge density of HPG-borate should be sufficient to promote interactions with DTAB below the cmc, indicating that the low overall charge density of the HPG-borate is not the explanation.

Another possible explanation involves the distribution of charges. Perhaps to initiate surfactant association with a soluble polymer, there must be a few areas of high

local negative charge density with charge spacing comparable to micelle head spacing. Furthermore we propose that these high charge domains nucleate polymer-surfactant complex formation. Once started, the cooperative characteristic of surfactant interaction will drive complex formation. In the case of carboxymethyl guar, areas of local high charge densities of carboxylate groups could either arise from the nature of the carboxymethylation process or the random approach of two chain segments.<sup>75</sup> By contrast, the labile nature of the bound borate groups is characterized by fast exchange with the HPG<sup>12</sup>, which means that bound borate groups will always maximize their spacing along the HPG chain to minimize borate-borate electrostatic repulsion. In other words, with HPG-borate we expect no high charge density sites on the HPG chain that might be required to nucleate DTAB association.

Yet another explanation of the absence of HPG-borate/DTAB interactions below the cmc might be due to the short lifetime of bound borate groups. If the borate ions are exchanging rapidly between the bound and unbound state, then DTAB groups near the HPG segments might, on average, experience only the negligible attraction associated with an unoccupied borate binding site on HPG. Clearly, our explanations are speculative at this time and much more work needs to be done on the fundamental nature of these labile polyelectrolytes.

HPG-borate reverts to more typical polyelectrolyte behavior when the DTAB micelles already exist. The upturn at low  $Q$  in the SANS results in Figure 4.9 is direct evidence of micellar complexation within HPG-borate.

## 4.5 Conclusions

Two conclusions result from this work:

1. HPG-borate or HPG-methylboronate does not promote DTAB micellization below the cmc of DTAB. In other words, there is no cac. We do not know why – one proposed explanation is that the labile nature of the HPG-bound borate groups precludes the formation of high charge density domains along the HPG chain that are necessary to nucleate DTAB micellization.
2. HPG-borate does bind to and aggregate existing DTAB micelles.

## 4.6 Tables

**Table 4.1** Parameter values used to fit the neutron scattering data.

Parameter	Figure 4.7	Figure 4.8	Figure 4.9
$\Delta\rho^2/\text{\AA}^{-2}$	$7.60\times 10^{-6}$	$6.58\times 10^{-6}$	$6.58\times 10^{-6}$
Volume fraction	$2.66\times 10^{-3}$	$2.90\times 10^{-3}$	$3.00\times 10^{-3}$
Hard sphere radius/ $\text{\AA}$	17.8	17.8	17.8
Polydispersity**	0.13	0.13	0.13
Total surface charge	10.2	10.2	10.2
Debye screen length/ $\text{\AA}$	32.4	32.4	32.4
Scaler*	1.0	0.79	0.9
Background	0.991	0.78	0.7

\* Factor to scale S(Q) \*\* Fixed during interactions

## 4.7 Figures

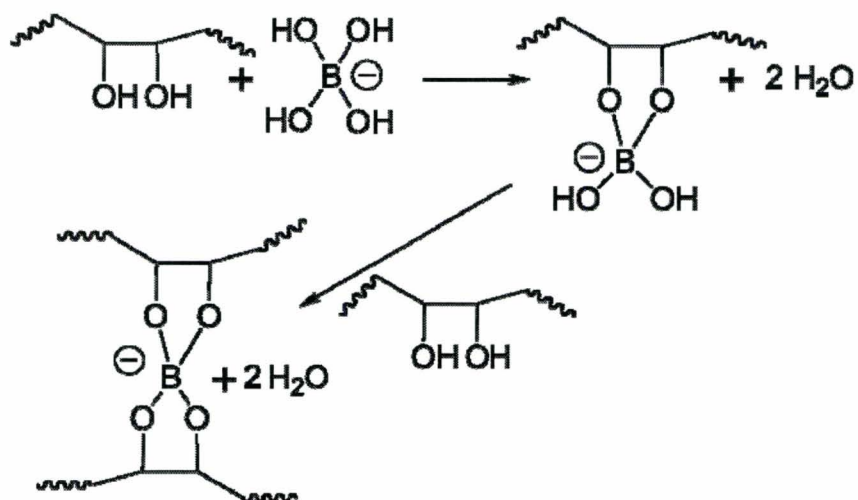


Figure 4.1 Cross-linking of water-soluble polymers containing cis-diol groups with the borate ion.

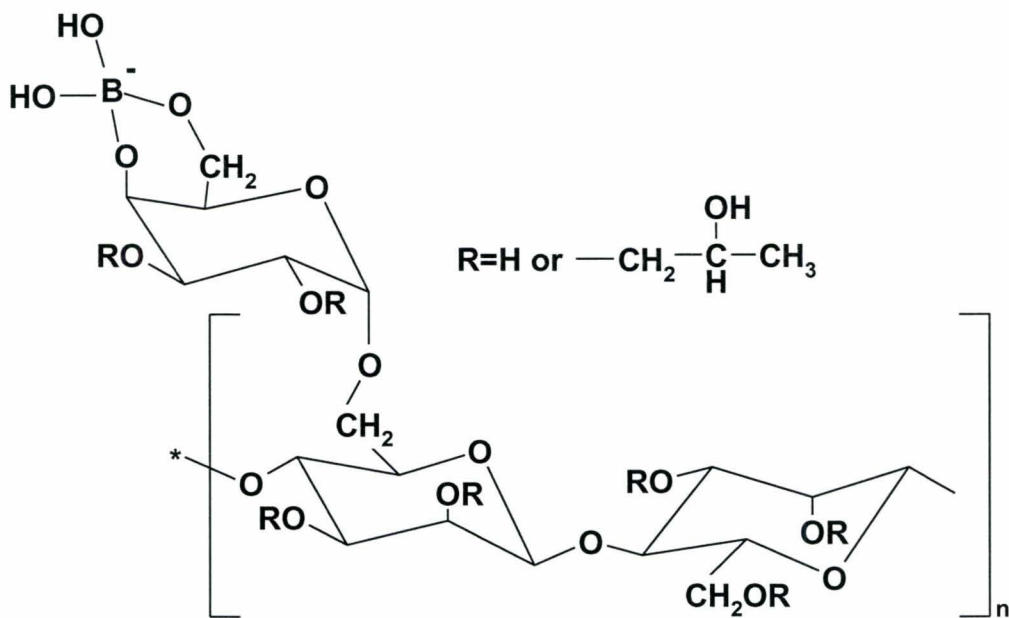


Figure 4.2 The condensation of borate with HPG to form HPG-borate.

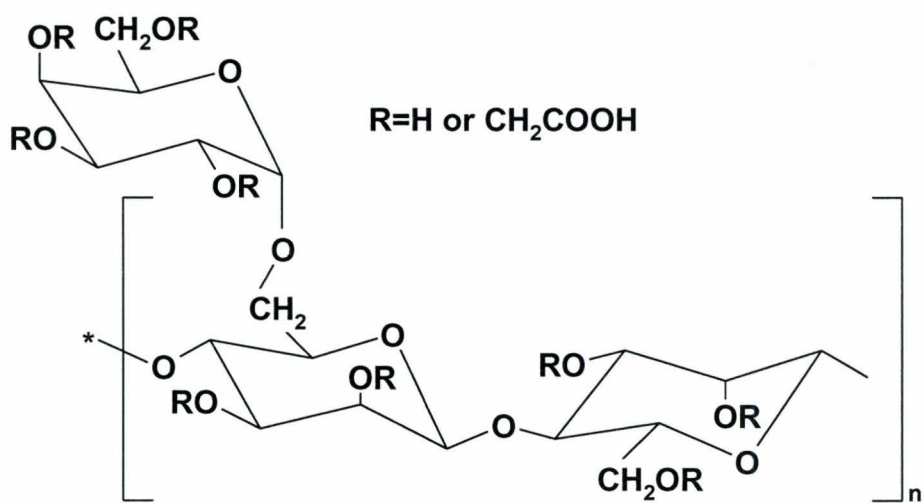


Figure 4.3 Structure of carboxymethyl guar (CMG).

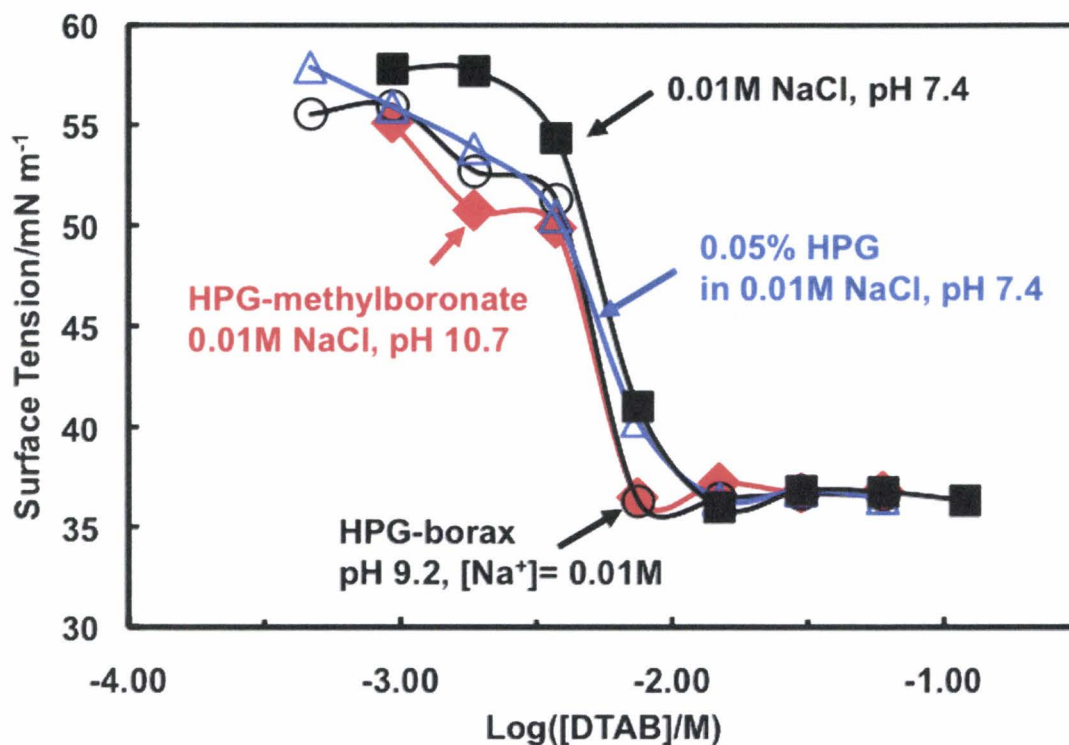


Figure 4.4 Surface tension as a function of DTAB concentration. The HPG concentrations were 0.05% (w/w) and the total boron concentrations in the borax (open circles) and methylboronate (red triangles) experiments were 0.02M.

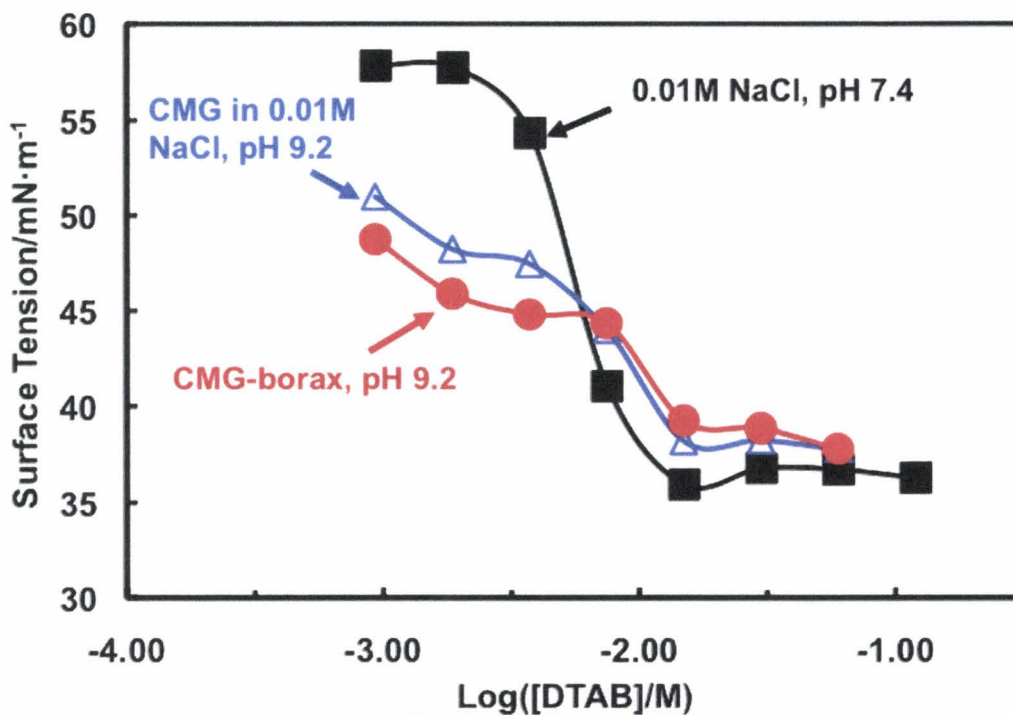


Figure 4.5 Influence of 0.05% carboxymethyl guar (CMG) on the DTAB surface tension. The degree of carboxymethyl substitution was 0.39. The total boron concentration for the borax experiments was 0.02M.

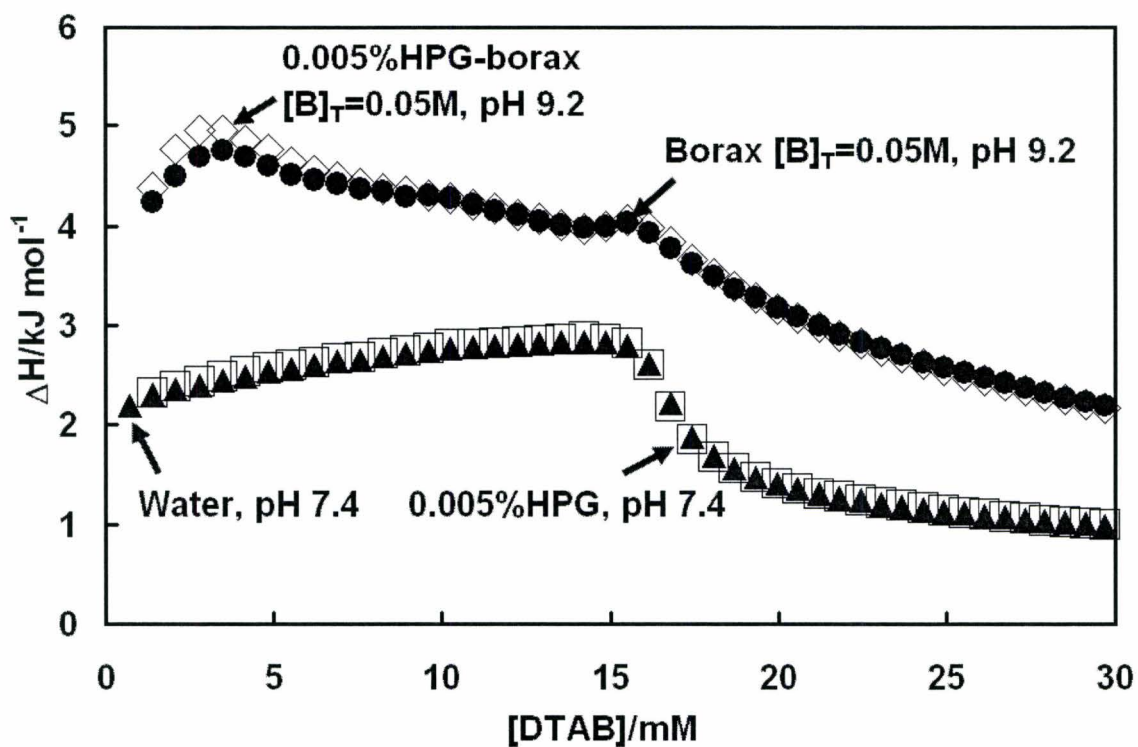


Figure 4.6 Isothermal calorimetric titration with concentrated (0.2 M) DTAB. The pH of the borate solutions was 9.2.

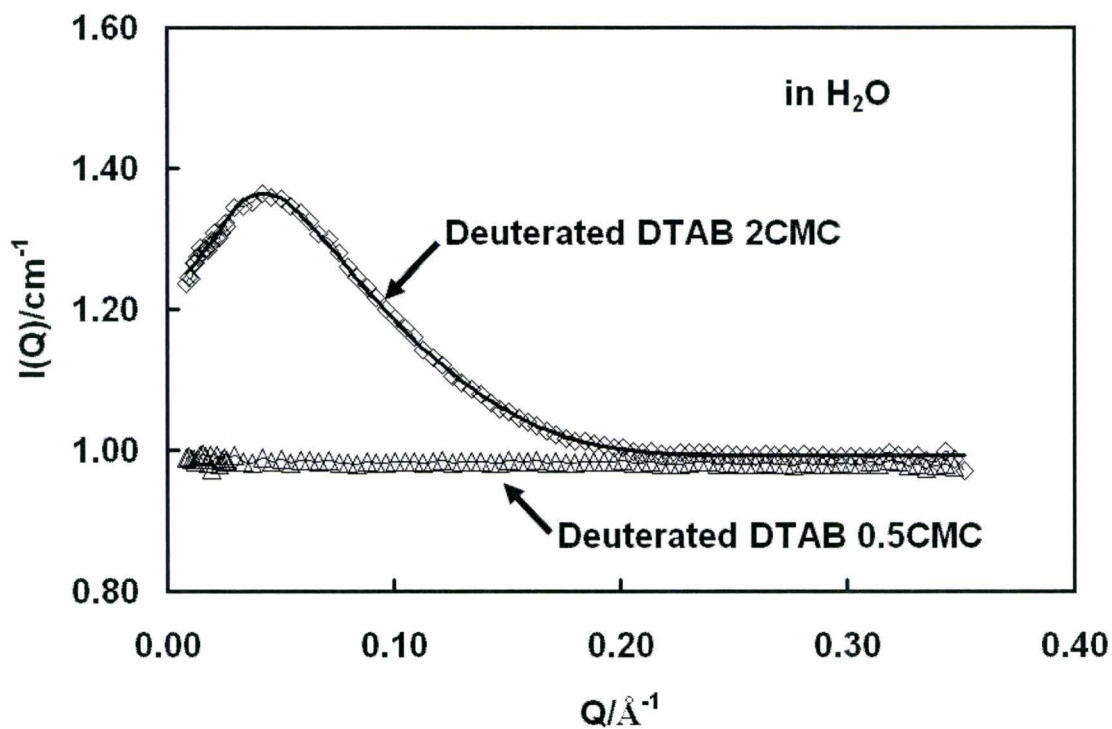


Figure 4.7 Small-angle neutron scattering results for D-DTAB in H<sub>2</sub>O. Surfactant concentrations are expressed as functions of the cmc (15 mM). The solid red line was fitted using parameters in Table 4.1.

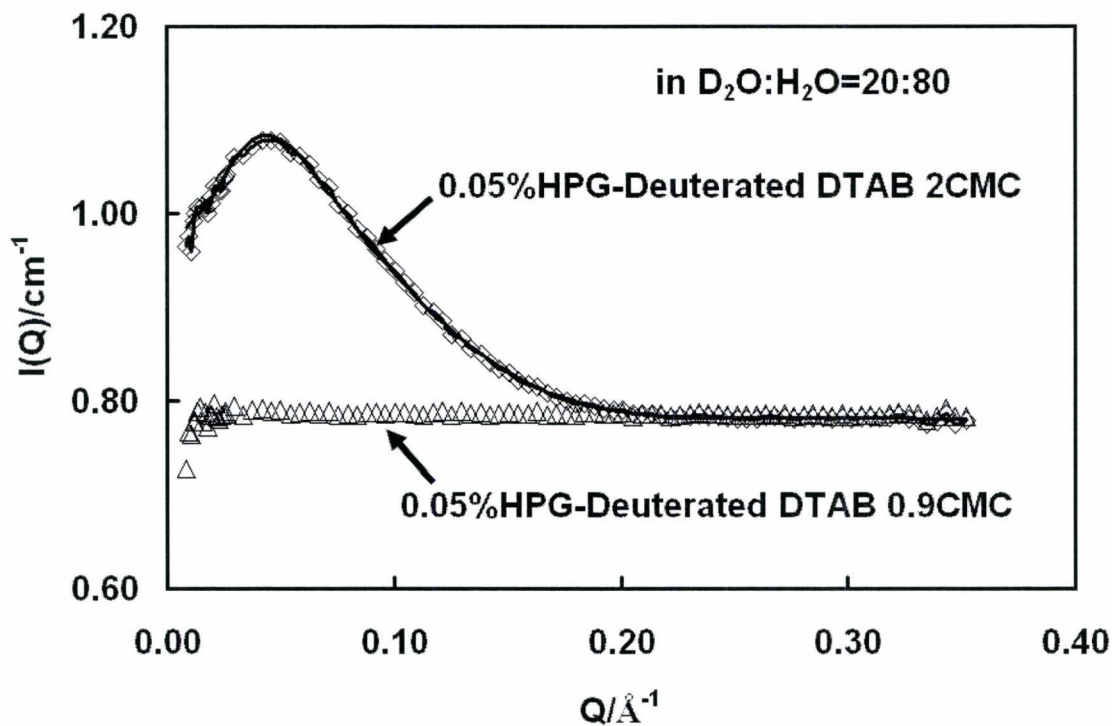


Figure 4.8 Influence of HPG (0.05% w/w) on the scattering behavior D-DTAB above and below the cmc in 20  $\text{D}_2\text{O}$ : 80  $\text{H}_2\text{O}$  (vol%).

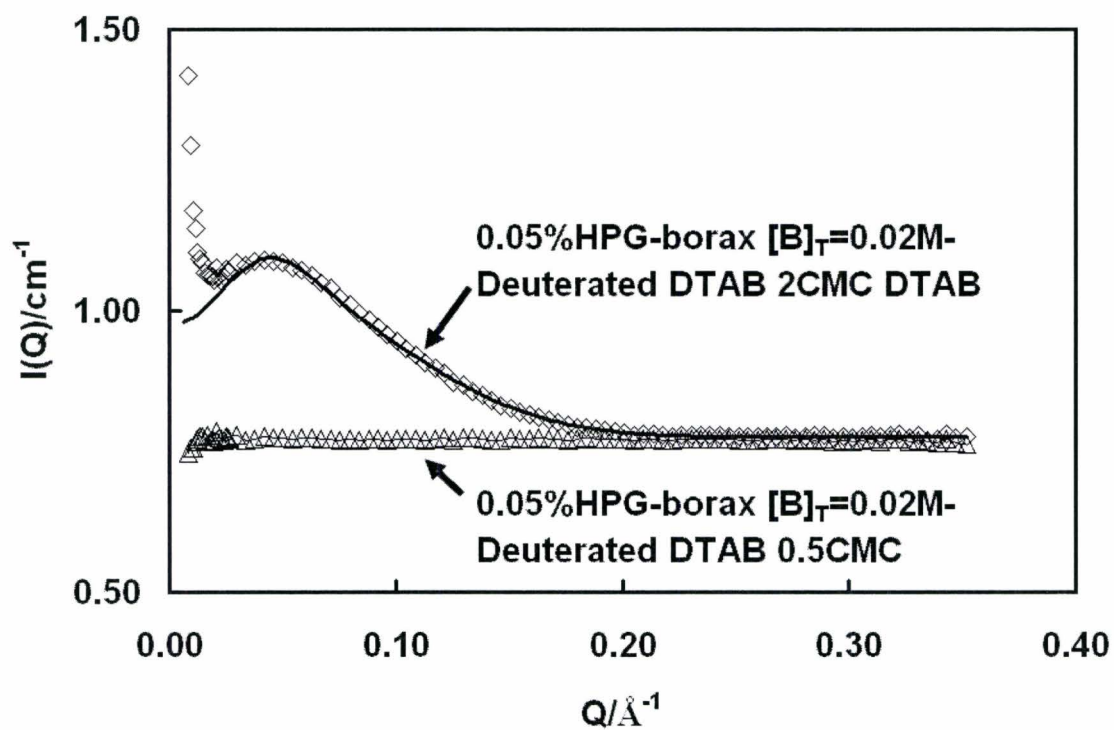


Figure 4.9 D-DTAB and HPG (0.05%) in 20% D<sub>2</sub>O 80% H<sub>2</sub>O (which is contrast matched to guar) with added borax (10 mM, pH 9.2).

## 4.8 References

1. Cui, Y. G.; Pelton, R.; Ketelson, H., Shapes of polyelectrolyte titration curves. 2. The deviant behavior of labile polyelectrolytes. *Macromolecules* 2008, 41, (21), 8198-8203.
2. Pelton, R.; Hu, Z.; Ketelson, H.; Meadows, D., Reversible flocculation with hydroxypropyl guar-borate, a labile anionic polyelectrolyte. *Langmuir* 2009, 25, (1), 192-195.
3. Cheng, Y.; Brown, K. M.; Prud'homme, R. K., Characterization and intermolecular interactions of hydroxypropyl guar solutions. *Biomacromolecules* 2002, 3, (3), 456-461.
4. McNeil, M.; Albersheim, P., A quantitative method to determine the points of ortho-(2-hydroxypropyl) substitution in ortho-(2-hydroxypropyl)-guar. *Carbohydrate Research* 1984, 131, (1), 131-137.
5. Christensen, M. T.; Cohen, S.; Rinehart, J.; Akers, F.; Pemberton, B.; Bloomenstein, M.; Leshner, M.; Kaplan, D.; Meadows, D.; Meuse, P.; Hearn, C.; Stein, J. M., Clinical evaluation of an hp-guar gellable lubricant eye drop for the relief of dryness of the eye. *Current Eye Research* 2004, 28, (1), 55-62.
6. Ubels, J. L.; Aupperlee, M. D.; Meadows, D. L., Artificial tear solutions and protection of the corneal epithelium from desiccation. *Journal of Toxicology-Cutaneous and Ocular Toxicology* 2002, 21, (4), 273-281.
7. Ubels, J. L.; Clousing, D. P.; Van Haitsma, T. A.; Hong, B. S.; Stauffer, P.; Asgharian, B.; Meadows, D., Pre-clinical investigation of the efficacy of an artificial tear solution containing hydroxypropyl-guar as a gelling agent. *Current Eye Research* 2004, 28, (6), 437-444.
8. Young, N. W. G.; Williams, P. A.; Meadows, J.; Allen, E., A promising hydrophobically-modified guar for completion applications. *Proceedings - SPE/DOE Symposium on Improved Oil Recovery, 11th, Tulsa, Okla., Apr. 19-22, 1998* 1998, 2, 463-470.
9. Lu, C.; Kostanski, L.; Ketelson, H.; Meadows, D.; Pelton, R., Hydroxypropyl guar-borate interactions with tear film mucin and lysozyme. *Langmuir* 2005, 21, (22), 10032-10037.
10. Parris, M. D.; MacKay, B. A.; Rathke, J. W.; Klingler, R. J.; Gerald, R. E., Influence of pressure on boron cross-linked polymer gels. *Macromolecules* 2008, 41, (21), 8181-8186.
11. Lei, C. Y.; Clark, P. E. In *Crosslinking of guar and guar derivatives*, 2007; Soc Petroleum Eng: 2007; pp 316-321.
12. Rietjens, M.; Steenbergen, P. A., Crosslinking mechanism of boric acid with diols revisited. *European Journal of Inorganic Chemistry* 2005, (6), 1162-1174.
13. Martin, S.; Freitas, R. A.; Obayashi, E.; Sierakowski, M. R., Physico-chemical aspects of galactoxyloglucan from the seeds of *hymenaea courbaril* and its tetraborate complex. *Carbohydrate Polymers* 2003, 54, (3), 287-295.

14. Goel, N.; Shah, S. N.; Yuan, W. L.; O'Rear, E. A., Suspension characteristics of borate-crosslinked gels: Rheology and atomic force microscopy measurements. *Journal of Applied Polymer Science* 2001, 82, (12), 2978-2990.
15. Tayal, A.; Pai, V. B.; Khan, S. A., Rheology and microstructural changes during enzymatic degradation of a guar-borax hydrogel. *Macromolecules* 1999, 32, (17), 5567-5574.
16. Kesavan, S.; Prudhomme, R. K., Rheology of guar and HPG cross-linked by borate. *Macromolecules* 1992, 25, (7), 2026-2032.
17. Pezron, E.; Ricard, A.; Leibler, L., Rheology of galactomannan-borax gels. *Journal of Polymer Science Part B-Polymer Physics* 1990, 28, (13), 2445-2461.
18. Noble, O.; Turquois, T.; Tavel, F. R., Rheological properties of galactomannan-based gels .1. Guar and hydroxypropylguar gels in alkaline media. *Carbohydrate Polymers* 1990, 12, (2), 203-217.
19. Noble, O.; Tavel, F. R., Rheological properties of galactomannan-based gels .2. Ion cross-linked galactomannan gels. *Carbohydrate Polymers* 1990, 12, (3), 279-293.
20. Leibler, L.; Pezron, E.; Pincus, P. A., Viscosity behavior of polymer-solutions in the presence of complexing ions. *Polymer* 1988, 29, (6), 1105-1109.
21. Pezron, E.; Leibler, L.; Ricard, A.; Audebert, R., Reversible gel formation induced by ion complexation .2. Phase-diagrams. *Macromolecules* 1988, 21, (4), 1126-1131.
22. Pezron, E.; Ricard, A.; Lafuma, F.; Audebert, R., Reversible gel formation induced by ion complexation .1. Borax galactomannan interactions. *Macromolecules* 1988, 21, (4), 1121-1125.
23. Pezron, E.; Leibler, L.; Lafuma, F., Complex-formation in polymer-ion solutions .2. Poly-electrolyte effects. *Macromolecules* 1989, 22, (6), 2656-2662.
24. Pezron, E.; Leibler, L.; Ricard, A.; Lafuma, F.; Audebert, R., Complex-formation in polymer ion solutions .1. Polymer concentration effects. *Macromolecules* 1989, 22, (3), 1169-1174.
25. Jasinski, R.; Redwine, D.; Rose, G., Boron equilibria with high molecular weight guar: An NMR study. *Journal of Polymer Science, Part B: Polymer Physics* 1996, 34, (8), 1477-1488.
26. Goddard, E. D., Polymer surfactant interaction .1. Uncharged water-soluble polymers and charged surfactants. *Colloids and Surfaces* 1986, 19, (2-3), 255-300.
27. Goddard, E. D., Polymer surfactant interaction .2. Polymer and surfactant of opposite charge. *Colloids and Surfaces* 1986, 19, (2-3), 301-329.
28. Li, Y.; Dubin, P. L., Polymer-surfactant complexes. *ACS Symp. Ser.* 1994, 578, (Structure and Flow in Surfactant Solutions), 320-36.
29. Hansson, P.; Lindman, B., Surfactant-polymer interactions. *Current Opinion in Colloid & Interface Science* 1996, 1, (5), 604-613.
30. Winnik, F. M.; Regismond, S. T. A., Fluorescence methods in the study of the interactions of surfactants with polymers. *Colloids and Surfaces a-Physicochemical and Engineering Aspects* 1996, 118, (1-2), 1-39.
31. Kwak, J. C. T.; Editor, *Polymer-surfactant systems. [in: Surfactant sci. Ser., 1998; 77].* 1998; p 482 pp.

32. Barany, S. In *Interaction between water soluble polymers and surfactants*, 2001; Wiley-V C H Verlag Gmbh: 2001; pp 71-92.
33. Miguel, M. D., Association of surfactants and polymers studied by luminescence techniques. *Advances in Colloid and Interface Science* 2001, 89, 1-23.
34. Hansson, P., Interaction between polyelectrolyte gels and surfactants of opposite charge. *Current Opinion in Colloid & Interface Science* 2006, 11, (6), 351-362.
35. Penfold, J.; Thomas, R. K.; Taylor, D. J. F., Polyelectrolyte/surfactant mixtures at the air-solution interface. *Current Opinion in Colloid & Interface Science* 2006, 11, (6), 337-344.
36. Lapitsky, Y.; Parikh, M.; Kaler, E. W. In *Calorimetric determination of surfactant/polyelectrolyte binding isotherms*, 2007; Amer Chemical Soc: 2007; pp 8379-8387.
37. Cooper, C. L.; Goulding, A.; Kayitmazer, A. B.; Ulrich, S.; Stoll, S.; Turksen, S.; Yusa, S.; Kumar, A.; Dubin, P. L., Effects of polyelectrolyte chain stiffness, charge mobility, and charge sequences on binding to proteins and micelles. *Biomacromolecules* 2006, 7, (4), 1025-1035.
38. Liu, J.; Shirahama, K.; Miyajima, T.; Kwak, J. C. T., Interaction of a cationic surfactant to sodium polyphosphates with different degrees of polymerization. *Colloid and Polymer Science* 1998, 276, (1), 40-45.
39. Berret, J. F.; Cristobal, G.; Herve, P.; Oberdisse, J.; Grillo, I., Structure of colloidal complexes obtained from neutral/polyelectrolyte copolymers and oppositely charged surfactants. *European Physical Journal E* 2002, 9, (4), 301-311.
40. Cabane, B.; Lindell, K.; Engstrom, S.; Lindman, B., Microphase separation in polymer plus surfactant systems. *Macromolecules* 1996, 29, (9), 3188-3197.
41. Penfold, J.; Tucker, I.; Thomas, R. K.; Taylor, D. J. F.; Zhang, J.; Zhang, X. L., The impact of electrolyte on the adsorption of sodium dodecyl sulfate/polyethyleneimine complexes at the air-solution interface. *Langmuir* 2007, 23, (7), 3690-3698.
42. Penfold, J.; Tucker, I.; Thomas, R. K.; Zhang, J., Adsorption of polyelectrolyte/surfactant mixtures at the air-solution interface: Poly(ethyleneimine)/sodium dodecyl sulfate. *Langmuir* 2005, 21, (22), 10061-10073.
43. Purcell, I. P.; Lu, J. R.; Thomas, R. K.; Howe, A. M.; Penfold, J., Adsorption of sodium dodecyl sulfate at the surface of aqueous solutions of poly(vinylpyrrolidone) studied by neutron reflection. *Langmuir* 1998, 14, (7), 1637-1645.
44. Richardson, R. M.; Pelton, R.; Cosgrove, T.; Zhang, J., A neutron reflectivity study of poly(n-isopropylacrylamide) at the air-water interface with and without sodium dodecyl sulfate. *Macromolecules* 2000, 33, (17), 6269-6274.
45. Wang, H.; Wang, Y. L.; Yan, H.; Zhang, J.; Thomas, R. K., Binding of sodium dodecyl sulfate with linear and branched polyethyleneimines in aqueous solution at different pH values. *Langmuir* 2006, 22, (4), 1526-1533.
46. Wesley, R. D.; Cosgrove, T.; Thompson, L.; Armes, S. P.; Baines, F. L., Structure of polymer/surfactant complexes formed by poly(2-(dimethylamino)ethyl methacrylate) and sodium dodecyl sulfate. *Langmuir* 2002, 18, (15), 5704-5707.
47. Zhang, J.; Thomas, R. K.; Penfold, J., Interaction of oppositely charged polyelectrolyte-ionic surfactant mixtures: Adsorption of sodium poly(acrylic acid)-

- dodecyl trimethyl ammonium bromide mixtures at the air-water interface. *Soft Matter* 2005, 1, (4), 310-318.
48. Feng, X. H.; Dubin, P. L.; Zhang, H. W.; Kirton, G. F.; Bahadur, P.; Parotte, J., Critical conditions for binding of dimethyldodecylamine oxide micelles to polyanions of variable charge density. *Macromolecules* 2001, 34, (18), 6373-6379.
49. Ranganathan, S.; Kwak, J. C. T., Effect of polymer charge density on the phase behavior of sodium poly(acrylate-co-acrylamide)-DTAB systems. *Langmuir* 1996, 12, (5), 1381-1390.
50. Shimizu, T.; Kwak, J. C. T., The binding of cationic surfactants by hydrophobic alternating copolymers of maleic-acid charge-density dependence. *Colloids and Surfaces a-Physicochemical and Engineering Aspects* 1994, 82, (2), 163-171.
51. Thalberg, K.; Lindman, B.; Bergfeldt, K., Phase-behavior of systems of polyacrylate and cationic surfactants. *Langmuir* 1991, 7, (12), 2893-2898.
52. Wang, C.; Tam, K. C., Interaction between polyelectrolyte and oppositely charged surfactant: Effect of charge density. *Journal of Physical Chemistry B* 2004, 108, (26), 8976-8982.
53. Yoshida, K.; Dubin, P. L. In *Complex formation between polyacrylic acid and cationic/nonionic mixed micelles: Effect of pH on electrostatic interaction and hydrogen bonding*, 1999; Elsevier Science Bv: 1999; pp 161-167.
54. Zhou, S. Q.; Burger, C.; Yeh, F. J.; Chu, B., Charge density effect of polyelectrolyte chains on the nanostructures of polyelectrolyte-surfactant complexes. *Macromolecules* 1998, 31, (23), 8157-8163.
55. Dubin, P. L.; Rigsbee, D. R.; Gan, L. M.; Fallon, M. A., Equilibrium binding of mixed micelles to oppositely charged poly-electrolytes. *Macromolecules* 1988, 21, (8), 2555-2559.
56. Rigsbee, D. R.; Dubin, P. L., Microcalorimetry of polyelectrolyte micelle interactions. *Langmuir* 1996, 12, (7), 1928-1929.
57. Kastner, U.; Zana, R., Interactions between quaternary ammonium surfactant oligomers and water-soluble modified guar. *Journal of Colloid and Interface Science* 1999, 218, (2), 468-479.
58. Fijan, R.; Sostar-Turk, S.; Lapasin, R., Rheological study of interactions between non-ionic surfactants and polysaccharide thickeners used in textile printing. *Carbohydrate Polymers* 2007, 68, (4), 708-717.
59. Anthony, O.; Marques, C. M.; Richetti, P., Bulk and surface behavior of cationic guar in solutions of oppositely charged surfactants. *Langmuir* 1998, 14, (21), 6086-6095.
60. Bahamdan, A.; Daly, W. H., Poly(oxyalkylene) grafts to guar gum with applications in hydraulic fracturing fluids. *Polym. Adv. Technol.* 2006, 17, (9-10), 679-681.
61. Hoare, T.; Pelton, R., Functional group distributions in carboxylic acid containing poly(n-isopropylacrylamide) microgels. *Langmuir* 2004, 20, (6), 2123-2133.
62. Favaro, Y. L.; Reinsborough, V. C., Micellar catalysis in mixed anionic/cationic surfactant systems. *Canadian Journal of Chemistry-Revue Canadienne De Chimie* 1994, 72, (12), 2443-2446.

63. Wang, C.; Tam, K. C.; Jenkins, R. D.; Tan, C. B., Interactions between methacrylic acid/ethyl acrylate copolymers and dodecyltrimethylammonium bromide. *Journal of Physical Chemistry B* 2003, 107, (19), 4667-4675.
64. Wiseman, T.; Williston, S.; Brandts, J. F.; Lin, L. N., Rapid measurement of binding constants and heats of binding using a new titration calorimeter. *Analytical Biochemistry* 1989, 179, (1), 131-137.
65. Wang, G.; Olofsson, G., Titration calorimetric study of the interaction between ionic surfactants and uncharged polymers in aqueous solution. *Journal of Physical Chemistry B* 1998, 102, (46), 9276-9283.
66. Wang, Y.; Chen, X. N.; Pelton, R., Interactions of hydrophobically modified polyvinylamine with pluronic triblock copolymer micelles. *Langmuir* 2006, 22, (11), 4952-4958.
67. Mears, S. J.; Deng, Y.; Cosgrove, T.; Pelton, R., Structure of sodium dodecyl sulfate bound to a poly(nipam) microgel particle. *Langmuir* 1997, 13, (7), 1901-1906.
68. Penfold, J.; Thomas, R. K.; Dong, C. C.; Tucker, I.; Metcalfe, K.; Golding, S.; Grillo, I., Equilibrium surface adsorption behavior in complex anionic/nonionic surfactant mixtures. *Langmuir* 2007, 23, (20), 10140-10149.
69. Penfold, J.; Staples, E.; Thompson, L.; Tucker, I.; Hines, J.; Thomas, R. K.; Lu, J. R., Solution and adsorption behavior of the mixed surfactant system sodium dodecyl sulfate/n-hexaethylene glycol monododecyl ether. *Langmuir* 1995, 11, (7), 2496-2503.
70. Hayter, J. B.; Penfold, J., An analytic structure factor for macroion solutions. *Mol. Phys.* 1981, 42, (1), 109-18.
71. Hayter, J. B.; Penfold, J., Self-consistent structural and dynamic study of concentrated micelle solutions. *J. Chem. Soc., Faraday Trans. 1* 1981, 77, (8), 1851-63.
72. Hansen, J. P.; Hayter, J. B., A rescaled msa structure factor for dilute charged colloidal dispersions. *Mol. Phys.* 1982, 46, (3), 651-656.
73. Bergstrom, M.; Pedersen, J. S., A small-angle neutron scattering (sans) study of tablet-shaped and ribbonlike micelles formed from mixtures of an anionic and a cationic surfactant. *Journal of Physical Chemistry B* 1999, 103, (40), 8502-8513.
74. Gittings, M. R.; Cipelletti, L.; Trappe, V.; Weitz, D. A.; In, M.; Marques, C., Structure of guar in solutions of h<sub>2</sub>o and d<sub>2</sub>o: An ultra-small-angle light-scattering study. *Journal of Physical Chemistry B* 2000, 104, (18), 4381-4386.
75. McNeil, M.; Szalecki, W.; Albersheim, P., Quantitative methods for determining the points of ortho-(carboxymethyl) substitution in ortho-(carboxymethyl)-guar. *Carbohydrate Research* 1984, 131, (1), 139-148.

## Chapter 5 HPG-Borate and Modified Guar Interactions with Lysozyme

### Abstract

The interactions of HPG-borate and modified guar with lysozyme were studied using turbidity measurement, electrophoretic mobility, dynamic light scattering, isothermal titration calorimetry and surface plasmon resonance. Although borate ion condensation on HPG converted HPG into a negatively charged polyelectrolyte, HPG-borate behaved differently from typical polyelectrolytes. HPG-borate does not interact with oppositely charged lysozyme at both pH 7.4 and pH 9.2, corresponding respectively to low charge density and high charge density on HPG polymer chains. The presence of salt screens the electrostatic attraction between HPG-borate and lysozyme. By contrast, carboxymethyl guar forms insoluble complexes with lysozyme at low polymer concentrations, or colloids at high polymer concentrations and low salt concentrations. Salt concentration has a great effect on the electrostatic interaction of oppositely charged HPG-borate or CMG, with lysozyme. Hydrophobically modified guar forms complexes with lysozyme, as detected by isothermal titration calorimetry, implying hydrophobic interaction between them.

## 5.1 Introduction

HPG-borate may or may not behave as a typical polyelectrolyte as has been described in Chapter 3 and Chapter 4. For example, HPG-borate behaves like a typical polyelectrolyte in forming complexes with oppositely charged poly(diallyldimethyl) ammonium chloride (PDADMAC)<sup>1</sup> and flocculating cationic polystyrene latex.<sup>2</sup> By contrast, it deviates from typical polyelectrolyte behavior by inducing no micellization of cationic surfactant dodecyltrimethyl ammonium bromide (DTAB) below the critical micelle concentration (cmc) of the surfactant.<sup>3</sup> Further, in polyelectrolyte titration, neutralization of HPG-borate by PDADMAC induced further binding of borate onto HPG polymer chains.<sup>1</sup> Fructose competitive binding, or lowering of the pH, results in detachment of the borate from the HPG polymer chains.<sup>2</sup> Because borate can attach to, and detach from, HPG polymer chains upon environment stimulation, we classify HPG-borate a labile polyelectrolyte, different from conventionally defined (strong and weak) polyelectrolytes.

However, labile polyelectrolyte HPG-borate interactions with one of the most important tear film components – proteins, have rarely been studied. Proteins exist mainly in the aqueous phase of the tear film.<sup>4, 5</sup> Among these proteins, lysozyme is one of the most abundant<sup>6</sup> and important, and is positively charged at physiological conditions.<sup>7</sup> Therefore, lysozyme is a good model protein in studying HPG-borate interaction with proteins. Does HPG-borate behave as a polyelectrolyte to form complexes with lysozyme or not?

Lysozyme is abundant in chicken egg white. Chicken egg white lysozyme is similar in structure to human lysozyme<sup>8</sup> and is one of the most studied proteins.<sup>9</sup> Chicken egg white lysozyme is a globular protein with a size of 3nm×3nm×4.5nm and apparent Stokes radius of 2nm.<sup>10, 11</sup> Its primary structure consists of 129 amino acid residues and four disulfide bonds<sup>8, 12, 13</sup> with molecular weight of about 14600 Dalton with a well – determined sequence.<sup>14</sup> Blake et al<sup>7</sup> first reported the secondary structure of lysozyme, which can be divided into two parts: an  $\alpha$  domain at one side with a core of hydrophobic side groups, and a  $\beta$  domain at the other side (see Figure 5.1).<sup>9</sup> The isoelectric point of lysozyme is about 11.<sup>15</sup> At neutral pH it has seventeen positive charges and nine negative charges yielding a total of eight positive net charges.<sup>16</sup> At the lysozyme surface, there are about 6.8 positive net charges at pH 7.4<sup>17, 18</sup> and 6 positive net charges at pH 9.<sup>19</sup> Because most of the hydrophobic side groups are buried inside the  $\alpha$  domain, only 11% of the hydrophobic side groups are exposed to the surface<sup>20</sup>, residing mainly at the  $\beta$  domain; there are hydrophobic side groups such as in residue 62 of Tryptophan.<sup>12, 21, 22</sup>

Polymer and protein interaction has long been an interesting subject due to its application to the food industry, especially the dairy industry.<sup>23-29</sup> Polymers may serve to stabilize proteins or precipitate proteins via formation of complexes with proteins. However, complexes of polymer and protein can be soluble.<sup>29-34</sup> Although few techniques

have been used to investigate precipitation, soluble complexes can be studied by techniques such as turbidity measurement, electrophoretic mobility, dynamic light scattering and static light scattering.<sup>35</sup> In addition, isothermal titration calorimetry, surface plasmon resonance, quartz crystal microbalance and fluorescence have also been used to probe complex formation.<sup>30</sup> Theoretical methods were developed to study the mechanism involving interaction forces and complex structures.<sup>32, 36-42</sup> Electrostatic interactions and hydrophobic effects are the major contributions to the interaction of polymer and protein, especially for polyelectrolyte and oppositely charged protein.<sup>28, 30, 43-45</sup> The strength of complex formation was affected by the linear charge density of the polyelectrolyte and the global charge density of the protein that depends on chain flexibility and salt concentration.<sup>30, 34, 44</sup>

Petit et al.<sup>11</sup> studied the interaction of lysozyme with copolymers of hydrophobically modified poly(sodium acrylate) and poly(sodium acrylate) at pH 9, and concluded that hydrophobic effects contributed to polymer-lysozyme binding while electrostatic interaction did not. Although their experimental results confirmed their conclusion, they ignored salt effects on electrostatic interactions. The strength of the electrostatic interaction between lysozyme and the polymer was screened by salts, so that it seemed that there was no electrostatic interaction between them. Therefore, the hydrophobic effects appeared to dominate in their interaction. Interactions between sulfated chitosan and lysozyme showed that they formed complexes due to electrostatic attraction.<sup>46</sup> Complexes were formed at low salt concentration, and were seen to be dissociated at high salt concentration, indicating that salt concentration strongly affects the electrostatic interaction between polymer and lysozyme. Lysozyme interaction with poly(acrylic acid) microgel should depend on pH, and the salt concentration, indicated that electrostatic forces are also significant in their interactions.<sup>15</sup> Interaction between potassium poly(vinyl alcohol) sulfate (PVSK) and lysozyme was also studied; they were shown to form complexes with PVSK through electrostatic interaction in salt-free systems by the use of light scattering techniques.<sup>47, 48</sup> It was proposed that neutralization of PVSK with lysozyme led to aggregation of the complexes, forming uniformly larger aggregates. In the neutral polymer poly(N-isopropylacrylamide) interaction with lysozyme, it was suggested that hydrophobic interaction dominates.<sup>45</sup> Studies have shown that tryptophan residues on lysozyme contributed to hydrophobic interaction with hydrophobic groups on polymers.<sup>49</sup>

Previous dynamic light scattering work from our laboratory showed that there was a slight and slow interaction between HPG-borate and lysozyme under conditions close to the human tear fluid.<sup>50</sup> But a more detailed study of HPG-borate and lysozyme interactions is needed to clarify the mechanism of their interactions. The goal of this work is to define the conditions under which HPG-borate/lysozyme complexes form. Complexation was monitored with various techniques such as turbidity measurement, electrophoretic mobility, dynamic light scattering (DLS), isothermal titration calorimetry (ITC) and surface plasmon resonance (SPR). For comparison, carboxymethyl guar (CMG)

and hydrophobically modified guar (HMG) were also used to probe electrostatic interaction and hydrophobic interaction with lysozyme.

## 5.2 Experimental

### 5.2.1 Materials

Lysozyme from chicken egg white was purchased from Sigma-Aldrich and used without further purification. Hydroxypropyl guar (HPG) with 0.36 hydroxypropyl groups per sugar ring and molecular weight of  $1.75 \times 10^6$  Da was provided by Alcon Laboratories, Fort Worth, Texas. Carboxymethyl guar with degree of substitution (DS) 0.39 (0.39 carboxymethyl groups per sugar ring) and hydrophobically modified guar with DS 0.13 were synthesized as described in Chapter 1.

Sodium borate ( $\text{Na}_2\text{B}_4\text{O}_7 \cdot 10\text{H}_2\text{O}$ ) was purchased from Anachemia. Boric acid was purchased from Caledon Laboratories Ltd. *N*-(3-Dimethylaminopropyl)-*N*'-ethylcarbodiimide hydrochloride (EDC), 4-(2-hydroxyethyl)-1-piperazineethanesulfonic acid (HEPES), *N*-Hydroxysuccinimide (NHS), 2-(*N*-morpholino)ethanesulfonic acid (MES hydrate), hexyl amine, ethanolamine sodium hydroxide, NaOH, HCl and NaCl were purchased from Sigma-Aldrich. Standard titrant solution of potassium polyvinyl sulfate (PVSK) ( $1 \times 10^{-3}$  eq/L) with molecular weight of 19,100 Da was purchased from BTG Americas Inc. All samples were prepared in MilliQ water.

### 5.2.2 Methods

#### Preparation of Mixtures of HPG or Modified Guar with Lysozyme

HPG or modified guar and lysozyme mixtures were prepared in HEPES buffer or borate buffer. The salt concentration and pH were adjusted using NaCl, NaOH and HCl. The mixtures stood for 24 hours before measurements.

#### Turbidity Measurement

Absorbance of mixtures was measured using DU 800 Beckman Coulter UV Spectrophotometer at room temperature. The wavelength was fixed at 500 nm. High absorbance value represents high turbidity.

#### Electrophoretic Mobility

Electrophoretic mobility of mixtures was measured using Brookhaven Zetaplus Zeta Potential Analyzer operating in phase analysis light scattering mode with BIC Pals Zeta Potential Analyzer software (version 2.5). A total of 10 runs (15 cycles per run) were

performed at room temperature, and the mean and standard deviation of these runs were shown.

### **Dynamic Light Scattering**

Particle sizes of samples were measured using a Brookhaven Dynamic Light Scattering Instrument with a BI-9000AT autocorrelator, 35 mW laser with wavelength of 632.8nm at a scattering angle of 90°. Sample data were acquired using BIC dynamic light scattering software 9kdls32 (version 3.34). A cumulative statistical method was used to analyze the data. The sample cell temperature was controlled at 25°C with a NESLAB water bath.

### **Isothermal Titration Calorimetry (ITC)**

A Microcal VP-ITC microcalorimeter was used to measure the heat released or absorbed as a result of the interaction of HPG-borate or modified guar with lysozyme. Typically 297  $\mu\text{L}$  of titrant was loaded into the syringe and 1.431 mL of the sample was loaded into the titration cell. The reference cell was filled with MilliQ water. Both titrant and sample solutions were degassed before titration, using Microcal Thermovac sample degassing equipment. The titration was controlled with VPViewer 2000 ITC software. The release or absorption heat per injection (10  $\mu\text{L}$  of titrant was injected for each injection) was calculated by integrating the raw data of injection heat over time using Microcal ITC Data Analysis software (Origin 7.0). Titrants and samples were prepared in the same buffers. Blank tests of titrant injected into buffers were also conducted. All results were obtained after subtraction of blank test results.

### **Surface Plasmon Resonance (SPR) Experiment**

A Biacore Inc. 3000 surface plasmon resonance instrument was used to detect HPG-borate or CMG binding to lysozyme. A gold chip purchased from Biacore Inc. with gold thickness of 50 nm, coated with 100 nm of carboxymethyl dextran monolayer, was employed to immobilize the lysozyme and detect the binding of HPG-borate or CMG with lysozyme.

The lysozyme on the chip was immobilized by the reaction of amine groups in the lysozyme with carboxyl groups in carboxymethyl dextran, in the presence of EDC/NHS. The order of immobilization was: first a mixture of 100  $\mu\text{L}$  of EDC (0.39 mol/L) with 100  $\mu\text{L}$  NHS (0.1 mol/L) was injected over the chip at a flow rate of 10  $\mu\text{L}/\text{min}$  to activate the carboxyl groups. Then 0.1g/L of lysozyme in 0.01mol/L acetate buffer at pH 5.0 was injected over the chip at a flow rate of 10  $\mu\text{L}/\text{min}$  until a response of over 7,000 was achieved. Then 1 mol/L ethanolamine was injected over the chip to block any remaining activated carboxyl groups on carboxymethyl dextran. Finally, regeneration buffer (1mol/L NaCl in 0.001mol/L HCL) was injected over the chip to remove any non-covalently bound molecules.

HPG samples were prepared in 0.01 mol/L HEPES buffer and 0.15 mol/L NaCl at pH 7.4 and in 0.05 mol/L boric acid and 0.15 mol/L NaCl at pH 7.4, 8.0 and 9.0. CMG samples were prepared in 0.01 mol/L HEPES buffer and 0.15 mol/L NaCl at pH 7.4. For each run, 250  $\mu$ l of the sample was injected over the chip at a flow rate of 5  $\mu$ l/min. This ensured an adsorption equilibrium time of up to 50 minutes. Then, the same buffer was injected over the chip to remove the free polymers. The response of the chip upon adsorption and desorption of polymer was recorded using a Biacore 3000 software. After the runs, the chip was washed with 1 mol/L NaCl in 0.001 mol/L HCl to clean the binding polymers for the next injection. For each experiment, two runs were repeated.

## 5.3 Results

Three forms of guar, HPG-borate, carboxymethyl guar (CMG) and hydrophobically modified guar (HMG) were compared in terms of interaction with lysozyme. The polymer structures were shown in Chapter 2. We anticipated that CMG and HPG-borate would display electrostatic interaction with cationic lysozyme, whereas HMG would show hydrophobic interaction with lysozyme.

### 5.3.1 CMG Interaction with Lysozyme

#### 5.3.1.1 CMG Interaction with Lysozyme at Low Ionic Strength

Complex formation between oppositely charged polyelectrolyte and protein is usually accompanied by phase separation.<sup>29, 30, 33, 38, 44</sup> Therefore, turbidity can be a sensitive measure of complex formation. We measured the turbidity of mixtures of lysozyme and CMG with concentrations ranging from 0.0031 g/L to 0.5 g/L, at pH 7.4 in NaCl concentration as low as 0.01 mol/L. We observed clear solutions at CMG concentrations below 0.031 g/L, precipitates with CMG concentrations between 0.031 g/L and 0.125 g/L, and colloids at CMG concentrations above 0.125 g/L. As shown in Figure 5.2, absorbance of supernatants of the mixtures changed from 0.04 to 0.01 and then to above 0.1. This conformed to what we observed visually.

Because lysozyme is positively charged, CMG adsorption on lysozyme may convert lysozyme surface charge from positive to negative. This can be detected by electrophoretic mobility. As shown in Figure 5.3, at CMG concentrations as low as 0.0031 g/L, the electrophoretic mobility was  $0.6 \times 10^{-8} \text{ m}^2/\text{Vs}$ , a value close to the mobility of pure lysozyme. With increasing CMG concentration, the mobility was converted to negative value, remaining at approximately  $-2 \times 10^{-8} \text{ m}^2/\text{Vs}$ .

We could not get useful information by dynamic light scattering for CMG concentrations as low as 0.0031 g/L because of the poor fits to the autocorrelation functions. Also, in CMG concentrations that formed precipitates, no good correlation functions were obtained. But for those colloids at CMG concentrations higher than

0.125g/L, DLS gave a good fit to the autocorrelation functions and narrow particle size distributions, as shown in Figure 5.4. Particle sizes of those colloids were above 200 nm, as shown in Table 5.1. From the experiments of CMG interaction with lysozyme at low salt concentration, we can see that at CMG concentrations between 0.031g/L and 0.125g/L, CMG formed insoluble complexes with lysozyme by electrostatic attraction. At CMG concentrations higher than 0.125g/L, colloids with a uniform particle size were formed.

### 5.3.1.2 Salt Effect on CMG Interaction with Lysozyme

Salt concentration is an important factor influencing polyelectrolyte and protein interaction. No insoluble complexes or colloids formed when mixing CMG and lysozyme in HEPES buffer of pH 7.4 at a NaCl concentration as high as 0.10mol/L. Therefore, CMG and lysozyme mixtures in NaCl concentrations ranging from 0 mol/L to 0.1 mol/L were prepared and measured as well. As we can see from Figure 5.5, the absorbance of the mixtures of CMG and lysozyme at a CMG concentration of 0.1 g/L decreased from about 0.5 to below 0.05 as the NaCl concentrations increased from 0 to 0.1 mol/L (note that samples were measured before precipitation). But the curve is not monotonous. There is a maximum affinity between the CMG and lysozyme in 0.01 mol/L of NaCl concentration. This is because of the anisotropy of the electrostatic domains in the protein. When the Debye length is larger than half the lysozyme diameter, salt screens the electrostatic repulsions more than the attractions.<sup>51</sup> The electrophoretic mobility decreased from above  $-2 \times 10^{-8} \text{ m}^2/\text{Vs}$  to about  $-1 \times 10^{-8} \text{ m}^2/\text{Vs}$  with the increase of NaCl concentration, as shown in Figure 5.6. By visual observation, flocculates and colloids disappeared gradually with increasing NaCl concentration.

Although we did not observe the formation of insoluble complexes or colloids upon mixing CMG and lysozyme in high salt concentration of solutions, soluble complexes can be shown to form.<sup>29-31, 33, 34</sup> Formation of soluble complexes can be detected using ITC, which can measure the heat generated from complex formation. A typical result is that at low molar ratio of ligand to sample, heat is detected, decreasing gradually to about zero as more ligands are injected. Because we expected electrostatic interaction of CMG and HPG-borate with lysozyme, the charge ratio was used instead of the molar ratio. Charge ratios of CMG or HPG-borate to lysozyme were calculated.

From the ITC experiments shown in Figure 5.7, we can see that at high NaCl concentration (0.1mol/L), no heat was released or absorbed by titrating 0.5g/L CMG to 0.3g/L lysozyme (see appendix B.1 for charge density on lysozyme). But in the absence of NaCl, the interaction of CMG with lysozyme was accompanied by released heat. CMG interaction with lysozyme is an exothermic process. A one-site model (refer to appendix B.2) was applied to the titration curve of CMG to lysozyme (refer to appendix B.3 for charge ratio calculation), from which it was found that CMG binding with lysozyme released  $1372 \pm 18$  cal/mol heat, indicating a very weak electrostatic interaction. The entropy gain for this interaction was 28.4 cal/mol K (refer to

appendix B.4 for an example calculation).

To further study whether CMG and lysozyme form soluble complexes at high salt concentrations, surface plasmon resonance (SPR) was employed. This is a sensitive technique for detecting binding of proteins with polysaccharides. Rather than detecting the interaction in solution, SPR detects the CMG and lysozyme interaction at the solid/liquid interface, with lysozyme immobilized at the solid surface as described above. By monitoring the surface plasmon response, the interaction of CMG with lysozyme was investigated. As shown in Figure 5.8, injection of CMG over the chip in HEPES buffer and borate buffer, at pH 7.4 and NaCl concentration 0.15mol/L, induced a surface plasma response as low as about 50 and 140 respectively. After 50 minutes equilibration, buffers were injected and the CMG adsorbed on the chip was nearly all washed away immediately<sup>52</sup>. These results indicate that lysozyme cannot interact with CMG through electrostatic attraction at high NaCl concentration.

### 5.3.2 Hydrophobically Modified Guar Interaction with Lysozyme

To investigate hydrophobic interaction between HPG and lysozyme, hydrophobically modified guar interaction with lysozyme was studied. Lysozyme has amino acid residues containing hydrophobic groups exposed to the globular lysozyme surface.<sup>53</sup> Therefore, hydrophobic groups on the lysozyme surface may interact with hydroxypropyl group in HPG.

Because lysozyme has low mobility and the hydrophobically modified guar was not charged, electrophoretic mobility could not generate any useful information. Further, the interaction between lysozyme and hydrophobically modified guar is so weak that turbidity measurement and DLS cannot detect complex formation.

However, ITC can give information on complex formation via hydrophobic interaction. As can be seen from Figure 5.9, injecting lysozyme into HMG releases heat. By applying the one-site model to the titration curve, we deduce that the interaction of HMG and lysozyme is an exothermic process, generating  $828.9 \pm 60$  cal/mol apparent heat, indicating a weak hydrophobic interaction. The entropy gain for the interaction was 18.2 cal/mol K.

### 5.3.3 HPG-Borate Interaction with Lysozyme

#### 5.3.3.1 Determination of Charge Content on HPG Polymer Chain

In electrostatic interactions between oppositely charged polyelectrolyte and protein, both protein charge density and polyelectrolyte charge density are important factors in the interaction.<sup>44</sup> Therefore estimation of charge content on HPG at varying pH, HPG concentrations and total boron concentrations is necessary. Here we use total boron

concentration because boric acid may dissociate into borate ion in solution, with borate concentration depending on pH, whereas total boron concentration does not change with pH. It is commonly accepted that borate can bind with cis-diols such as those on HPG, whereas boric acid cannot. Borate and HPG binding can be represented as in equation (1):

$$K_1 = \frac{[BP]}{[BOH][P]} \quad (1)$$

where  $K_1$  is the binding constant of borate with HPG, 100L/mol according to Jasinski's binding constant<sup>54</sup> (because we believe that only one binding site on galactose in HPG molecule binds with borate);  $[BP]$  is the concentration of borate bound on the HPG polymer chain;  $[BOH]$  is the concentration of free borate; and  $[P]$  is the concentration of free borate binding sites on HPG. Here we calculated  $[BOH]$  according to the boron balance equation (2) and boric acid/borate equilibrium equation (3):

$$B_T = [B] + [BOH] \quad (2)$$

$$K_0 = \frac{[BOH]}{[B][OH]} \quad (3)$$

where  $B_T$  is the total boron concentration;  $[B]$  is the concentration of boric acid;  $K_0$  is dissociation constant of boric acid which can be calculated from the pKa of boric acid (9.2) as shown in equation (4):

$$K_0 = 10^{14-pKa} \quad (4)$$

$[OH]$  is the free hydroxyl ion concentration which can be calculated from the pH as shown in equation (5):

$$[OH] = 10^{pH-14} \quad (5)$$

and  $[P]$  can be calculated by polymer balance shown as follows:

$$P_T = [BP] + [P] \quad (6)$$

where  $P_T$  is the total concentration of HPG binding sites.

Combining equation (1)-(6),  $[BP]$ , which is borate concentration bound on HPG polymer chain can be determined as long as we know the pH, HPG concentration and the total boron concentration.

By calculation, the charge density on the HPG polymer chain with a total boron concentration of 0.04 mol/L at pH 7.4 is about 0.09 meq/g, corresponding to DS 0.017 (borate substitution per HPG sugar ring), while at pH 9.2 it is about 1.02 meq/g, corresponding to DS 0.19. We can see that although at pH 7.4 the charge content of borate (0.017) on HPG is much lower than that of CMG (0.39), at pH 9.2 they are comparable (0.19 for HPG vs 0.39 for CMG). We therefore conducted the same experiments at both pH 7.4 and pH 9.2, to compare the interactions of labile polyelectrolyte, HPG-borate, to weak polyelectrolyte CMG.

It should be noticed that here we used borate/HPG binding constant 100 L/mol based on the assumption: (1) borate only binds with galactose; (2) ideal solution behavior; (3) ignore the cross-linking reaction of HPG with borate. Example calculation refers to appendix B.5.

### 5.3.3.2 Experimental Results of HPG-Borate Interaction with Lysozyme

HPG and lysozyme mixtures in the presence of borate at both pH 7.4 and 9.2, and NaCl concentration of both 0.10mol/L and 0.01mol/L, were prepared. In appearance, no turbidity change was observed with the increase of HPG concentration from 0.003g/L to 0.5g/L. By measuring absorbance of the mixtures at 500 nm wavelength as shown in Figure 5.10, we showed that absorbance of mixtures was below 0.005 at an HPG concentration of 0.003 g/L, and only a little higher (below 0.05) at an HPG concentration of 0.5g/L. Turbidity was very low, with really clear solutions, for HPG concentrations from 0.003g/L to 0.5g/L. Turbidity measurements indicated no formation of insoluble HPG-borate/lysozyme complexes.

Electrophoretic mobility shows little change with HPG concentration, increasing from 0.003g/L to 0.5g/L for both pH values and both NaCl concentrations in the HEPES and borate buffers, as shown in Figure 5.11. No complex formation can be detected by electrophoretic mobility.

ITC was also employed to detect HPG-borate and lysozyme interactions. As shown in Figure 5.12, even at a low charge ratio of HPG-borate to lysozyme, the apparent heat (released or absorbed) is below 0.3 kcal/mol for each injection (each point representing one injection) as low as that of the dilution of HPG solution. No apparent heat exchange due to HPG-borate and lysozyme interaction was detected.

SPR was also employed to detect the interaction of HPG-borate and lysozyme in 0.15 mol/L NaCl solutions. From Figure 5.13, we can see that in the absence of borate, HPG was adsorbed onto the chip with a plasma response of only about 50. After 5 minutes adsorption, the chip was rinsed with the same buffer and nearly all the HPG was immediately rinsed off the chip, indicating very low HPG adsorption<sup>52</sup>. In the presence of boric acid at pH 7.4, HPG was adsorbed onto the chip with a plasma response of as low as 10. After 50 minutes adsorption, the chip was rinsed with the same buffer and almost all

the HPG was immediately rinsed off the chip. Although the borate presence increased the initial HPG adsorption to above 200 and 400 at pH 8.0 and 9.0 respectively, after 50 minutes adsorption, the same buffer was used to rinse the chip and nearly all the HPG was immediately rinsed off the chip. These SPR results show that HPG-borate does not bind with lysozyme in high salt concentration solutions.

## 5.4 Discussion

Negatively charged polyelectrolytes bind with oppositely charged proteins to form complexes, either soluble or insoluble, by electrostatic attraction. The insolubility of a complex can be due either to the insolubility of the primary complexes or to their further aggregation.<sup>30, 33, 34, 44</sup> CMG and lysozyme form insoluble complexes in low CMG concentrations, and form colloids in high CMG concentrations, via electrostatic attraction at low salt concentrations. The fact that this attraction was screened by salt addition further confirms the electrostatic attraction between them. In contrast, HPG-borate does not interact with lysozyme, as was demonstrated by the experiments above. HPG-borate and lysozyme mixtures appear not to form insoluble complexes, as seen in the turbidity measurements. ITC experiments detected no heat released or absorbed when HPG-borate was used to titrate lysozyme, implying that no soluble complexes had formed between them. SPR experiments confirmed that HPG-borate does not bind with lysozyme at high salt concentrations. ITC and SPR experiments indicate that neither enthalpy nor entropy contributes to the interaction of HPG-borate and lysozyme.

We will now list some factors affecting the HPG-borate/lysozyme interactions.

Firstly, both polyelectrolyte linear charge density and protein global charge density affect polyelectrolyte and protein interactions.<sup>30, 33, 34, 44</sup> By comparing CMG and HPG-borate, although the charge content (borate ions) of the HPG polymer chain at pH 7.4 is low, at pH 9.2 it is comparable to that of CMG. As for the protein charge density, lysozyme has 6 net positive surface charges at pH 9.2<sup>19</sup> and 6.8 at pH 7.4.<sup>17, 18</sup> Hence, lysozyme has similar surface charge at pH 9.2 and pH 7.4. With regard to polyelectrolyte linear charge density and lysozyme global charge density, HPG-borate and CMG should behave similarly when they interact with lysozyme. Hence, the non-binding of HPG-borate with lysozyme is neither a function of the polyelectrolyte linear charge density nor the lysozyme global charge density.

Secondly, polymer chain flexibility is an important factor in polyelectrolyte/protein interactions.<sup>44</sup> Because both CMG and HPG are both derived from guar, their chain flexibility should be similar. Hence, chain flexibility cannot be the reason why HPG-borate does not bind with lysozyme.

Finally, salt concentration is an important factor in the electrostatic interaction between guar and lysozyme.<sup>51</sup> From experimental results, we can see that salt

concentration strongly affects the interaction between CMG and lysozyme. But it seems from our work that interaction between HPG-borate and lysozyme does not occur at any salt concentration. Theoretically, there is a critical salt concentration that controls the adsorption behavior of polyelectrolyte on spheres. When the salt concentration of the solution is below the critical salt concentration, polyelectrolytes can adsorb on spheres. However, above this critical salt concentration, polyelectrolytes cannot adsorb on spheres.<sup>55-57</sup> In the interactions of HPG-borate and CMG with lysozyme, we can assume that the lysozyme molecule is a sphere. According to Muthukumar's model as shown in equation (7),<sup>58-60</sup> critical salt concentration is related to both polyelectrolyte and sphere charge density:

$$\kappa^3 = \frac{12\pi e_o \alpha \sigma_o}{\varepsilon b_{eff} b k_b T} (1 - \exp(-2\kappa a)) \quad (7)$$

where  $e_o$  is the elementary charge;  $k_b$  is Boltzmann constant;  $T$  is absolute temperature (298 K);  $\varepsilon$  is water permittivity;  $\alpha$  is the DS of borate per HPG sugar ring;  $a$  is the radius of the lysozyme molecule (2nm);  $b$  is the Kuhn length of HPG polymer chain, which is twice its persistence length for semi-flexible polymers. Because the persistence length of HPG is a little larger than that of guar (10nm),<sup>61</sup> we assume it to be 12 nm;  $b_{eff}$  is the effective step length, which can be calculated by equation (8)<sup>58, 62</sup>:

$$b_{eff} = C_\infty l_o \quad (8)$$

where  $C_\infty$  is the characteristic ratio of HPG (13),<sup>62</sup>  $l_o$  is the length of the monomer unit of HPG (0.54 nm).<sup>62</sup>

In equation (7),  $\sigma_o$  is the charge density of the lysozyme sphere surface. Because lysozyme has 6 net positive surface charges at pH 9.2<sup>19</sup> and 6.8 at pH 7.4<sup>17, 18</sup>, we assume an average net positive surface charge of 6.4 from pH 7.4 to 9.2. Hence, the lysozyme surface charge density can be calculated as in equation (9):

$$\sigma_o = \frac{6.4e_o}{4\pi a^2} \quad (9)$$

Also in equation (7),  $\kappa$  is the inverse of the Debye length. The calculation of  $\kappa$  is given by equation (10):

$$\kappa = \sqrt{\frac{e_o^2 N_{av}}{\varepsilon k_b T} 2c} \quad (10)$$

where  $N_{av}$  is Avogadro constant,  $c$  is salt concentration.

From equation (7), we can calculate the critical salt concentrations of the HPG-borate/lysozyme interaction as a function of the DS of borate per sugar ring (for a detailed calculation, refer to appendix B.6), plotted as data points for HPG-borate in Figure 5.14 (a). Because HPG-borate has a DS 0.017 (0.017 borate per HPG sugar ring) at pH 7.4, and 0.19 at 9.2, these give the data points in the critical salt concentration curve of Figure 5.14(a). The other four data points in Figure 5.14(a) are experimental salt concentrations in HPG-borate/lysozyme solutions with initial salt concentrations of 0.01 and 0.1 mol/L at pH 7.4 and 9.2, respectively. The salt concentrations are due to the initial salt concentrations, plus the NaOH and sodium borate added to increase the pH. From Figure 5.14(a), we can see that salt concentrations in experimental conditions for HPG-borate/lysozyme interactions are all higher than the critical salt concentration data points at both pH 7.4 and 9.2. We conclude that the HPG-borate/lysozyme electrostatic interaction is screened by salt.

In addition, the critical salt concentrations for the CMG/lysozyme interaction are constant because the average carboxymethyl groups per sugar ring are constant (0.39). In Figure 5.14(b), here concentrations for CMG also plotted. But as shown in Figure 5.14(b), as long as salt concentrations are lower than about 0.02 mol/L, CMG can interact with lysozyme through electrostatic interaction. Therefore the CMG/lysozyme interaction can be detected at a solution salt concentration of 0.01 mol/L, but not at a solution salt concentration of 0.1 mol/L.

## 5.5 Conclusions

1. HPG-borate does not form soluble or insoluble complexes with lysozyme at lysozyme concentrations from 0.1 g/L to 0.5 g/L. Neither entropy nor enthalpy contributes to complex formation.
2. CMG can form insoluble complexes or colloids with lysozyme via electrostatic attraction at low salt concentrations. Beyond the critical salt concentration, electrostatic attractions between CMG and lysozyme interactions were screened.
3. Hydrophobic interaction was detected using hydrophobically modified guar and lysozyme by ITC.
4. The reason for non-binding between oppositely charged HPG-borate and lysozyme is that the critical salt concentration for HPG-borate adsorption onto lysozyme is always below the ambient salt concentrations of the borate buffer.

## 5.6 Tables

**Table 5.1** DLS measurement of hydrodynamic diameter of CMG and lysozyme (0.3g/L) at pH 7.4, 0.01mol/L NaCl in 0.05mol/L HEPES buffer.

CMG conc./gL <sup>-1</sup>	Hydrodynamic diameter/nm
0.5	251.6±15.5
0.25	231.6±13.9
0.125	209.1±7.9

## 5.7 Figures

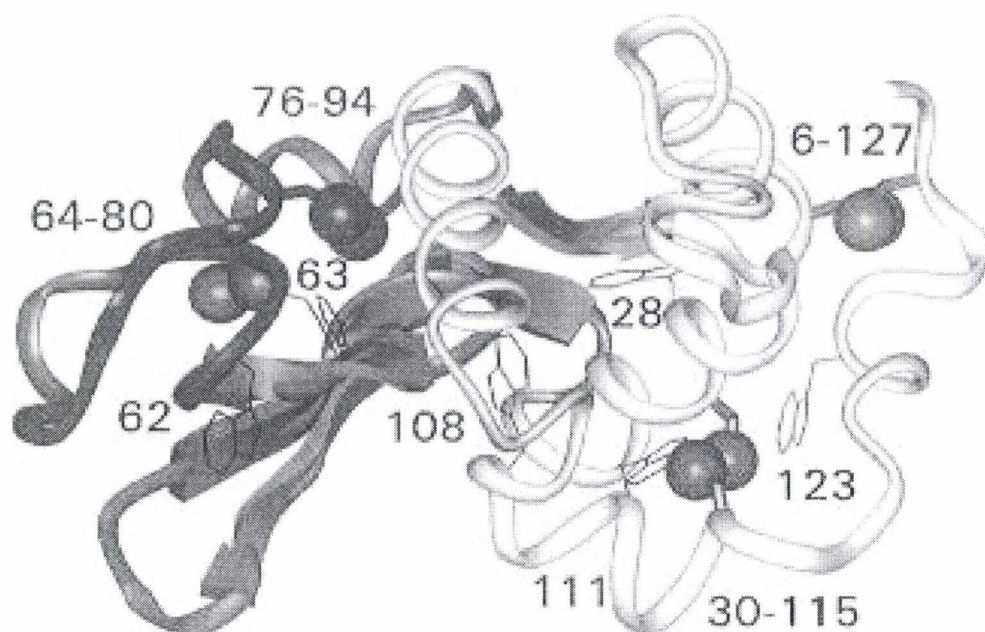


**Figure 5.1** Structure of hen egg white lysozyme (Adapted from Rothwarf 1996, see reference 12). The right white part and left black part represents  $\alpha$  domain and  $\beta$  domain respectively. The hydrophobic tryptophan side chains are shown. The double balls represent disulfide bonds.

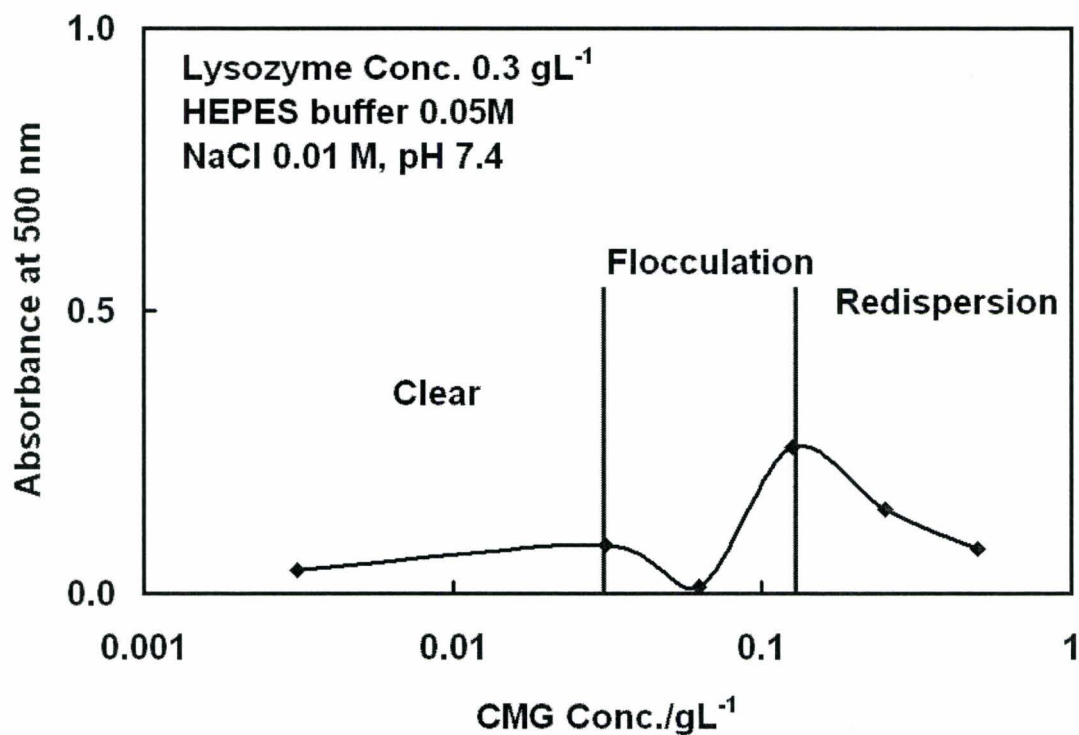


Figure 5.2 Turbidity measurement of CMG and lysozyme as a function of CMG concentration.

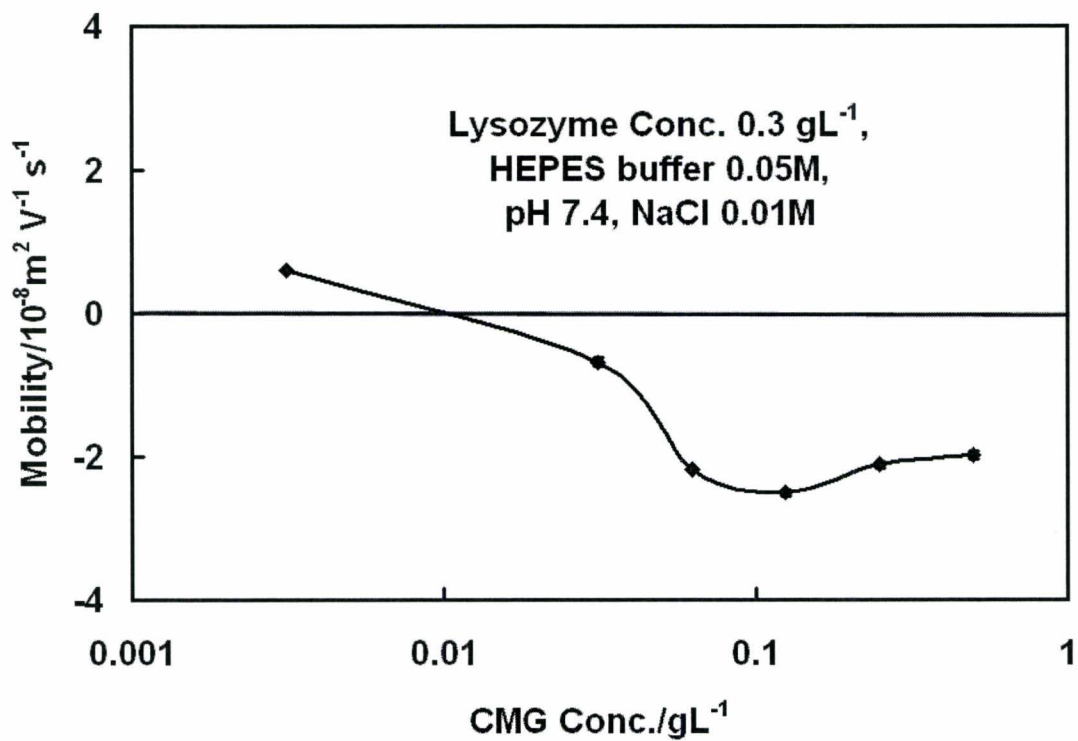
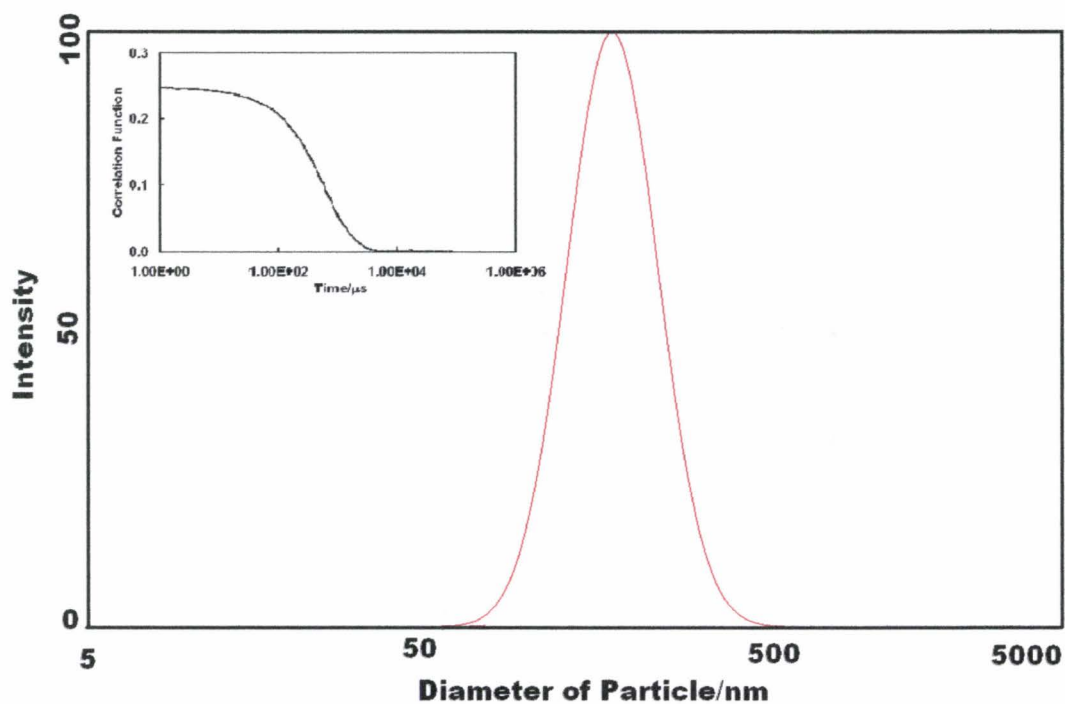


Figure 5.3 Electrophoretic mobility measurement of CMG and lysozyme as a function of CMG concentration.



**Figure 5.4 Particle Size Distribution and Correlation Function (Inlet) of Dynamic Light Scattering of 0.125 g/L CMG with 0.3 g/L Lysozyme at pH 7.4, NaCl Concentration of 0.01mol/L in 0.05mol/L HEPES Buffer, poly 0.113, intensity 235.7 kcps, average particle size 216.8 nm.**

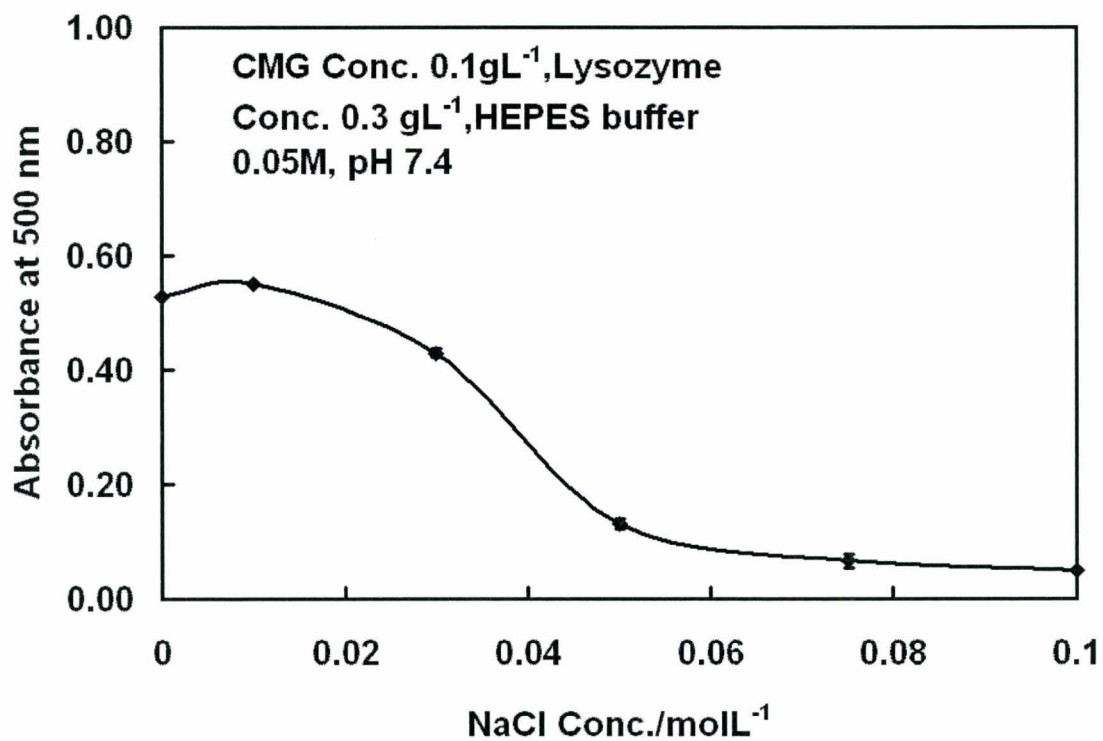


Figure 5.5 Salt effect on turbidity of CMG and lysozyme.

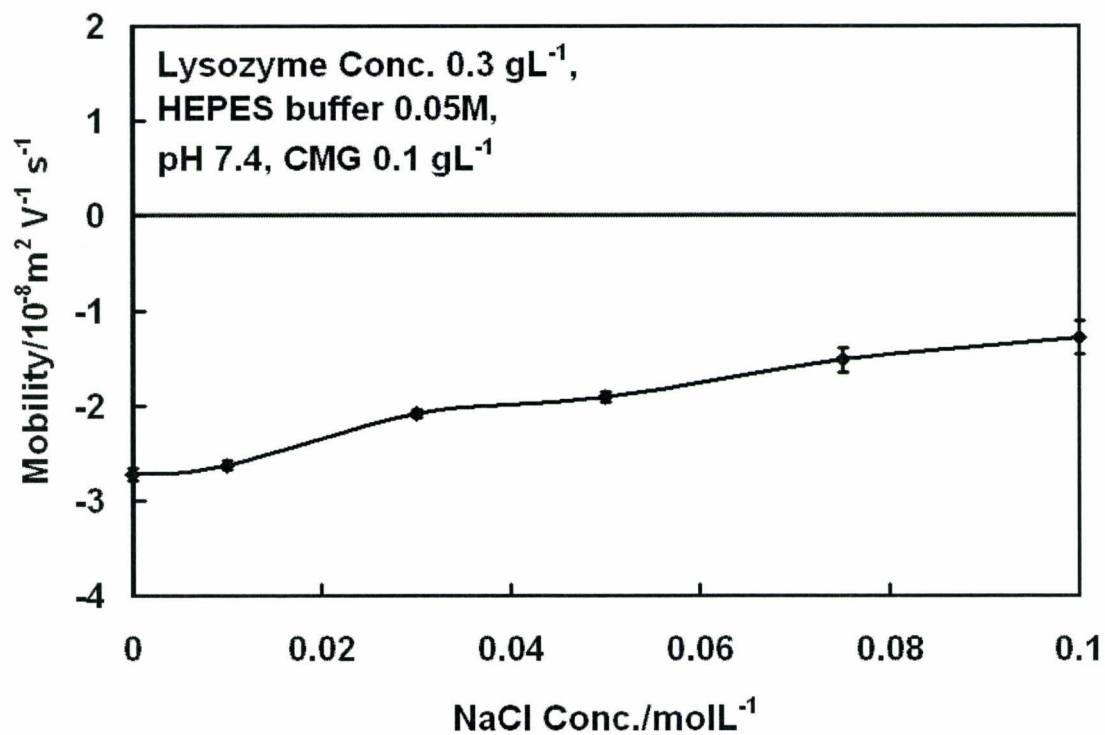


Figure 5.6 Salt effect on electrophoretic mobility of CMG and lysozyme.

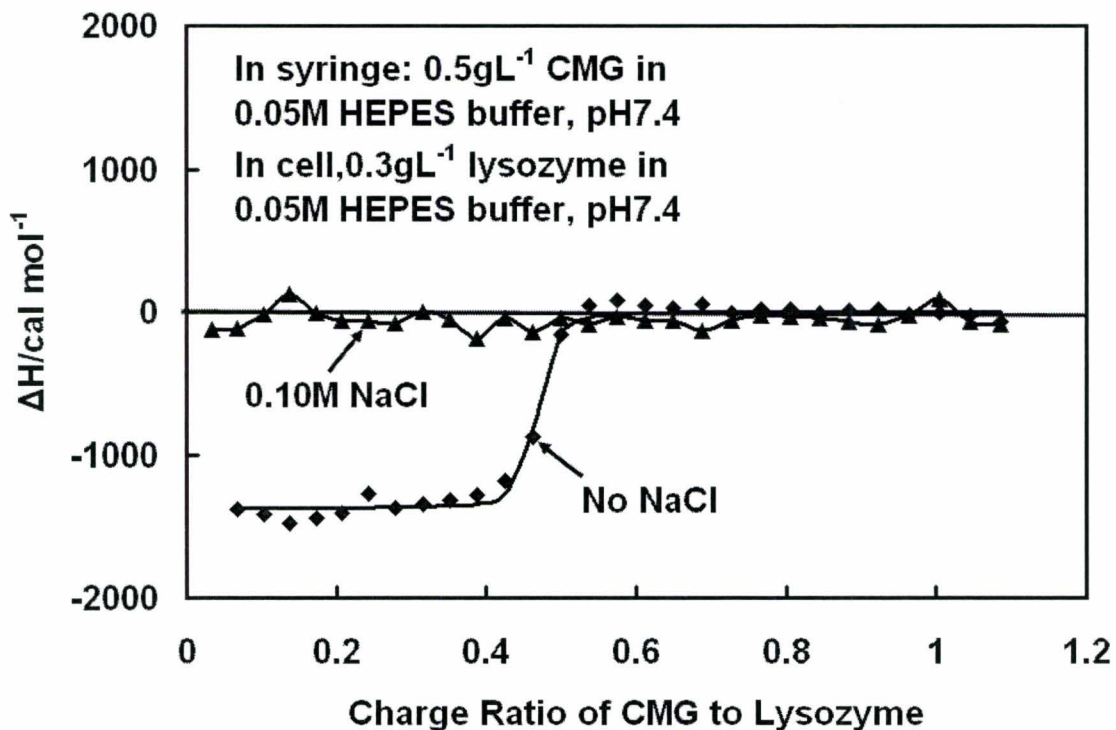


Figure 5.7 ITC measurement of CMG interaction with lysozyme.

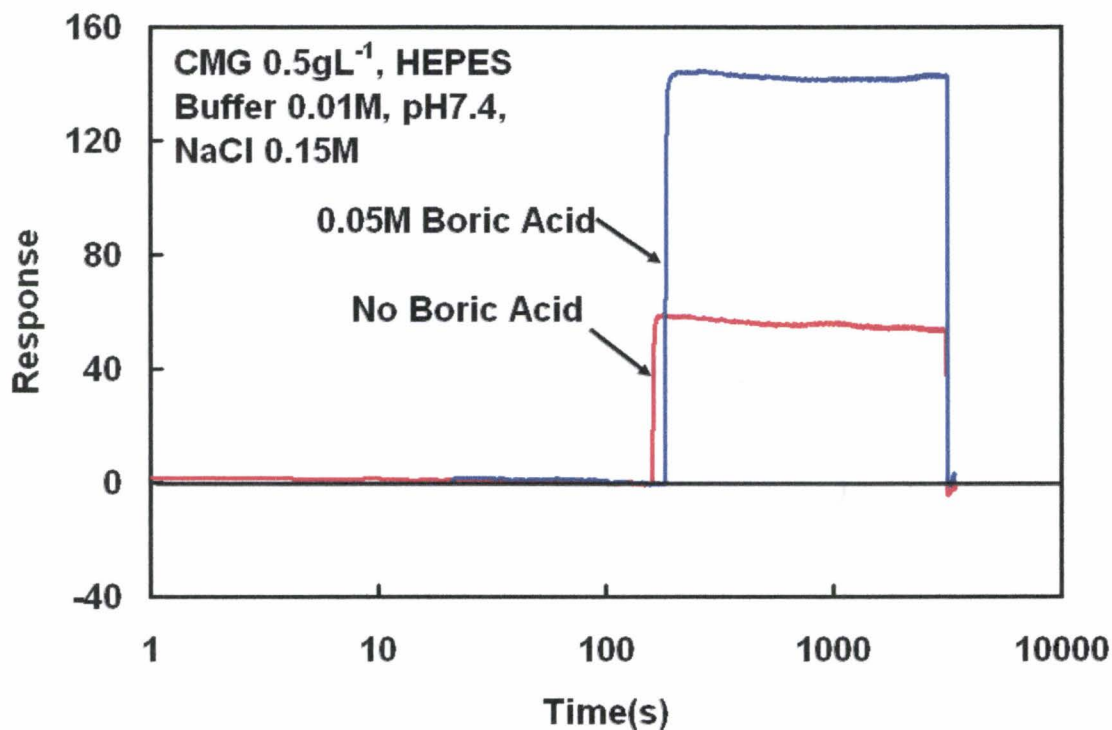


Figure 5.8 SPR measurement of CMG interaction with lysozyme.

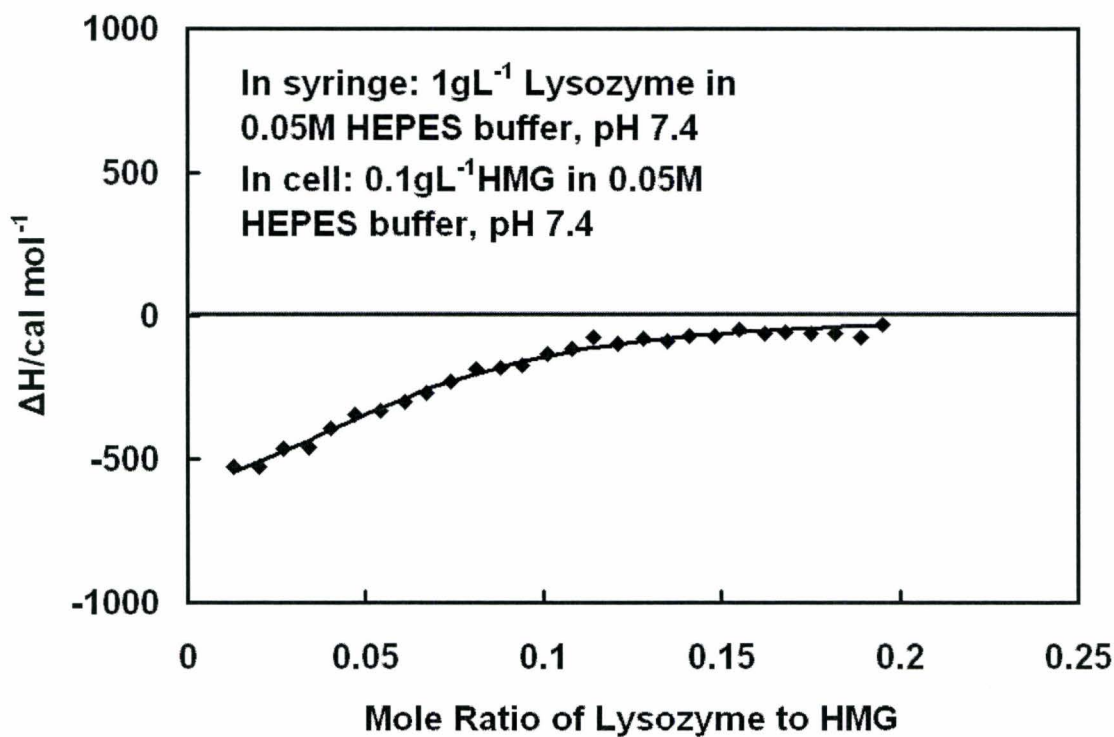


Figure 5.9 ITC measurement of hydrophobically modified guar interaction with lysozyme.

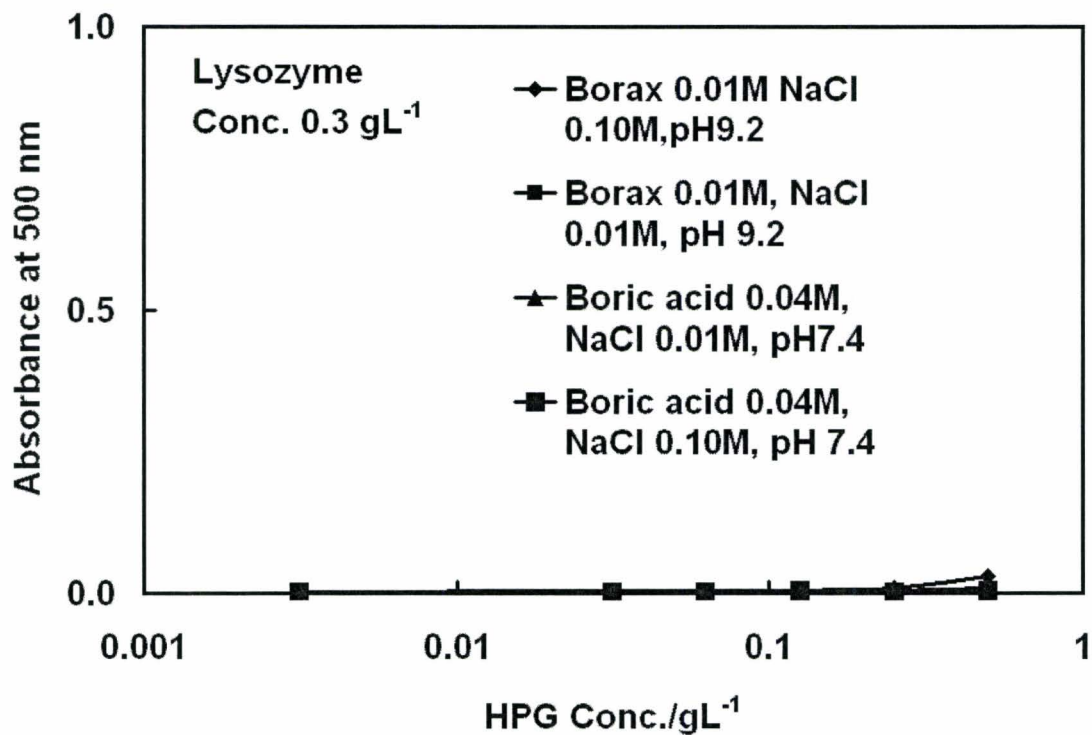


Figure 5.10 Turbidity measurement of HPG with lysozyme in the presence of borate as a function of HPG concentration.

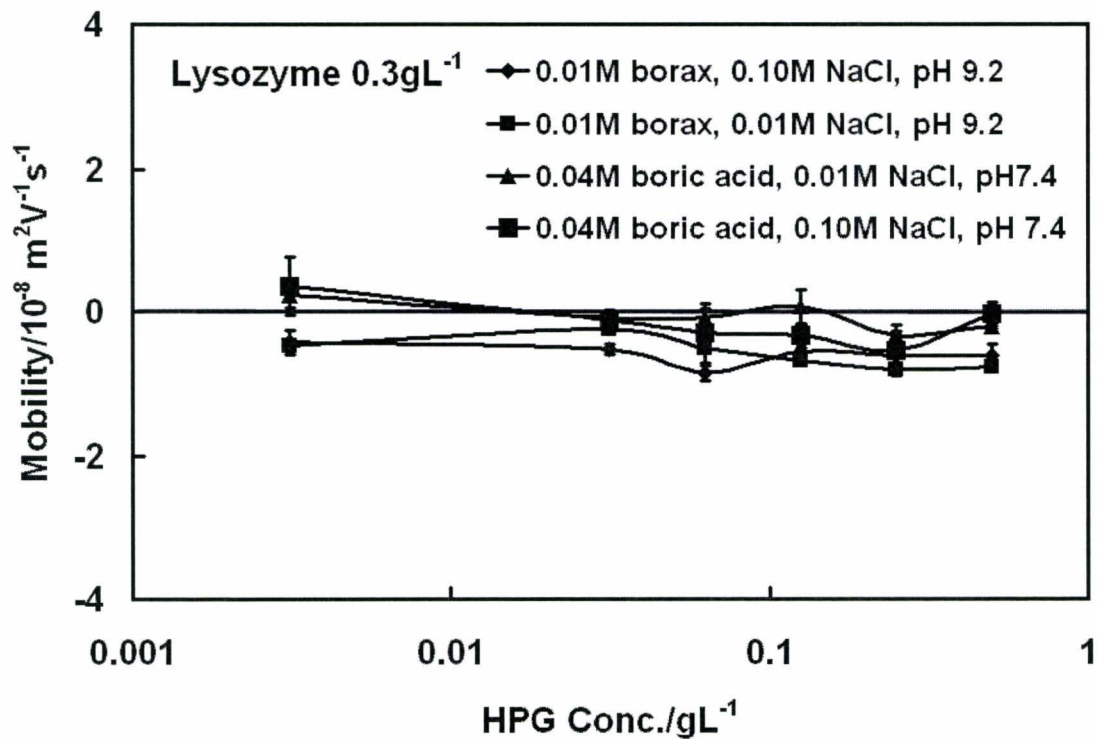


Figure 5.11 Electrophoretic mobility of HPG with lysozyme in the presence of borate as a function of HPG concentration.

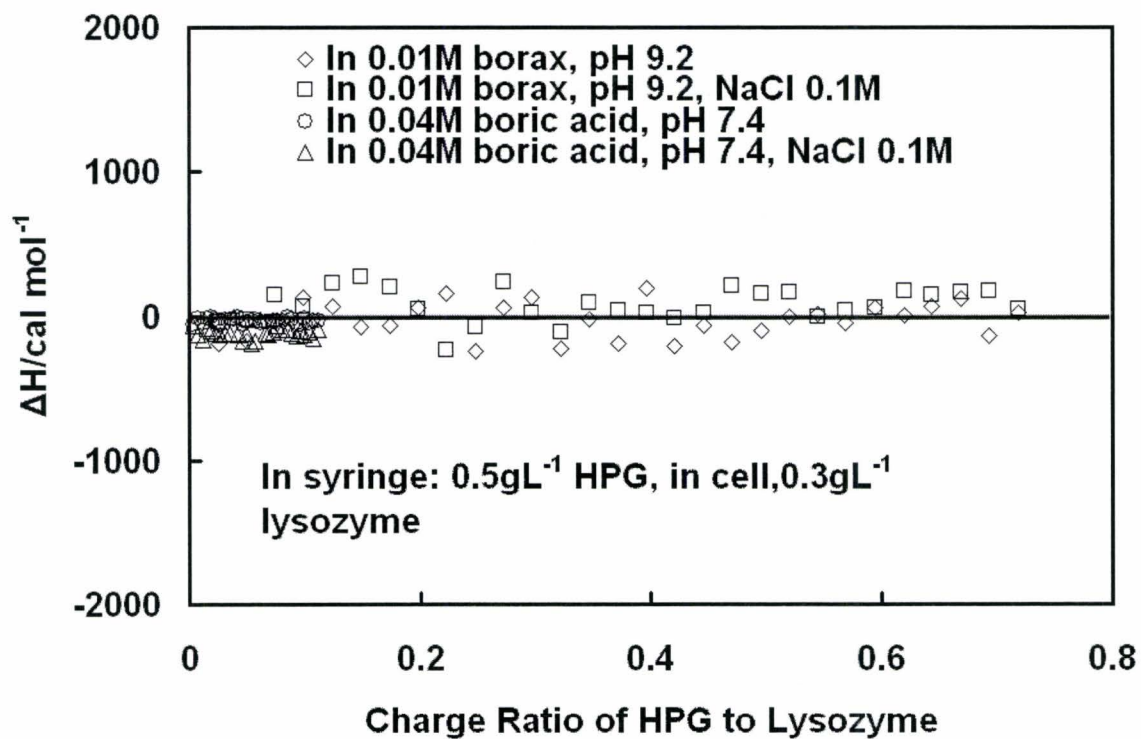


Figure 5.12 ITC measurement of HPG-borate interaction with lysozyme.

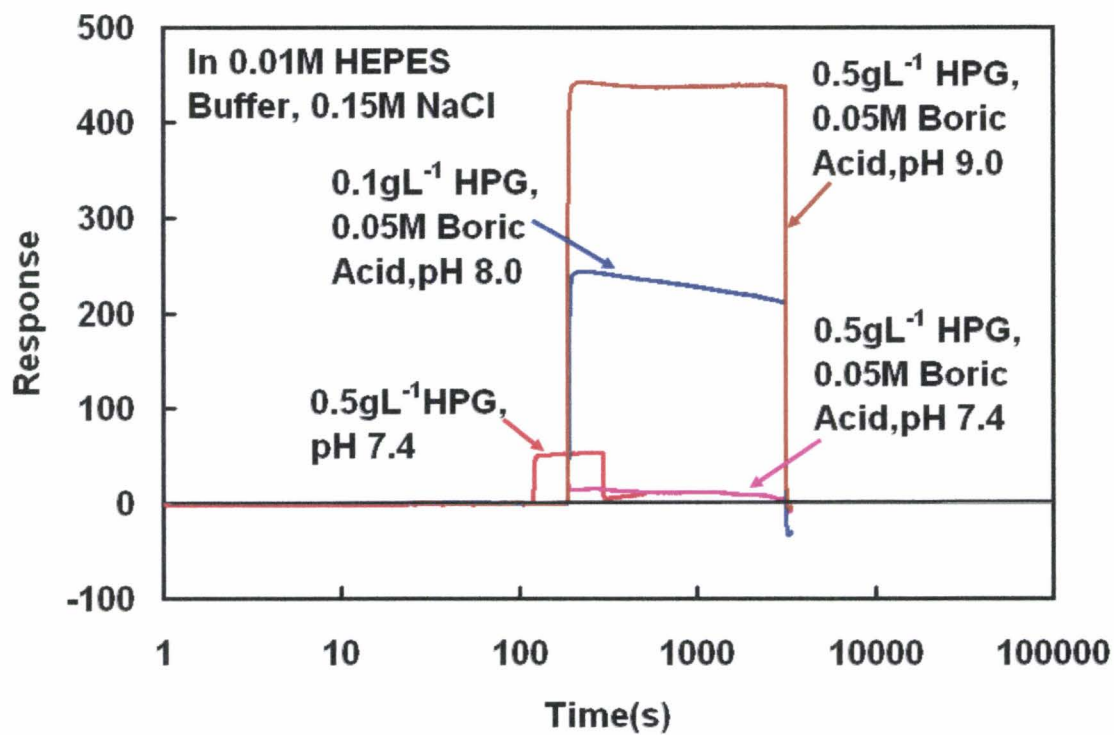


Figure 5.13 SPR measurement of HPG interaction with lysozyme in the presence of HEPES buffer and borate buffer.

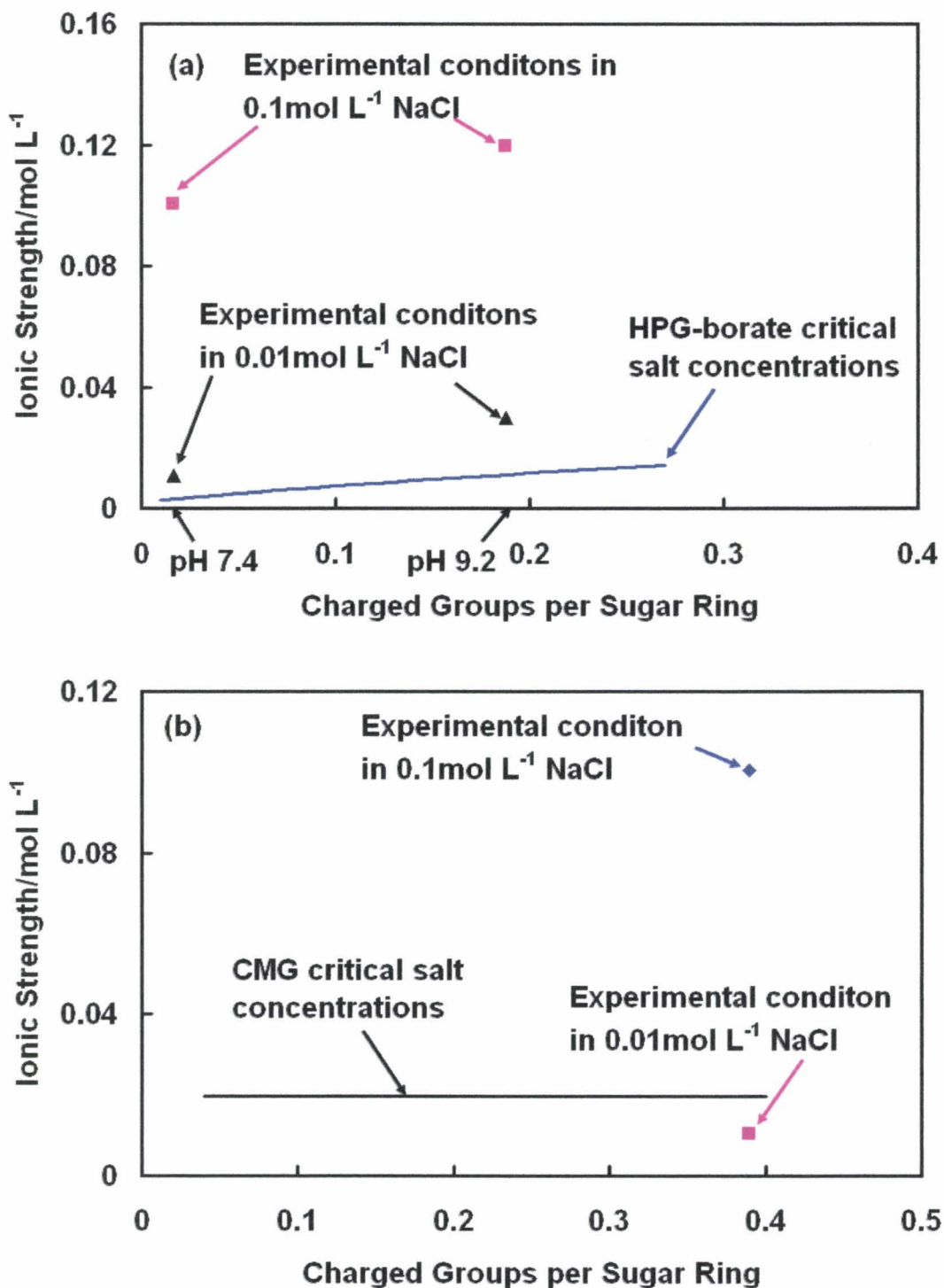


Figure 5.14 (a) Ionic strength effects on HPG-borate interaction with lysozyme. (b) Ionic strength effects on CMG interaction with lysozyme.

## 5.8 References

1. Cui, Y. G.; Pelton, R.; Ketelson, H., Shapes of polyelectrolyte titration curves. 2. The deviant behavior of labile polyelectrolytes. *Macromolecules* 2008, 41, (21), 8198-8203.
2. Pelton, R.; Hu, Z.; Ketelson, H.; Meadows, D., Reversible flocculation with hydroxypropyl guar-borate, a labile anionic polyelectrolyte. *Langmuir* 2009, 25, (1), 192-195.
3. Cui, Y. G.; Pelton, R.; Cosgrove, T.; Richardson, R.; Dai, S.; Prescott, S.; Grillo, I.; Ketelson, H.; Meadows, D., Not all anionic polyelectrolytes complex with DTAB. *Langmuir* 2009, 25, (24), 13712-13717.
4. Johnson, M. E.; Murphy, P. J., Changes in the tear film and ocular surface from dry eye syndrome. *Progress in Retinal and Eye Research* 2004, 23, (4), 449-474.
5. Van Haeringen, N. J., Clinical biochemistry of tears. *Survey of Ophthalmology* 1981, 26, (2), 84-96.
6. Davidson, H. J.; Kuonen, V. J., The tear film and ocular mucins. *Veterinary Ophthalmology* 2004, 7, (2), 71-77.
7. Blake, C. C. F.; Koenig, D. F.; Mair, G. A.; North, A. C. T.; Phillips, D. C.; Sarma, V. R., Structure of hen egg-white lysozyme: A three-dimensional fourier synthesis at 2 Å resolution. *Nature* 1965, 206, 757-761.
8. Mine, S.; Ueda, T.; Hashimoto, Y.; Imoto, T., Analysis of the internal motion of free and ligand-bound human lysozyme by use of N-15 NMR relaxation measurement: A comparison with those of hen lysozyme. *Protein Science* 2000, 9, (9), 1669-1684.
9. Schwalbe, H.; Grimshaw, S. B.; Spencer, A.; Buck, M.; Boyd, J.; Dobson, C. M.; Redfield, C.; Smith, L. J., A refined solution structure of hen lysozyme determined using residual dipolar coupling data. *Protein Science* 2001, 10, (4), 677-688.
10. Klose, T.; Welzel, P. B.; Werner, C., Protein adsorption from flowing solutions on pure and maleic acid copolymer modified glass particles. *Colloids and Surfaces B-Biointerfaces* 2006, 51, (1), 1-9.
11. Petit, F.; Audebert, R.; Iliopoulos, I., Interactions of hydrophobically-modified poly(sodium acrylate) with globular-proteins. *Colloid and Polymer Science* 1995, 273, (8), 777-781.
12. Rothwarf, D. M.; Scheraga, H. A., Role of non-native aromatic and hydrophobic interactions in the folding of hen egg white lysozyme. *Biochemistry* 1996, 35, (43), 13797-13807.
13. Sternberg, M. J.; Grace, D. E.; Phillips, D. C., Dynamic information from protein crystallography. An analysis of temperature factors from refinement of the hen egg-white lysozyme structure. *Journal of molecular biology* 1979, 130, (3), 231.
14. Thompson, A. R., Amino acid sequence in lysozyme. 1. Displacement chromatography of peptides from a partial hydrolysate on ion-exchange resins. *Biochemical Journal* 1955, 60, (3), 507.

15. Johansson, C.; Hansson, P.; Malmsten, M., Interaction between lysozyme and poly(acrylic acid) microgels. *Journal of Colloid and Interface Science* 2007, 316, 350-359.
16. Cheng, A. K. H.; Ge, B.; Yu, H. Z., Aptamer-based biosensors for label-free voltammetric detection of lysozyme. *Analytical Chemistry* 2007, 79, (14), 5158-5164.
17. Arai, T.; Norde, W., The behavior of some model proteins at solid liquid interfaces .1. Adsorption from single protein solutions. *Colloids and Surfaces* 1990, 51, 1-15.
18. Pasche, S.; Voros, J.; Griesser, H. J.; Spencer, N. D.; Textor, M., Effects of ionic strength and surface charge on protein adsorption at pegylated surfaces. *Journal of Physical Chemistry B* 2005, 109, (37), 17545-17552.
19. Carlsson, F.; Hyllner, E.; Arnebrant, T.; Malmsten, M.; Linse, P., Lysozyme adsorption to charged surfaces. A monte carlo study. *Journal of Physical Chemistry B* 2004, 108, (28), 9871-9881.
20. Takano, K.; Yamagata, Y.; Yutani, K., Contribution of polar groups in the interior of a protein to the conformational stability. *Biochemistry* 2001, 40, (15), 4853-4858.
21. Furness, E. L.; Ross, A.; Davis, T. P.; King, G. C., A hydrophobic interaction site for lysozyme binding to polyethylene glycol and model contact lens polymers. *Biomaterials* 1998, 19, (15), 1361-1369.
22. Li, S. J.; Nakagawa, A.; Tsukihara, T., Ni<sup>2+</sup> binds to active site of hen egg-white lysozyme and quenches fluorescence of trp62 and trp108. *Biochemical and Biophysical Research Communications* 2004, 324, (2), 529-533.
23. Bourriot, S.; Garnier, C.; Doublier, J. L., Micellar-casein-kappa-carrageenan mixtures. I. Phase separation and ultrastructure. *Carbohydrate Polymers* 1999, 40, (2), 145-157.
24. Bourriot, S.; Garnier, C.; Doublier, J. L., Phase separation, rheology and microstructure of micellar casein-guar gum mixtures. *Food Hydrocolloids* 1999, 13, (1), 43-49.
25. Marozziene, A.; de Kruif, C. G., Interaction of pectin and casein micelles. *Food Hydrocolloids* 2000, 14, (4), 391-394.
26. Perissutti, G. E.; Bresolin, T. M. B.; Ganter, J., Interaction between the galactomannan from mimosa scabrella and milk proteins. *Food Hydrocolloids* 2002, 16, (5), 403-417.
27. Schorsch, C.; Jones, M. G.; Norton, I. T., Phase behaviour of pure micellar casein/kappa-carrageenan systems in milk salt ultrafiltrate. *Food Hydrocolloids* 2000, 14, (4), 347-358.
28. Tuinier, R.; Dhont, J. K. G.; De Kruif, C. G., Depletion-induced phase separation of aggregated whey protein colloids by an exocellular polysaccharide. *Langmuir* 2000, 16, (4), 1497-1507.
29. Ye, A. Q., Complexation between milk proteins and polysaccharides via electrostatic interaction: Principles and applications - a review. *International Journal of Food Science and Technology* 2008, 43, (3), 406-415.
30. Cooper, C. L.; Dubin, P. L.; Kayitmazer, A. B.; Turksen, S., Polyelectrolyte-protein complexes. *Current Opinion in Colloid & Interface Science* 2005, 10, (1-2), 52-78.

31. Cooper, C. L.; Goulding, A.; Kayitmazer, A. B.; Ulrich, S.; Stoll, S.; Turksen, S.; Yusa, S.; Kumar, A.; Dubin, P. L., Effects of polyelectrolyte chain stiffness, charge mobility, and charge sequences on binding to proteins and micelles. *Biomacromolecules* 2006, 7, (4), 1025-1035.
32. de Kruif, C. G.; Weinbreck, F.; de Vries, R., Complex coacervation of proteins and anionic polysaccharides. *Current Opinion in Colloid & Interface Science* 2004, 9, (5), 340-349.
33. Dickinson, E., Hydrocolloids at interfaces and the influence on the properties of dispersed systems. *Food Hydrocolloids* 2003, 17, (1), 25-39.
34. Doublier, J. L.; Garnier, C.; Renard, D.; Sanchez, C., Protein-polysaccharide interactions. *Current Opinion in Colloid & Interface Science* 2000, 5, (3-4), 202-214.
35. Li, Y. J.; Mattison, K. W.; Dubin, P. L.; Havel, H. A.; Edwards, S. L., Light scattering studies of the binding of bovine serum albumin to a cationic polyelectrolyte. *Biopolymers* 1996, 38, (4), 527-533.
36. Carlsson, F.; Linse, P.; Malmsten, M., Monte carlo simulations of polyelectrolyte-protein complexation. *Journal of Physical Chemistry B* 2001, 105, (38), 9040-9049.
37. da Silva, F. L. B.; Jonsson, B., Polyelectrolyte-protein complexation driven by charge regulation. *Soft Matter* 2009, 5, (15), 2862-2868.
38. da Silva, F. L. B.; Lund, M.; Jonsson, B.; Akesson, T., On the complexation of proteins and polyelectrolytes. *Journal of Physical Chemistry B* 2006, 110, (9), 4459-4464.
39. de Vries, R., Monte carlo simulations of flexible polyanions complexing with whey proteins at their isoelectric point. *Journal of Chemical Physics* 2004, 120, (7), 3475-3481.
40. Odijk, T., Many-body depletion interactions among protein spheres in a semidilute polymer solution. *Journal of Chemical Physics* 1997, 106, (8), 3402-3406.
41. Odijk, T., Depletion theory and the precipitation of protein by polymer. *Journal of Physical Chemistry B* 2009, 113, (12), 3941-3946.
42. Wang, S.; van Dijk, J.; Odijk, T.; Smit, J. A. M., Depletion-induced demixing in aqueous protein - polysaccharide solutions. *Biomacromolecules* 2001, 2, (4), 1080-1088.
43. Kulkarni, A. M.; Chatterjee, A. P.; Schweizer, K. S.; Zukoski, C. F., Depletion interactions in the protein limit: Effects of polymer density fluctuations. *Physical Review Letters* 1999, 83, (22), 4554-4557.
44. Mattison, K. W.; Wang, Y. F.; Grymonpre, K.; Dubin, P. L., Micro- and macro-phase behavior in protein-polyelectrolyte complexes. *Macromolecular Symposia* 1999, 140, 53-76.
45. Hiroshi, M. A.; Chiho, F. I. A.; Kazuyoshi, O. A. B.; Kokufuta, E., Static light scattering study of complex formation between protein and neutral water-soluble polymer. *Colloids and Surfaces B-Biointerfaces* 2007, 56, (1-2), 149-154.
46. Yuan, L.; Yue, Z.; Chen, H.; Huang, H.; Zhao, T. L., Biomacromolecular affinity: Interactions between lysozyme and regioselectively sulfated chitosan. *Colloids and Surfaces B-Biointerfaces* 2009, 73, (2), 346-350.
47. Takahashi, D.; Kubota, Y.; Kokai, K.; Izumi, T.; Hirata, M.; Kokufuta, E., Effects of surface charge distribution of proteins in their complexation with polyelectrolytes in an aqueous salt-free system. *Langmuir* 2000, 16, (7), 3133-3140.

48. Tsuboi, A.; Izumi, T.; Hirata, M.; Xia, J.; Dubin, P. L.; Kokufuta, E., Complexation of proteins with a strong polyanion in an aqueous salt-free system. *Langmuir* 1996, 12, (26), 6295-6303.
49. Lu, M.; Tjerneld, F., Interaction between tryptophan residues and hydrophobically modified dextran - effect on partitioning of peptides and proteins in aqueous two-phase systems. *Journal of Chromatography A* 1997, 766, (1-2), 99-108.
50. Lu, C.; Kostanski, L.; Ketelson, H.; Meadows, D.; Pelton, R., Hydroxypropyl guar-borate interactions with tear film mucin and lysozyme. *Langmuir* 2005, 21, (22), 10032-10037.
51. Seyrek, E.; Dubin, P. L.; Tribet, C.; Gamble, E. A., Ionic strength dependence of protein-polyelectrolyte interactions. *Biomacromolecules* 2003, 4, (2), 273-282.
52. Karlsson, R.; Falt, A., Experimental design for kinetic analysis of protein-protein interactions with surface plasmon resonance biosensors. *Journal of Immunological Methods* 1997, 200, (1-2), 121-133.
53. Gilquin, B.; Guilbert, C.; Perahia, D., Unfolding of hen egg lysozyme by molecular dynamics simulations at 300k: Insight into the role of the interdomain interface. *Proteins-Structure Function and Genetics* 2000, 41, (1), 58-74.
54. Jasinski, R.; Redwine, D.; Rose, G., Boron equilibria with high molecular weight guar: An nmr study. *Journal of Polymer Science, Part B: Polymer Physics* 1996, 34, (8), 1477-1488.
55. Evers, O. A.; Fler, G. J.; Scheutjens, J.; Lyklema, J., Adsorption of weak polyelectrolytes from aqueous-solution. *Journal of Colloid and Interface Science* 1986, 111, (2), 446-454.
56. Fler, G. J.; Scheutjens, J., Interaction between adsorbed layers of macromolecules. *Journal of Colloid and Interface Science* 1986, 111, (2), 504-515.
57. Scheutjens, J.; Fler, G. J.; Stuart, M. A. C., End effects in polymer adsorption - a tale of tails. *Colloids and Surfaces* 1986, 21, 285-306.
58. Muthukumar, M., Adsorption of a polyelectrolyte chain to a charged surface. *Journal of Chemical Physics* 1987, 86, (12), 7230-7235.
59. Muthukumar, M., Pattern-recognition by polyelectrolytes. *Journal of Chemical Physics* 1995, 103, (11), 4723-4731.
60. Vongoele, F.; Muthukumar, M., Adsorption of polyelectrolytes onto curved surfaces. *Journal of Chemical Physics* 1994, 100, (10), 7796-7803.
61. Morris, G. A.; Patel, T. R.; Picout, D. R.; Ross-Murphy, S. B.; Ortega, A.; de la Torre, J. G.; Harding, S. E., Global hydrodynamic analysis of the molecular flexibility of galactomannans. *Carbohydrate Polymers* 2008, 72, (2), 356-360.
62. Cheng, Y.; Brown, K. M.; Prud'homme, R. K., Characterization and intermolecular interactions of hydroxypropyl guar solutions. *Biomacromolecules* 2002, 3, (3), 456-461.

## **Chapter 6 HPG-Borate and Modified Guar Interactions with Phosphatidic Acid Liposomes**

### **Abstract**

The interactions of HPG-borate, guar-borate, partially hydrolyzed guar-borate and modified guar (respectively) with negatively charged phosphatidic acid (PA) liposomes were investigated using turbidity measurement, electrophoretic mobility and dynamic light scattering. HPG-borate, guar-borate and partially hydrolyzed guar-borate did not adsorb onto PA liposomes, but induced flocculation of PA liposomes through a depletion mechanism. Depletion flocculation was observed at polymer concentrations close to the critical overlap concentration,  $c^*$ , which depends on polymer molecular weight. Hydrophobically modified guar (HMG) did not adsorb onto PA liposomes because of the low hydrophobicity of short hydrophobic groups in HMG. HMG can also flocculate PA liposomes via a depletion mechanism. By contrast, cationic guar adsorbs onto PA liposomes through electrostatic attraction, and flocculates PA liposomes via a bridging flocculation mechanism.

## 6.1 Introduction

In previous chapters, we have described the interaction of HPG-borate and modified guar with tear film components or with model components such as the oppositely charged polyelectrolyte, poly(diallyldimethyl) ammonium chloride (PDADMAC),<sup>1</sup> the cationic surfactant, dodecyldimethyl ammonium bromide (DTAB)<sup>2</sup>, and positively charged protein-lysozyme at physiological conditions. The interaction of HPG-borate with a model hydrophobic surface, a polystyrene (PS) latex, was also examined.<sup>3</sup> But the interaction of HPG-borate with one of the most important components, lipid, has so far not been investigated. In this chapter, we will study this interaction.

The external layer of the tear film is mainly composed of lipid. It consists mainly of meibomian lipids which excrete from the meibomian glands.<sup>4</sup> It is generally agreed that the lipid layer thickness is less than 100 nm.<sup>5,6</sup> The lipid layer is present at the air/water interface as a continuous sheet, to prevent water evaporation. With regard to chemical composition, the lipid layer consists mainly of non-polar lipids (wax ester, cholesterol and cholesterol ester), polar lipids (phospholipids and glycolipids)<sup>4</sup> and a small fraction of fatty acids, alcohols, glycerides, neutral fats<sup>7</sup> and hydrocarbons<sup>8</sup>. It has been suggested that in the tear film, at first polar lipids spread onto the aqueous surface, followed by non-polar lipids, which interact with the non-polar tails of polar lipids.<sup>9</sup> Although polar lipids make up only less than 20% of the lipid composition, the polar head of such a lipid gives it the potential to interact with other components, such as proteins in aqueous phase. To simplify the study of HPG/lipid interaction, one of the phospholipids, phosphatidic acid (PA) (with structure shown in Figure 6.1 ) was selected as a model lipid to study the interaction of lipids with HPG-borate.

The interactions of lipids with polymer such as proteins were studied by Millar's group using the Langmuir trough method, in which the lipids were spread onto an aqueous surface and proteins were injected into the aqueous phase.<sup>10-13</sup> The interactions between lipids and proteins were investigated by observing the surface pressure change as a function of surface area and using fluorescence microscopy. The uptake of polymers from the aqueous phase to the lipid layer can be detected using the Langmuir trough.

In 1965, Bangham first discovered liposome, a lipid vesicle that can be dispersed in the aqueous phase.<sup>14</sup> Using sonication or extrusion techniques, unilamellar liposome with narrow size distribution can be prepared as shown in Figure 6.2. We can thus investigate the interaction of HPG-borate with lipid in the form of liposome, with the methods usually employed in studying polyelectrolyte/colloid interactions, such as turbidity measurement, electrophoretic mobility and dynamic light scattering.

The possible interactions of HPG with liposome are analogous to the interactions of HPG with colloidal particles. The adsorption of polymer at surfaces of spherical particles may lead to two results. One is to flocculate spherical particles via a bridging

flocculation mechanism at low polymer concentration, and induce aggregation of spherical particles at high polymer concentration. Another is to stabilize spherical particles by the steric effect of adsorbed polymers at high polymer concentration.<sup>15, 16</sup> The non-adsorbing polymer could also induce flocculation of spherical particles by a depletion mechanism, as first reported by Asakura and Oosawa.<sup>17</sup> The aggregation of egg lecithin liposomes, induced by polysaccharide such as pullulan and dextran, was reported by Sunamoto et al.<sup>18</sup> It was suggested that these polysaccharides could adsorb onto a liposome surface, and induce the aggregation of liposomes by a bridging mechanism. However, Kawasaki et al.<sup>19</sup> suggested that pullulan and dextran do not adsorb onto a lecithin liposome surface, and induce the aggregation of liposomes by a depletion mechanism. By contrast, charged polymers such as sodium alginate and carboxymethyl cellulose, or surface active polymers such as poly(vinyl alcohol) adsorbed onto liposome surfaces due to electrostatic or hydrophobic interaction, could stabilize liposomes at high polymer concentrations.

However, HPG-borate interactions with lipid liposome have rarely been studied. In our previous study, at physiological conditions (pH 7.4, NaCl 0.1mol/L) neither HPG nor the polyelectrolyte HPG-borate adsorbed onto cationic 1,2-dioleoyl-3-trimethylammonium-propane (DOTAP) liposome, and the electrostatic attraction between HPG-borate and cationic DOTAP was screened by salt.<sup>20</sup> The non-adsorbing polymer or polyelectrolyte induced the aggregation of liposomes due to the depletion potential generated by the decrease of osmotic pressure between liposomes, because of the HPG concentration increase. It is reasonable to predict that HPG and HPG-borate also do not adsorb onto PA liposomes, because HPG-borate and PA are both negatively charged and electrostatic repulsion prevents this adsorption. As with its interaction with DOTAP liposomes, HPG does not adsorb onto PA liposomes either. Therefore, depletion flocculation of PA liposomes is expected, induced by the addition of HPG. We also investigated the adsorbing cationic guar interaction with PA liposomes, and the hydrophobically modified guar (HMG) interaction with PA liposomes.

## 6.2 Experimental

### 6.2.1 Materials

L- $\alpha$ -phosphatidic acid from chicken egg was purchased from Avanti Polar Lipids Inc. Hydroxypropyl guar (HPG) with DS (degree of substitution) 0.36 (0.36 hydroxypropyl groups per sugar ring), and molecular weight  $1.75 \times 10^6$  Da, purified native guar with molecular weight  $3 \times 10^6$  Da and partially hydrolyzed guar (PHG) with molecular weight 15,000 Da were provided by Alcon Laboratories, Fort Worth, Texas. Sodium borate (borax) was purchased from Anachemia. Boric acid was purchased from Caledon Laboratories Ltd. Sodium chloride and HEPES (4-(2-hydroxyethyl)-1-piperazineethanesulfonic acid) were purchased from Sigma-Aldrich. Cationic guar with DS 0.09 (0.09 cationic groups per sugar ring) and hydrophobic modified guar with DS

0.13 (0.13 hydrophobic group per sugar ring) were synthesized as described in Chapter 2. The structure of cationic guar is shown in Figure 2.2 of Chapter 2. The structure of HMG is shown in Figure 2.3 of Chapter 2 and a HMG with 6 carbons in the hydrophobic groups ( $n=4$  in R') was used in this study. All samples were prepared in MilliQ water.

## 6.2.2 Methods

### Phosphatidic Acid Liposome Preparation

First, 100-200 mg of phosphatidic acid lipid was dissolved for one hour in 10 mL solvent of chloroform and methanol (1:1 mixture). The solvent was then evaporated in a one-neck round-bottom flask using a rotary vacuum evaporator at 42°C, and the lipid formed a thin film on the flask wall. The lipid film was then purged by nitrogen gas for half an hour. Finally, the lipid film was dispersed in MilliQ water at 47°C for one hour and sonicated for several hours, until a clear solution of phosphatidic acid liposome was formed.<sup>21</sup>

### Preparation of Mixtures of Polymer with Liposome

Mixtures of guar polymers and liposomes were prepared in a HEPES or borate buffer. The ionic strength and pH were adjusted using sodium chloride, sodium hydroxide and hydrochloric acid. The mixtures were left for 24 hours before measurements.

### Turbidity Measurement

Absorbance (turbidity) of the mixtures was measured using a DU 800 Beckman Coulter UV Spectrophotometer at room temperature. The wavelength was fixed at 500 nm.

### Electrophoretic Mobility

Electrophoretic mobility of the mixtures was measured using a Brookhaven Zetaplus Zeta Potential Analyzer operating in phase analysis light scattering mode with BIC Pals Zeta Potential Analyzer software (version 2.5). A total of 10 runs (15 cycles per run) were performed at room temperature and the mean and standard deviation of these runs was read off.

### Dynamic Light Scattering (DLS)

Particle sizes of samples were measured using a Brookhaven Dynamic Light Scattering Instrument with a BI-9000AT autocorrelator and 35 mW laser of 632.8nm wavelength at a scattering angle of 90°. Sample data were acquired using BIC dynamic light scattering software 9kdls32 (version 3.34). The cumulative statistical method was

used to analyze the data. The sample temperature was controlled at  $25 \pm 1$  °C using a NESLAB water bath.

## 6.3 Results

The head group (phosphate) in phosphatidic acid (PA) has dissociation constant of  $pK_{a1}=3$  and  $pK_{a2}=7$ .<sup>22</sup> The charge density of PA liposomes increases with the increasing of pH. In our experimental conditions, the charge density of PA liposomes increases slightly from pH 7.4 to pH 9.2 according to zeta potentials of PA liposomes (about 30-40 mV).

To clarify whether electrostatic and hydrophobic interactions dominate in guar/PA liposomes interactions, cationic guar and HMG were used. Guar/ liposome interactions can be demonstrated using turbidity measurements if insoluble complexes are formed. Electrophoretic mobility detects changes in liposome surface charges, and so can be used to monitor the adsorption of guar on liposomes. Particle size changes, measured by DLS, can demonstrate complex formation between guar and PA liposomes.

### 6.3.1 Cationic Guar Interaction with PA Liposomes

In the study of interactions between cationic guar and phosphatidic acid liposomes, cationic guar with DS 0.09 was used. The molecular weight of cationic guar is similar to that of guar (about  $3 \times 10^6$  Dalton). The molecular weight of guar that synthesized in an identical manner to that of cationic guar was measured using gel permeation chromatography (GPC), and found to be same as native guar used to synthesize cationic guar (results not shown here). The structure of cationic guar was shown in Chapter 2.

From Figure 6.3 and Figure 6.4, the turbidity, mobility and particle size were measured for a wide range of cationic guar concentrations from about  $2 \times 10^{-4}$  g/L to above 3 g/L, with a PA concentration of  $1 \times 10^{-3}$  mol/L in 0.05 mol/L HEPES buffer at pH 7.4 and a sodium chloride concentration of 0.1 mol/L. At a low cationic guar concentration (up to 0.01 g/L), turbidity, mobility and particle size did not change with the variation of this concentration. The turbidity remained at around 0.02, which is as low as the turbidity of water. The mobility remained at about  $-3 \times 10^{-8} \text{ m}^2/\text{Vs}$ , and the particle sizes were consistent with that of PA liposome: about 95 nm. Starting from a cationic guar concentration of 0.01 g/L, precipitation was observed, and the turbidity of the supernatant were not very different from that in low cationic guar concentration, due to the low turbidity of the PA liposome solution. Although electrophoretic mobility remained about  $-3 \times 10^{-8} \text{ m}^2/\text{Vs}$ , particle size increased from around 100 nm to 130 nm, indicating cationic guar adsorption on the PA liposome. As the cationic guar concentration further increased to above 0.1 g/L, precipitation continued to be observed, and the turbidity increased to about 0.6, indicative of large size colloid formation. The mobility decreased to about zero, indicating the neutralization of negatively charged PA liposome by cationic guar

adsorption. At the same time, the particle sizes sharply increased to about 1  $\mu\text{m}$ , suggesting PA liposome flocculation induced by cationic guar adsorption onto PA liposome through electrostatic attraction, i.e. bridging flocculation mechanism.

### 6.3.2 Hydrophobically Modified Guar (HMG) Interaction with PA Liposome

To clarify the hydrophobic interaction between guar and PA liposome, the same experiments with cationic guar were repeated for HMG. HMG has a saturation point of 0.1g/L. Therefore, only HMG with concentrations below 0.1g/L was studied.

In contrast to cationic guar, no precipitation was observed for HMG over a wide range of concentrations. At HMG concentrations below 0.1g/L, the turbidity of HMG/PA liposome mixtures remained at below 0.02, and the mobility remained about  $-3 \times 10^{-8} \text{m}^2/\text{Vs}$ , as shown in Figure 6.5. At the same time, the particle sizes remained at about 100 nm, as shown in Figure 6.6. This indicates an absence of adsorption of HMG onto PA liposomes. However, at HMG concentrations close to 0.1g/L, the turbidity of HMG/PA liposome mixtures slightly increased to above 0.02. The particle sizes increased to as large as about 150 nm, suggesting the aggregation of PA liposomes. The mobility remained about  $-3 \times 10^{-8} \text{m}^2/\text{Vs}$ , indicating no adsorption of HMG onto PA liposomes at these HMG concentrations. It is suggested that PA liposomes can also possibly be flocculated by HMG through a depletion mechanism.

### 6.3.3 HPG-Borate Interaction with PA Liposome

For the HPG - borate and PA liposome mixtures, we fixed the PA concentration at  $1 \times 10^{-3} \text{mol/L}$ , and the sodium chloride concentration at 0.1mol/L. The HPG /PA liposome mixtures were prepared in HEPES buffer without borate at pH 7.4, in boric acid at pH 7.4, and in borax buffer at pH 9.2, in a wide range of HPG concentration. From our calculation, at pH 7.4, the degree of ionization of HPG with borate ions is 0.017 (0.017 borate ion per sugar ring) while at pH 9.2 it is 0.19. The linear charge density of HPG - borate at pH 9.2 is nearly ten times that at pH 7.4.

Turbidity, mobility, and DLS experiments were also done for the above samples. The results are shown in Figure 6.7, Figure 6.8 and Figure 6.9. From these figures, we can see that at HPG concentrations below 0.55 g/L, the turbidity remained at about 0.01 for varying buffers and pH. The mobility remained constant: about  $-3 \times 10^{-8} \text{m}^2/\text{Vs}$  in boric acid at pH 7.4; about  $-2.5 \times 10^{-8} \text{m}^2/\text{Vs}$  in sodium borate buffer at pH 9.2; and about  $-1.5 \times 10^{-8} \text{m}^2/\text{Vs}$  in HEPES buffer at pH 7.4. The particle sizes remained at 80-100 nm. At HPG concentrations above 0.55g/L, although no precipitation was observed, the turbidity sharply increased to 0.03-0.04 for varying buffers and pH. The mobility decreased to about  $-1.5 \times 10^{-8} \text{m}^2/\text{Vs}$  in boric acid at pH 7.4, about  $-1 \times 10^{-8} \text{m}^2/\text{Vs}$  in sodium borate buffer at pH 9.2, and about  $-0.8 \times 10^{-8} \text{m}^2/\text{Vs}$  in HEPES buffer at pH 7.4, due to the

viscosity increase with the increase of HPG concentration (example calculation of the HPG viscosity effect on the mobility of HPG/PA liposome is shown in Appendix C.1). The particle sizes increased sharply up to 1 $\mu$ m. This indicates that aggregation of PA liposomes occurred due to the increase of HPG concentration whereas HPG does not adsorb onto PA liposomes. It is reasonable to attribute the aggregation of PA liposomes to depletion forces, because the HPG concentration which induced the aggregation of PA liposomes is close to the critical overlap concentration of HPG, namely 0.8g/L, calculated as the inverse of intrinsic viscosity of HPG which was measured using Ubbelohde viscometer.

### 6.3.4 Guar and Partially Hydrolyzed Guar Interaction with PA Liposome

To further investigate the aggregation behavior of PA liposome, native guar with molecular weight of  $3 \times 10^6$  Da and partially hydrolyzed guar with molecular weight 15,000 Da were employed, and the DLS results were compared with those of HPG and PA liposomes. As shown in Figure 6.10 and 6.11, in both a HEPES buffer and a boric acid solution at pH 7.4 and 0.1mol/L sodium chloride, the particle sizes in 1mmol/L PA lipid started to increase at a native guar concentration of 0.3 g/L, HPG concentration of above 0.5 g/L and PHG concentration of above 3 g/L. However, in a borax buffer at pH 9.2 and 0.1M sodium chloride, the onset concentrations of guar, for an increase in PA liposome particle size, were 0.15 g/L for native guar, close to 0.3 g/L for HPG, and above 1.5 g/L for PHG respectively, as shown in Figure 6.12. The mobility also slightly decreased above the onset guar and PHG concentration for PA liposomes to aggregate as shown in Figure 6.13 and Figure 6.14. This is due to the viscosity increase not the adsorption of guar and PHG onto PA liposomes. Once more, the particle size increase is due to the aggregation of PA liposomes by depletion force induced by guar polymer addition.

## 6.4 Discussion

Cationic guar adsorbed onto PA liposomes and induced the aggregation of PA liposomes (see Figure 6.3). Thus, electrostatic attraction dominates the behavior of cationic guar/PA liposome mixtures, and cationic guar flocculates PA liposomes via a bridging flocculation mechanism.

Hydrophobic interaction plays an important role in hydrophobic polymer interaction with liposomes. Hydrophobic groups (anchors) on polymer chains can penetrate into the bilayer of liposomes and associate with the hydrophobic parts of lipid molecules.<sup>23</sup> The association of hydrophobic anchors on polymers with hydrophobic tails on lipids can induce adsorption of polymers on liposomes, thus inducing either aggregation or stabilization of liposomes.<sup>24-27</sup> Also the penetration of hydrophobic anchors on polymers into a bilayer of liposomes can induce fusion or fission of

liposomes.<sup>28, 29</sup> The strength of the hydrophobic association depends on the hydrophobicity of the hydrophobic groups on polymer chains: the more hydrophobic the hydrophobic group, the stronger the hydrophobic interaction.<sup>30</sup> In our experiments, HMG did not adsorb onto PA liposome. This is probably due to the low hydrophobicity of short hexyl chains on guar molecules. However, HMG is able to aggregate PA liposomes through depletion flocculation mechanism.

Although HPG-borate, the negatively charged polyelectrolyte, did not adsorb onto identically charged PA liposome because of electrostatic repulsion between them, HPG-borate still induced the aggregation of PA liposome. Similarly, native guar-borate and PHG-borate also induced the aggregation of PA liposome. From Figure 6.11, it is seen that the onset concentration for PA liposome aggregation depends on the molecular weight of the guar: the higher the molecular weight, the lower the onset concentration for PA liposome aggregation. We also found the onset concentration for guar aggregation to be close to critical overlap concentration  $c^*$ . We propose that the aggregation of PA liposome here is due to depletion flocculation induced at high guar (HPG, PHG, native guar and HMG) concentration. In addition, it should be noticed that the onset concentrations of guar for PA liposome aggregation slightly decreased in the presence of borax buffer. The increase of the HPG-borate linear charge density, for a pH increase from 7.4 to 9.2 induced an increase in electrostatic repulsion between HPG-borate and PA liposomes, facilitating the aggregation of liposomes.

Theoretically, the stability of PA liposome in the aqueous phase is controlled by the total potential energy between liposome vesicles. In the guar-borate/PA liposome system, the total potential energy can be estimated as the sum of that given by DLVO theory<sup>31, 32</sup> and the depletion energy<sup>17</sup> as described by the following equation:

$$V_t = V_{el} + V_{vdW} + V_{dep} \quad (1)$$

where  $V_t$  is the total potential energy;  $V_{el}$  is potential energy arising from the electrostatic repulsion between PA liposomes;  $V_{vdW}$  is the potential energy from the van der Waals force which is the attractive force between liposomes; and  $V_{dep}$  is the depletion potential energy induced by non-adsorbing polymers such as guar in our system.

The electrostatic repulsion potential energy with constant surface potential can be calculated by the following equation.<sup>33</sup>

$$V_{el} = 2\pi\epsilon a\psi_o^2 \ln(1 + \exp(-\kappa h)) \quad (2)$$

where  $\epsilon$  is aqueous permittivity,  $a$  is the radius of PA liposome (40 nm),  $\psi_o$  is surface potential of PA liposome (38 mV as measured zeta potential),  $h$  is the separation distance between PA liposomes, and  $\kappa$  is the inverse of the Debye length, which can be calculated by:

$$\kappa = \left( \frac{2e_o^2 N_A c_{NaCl}}{\epsilon k_b T} \right)^{\frac{1}{2}} \quad (3)$$

where  $e_o$  is elementary charge,  $N_A$  is the Avogadro constant,  $c_{NaCl}$  is the sodium chloride concentration (0.1 mol/L),  $k_b$  is the Boltzmann constant, and  $T$  is absolute temperature.

The van der Waals attractive potential energy can be described as<sup>34</sup>:

$$V_{vdW} = \frac{-A}{12} \left[ \frac{4a^2}{h^2 + 4ah} + \frac{4a^2}{h^2 + 4ah + 4a^2} + 2 \ln \left( \frac{h^2 + 4ah}{h^2 + 4ah + 4a^2} \right) \right] \quad (4)$$

where  $A$  is the Hamaker constant of PA liposome in the aqueous phase ( $7 \times 10^{-21}$  J, the same value as reported for the Hamaker constant of phosphatidylcholines).<sup>35</sup>

For the depletion potential energy, we used the equation given by Fleer et al.<sup>36</sup>:

$$V_{dep} = -\frac{2}{3} \pi \Pi \left( \Delta - \frac{h}{2} \right)^2 \left( 3a + 2\Delta + \frac{h}{2} \right) \quad (5)$$

where  $\Delta$  is the depletion layer thickness, and  $\Pi$  is the osmotic pressure between PA liposomes. The osmotic pressure we used is a virial expansion, valid for dilute solutions (Seebergh and Berg<sup>34</sup>).

$$\Pi = RT \rho \phi \left( \frac{1}{M} + B_2 \rho \phi \right) \quad (6)$$

where  $R$  is the gas constant,  $\rho$  is the guar density (about 1 g/cm<sup>3</sup>),  $\phi$  is the guar volume fraction,  $M$  is the guar molecular weight ( $1.75 \times 10^6$  Da for HPG), and  $B_2$  is the second virial coefficient (0.0003 cm<sup>3</sup> mol/g<sup>2</sup> for HPG)<sup>37</sup>.

The depletion layer thickness in equation (5) was calculated by the equation proposed by Seebergh and Berg<sup>34</sup>, which was derived from Vincent et al<sup>38</sup>:

$$\left( \frac{\Delta}{\Delta_0} - \frac{1}{\Delta} \right) = -\frac{N_A \rho}{2} \left( \frac{v}{\phi} \right)^{\frac{2}{3}} \left[ \frac{\phi}{M} + B_2 \rho \phi^2 \right] \quad (7)$$

where  $\Delta_0$  is the depletion layer thickness without addition of guar ( $1.4r_g$  according to Fleer et al<sup>36</sup>),  $r_g$  is the radius of gyration of guar (128 nm for HPG with molecular weight  $1.75 \times 10^6$  Da)<sup>39</sup>,  $v$  is the molecular volume of the free guar chain which can be calculated by  $M/\rho$ .

An example calculation of the normalized potentials, divided by the thermal energy  $k_b T$ , as a function of the separation distance of PA liposomes, is shown in

Figure 6.15 (see Appendix C.2 for detail calculation). It can be seen that there is a secondary minimum for the sum of potentials at PA liposomes separation distances about 4-6 nm. The secondary potential minimum for HPG volume fraction of 0.05% is about  $-3k_bT$ . This is a weak attractive potential energy for depletion flocculation.<sup>40, 41</sup> The experimental results, that flocculation cannot be observed visually but can be measured (see Figure 6.7 and Figure 6.9), show that HPG induced flocculation is caused by weak depletion forces. For strong depletion flocculation, a secondary minimum of  $-7k_bT$  is widely accepted.<sup>41, 42</sup> The secondary minimum of the sum of potentials as a function of HPG concentration is shown in Figure 6.16. It can be seen that the secondary minimum is smaller than  $-k_bT$  at HPG concentration below 0.1g/L whereas larger than  $-3k_bT$  at HPG concentration above 0.5g/L. Therefore, 0.5g/L is the onset concentration for HPG to aggregate PA liposomes. Similarly, for native guar (molecular weight  $3 \times 10^6$  Da, radius of gyration 177 nm) and PHG (molecular weight 15000 Da, radius of gyration 7.4 nm), 0.4 g/L and 3 g/L (respectively) were needed to achieve a secondary minimum potential of above  $-3k_bT$ , therefore are the onset concentration of native guar and PHG (respectively) for the aggregation of PA liposomes. In calculating the potentials of native guar/PA liposome and PHG/PA liposome, all the parameters are the same as those in calculating HPG/PA liposome except the molecular weight and radius of gyration. The estimation of radius of gyration of HPG, native guar and PHG is shown in Appendix C.3. The onset concentration of guar to aggregate PA liposomes depends on guar molecular weight as shown in Figure 6.17. The higher the molecular weight, the lower the onset guar concentration needed to aggregate PA liposomes. We conclude that the aggregation of PA liposomes is due to the depletion forces of guar molecules.

As for the polyelectrolyte (guar-borate) effect on the aggregation of PA liposome, another term  $V_{pl}$  should be added to the total potential energy equation. This is the potential energy resulting from guar-borate/liposome repulsion which also promotes the aggregation of liposomes.<sup>43</sup> Therefore, the onset concentration of guar to aggregate PA liposomes in borax buffer is decreased compared with those in HEPES buffer and boric acid solution.

## 6.5 Conclusions

1. The negatively charged polyelectrolyte, HPG-borate, does not adsorb on PA liposomes, but induces the aggregation of PA liposomes by depletion forces.
2. The onset guar concentration for PA liposomes aggregation depends on the molecular weight of the guar. The higher the molecular weight, the lower the onset guar concentration needed to aggregate PA liposomes.
3. Cationic guar is adsorbed onto PA liposome through electrostatic attraction, and induces the aggregation of PA liposomes through bridging flocculation mechanism.

4. HMG does not adsorb onto PA liposomes by hydrophobic interaction. This is probably due to the low hydrophobicity of hydrophobic groups on HMG. Therefore, hydrophobic groups on HMG have less ability to penetrate into the liposome bilayer. However, HMG can also possibly induce flocculation of PA liposomes through a depletion mechanism.

## 6.6 Figures

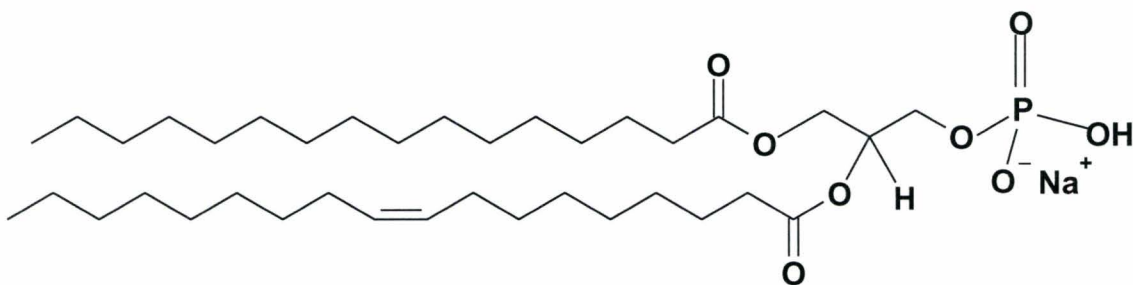
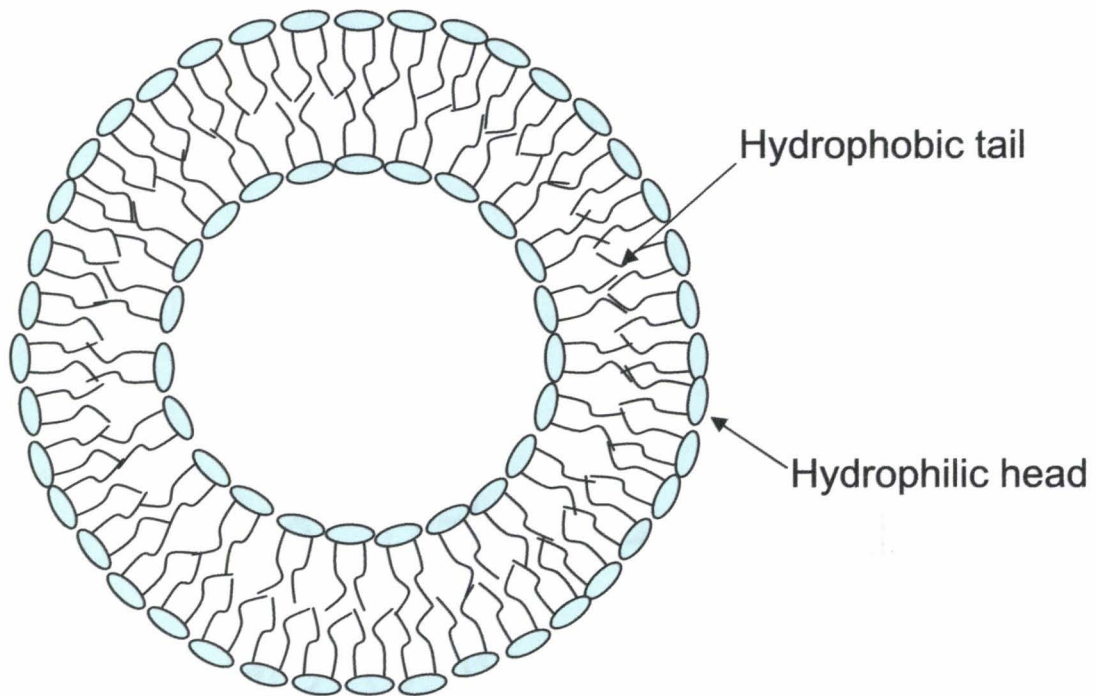


Figure 6.1 Phosphatidic acid sodium salt.



**Figure 6.2** Schematic representation of a cross-section of a unilamellar liposome structure.

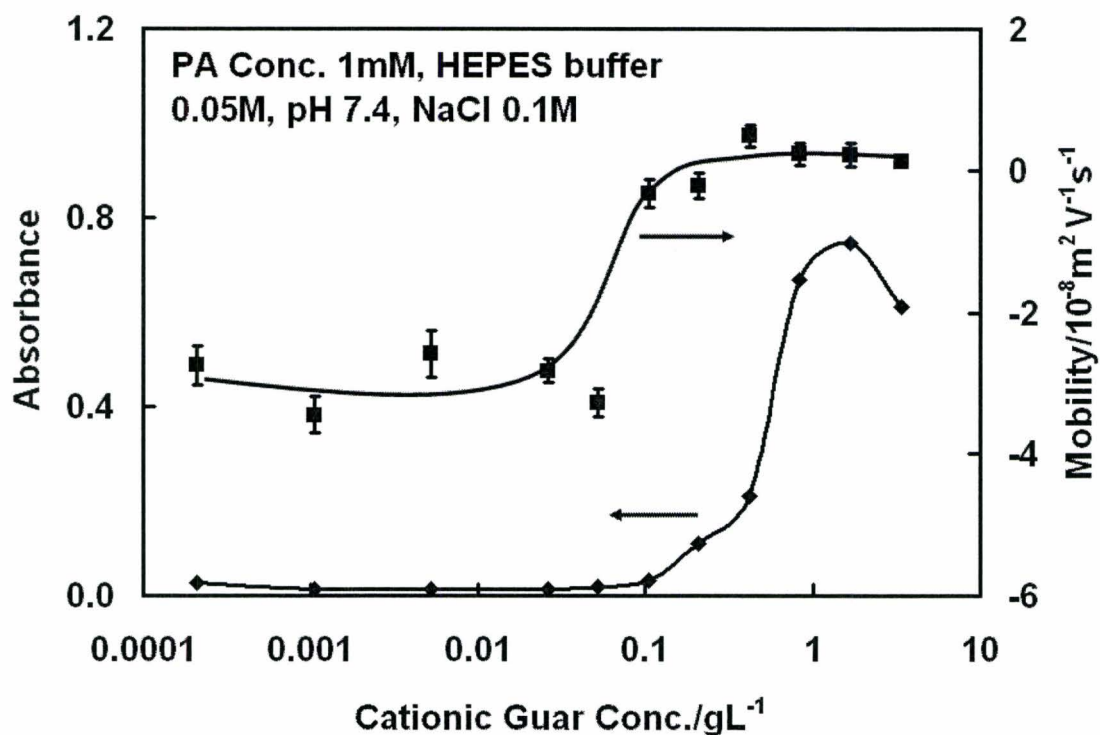


Figure 6.3 Turbidity and mobility measurement of PA liposomes interaction with cationic guar in HEPES buffer (The degree of substitution (DS) of cationic guar is 0.09 (0.09 cationic group per sugar unit) and molecular weight of cationic guar is about  $3 \times 10^6$  Da.).

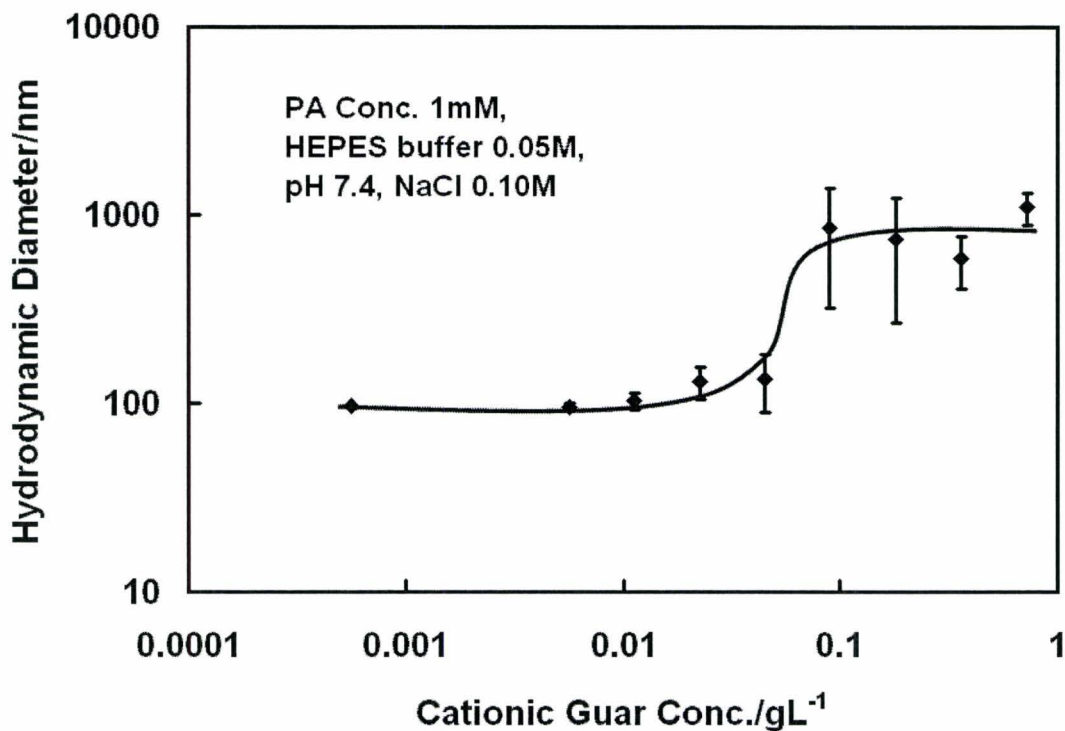
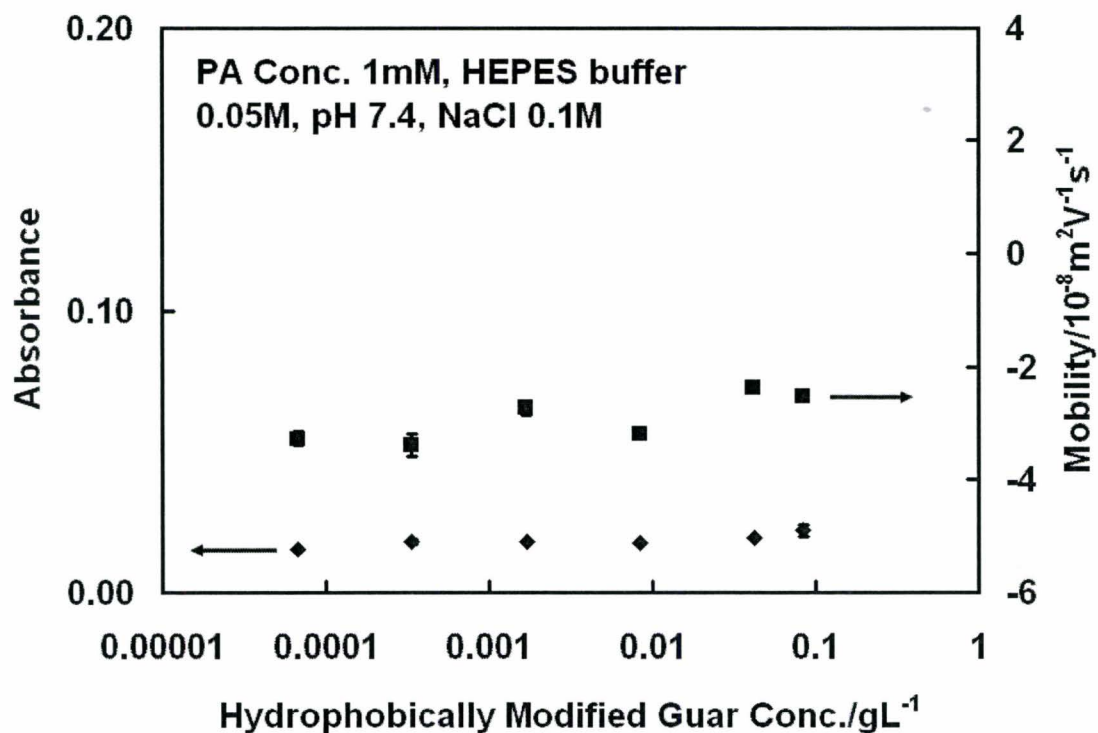
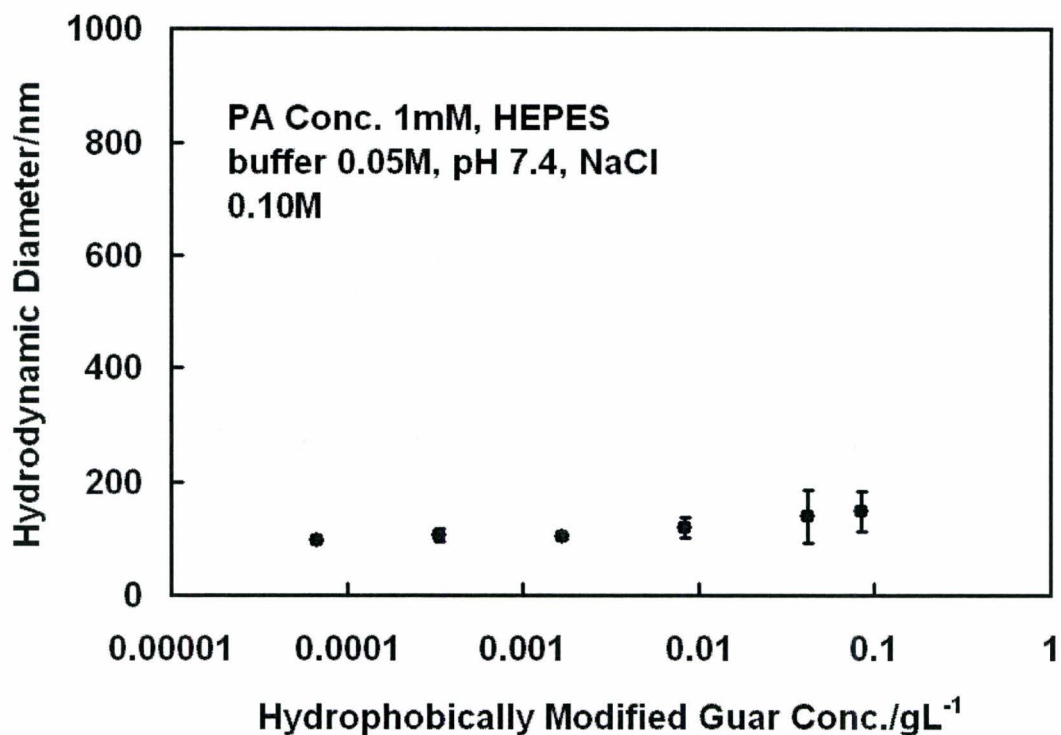


Figure 6.4 DLS measurement of PA liposomes sizes in the presence of cationic guar in HEPES buffer (The degree of substitution (DS) of cationic guar is 0.09 (0.09 cationic group per sugar unit) and molecular weight of cationic guar is about  $3 \times 10^6$  Da.).



**Figure 6.5** Turbidity and mobility measurement of PA liposomes interaction with hydrophobically modified guar in HEPES buffer (The degree of substitution (DS) of HMG is 0.13 (0.13 hydrophobic group per sugar unit) and molecular weight of HMG is about  $3 \times 10^6$  Da.).



**Figure 6.6** DLS measurement of PA liposomes sizes in the presence of hydrophobically modified guar in HEPES buffer (The degree of substitution (DS) of HMG is 0.13 (0.13 hydrophobic group per sugar unit) and molecular weight of HMG is about  $3 \times 10^6$  Da.).

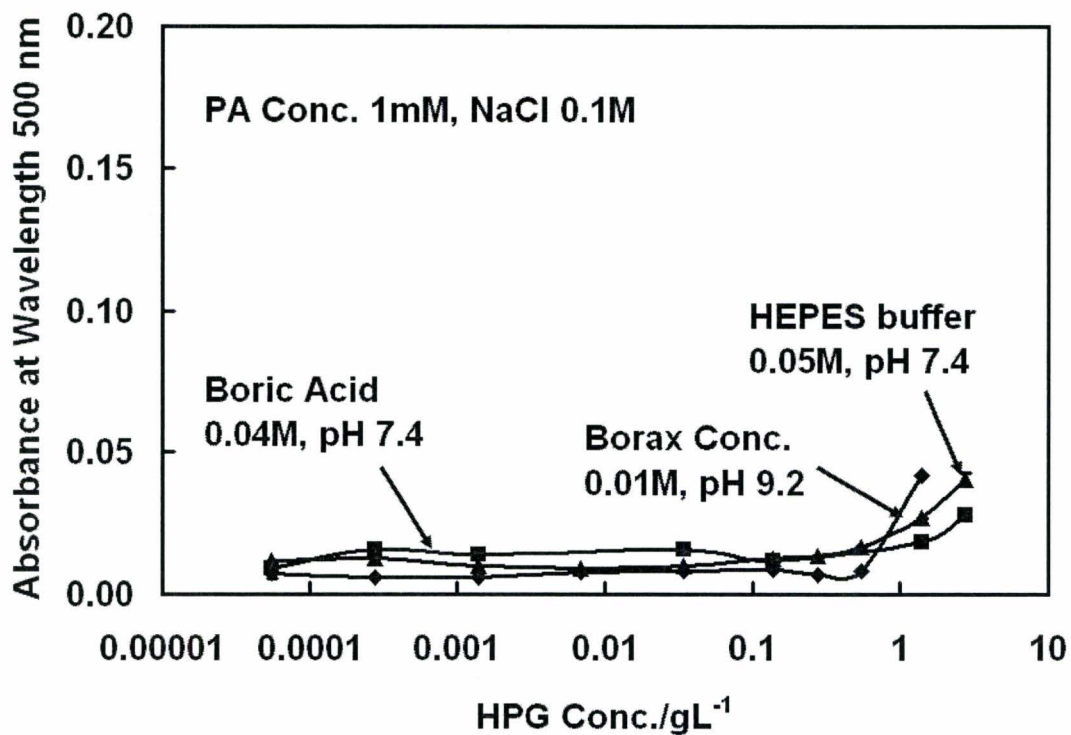


Figure 6.7 Turbidity measurement of HPG interaction with PA liposome in HEPES buffer and borate buffer.

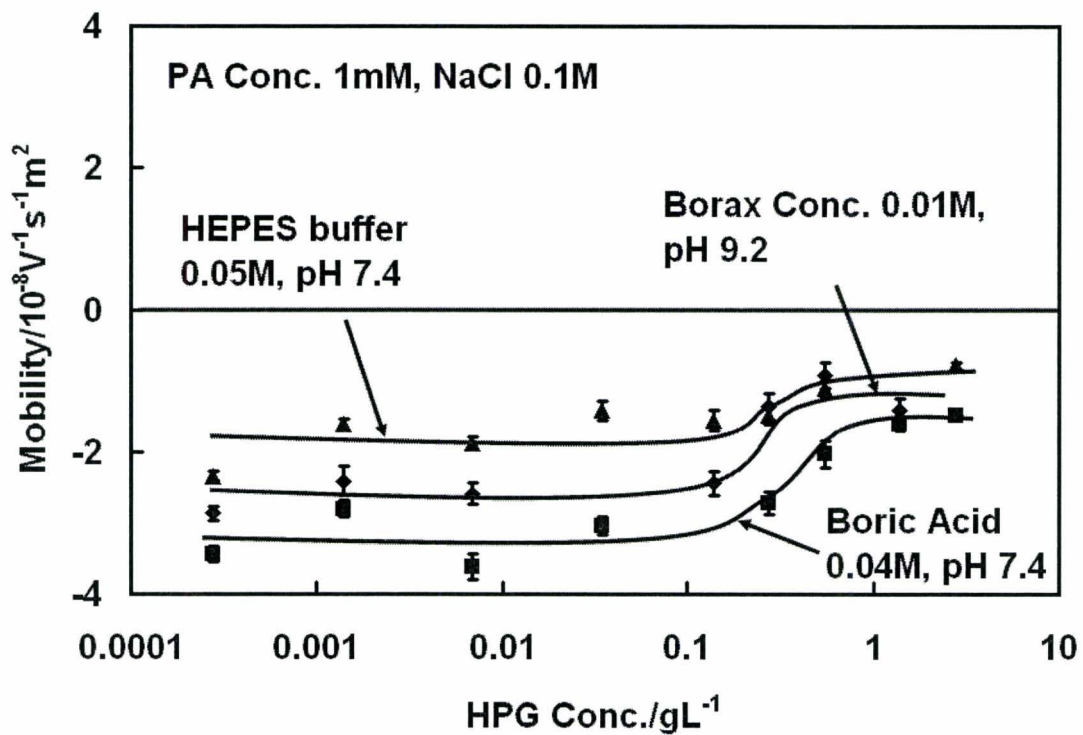


Figure 6.8 Mobility measurement of PA liposomes in the presence of HPG in HEPES buffer and borate buffer.

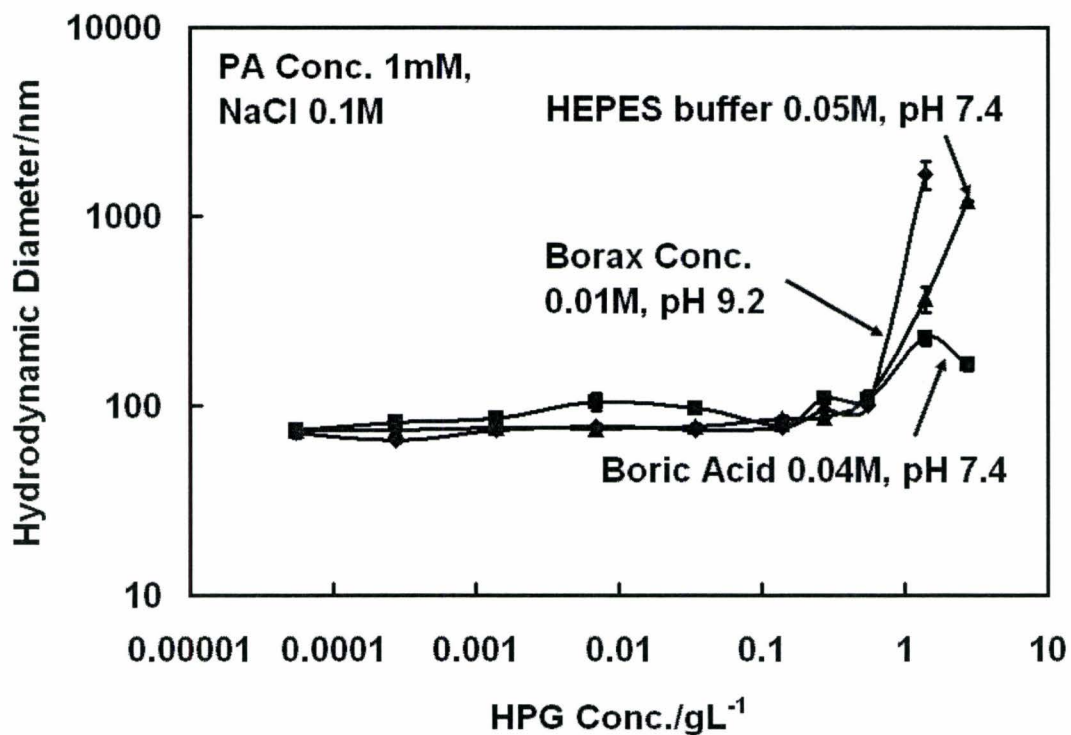


Figure 6.9 DLS measurement of PA liposomes sizes in the presence of HPG in HEPES buffer and borate buffer.

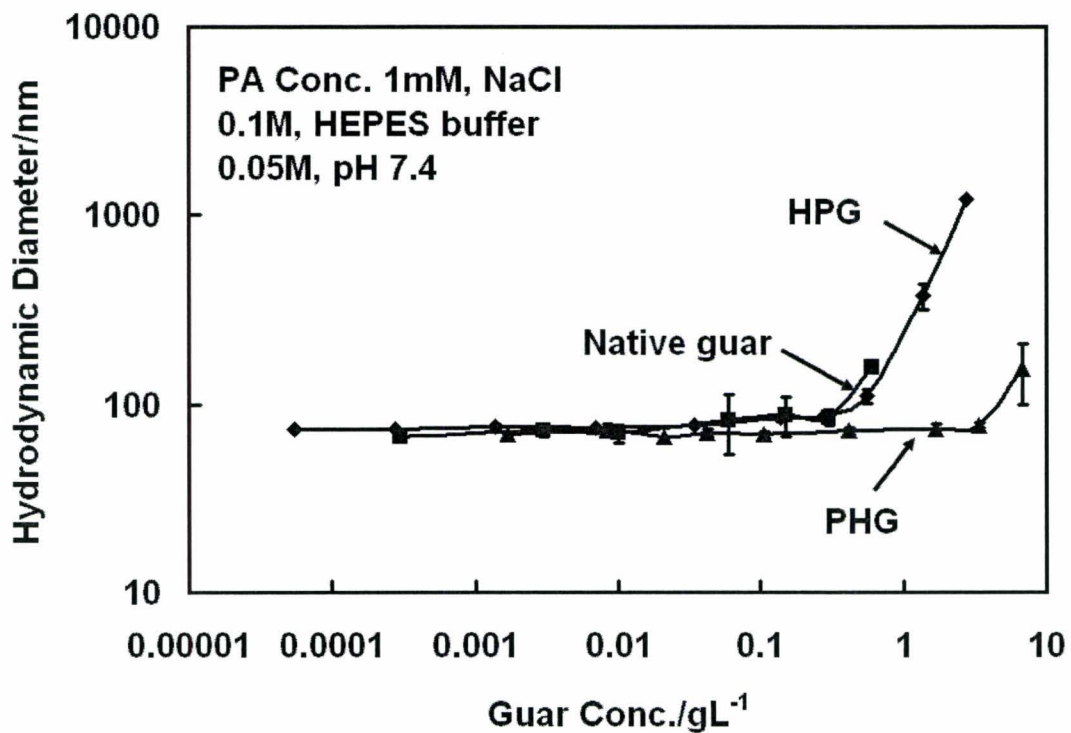


Figure 6.10 DLS measurement of PA liposomes sizes in the presence of guar with different molecular weights in HEPES buffer at pH 7.4.

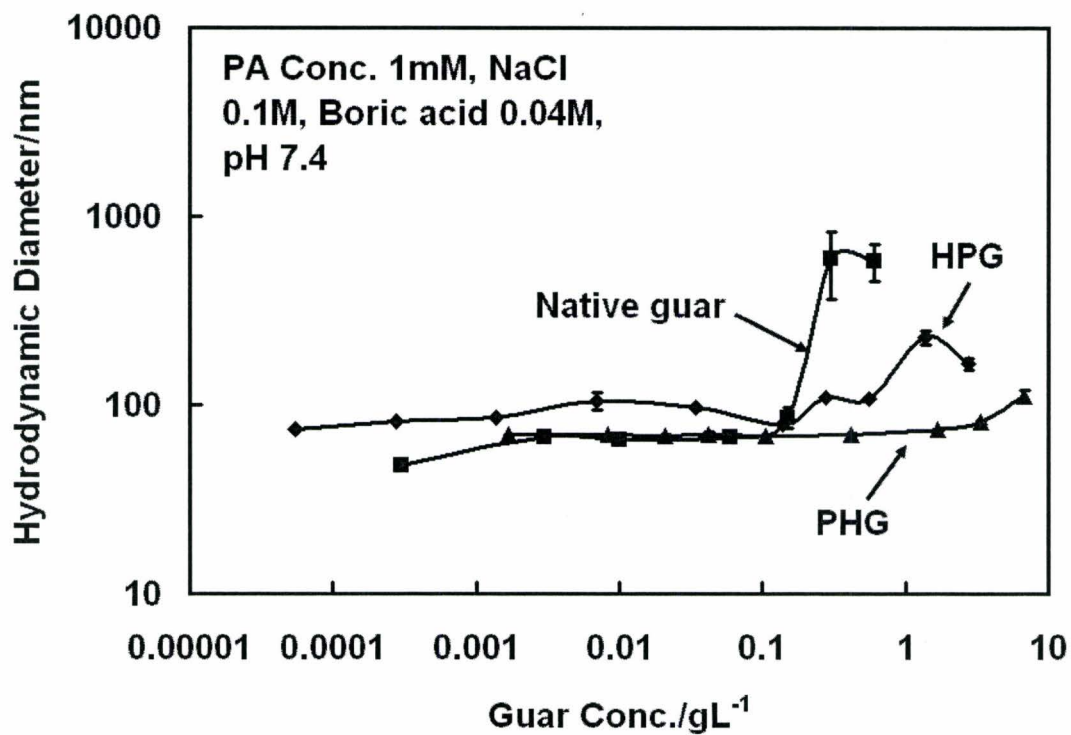


Figure 6.11 DLS measurement of PA liposomes sizes in the presence of guar with different molecular weights in boric acid at pH 7.4.

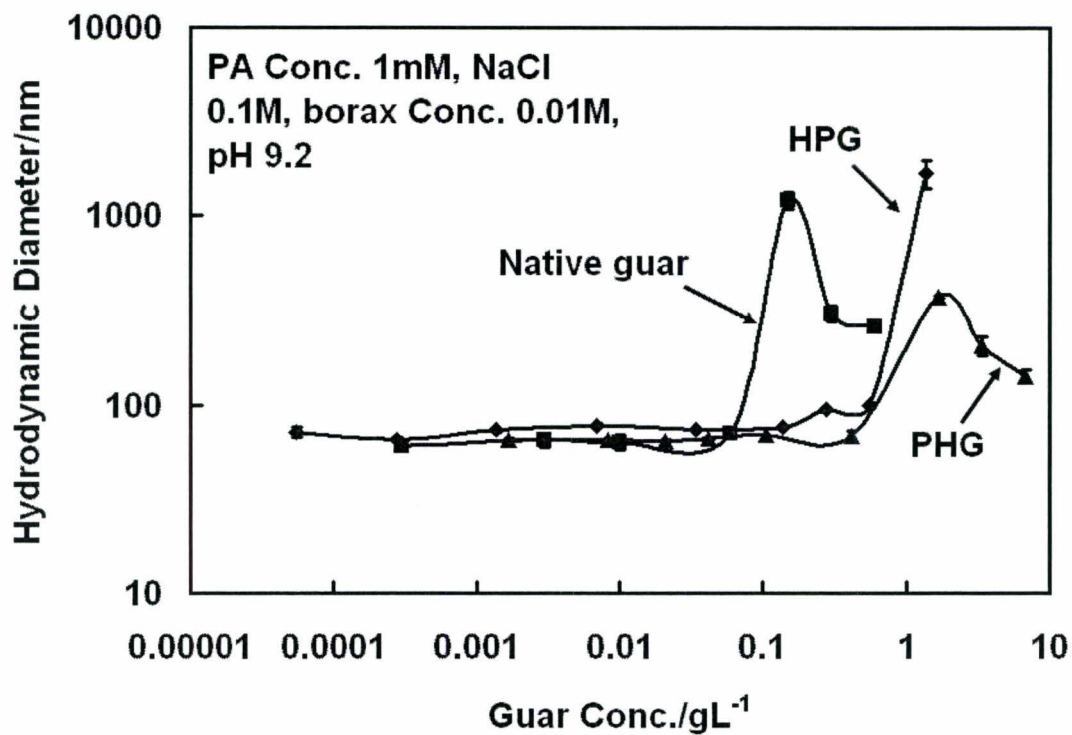


Figure 6.12 DLS measurement of PA liposomes particle sizes in the presence of guar with different molecular weights in borax buffer at pH 9.2.

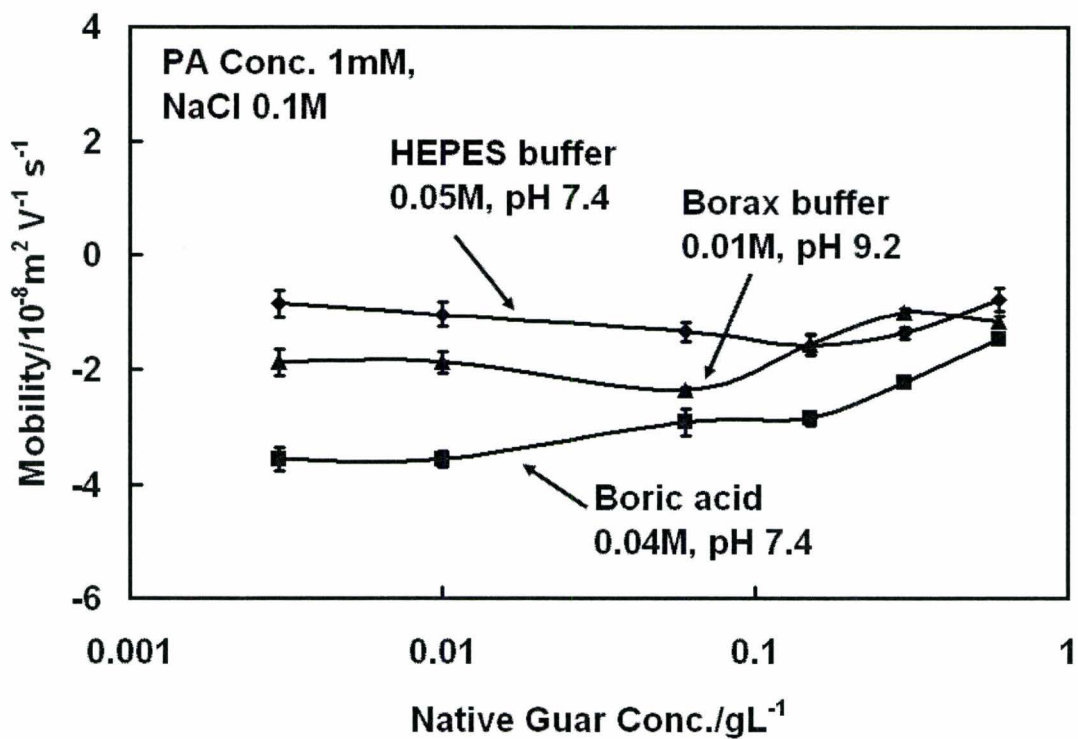


Figure 6.13 Mobility measurement of PA liposomes in the presence of native guar in HEPES buffer and borate buffer.

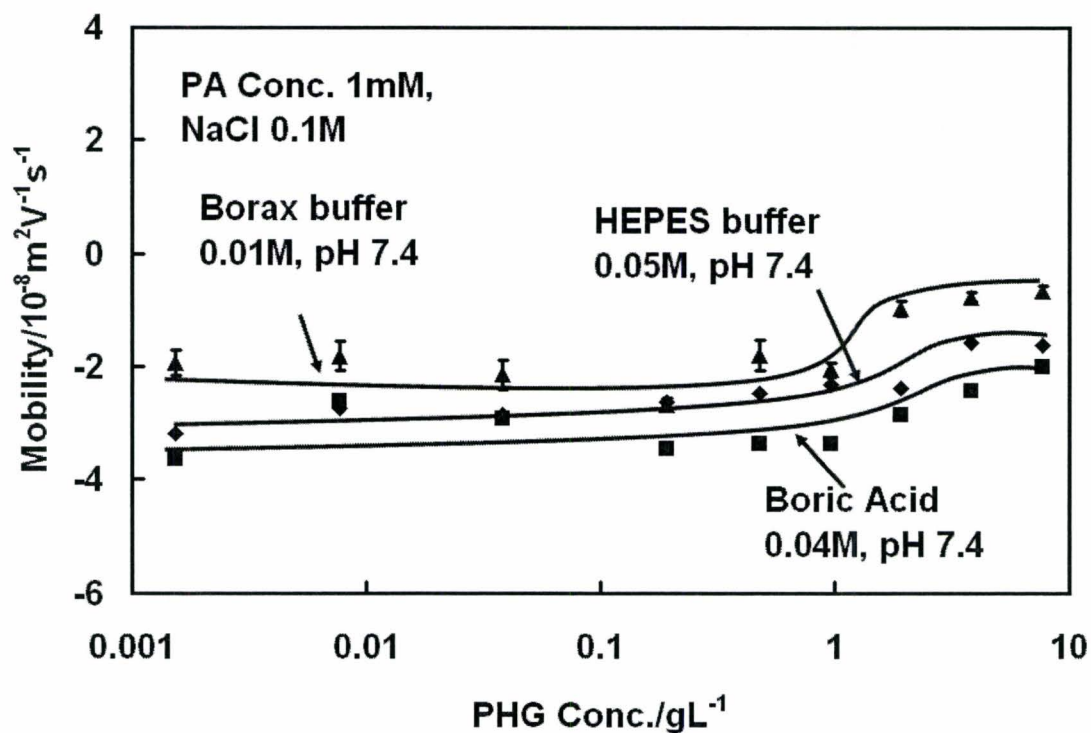
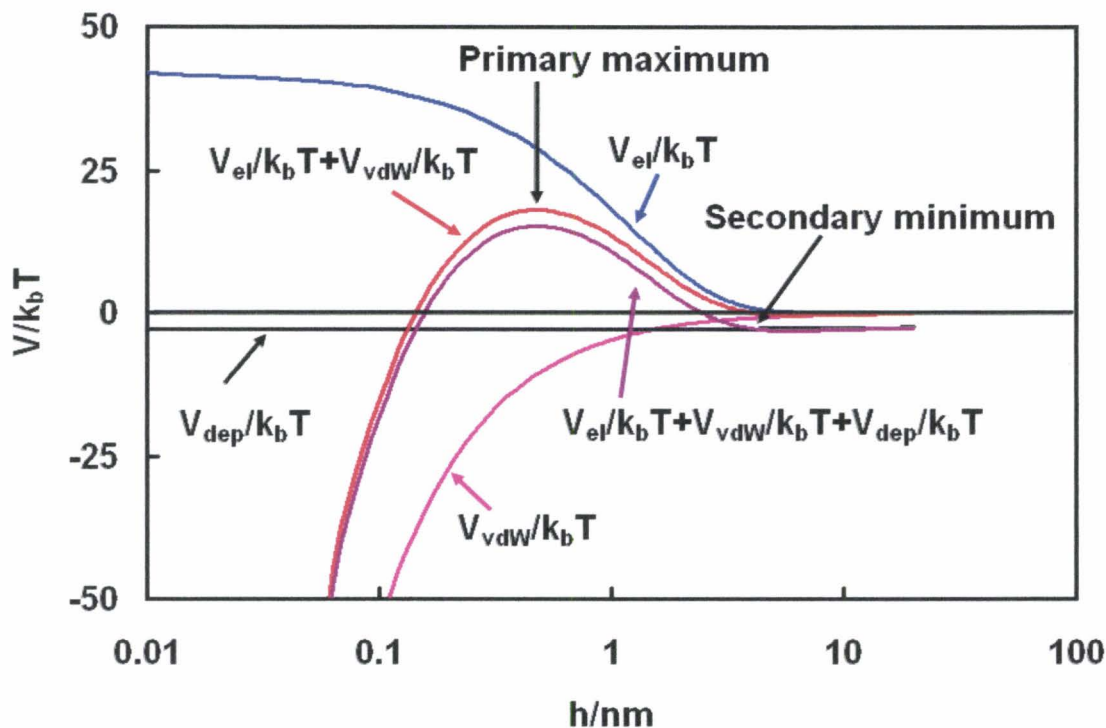


Figure 6.14 Mobility measurement of PA liposomes in the presence of PHG in HEPES buffer and borate buffer.



**Figure 6.15** Potential energy as a function of PA liposomes separation distance. The calculation of above potentials is based on the conditions: HPG volume fraction 0.05%, radius of gyration of HPG 128 nm, HPG molecular weight 1750000 Da, HPG second virial coefficient  $0.00003 \text{ cm}^3 \text{ mol/g}^2$ ; radius of PA liposome 40 nm, surface potential of PA liposome 38 mV, Hamaker constant of PA liposome  $7 \times 10^{-21} \text{ J}$ ; NaCl concentration 0.1 mol/L.

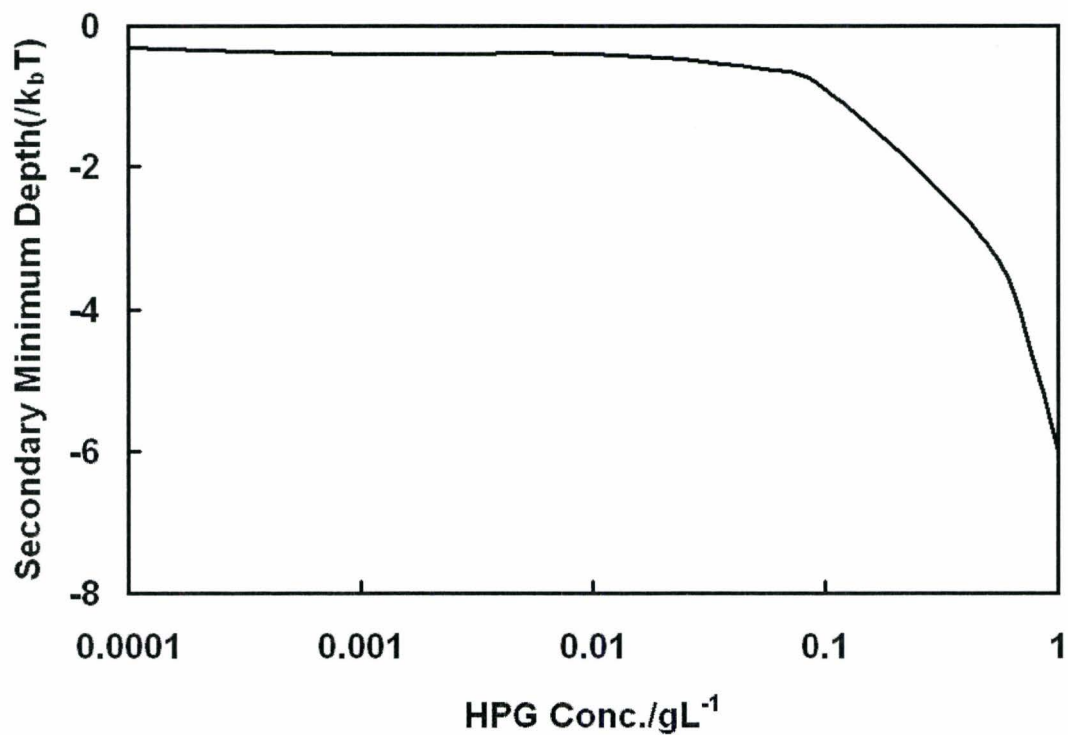


Figure 6.16 Secondary minimums of the sum of the potentials between PA liposomes as a function of HPG concentration.

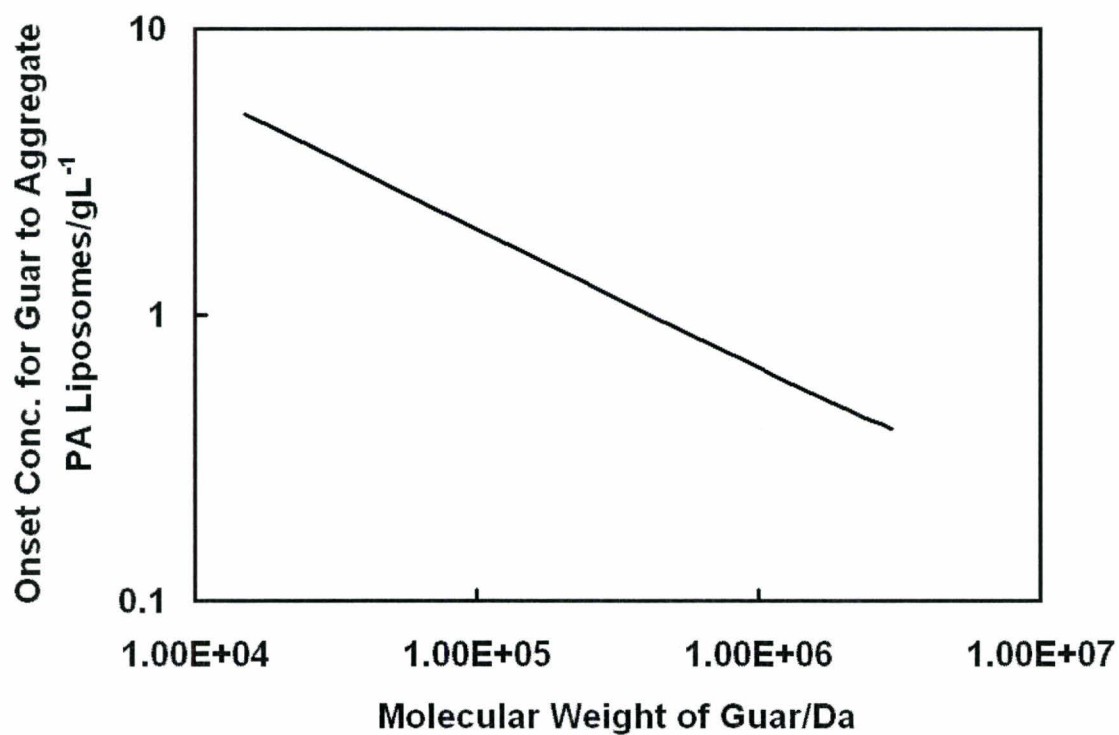


Figure 6.17 Molecular weight dependence of onset concentration for guar to aggregate PA liposomes.

## 6.7 References

1. Cui, Y. G.; Pelton, R.; Ketelson, H., Shapes of polyelectrolyte titration curves. 2. The deviant behavior of labile polyelectrolytes. *Macromolecules* 2008, 41, (21), 8198-8203.
2. Cui, Y. G.; Pelton, R.; Cosgrove, T.; Richardson, R.; Dai, S.; Prescott, S.; Grillo, I.; Ketelson, H.; Meadows, D., Not all anionic polyelectrolytes complex with DTAB. *Langmuir* 2009, 25, (24), 13712-13717.
3. Pelton, R.; Hu, Z.; Ketelson, H.; Meadows, D., Reversible flocculation with hydroxypropyl guar-borate, a labile anionic polyelectrolyte. *Langmuir* 2009, 25, (1), 192-195.
4. Bron, A. J.; Tiffany, J. M.; Gouveia, S. M.; Yokoi, N.; Voon, L. W., Functional aspects of the tear film lipid layer. *Experimental Eye Research* 2004, 78, (3), 347-360.
5. Norn, M. S., Semi-quantitative interference study of fatty layer of pre-corneal film. *Acta Ophthalmologica* 1979, 57, (5), 766-774.
6. Olsen, T., Reflectometry of the precorneal film. *Acta Ophthalmologica* 1985, 63, (4), 432-438.
7. Nicolaides, N.; Kaitaranta, J. K.; Rawdah, T. N.; Macy, J. I.; Boswell, F. M.; Smith, R. E., Meibomian gland studies - comparison of steer and human lipids. *Investigative Ophthalmology & Visual Science* 1981, 20, (4), 522-536.
8. Tiffany, J. M., The lipid secretion of the meibomian glands. *Advances in Lipid Research* 1987, 22, 1-62.
9. McCulley, J. P.; Shine, W. E., Meibomian gland and tear film lipids: Structure, function and control. In *Lacrimal gland, tear film, and dry eye syndromes 3: Basic science and clinical relevance, pts a & b*, Sullivan, D. A.; Stern, M. E.; Tsubota, K.; Dartt, D. A.; Sullivan, R. M.; Bromberg, B. B., Eds. 2002; Vol. 506, pp 373-378.
10. Miano, F.; Calcara, M.; Millar, T. J.; Enea, V., Insertion of tear proteins into a meibomian lipids film. *Colloids and Surfaces B-Biointerfaces* 2005, 44, (1), 49-55.
11. Millar, T. J.; Mudgil, P., Penetration of tear proteins into a meibomian lipid layer. *Investigative Ophthalmology & Visual Science* 2005, 46, 4418.
12. Millar, T. J.; Tragoulias, S. T.; Anderton, P. J.; Ball, M. S.; Miano, F.; Dennis, G. R.; Mudgil, P., The surface activity of purified ocular mucin at the air-liquid interface and interactions with meibomian lipids. *Cornea* 2006, 25, (1), 91-100.
13. Mudgil, P.; Torres, M.; Millar, T. J., Adsorption of lysozyme to phospholipid and meibomian lipid monolayer films. *Colloids and Surfaces B-Biointerfaces* 2006, 48, (2), 128-137.
14. Bangham, A. D., Liposomes - the babraham connection. *Chemistry and Physics of Lipids* 1993, 64, (1-3), 275-285.
15. Dickinson, E., Hydrocolloids at interfaces and the influence on the properties of dispersed systems. *Food Hydrocolloids* 2003, 17, (1), 25-39.
16. Dickinson, E.; Eriksson, L., Particle flocculation by adsorbing polymers. *Advances in Colloid and Interface Science* 1991, 34, 1-29.
17. Asakura, S.; Oosawa, F., Interaction between particles suspended in solutions of macromolecules. *Journal of Polymer Science* 1958, 33, (126), 183-192.

18. Sunamoto, J.; Iwamoto, K.; Kondo, H.; Shinkai, S., Liposomal membranes: Vi. Polysaccharide-induced aggregation of multilamellar liposomes of egg lecithin. *Journal of Biochemistry* 1980, 88, (5), 1219.
19. Kawakami, K.; Nishihara, Y.; Hirano, K., Effect of hydrophilic polymers on physical stability of liposome dispersions. *Journal of Physical Chemistry B* 2001, 105, (12), 2374-2385.
20. Anil Khanal, Y. C., Liang Zhang, Robert Pelton, Yuanyuan Ren, Howard Ketelson, Davies James, Bridging and depletion flocculation of cationic liposome by hydroxypropyl guar-borate, a labile anionic polyelectrolyte In preparation.
21. Bangham, A. D.; Hill, M. W.; Miller, N. G. A., Preparation and use of liposomes as models of biological membranes. *Methods Membr. Biol* 1974, 1, (1).
22. Jain, M. K., Introduction to biological membranes. *John Wiley & Sons* 1988, 98.
23. Antunes, F. E.; Marques, E. F.; Miguel, M. G.; Lindman, B., Polymer-vesicle association. *Advances in Colloid and Interface Science* 2009, 147-48, 18-35.
24. Ringsdorf, H.; Schlarb, B.; Venzmer, J., Molecular architecture and function of polymeric oriented systems - models for the study of organization, surface recognition, and dynamics of biomembranes. *Angewandte Chemie-International Edition in English* 1988, 27, (1), 113-158.
25. Hara, M.; Miyake, M.; Iijima, S.; Yang, Q.; Arai, T.; Yuan, H. Q.; Miyake, J., Interaction between a novel amphiphilic polymer and liposomes. *Supramolecular Science* 1998, 5, (5-6), 777-781.
26. Hayashi, H.; Kono, K.; Takagishi, T., Temperature-controlled release property of phospholipid vesicles bearing a thermo-sensitive polymer. *Biochimica Et Biophysica Acta-Biomembranes* 1996, 1280, (1), 127-134.
27. Torchilin, V. P.; Levchenko, T. S.; Whiteman, K. R.; Yaroslavov, A. A.; Tsatsakis, A. M.; Rizos, A. K.; Michailova, E. V.; Shtilman, M. I., Amphiphilic poly-n-vinylpyrrolidones: Synthesis, properties and liposome surface modification. *Biomaterials* 2001, 22, (22), 3035-3044.
28. Polozova, A.; Winnik, F. M., Mechanism of the interaction of hydrophobically-modified poly-(n-isopropylacrylamides) with liposomes. *Biochimica Et Biophysica Acta-Biomembranes* 1997, 1326, (2), 213-224.
29. Vial, F.; Rabhi, S.; Tribet, C., Association of octyl-modified poly(acrylic acid) onto unilamellar vesicles of lipids and kinetics of vesicle disruption. *Langmuir* 2005, 21, (3), 853-862.
30. Okumura, Y.; Mizushima, H.; Fujinaga, K.; Sunamoto, J., Immobilization of liposomes on hydrophobically modified polymer gel particles in batch mode interaction. *Colloids and Surfaces B-Biointerfaces* 2007, 55, (2), 235-240.
31. Derjaguin, B.; Landau, L., A theory of the stability of strongly charged lyophobic sols and the coalescence of strongly charged particles in electrolytic solution. *Acta Phys.-Chim. USSR* 1941, 14, 633-662.
32. Verwey, E. J. W.; Overbeek, J., Th. G.(1948) theory of the stability of lyophobic colloids. *Elsevier Publ. Co. Inc., London* 8, (8), 9.
33. Hunter, R. J.; White, L. R.; Chan, D. Y. C., *Foundations of colloid science*. Clarendon Press Oxford: 1987, 415.

34. Seebergh, J. E.; Berg, J. C., Depletion flocculation of aqueous, electrosterically-stabilized latex dispersions. *Langmuir* 1994, 10, (2), 454-463.
35. Marra, J.; Israelachvili, J., Direct measurements of forces between phosphatidylcholine and phosphatidylethanolamine bilayers in aqueous electrolyte solutions. *Biochemistry* 1985, 24, (17), 4608-4618.
36. Fleer, G. J.; Scheutjens, J.; Vincent, B., The stability of dispersions of hard spherical-particles in the presence of nonadsorbing polymer. *Acs Symposium Series* 1984, 240, 245-263.
37. Simonet, F.; Garnier, C.; Doublier, J. L., Description of the thermodynamic incompatibility of the guar-dextran aqueous two-phase system by light scattering. *Carbohydrate Polymers* 2002, 47, (4), 313-321.
38. Vincent, B., The calculation of depletion layer thickness as a function of bulk polymer concentration. *Colloids and Surfaces* 1990, 50, 241-249.
39. Picout, D. R.; Ross-Murphy, S. B.; Errington, N.; Harding, S. E., Pressure cell assisted solution characterization of polysaccharides. 1. Guar gum. *Biomacromolecules* 2001, 2, (4), 1301-1309.
40. Rawson, S.; Ryan, K.; Vincent, B., Depletion flocculation in sterically stabilized aqueous systems using poly-electrolytes. *Colloids and Surfaces* 1988, 34, (1), 89-93.
41. Snowden, M. J.; Clegg, S. M.; Williams, P. A.; Robb, I. D., Flocculation of silica particles by adsorbing and nonadsorbing polymers. *Journal of the Chemical Society-Faraday Transactions* 1991, 87, (14), 2201-2207.
42. Dickinson, E.; Goller, M. I.; Wedlock, D. J., Osmotic-pressure, creaming, and rheology of emulsions containing nonionic polysaccharide. *Journal of Colloid and Interface Science* 1995, 172, (1), 192-202.
43. Tuinier, R.; Rieger, J.; de Kruif, C. G., Depletion-induced phase separation in colloid-polymer mixtures. *Advances in Colloid and Interface Science* 2003, 103, (1), 1-31.

## Chapter 7 Concluding Remarks

In this work, I have investigated the properties of HPG-borate by polyelectrolyte titration and behaviors of HPG-borate in solutions as a polyelectrolyte, such as interaction with oppositely charged surfactant. The interaction of HPG-borate with proteins mostly existing in aqueous phase of tear film has been investigated using model protein, lysozyme. The effect of HPG-borate on lipid layer stability has been evaluated using phosphatidic acid (PA) liposome as a model. The research objectives set in Chapter 1 have been fulfilled.

### 7.1 Key Findings and Contributions

The key findings and major contributions of this research are:

The research findings in this thesis suggest that HPG-borate/lysozyme do not form complexes through electrostatic attraction in physiological conditions. HPG-borate behaves like a neutral polymer not a polyelectrolyte in physiological conditions. High concentration of salt screens the electrostatic interaction between HPG-borate and lysozyme. Considering that lysozyme is the protein that can most possibly interact with HPG-borate through electrostatic attraction because they are oppositely charged in physiological conditions, other proteins probably do not interact with HPG-borate as well in physiological conditions.

For the first time, HPG-borate is proposed of being able to flocculate phosphatidic acid (PA) liposomes by depletion mechanism in tear film at high HPG concentrations. High concentrations of guar and neutral guar derivatives can also induce the aggregation of PA liposomes due to depletion forces. Therefore, HPG-borate, guar and neutral guar derivatives have the potential to inhibit the emulsification of PA lipid so as to stabilize the lipid layer.

Our findings suggest that dilute HPG in the presence of borate does not interact with oppositely charged surfactant with the concentration below critical micelle concentration (cmc) of the surfactant. But it does induce some aggregation of micelles through bridging mechanism. These findings suggest that the concentrations of surfactants should be carefully controlled to be below cmc in artificial tear formulations if cationic surfactants are going to be used.

Behaving as a polyelectrolyte, HPG-borate does form insoluble complexes with oppositely charged polyelectrolyte, such as PDADMAC, by electrostatic attraction. This suggests that we should be careful when importing any new artificial tear components because HPG-borate may interact with some cationic additives, such as polyquad (polyquaternium preservative).

Borate can cross-link HPG so as to form gels especially in high concentrations of HPG solutions. We suggest from our findings that monoborate such as phenyl borate and methyl borate can be applied as a substitute to borate to avoid the cross-linking of HPG.

Our findings suggest that some behaviors of HPG-borate are different from conventionally defined strong and weak polyelectrolyte. For example, the complexes formation between HPG-borate and PDADMAC facilitates the further binding of borate to HPG polymer chain and HPG-borate flocculates oppositely charged polystyrene latex particle reversibly<sup>1</sup>. Therefore, for the first time we name HPG-borate a labile polyelectrolyte.

A model is developed to predict the polyelectrolyte titration curve of the labile polyelectrolytes such as HPG-borate. Polyelectrolyte titration results also show that the borate binding sites on HPG are possibly only on galactoses.

In general, electrostatic interaction is not the major mechanism in the interaction of HPG-borate with tear film components. High concentration of salt screens the electrostatic interaction in physiological conditions. In addition, low charge density of HPG-borate weakens the strength of electrostatic interaction at low pH (7.4) in physiological conditions. The major interaction mechanism in tear film as we suggest is depletion mechanism. Tear film components such as PA liposome tend to be flocculated by HPG-borate, HPG, guar and its neutral derivatives at high concentrations by depletion mechanism.

## 7.2 Future Work

The future work we suggest:

Design experiments to find evidence that HPG-borate induce flocculation of liposome formed from lipid layer components by depletion mechanism.

All the experiments were done assuming that the interaction of HPG-borate and model tear film components reached equilibrium. In the future, the kinetics of HPG-borate interaction with these model tear film components will be helpful to assess HPG-borate application as an artificial tear component.

### 7.3 References

1. Pelton, R.; Hu, Z.; Ketelson, H.; Meadows, D., Reversible flocculation with hydroxypropyl guar-borate, a labile anionic polyelectrolyte. *Langmuir* 2009, 25, (1), 192-195.

## Appendices

### Appendix A: Modeling of polyelectrolyte titration of HPG/borate with PDADMAC

**Objective:** This calculation is to model polyelectrolyte titration of HPG/borate with PDADMAC

**Assumptions:**

1. The SCD output is proportional to the streaming current which in turn proportional to streaming potential. (Walker et al. 1996).

$$SCD = \alpha \xi$$

2. The titrant is uniformly distributed on the detector walls and in solution so that the titrant corresponding to isoelectric point of the adsorbed layer represent the isoelectric point of the polyelectrolyte complex species in solution.

3. Every added PDADMAC chain binds to a HPG chain and PDADMAC binds to HPG in solution and on surface in the same amount.

4. The addition of PDADMAC which form polyelectrolyte complex with borate bound HPG facilitates the binding of borate on HPG binding sites.

#### Symbols

B - uncharged  $B(OH)_3$ ; P - concentration of HPG binding sites; BP - concentration of HPG bound borate; BOH - borate anion,  $B_T$  - total boron concentration, OH - hydroxy ion concentration, H - hydrogen ion concentration

**The equation set**

$$P_T = P + BP \quad \text{polymer balance}$$

$$B_T = B + BOH + BP \quad \text{boron balance}$$

$$K_0 = \frac{BOH}{B \cdot OH} \quad \text{borate buffer}$$

$$K_1 = \frac{BP}{BOH_s \cdot P} \quad \text{borate binding constant}$$

BOH<sub>s</sub> is borate anion concentration at the surface which is lower because of electrostatic repulsion. Thus a charged surface inhibits binding

From the Boltzmann equation

$$BOH_s = BOH \cdot \exp\left(\frac{e_0 \cdot \psi \cdot \gamma}{k_b \cdot T}\right) = \lambda \cdot BOH$$

The is equivalent to equation 6 in Leibler, L.; Pezron, E.; Pincus, P. A. Polymer 1988, 29, (6), 1105-1109.

Term  $\gamma$  is an adjustable correction term

$$\frac{B_T}{2} = OH + BOH + BP - H$$

Charge balance - ignoring PDADMAC, the only source of cations is the initial borax addition and protons.

$$K_w = OH \cdot H \quad \text{Dissociation of water}$$

$$\psi = 2 \cdot \frac{\operatorname{asinh}\left(-\frac{1}{2} \cdot \sigma_d \cdot \frac{\epsilon_0}{\epsilon_0 \cdot \epsilon_r \cdot k_b \cdot T \cdot \kappa(\text{NaCl})}\right)}{\epsilon_0} \cdot k_b \cdot T$$

equation 4 from Pelton, R.;  
Cabane, B.; Cui, Y.;  
Ketelson, H. Anal. Chem.  
2007, 79, 8114-8117.

collecting constants

$$\omega = \frac{\epsilon_0}{\epsilon_0 \cdot \epsilon_r \cdot k_b \cdot T}$$

$$\psi = 2 \cdot \frac{\operatorname{asinh}\left(-\frac{1}{2} \cdot \sigma_d \cdot \frac{\omega}{\kappa(\text{NaCl})}\right)}{\epsilon_0} \cdot k_b \cdot T$$

$$\sigma_d = \sigma_{dl} + \sigma_{HPG} + \sigma_{DAD}$$

$\sigma_d$  is the total surface charge density

$\sigma_{dl}$  is the original value in the cell

$\sigma_{HPG}$  is the contribution due to HPG-borate

$\sigma_{DAD}$  is the contribution due to PDADMAC

Defining the surface polymer layer

$$\sigma_{HPG} = \frac{\Gamma_{HPG}}{EW_{max}} \cdot \frac{BP}{BT} \cdot F$$

$\Gamma_{HPG}$  is the amount of adsorbed HPG - a parameter and is assumed to be constant

$EW_{max}$  is the equivalent weight of fully charged HPG.

$$\Gamma_{DAD} = \frac{C_{DAD}}{C_{HPG}} \cdot \Gamma_{HPG}$$

$C_{DAD}$  is the mass concentration of added PDADMAC in the cell

$C_{HPG}$  is the mass concentration of HPG in the cell

**Assume:**

1. Every added PDADMAC chain binds to a HPG
2. Adsorbed and solution polymers are the same

$$\sigma_{\text{DAD}} = \frac{\Gamma_{\text{DAD}} \cdot F}{\text{EW}_{\text{DAD}}} = \frac{C_{\text{DAD}}}{C_{\text{HPG}}} \cdot \frac{\Gamma_{\text{HPG}} \cdot F}{\text{EW}_{\text{DAD}}}$$

$$\sigma_{\text{d}} = \sigma_{\text{dl}} - \frac{\Gamma_{\text{HPG}}}{\text{EW}_{\text{max}}} \cdot \frac{\text{BP}}{P_{\text{T}}} \cdot F + \frac{C_{\text{DAD}}}{C_{\text{HPG}}} \cdot \frac{\Gamma_{\text{HPG}} \cdot F}{\text{EW}_{\text{DAD}}}$$

**Recasting equations for Numerical solution**

$\frac{\text{BP}}{P_{\text{T}}}$  is the fraction of occupied borate binding sites

$$K_1 = \frac{\text{BP}}{\lambda \cdot \text{BOH} \cdot P} \quad \text{Rearranging} \quad \text{BOH} = \frac{\text{BP}}{\lambda \cdot K_1 \cdot P}$$

$$\text{Substituting polymer balance gives} \quad \text{BOH} = \frac{\text{BP}}{\lambda \cdot K_1 \cdot (P_{\text{T}} - \text{BP})}$$

$$\text{Substituting in } \lambda \text{ gives} \quad \text{BOH} = \frac{\text{BP}}{\exp\left(\frac{e_0 \cdot \gamma \cdot \psi}{k_{\text{b}} \cdot T}\right) \cdot K_1 \cdot (P_{\text{T}} - \text{BP})}$$

$$\text{Substituting} \quad \psi(\text{NaCl}) = 2 \cdot \frac{\text{asinh}\left(\frac{1}{2} \cdot \sigma_{\text{d}} \cdot \frac{\omega}{\kappa(\text{NaCl})}\right)}{e_0} \cdot k_{\text{b}} \cdot T$$

$$\text{BOH} = \frac{\text{BP}}{[K_1 \cdot (P_{\text{T}} - \text{BP})]} \cdot \exp\left(e_0 \cdot \gamma \cdot 2 \cdot \frac{\text{asinh}\left(\frac{1}{2} \cdot \sigma_{\text{d}} \cdot \frac{\omega}{\kappa(\text{NaCl})}\right)}{e_0}\right)^{-1}$$

$$K_0 = \frac{BOH}{B \cdot OH} \quad \text{Rearranging} \quad BOH = K_0 \cdot OH \cdot B$$

Substitute from boron balance

$$BOH = K_0 \cdot OH \cdot (B_T - BOH - BP) \quad \text{solve, BOH} \rightarrow -\frac{K_0 \cdot OH \cdot (BP - B_T)}{K_0 \cdot OH + 1}$$

$$BOH = -K_0 \cdot OH \cdot \frac{-B_T + BP}{1 + K_0 \cdot OH}$$

Substituting  $K_w$  into charge balance to eliminate proton ion

$$\frac{B_T}{2} = OH + BOH + BP - \frac{K_w}{OH}$$

## Constants

$$\epsilon_r := 78$$

Relative permittivity

$$T := 298K$$

Temperature

$$NaCl := 0.01 \frac{\text{mol}}{L}$$

Background electrolyte

$$\kappa(NaCl) := \left( \frac{\epsilon_0^2 \cdot N_{av}}{\epsilon_r \epsilon_0 \cdot k_b \cdot T} \cdot 2 \cdot NaCl \right)^{0.5}$$

Corresponding kappa

$$EW_{DAD} := 161.5Da$$

Equivalent molecular weight of PDADMAC

$$\rho := \frac{\text{gm}}{\text{mL}}$$

Density of solutions

**Borate binding constant**

$$pK_a := 9.2$$

$$K_w := 10^{-14} \left( \frac{\text{mol}}{\text{L}} \right)^2$$

$$K_0 := 10^{14-pK_a} \frac{\text{L}}{\text{mol}}$$

$$K_0 = 6.3096 \times 10^4 \frac{\text{L}}{\text{mol}} \quad \text{Boric acid association constant}$$

**SCD and HPG Properties**

$$\sigma_{d1} := -0.06 \frac{\text{C}}{\text{m}^2} \quad \text{Initial charge on the cell}$$

$$\Gamma_{\text{HPG}} := 2 \frac{\text{mg}}{\text{m}^2} \quad \text{Amount adsorbed HPG}$$

$$EW_{\text{max}} := 650 \text{Da} \quad \text{Minimum equivalent molecular weight of HPG/borate}$$

$$\omega := \frac{e_0}{\epsilon_0 \cdot \epsilon_r \cdot k_b \cdot T} \quad \text{Collection of constants}$$

$$\omega = 5.6385 \times 10^{10} \text{C}^{-1} \cdot \text{m}$$

**Input variables for calculation - these can be varied**

$$P_T := \frac{0.01\% \cdot \rho}{EW_{\max}}$$

HPG concentration expressed as molarity of borate binding sites

$$P_T = 1.5385 \times 10^{-4} \cdot \frac{\text{mol}}{\text{L}}$$

$$C_{\text{HPG}}(P_T) := \frac{P_T \cdot EW_{\max}}{\rho}$$

Function gives corresponding mass fraction of HPG

$$C_{\text{HPG}}(P_T) = 1 \times 10^{-4}$$

$$B_T := 0.019 \frac{\text{mol}}{\text{L}}$$

Total boron concentration

$$K_1 := 100.0 \frac{\text{L}}{\text{mol}}$$

Borate/HPG binding constant

$$\text{OH}_I := 10^{-(14-pK_a)} \frac{\text{mol}}{\text{L}}$$

Initial hydroxyl ion concentration from borax

$$\text{OH}_I = 1.5849 \times 10^{-5} \cdot \frac{\text{mol}}{\text{L}}$$

$$D_{\text{ad}} := 0.0001 \frac{\text{mole}}{\text{L}}$$

Molar concentration of quaternary groups from PDADMAC

$$C_{\text{Dad}}(D_{\text{ad}}) := \frac{D_{\text{ad}} \cdot EW_{\text{DAD}}}{\rho}$$

Corresponding mass fraction of PDADMAC in cell

$$\gamma := 3$$

An adjustable parameter used in Boltzmann equation

$$\text{BOH}_s = \text{BOH} \cdot \exp\left(\frac{e_0 \cdot \psi \cdot \gamma}{k_b \cdot T}\right) = \lambda \cdot \text{BOH}$$

## Solving simultaneous equations using Mathcad solver

### Initial guesses

$$\text{BOH} := 0.5 \cdot \text{B}_T$$

Free borate

$$\text{OH} := \text{OH}_I$$

$$\text{BP} := 0.05 \cdot \text{P}_T$$

Bound borate

$$\psi := -100\text{mV}$$

### Solve block

Given

$$\text{BOH} = -K_0 \cdot \text{OH} \cdot \frac{-\text{B}_T + \text{BP}}{1 + K_0 \cdot \text{OH}}$$

$$\text{BOH} = \frac{\text{BP}}{[K_1 \cdot (\text{P}_T - \text{BP})]} \cdot \exp \left[ \gamma \cdot 2 \cdot \text{asinh} \left[ \frac{1}{2} \cdot \left( \sigma_{d1} - \frac{\Gamma_{\text{HPG}}}{\text{EW}_{\text{max}}} \cdot \frac{\text{BP}}{\text{P}_T} \cdot \text{F} + \frac{\text{Dad}}{\text{P}_T \cdot \text{EW}_{\text{max}}} \cdot \Gamma_{\text{HPG}} \cdot \text{F} \right) \cdot \frac{\omega}{\kappa(\text{NaCl})} \right] \right]^{-1}$$

$$\frac{\text{B}_T}{2} = \text{OH} + \text{BOH} + \text{BP} - \frac{K_w}{\text{OH}}$$

$$0 \frac{\text{mol}}{\text{L}} \leq \text{BOH} \leq \text{B}_T$$

$$0 \frac{\text{mol}}{\text{L}} \leq \text{BP} \leq \text{B}_T$$

$$0 \frac{\text{mol}}{\text{L}} \leq \text{BP} \leq \text{P}_T$$

$$f(\text{B}_T, \text{P}_T, K_1, \text{NaCl}, \text{Dad}, \Gamma_{\text{HPG}}, \gamma, \sigma_{d1}) := \text{Find}(\text{BOH}, \text{BP}, \text{OH})$$

### Example calculation

$$f(\text{B}_T, \text{P}_T, K_1, \text{NaCl}, \text{Dad}, \Gamma_{\text{HPG}}, \gamma, \sigma_{d1}) = \begin{pmatrix} 9.4153 \times 10^{-3} \\ 6.9054 \times 10^{-5} \\ 1.5682 \times 10^{-5} \end{pmatrix} \cdot \frac{\text{mol}}{\text{L}}$$

BOH

BP

OH

$$\psi(B_T, P_T, K_1, NaCl, Dad, \Gamma_{HPG}, \gamma, \sigma_{d1}) := \frac{2 \cdot k_b \cdot T}{e_0} \cdot \operatorname{asinh} \left[ \frac{1}{2} \cdot \left[ \frac{\left[ \begin{array}{l} \sigma_{d1} \dots \\ + \left( \frac{-\Gamma_{HPG}}{EW_{max}} \cdot \frac{f(B_T, P_T, K_1, NaCl, Dad, \Gamma_{HPG}, \gamma, \sigma_{d1})}{P_T} \right) \cdot F \right]}{C_{Dad}(Dad) \cdot \frac{\Gamma_{HPG} \cdot F}{CHPG(P_T)} \cdot \frac{1}{EW_{DAD}}} \right]}{\frac{\kappa(NaCl)}{\omega}} \right] \right]$$

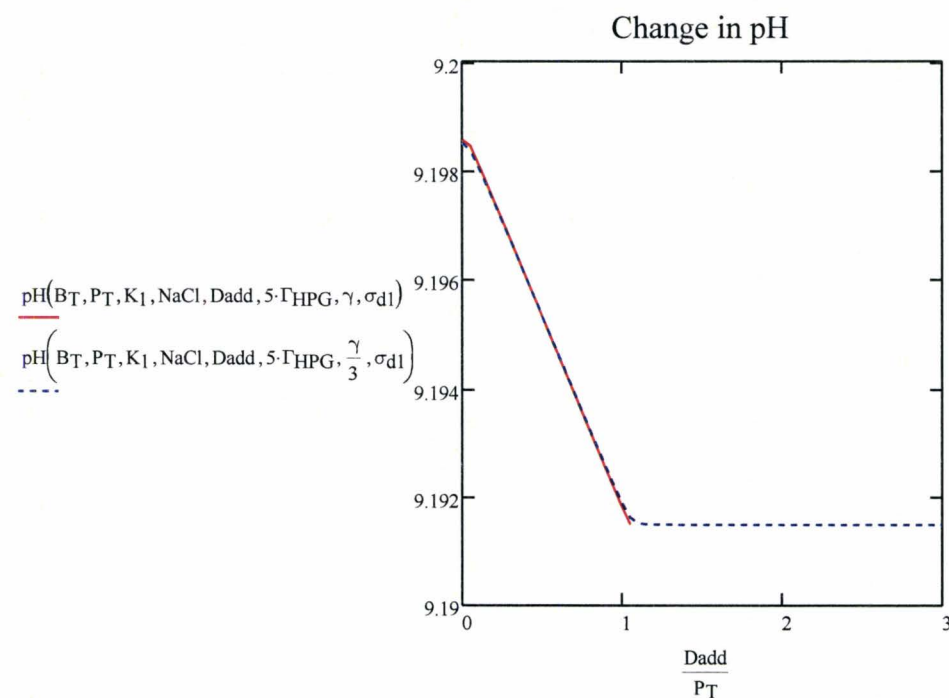
$$\psi(B_T, P_T, K_1, NaCl, Dad, \Gamma_{HPG}, \gamma, \sigma_{d1}) = -1.2418 \cdot mV$$

$$pH(B_T, P_T, K_1, NaCl, Dad, \Gamma_{HPG}, \gamma, \sigma_{d1}) := 14 + \log \left( \frac{f(B_T, P_T, K_1, NaCl, Dad, \Gamma_{HPG}, \gamma, \sigma_{d1})}{\frac{\text{mole}}{L}} \right)$$

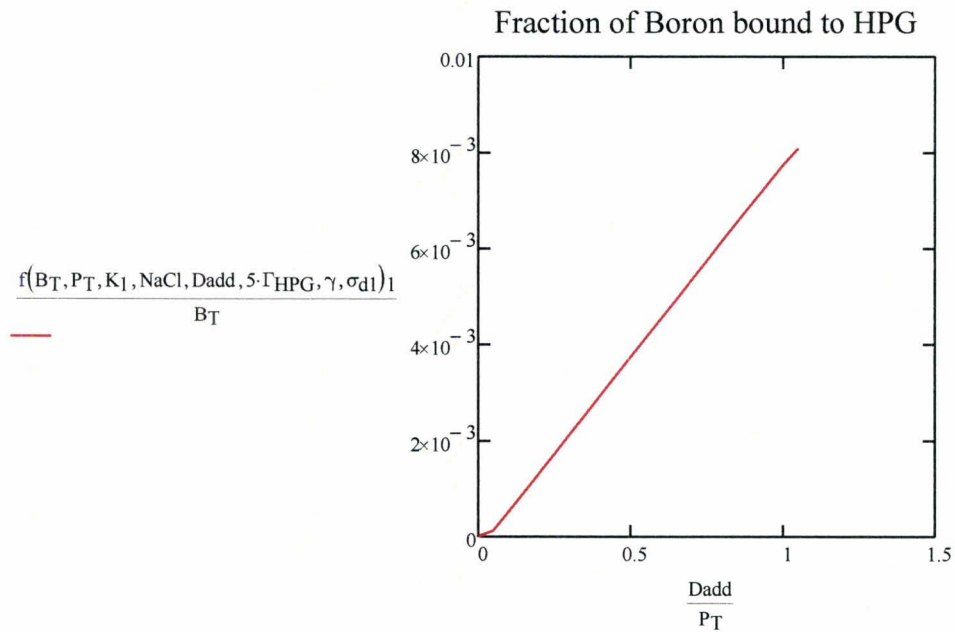
### Simulating Polyelectrolyte Titrations

Dadd := 0·P<sub>T</sub>, 0.05·P<sub>T</sub>.. 3·P<sub>T</sub>      Range of PDADM<sub>AC</sub> concentrations during a titration

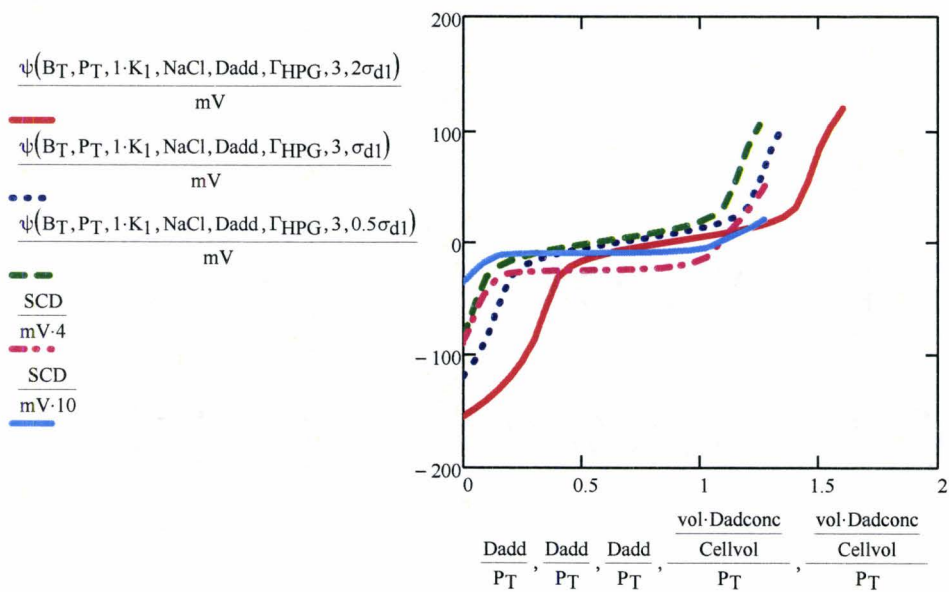
Binding of boric acid to HPG lowers pH



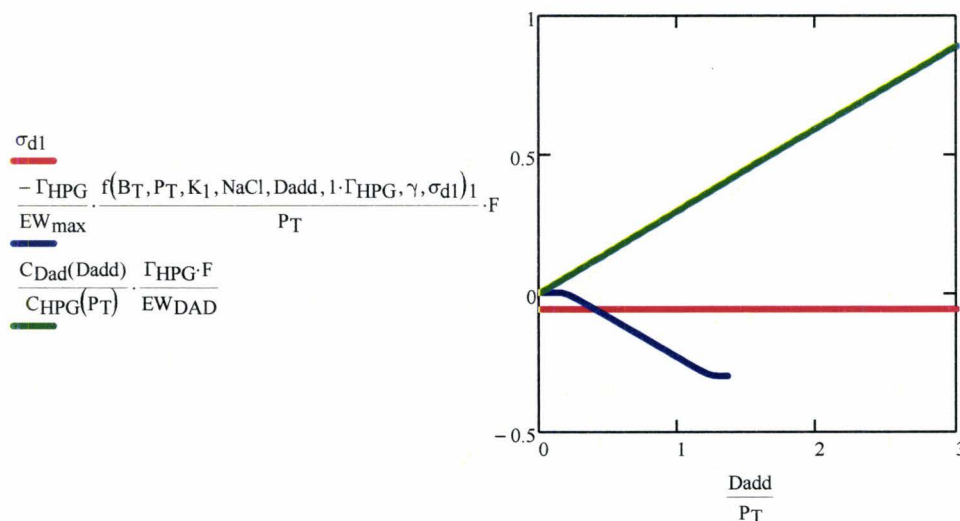
In this case only a small fraction of the borate is bound to HPG



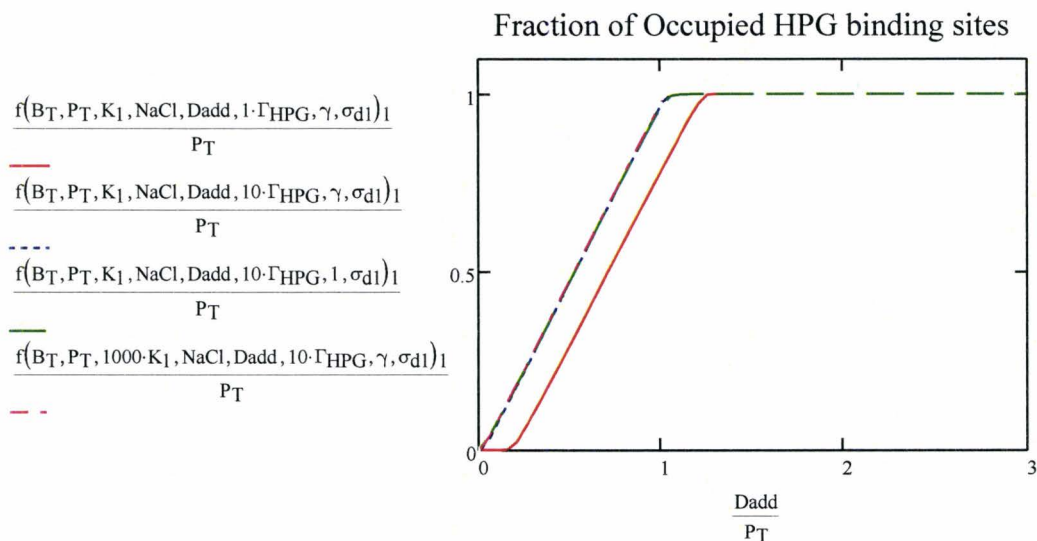
The effect of initial charge density on the cell



Components of surface charge density

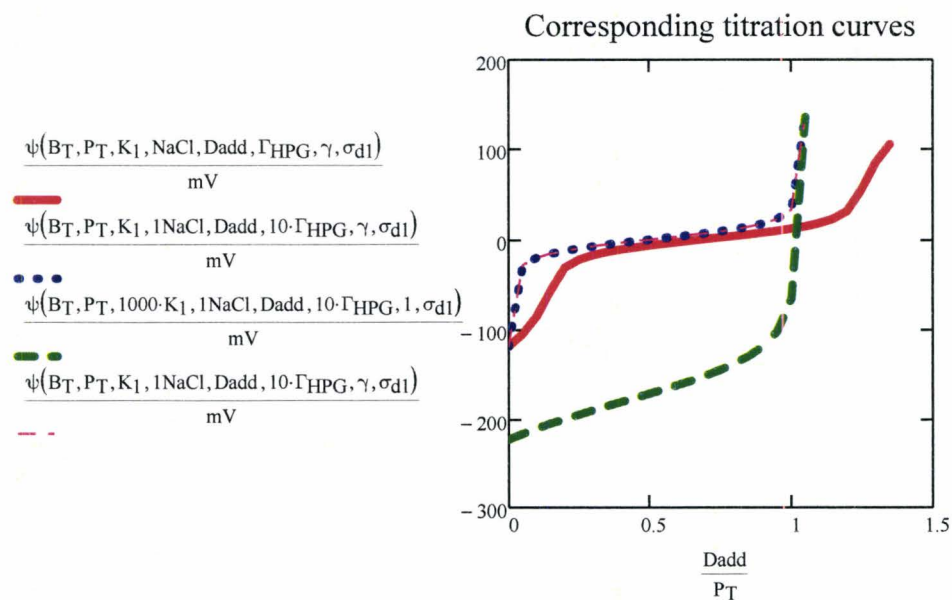


The Titration Endpoint

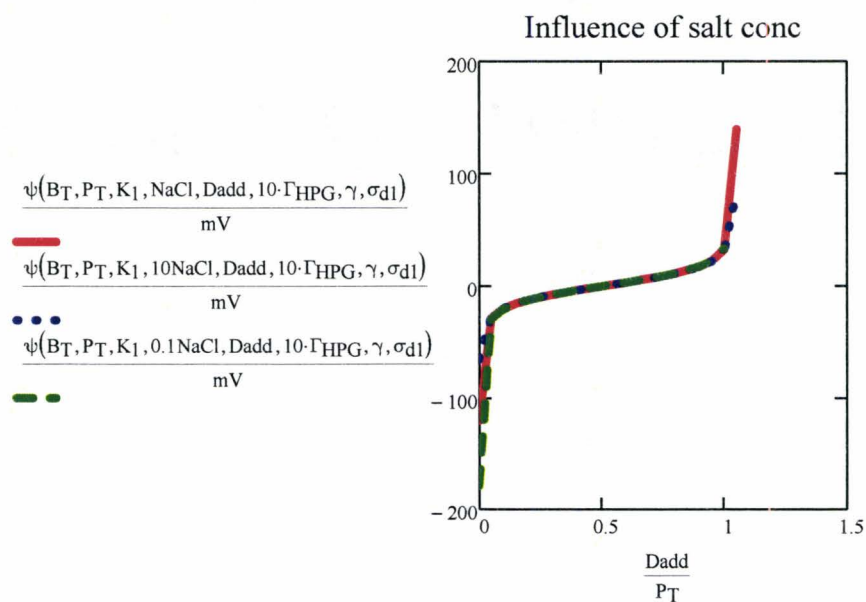


All titrations saturate the HPG. However, endpoint stoichiometry is only achieved if there is sufficient adsorbed HPG. Endpoint is not sensitive to  $\gamma$  or  $K_1$ , whereas shape of titration curves is.

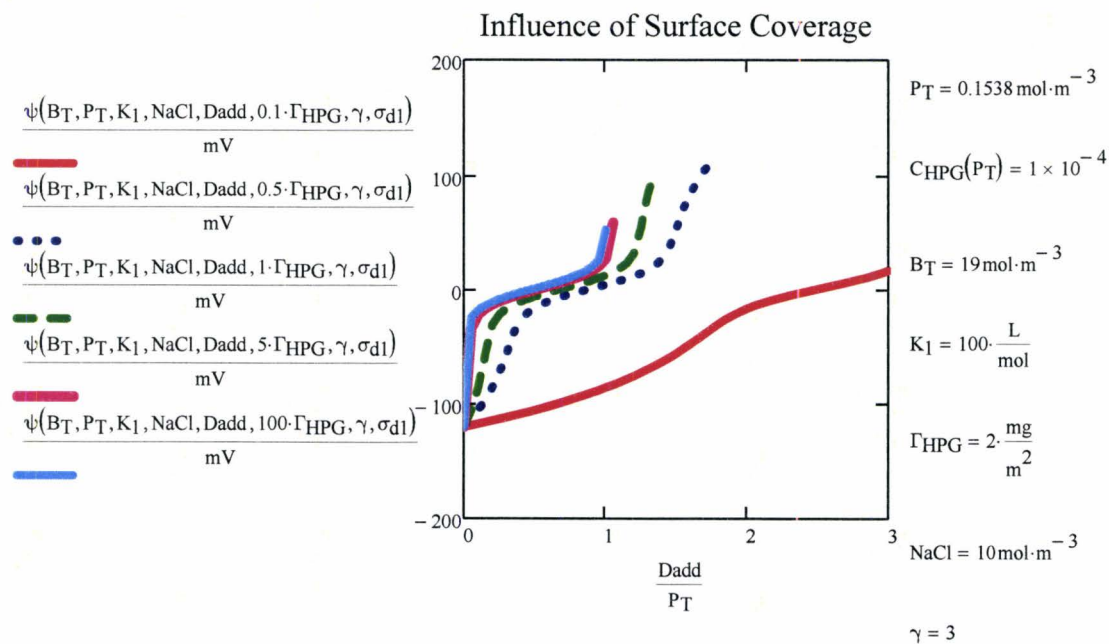
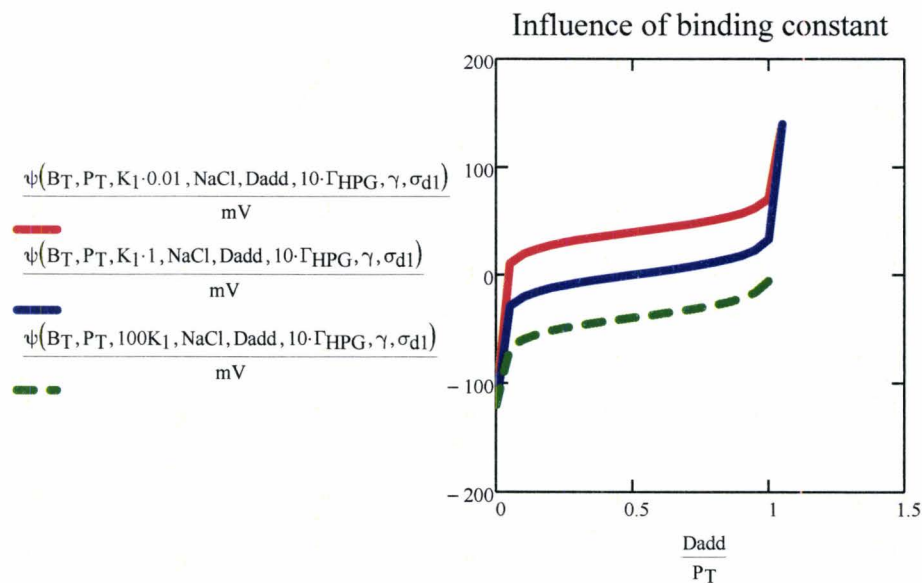
The corresponding titration curves, shown below, indicate that although the endpoints are stoichiometric if  $\Gamma$  is big enough, the shapes vary - When  $K_1$  is large, the behavior is the same as a strong polyelectrolyte.

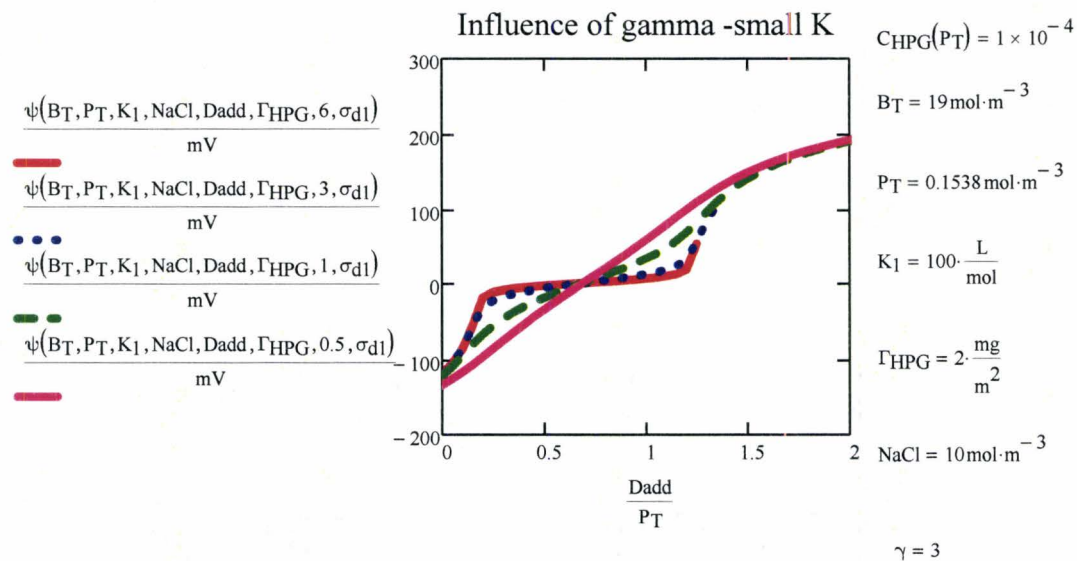
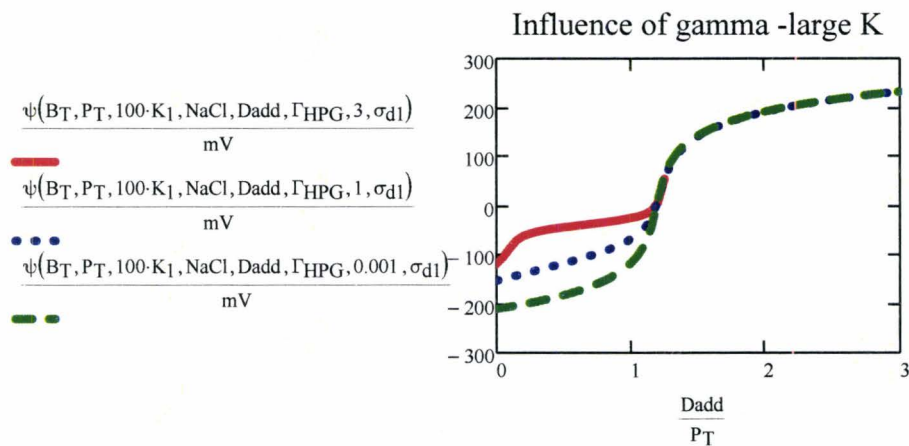


Ionic strength influences initial potential shape at the end

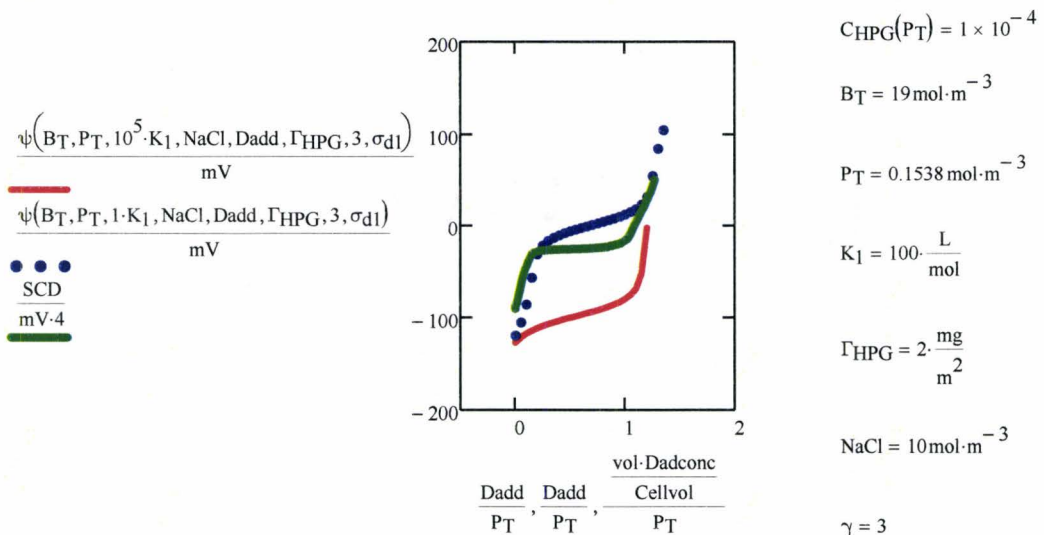


The binding constant dictates the potential corresponding to the flat part of the curve

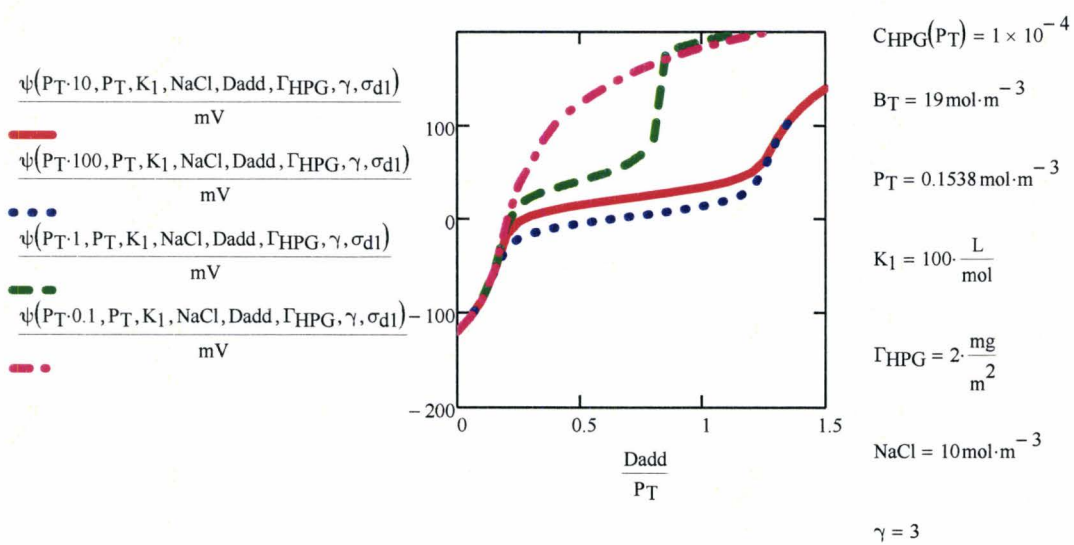




**Fitting experimental data**

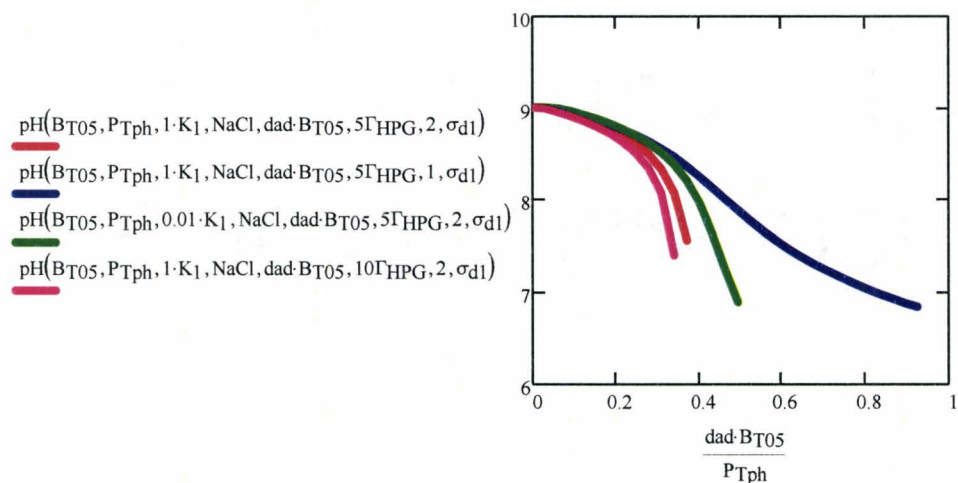
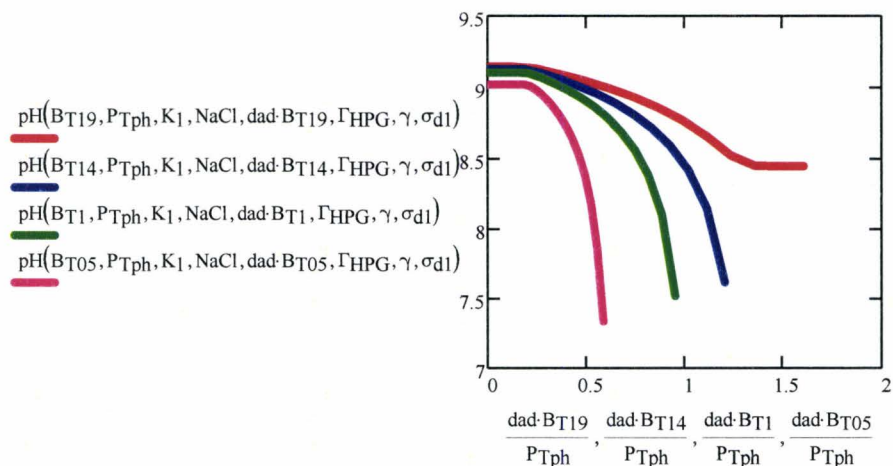


**Influence of Boron Content**



### Simulating pH Change During Titration

dad := 0, 0.05 .. 2



Gamma has biggest effect on shape.

Weakening the binding constant also has an influence.

## Appendix B

### Appendix B.1: Determination of Charge Density on Lysozyme by Polyelectrolyte Titration

The detailed procedure of polyelectrolyte titration was described in Chapter 3. In determining the charge density on lysozyme, we used  $1 \times 10^{-3}$  eq/L of PVSK as standard titrant, and the ionic strength in PVSK solution was adjusted to 0.01 mol/L using solid NaCl. Sample solutions with 0.3 g/L lysozyme in 0.01 mol/L NaCl were prepared. The pH of solutions was adjusted using 0.01 mol/L sodium borate buffer and 0.05 mol/L HEPES buffer to 9.2 and 7.4 respectively. The zero signal of a streaming current detector was used to determine the endpoint of polyelectrolyte titration. The results showed that 2.18 and 1.85 mL of PVSK were consumed to neutralize 10 mL of lysozyme at pH 7.4 and 9.2 respectively. The charge concentration of lysozyme was calculated using equation (1):

$$C_{lyso} = \frac{C_{PVSK} V_{PVSK}}{V_{lyso}} \quad (1)$$

where  $C_{lyso}$  is the charge concentration of lysozyme,  $C_{PVSK}$  is the charge concentration of PVSK ( $1 \times 10^{-3}$  eq/L),  $V_{PVSK}$  is the volume of PVSK consumed at endpoint,  $V_{lyso}$  is the volume of lysozyme solution loaded (10 mL). The calculated charge concentration of lysozyme at pH 7.4 and 9.2 were  $2.18 \times 10^{-4}$  eq/L and  $1.85 \times 10^{-4}$  eq/L respectively.

## Appendix B.2: One site binding model for isothermal titration calorimetry (ITC)

From the MicroCal ITC tutorial guide, the binding constant for the ligand and macromolecules can be expressed as:

$$K = \frac{\Theta}{(1-\Theta)[X]} \quad (1)$$

where  $\Theta$  is fraction of sites occupied by ligand X, and  $[X]$  is the free concentration of ligand. The total ligand concentration can be calculated by:

$$X_t = [X] + n\Theta M_t \quad (2)$$

where  $n$  is number of sites,  $X_t$  is the total ligand concentration,  $M_t$  is the total concentration of macromolecules. Combining equation (1) and (2) gives

$$\Theta^2 - \Theta \left[ 1 + \frac{X_t}{nM_t} + \frac{1}{nKM_t} \right] + \frac{X_t}{nM_t} = 0 \quad (3)$$

The total released heat at fractional saturation  $\Theta$  is

$$Q = n\Theta M_t \Delta H V_0 \quad (4)$$

where  $\Delta H$  is the molar heat of ligand binding, and  $V_0$  is the volume of the titration cell. Solving equation (3) for  $\Theta$  and then substituting into equation (4) gives

$$Q = \frac{nM_t \Delta H V_0}{2} \left[ 1 + \frac{X_t}{nM_t} + \frac{1}{nKM_t} - \sqrt{\left( 1 + \frac{X_t}{nM_t} + \frac{1}{nKM_t} \right)^2 - \frac{4X_t}{nM_t}} \right] \quad (5)$$

The  $Q$  of the  $i^{\text{th}}$  injection,  $Q(i)$ , can be calculated using above equation. But volume correction must be made for the injections of ligand liquid. The correct expression for heat released,  $\Delta Q(i)$ , from the  $i^{\text{th}}$  injection is

$$\Delta Q(i) = Q(i) - Q(i-1) + \frac{dV_i}{V_0} \left[ \frac{Q(i) + Q(i-1)}{2} \right] \quad (6)$$

The procedure of fitting using Origin, involves

1. initial guesses for  $n$ ,  $K$  and  $\Delta H$ ,

2. calculation of  $\Delta Q(i)$  for each injection and comparison of these values with the measured heat for the corresponding experimental injections,
3. improvement in the values of  $n$ ,  $K$  and  $\Delta H$ ,
4. iteration of the above procedure until no further improvement is needed.

The one site model finally gives  $n$ ,  $K$  and  $\Delta H$  for the specific experimental data.

### Appendix B.3: Calculation of charge ratio of CMG or HPG-borate to lysozyme and molar ratio of HMG to lysozyme

$$\text{eq} := \text{mol}$$

In isothermal titration calorimetry of CMG titrating lysozyme, lysozyme was in cell and CMG was in syringe at pH 7.4 and 25°C both in 0.05 mol L<sup>-1</sup> HEPES buffer.

$$V_{\text{cell}} := 1.431 \text{ mL}$$

Volume of cell

$$V_{\text{s}} := 0.01 \text{ mL}$$

Volume of each drop titrated from syringe to cell

$$c_{\text{lyso}} := 2.18 \cdot 10^{-4} \frac{\text{eq}}{\text{L}}$$

Charge concentration of 0.3 g L<sup>-1</sup> lysozyme at pH 7.4, see Appendix B.1

$$\text{DS} := 0.39$$

Degree of substitution of carboxymethyl group in CMG

$$M_{\text{wCMG}} := (162 + \text{DS} \cdot 58) \frac{\text{gm}}{\text{mol}}$$

162 is molecular weight of one sugar unit, 58 is molecular weight of carboxymethyl group

$$M_{\text{wCMG}} = 0.185 \frac{\text{kg}}{\text{mol}}$$

Molecular weight of CMG per sugar unit

$$\text{CMG} := 0.5 \frac{\text{gm}}{\text{L}}$$

Mass concentration of CMG

$$c_{\text{CMG}} := \frac{\text{DS} \cdot \text{CMG}}{M_{\text{wCMG}}} = 1.056 \times 10^{-3} \frac{\text{eq}}{\text{L}}$$

CMG charge concentration

$$r_{\text{cCMG}}(V_{\text{s}}) := \frac{c_{\text{CMG}} \cdot V_{\text{s}}}{c_{\text{lyso}} \cdot V_{\text{cell}}}$$

Charge ratio of CMG to lysozyme

Accumulated volume of CMG solution titrated from syringe into cell

$$V_s := 0.01\text{mL}, 0.02\text{mL}.. 0.29\text{mL}$$

$$r_{\text{cCMG}}(V_s) = \begin{pmatrix} 0.034 \\ 0.068 \\ 0.102 \\ 0.135 \\ 0.169 \\ 0.203 \\ 0.237 \\ 0.271 \\ 0.305 \\ 0.339 \\ 0.372 \\ 0.406 \\ 0.44 \\ 0.474 \\ 0.508 \\ 0.542 \\ 0.576 \\ 0.609 \\ 0.643 \\ 0.677 \\ 0.711 \\ 0.745 \\ 0.779 \\ 0.813 \\ 0.846 \\ 0.88 \\ 0.914 \\ 0.948 \\ 0.982 \end{pmatrix}$$

Charge ratio of CMG to lysozyme for accumulated volume of CMG solution titrated from syringe into cell

In isothermal titration calorimetry of HPG-borate titrating lysozyme, lysozyme was in cell and HPG-borate was in syringe at pH 7.4 in 0.04 mol L<sup>-1</sup> boric acid and pH 9.2 in 0.01 mol L<sup>-1</sup> sodium borate buffer at 25°C.

At pH 7.4

$$c_{\text{lyso}7.4} := 2.18 \cdot 10^{-4} \frac{\text{eq}}{\text{L}}$$

At pH 9.2

$$c_{\text{lyso}9.2} := 1.85 \cdot 10^{-4} \frac{\text{eq}}{\text{L}}$$

Lysozyme charge concentration at pH 7.4 and pH 9.2, see Appendix B.1

$$\text{HPG} := 0.5 \frac{\text{gm}}{\text{L}}$$

HPG mass concentration

$$M_{\text{wHPG}} := (162 + 0.36 \cdot 58) \frac{\text{gm}}{\text{mol}}$$

$$M_{\text{wHPG}} = 182.88 \frac{\text{gm}}{\text{mol}}$$

Molecular weight of HPG with degree of substitution of hydroxypropyl groups of 0.36

At pH 7.4

$$\text{DS}_{\text{b}7.4} := 0.017$$

At pH 9.2

Degree of substitution of borate per sugar unit on HPG at pH 7.4 and pH 9.2, see Appendix B.5

$$\text{DS}_{\text{b}9.2} := 0.19$$

Charge concentration of HPG-borate in syringe at pH 7.4 and pH 9.2

At pH 7.4

$$c_{\text{HPG}7.4} := \frac{\text{HPG} \cdot \text{DS}_{\text{b}7.4}}{\text{Mw}_{\text{HPG}}} = 4.648 \times 10^{-5} \frac{\text{eq}}{\text{L}}$$

At pH 9.2

$$c_{\text{HPG}9.2} := \frac{\text{HPG} \cdot \text{DS}_{\text{b}9.2}}{\text{Mw}_{\text{HPG}}} = 5.195 \times 10^{-4} \frac{\text{eq}}{\text{L}}$$

Charge ratio of HPG-borate to lysozyme at pH 7.4 and pH 9.2

At pH 7.4

$$r_{\text{cHPG}7.4}(V_s) := \frac{c_{\text{HPG}7.4} \cdot V_s}{c_{\text{lyso}7.4} \cdot V_{\text{cell}}}$$

At pH 9.2

$$r_{\text{cHPG}9.2}(V_s) := \frac{c_{\text{HPG}9.2} \cdot V_s}{c_{\text{lyso}9.2} \cdot V_{\text{cell}}}$$

Charge ratio of HPG-borate to lysozyme for accumulated volume of HPG-borate solution titrated from syringe into cell at pH 7.4 and pH 9.2

$$\tau_{\text{cHPG7.4}}(V_s) = \begin{pmatrix} 1.49 \times 10^{-3} \\ 2.98 \times 10^{-3} \\ 4.47 \times 10^{-3} \\ 5.96 \times 10^{-3} \\ 7.449 \times 10^{-3} \\ 8.939 \times 10^{-3} \\ 0.01 \\ 0.012 \\ 0.013 \\ 0.015 \\ 0.016 \\ 0.018 \\ 0.019 \\ 0.021 \\ 0.022 \\ 0.024 \\ 0.025 \\ 0.027 \\ 0.028 \\ 0.03 \\ 0.031 \\ 0.033 \\ 0.034 \\ 0.036 \\ 0.037 \\ 0.039 \\ 0.04 \\ 0.042 \\ 0.043 \end{pmatrix}$$

$$\tau_{\text{cHPG9.2}}(V_s) = \begin{pmatrix} 0.02 \\ 0.039 \\ 0.059 \\ 0.078 \\ 0.098 \\ 0.118 \\ 0.137 \\ 0.157 \\ 0.177 \\ 0.196 \\ 0.216 \\ 0.235 \\ 0.255 \\ 0.275 \\ 0.294 \\ 0.314 \\ 0.334 \\ 0.353 \\ 0.373 \\ 0.392 \\ 0.412 \\ 0.432 \\ 0.451 \\ 0.471 \\ 0.491 \\ 0.51 \\ 0.53 \\ 0.549 \\ 0.569 \end{pmatrix}$$

In isothermal titration calorimetry of lysozyme titrating hydrophobically modified guar (HMG), HMG was in cell and lysozyme was in syringe at pH 7.4 in 0.05 mol L<sup>-1</sup> HEPES buffer at 25°C.

$$Da := \frac{\text{gm}}{\text{mol}} \quad DS_{\text{HMG}} := 0.13$$

$$Mw_{\text{HMG}} := (162 + 159 \cdot DS_{\text{HMG}}) \frac{\text{gm}}{\text{mol}} = 182.67 \cdot \frac{\text{gm}}{\text{mol}}$$

Molecular weight of HMG sugar unit

$$\text{HMG} := 0.1 \frac{\text{gm}}{\text{L}} \quad \text{HMG mass concentration}$$

$$c_{\text{HMG}} := \frac{\text{HMG} \cdot DS_{\text{HMG}}}{Mw_{\text{HPG}}} \quad \text{HMG binding sites molar concentration}$$

$$c_{\text{HMG}} = 7.108 \times 10^{-5} \cdot \frac{\text{mol}}{\text{L}}$$

$$Mw_{\text{lyso}} := 14600 \text{Da} \quad \text{Molecular weight of lysozyme}$$

$$\text{Lyso} := 1 \frac{\text{gm}}{\text{L}} \quad \text{Mass concentration of lysozyme}$$

$$c_{\text{lysozyme}} := \frac{\text{Lyso}}{Mw_{\text{lyso}}}$$

$$c_{\text{lysozyme}} = 6.849 \times 10^{-5} \cdot \frac{\text{mol}}{\text{L}} \quad \text{Molar concentration of lysozyme}$$

$$r(V_s) := \frac{c_{\text{lysozyme}} \cdot V_s}{c_{\text{HMG}} \cdot V_{\text{cell}}} \quad \text{Molar ratio of lysozyme to HMG}$$

Molar ratio of lysozyme to HMG for accumulated volume of lysozyme solution titrated from syringe into cell

$$r(V_s) = \begin{pmatrix} 6.733 \times 10^{-3} \\ 0.013 \\ 0.02 \\ 0.027 \\ 0.034 \\ 0.04 \\ 0.047 \\ 0.054 \\ 0.061 \\ 0.067 \\ 0.074 \\ 0.081 \\ 0.088 \\ 0.094 \\ 0.101 \\ 0.108 \\ 0.114 \\ 0.121 \\ 0.128 \\ 0.135 \\ 0.141 \\ 0.148 \\ 0.155 \\ 0.162 \\ 0.168 \\ 0.175 \\ 0.182 \\ 0.189 \\ 0.195 \end{pmatrix}$$

## Appendix B.4: Example calculation of Gibbs free energy and entropy in ITC

From one site binding model results for CMG titration to lysozyme in the absence of salt

$$K_1 := 1.61 \cdot 10^7 \quad \text{Binding constant of CMG with lysozyme}$$

$$\Delta H := -1372 \frac{\text{cal}}{\text{mol}} \quad \text{Molar enthalpy released from CMG binding with lysozyme}$$

$$R := 8.314 \frac{\text{J}}{\text{mol} \cdot \text{K}} \quad \text{Gas constant}$$

$$T := 298\text{K} \quad \text{Absolute temperature}$$

Calculation of Gibbs free energy and entropy

$$\Delta G := -R \cdot T \cdot \ln(K_1)$$

$$\Delta G = -9.82 \times 10^3 \frac{1}{\text{mol}} \cdot \text{cal} \quad \text{Molar Gibbs free energy from CMG/lysozyme binding}$$

$$\Delta S := \frac{\Delta H - \Delta G}{T}$$

$$\Delta S = 28.348 \cdot \frac{\text{cal}}{\text{mol} \cdot \text{K}} \quad \text{Molar entropy from CMG/lysozyme binding}$$

## Appendix B.5: Example calculation of borate content on HPG polymer chain

The objective of this model is to calculate borate binding to guar as a function of pH

B - uncharged  $B(OH)_3$ ; P - conc. of HPG binding sites; BP - conc of HPG bound borate; BOH - borate anion

### The equation set

$$K_0 = \frac{BOH}{B \cdot OH} \quad \text{borate buffer}$$

$$K_1 = \frac{BP}{BOH \cdot P} \quad \text{borate binding constant}$$

$$P_T = P + BP \quad \text{polymer balance}$$

$$B_T = B + BOH + BP \quad \text{boron balance}$$

rearranging equations for solver

$$K_1 = \frac{BP}{BOH \cdot P} \quad \text{rearranging} \quad BOH = \frac{BP}{K_1 \cdot P}$$

$$\text{substituting polymer balance gives} \quad BOH = \frac{BP}{K_1 \cdot (P_T - BP)}$$

$$K_0 = \frac{BOH}{B \cdot OH} \quad \text{rearranging} \quad BOH = K_0 \cdot OH \cdot B$$

$$\text{substitute from boron balance} \quad BOH = -K_0 \cdot OH \cdot \frac{-B_T + BP}{1 + K_0 \cdot OH}$$

$$BOH = K_0 \cdot OH \cdot (B_T - BOH - BP) \quad \text{solve, BOH} \rightarrow -\frac{K_0 \cdot OH \cdot (BP - B_T)}{K_0 \cdot OH + 1}$$

We assume we know total polymer and boron concentration as well as final pH

Want to calculate concentration of HPG bound borate and related quantities

### Constants

$TOL := 10^{-12}$  tolerance for solver

$\rho := \frac{\text{gm}}{\text{mL}}$  density of solutions

$pKa := 9.2$

$K_0 := 10^{14-pKa} \cdot \frac{\text{L}}{\text{mol}}$

$K_0 = 6.3096 \times 10^4 \cdot \frac{\text{L}}{\text{mol}}$  boric acid association constant

$C_{\text{hpg}} := 0.01\%$  mass fraction of HPG

$EW_{\text{HPG}} := 650\text{Da}$  equivalent weight of HPG

### Input variables for Calculation

$P_T := \frac{C_{\text{hpg}} \cdot \rho}{EW_{\text{HPG}}}$  total polymer conc.  $P_T = 0.1538 \text{ m}^{-3} \cdot \text{mol}$

$B_T := 40 \frac{\text{mol}}{\text{m}^3}$  total boron conc.

$OH := \frac{\text{mol}}{\text{L}} \cdot 10^{-(14-9)}$  hydroxyl ion conc.

$K_1 := 100 \frac{\text{L}}{\text{mol}}$  Borate/HPG binding constant

### Solving two simultaneous equations using Mathcad solver

Initial guesses

$$\text{BOH} := 0.5 \text{B}_T \quad \text{free borate conc.} \quad \text{BP} := 0.05 \cdot \text{P}_T \quad \text{bound borate conc.}$$

Given

$$\text{BOH} = -K_0 \cdot \text{OH} \cdot \frac{-\text{B}_T + \text{BP}}{1 + K_0 \cdot \text{OH}}$$

Solve block - two equations for two unknowns

$$\text{BOH} = \frac{\text{BP}}{K_1 \cdot (\text{P}_T - \text{BP})}$$

$$0 \frac{\text{mol}}{\text{L}} \leq \text{BOH} \leq \text{B}_T$$

Helps to restrict solutions

$$\text{xxx}(\text{B}_T, \text{P}_T, \text{OH}, K_1) := \text{Find}(\text{BOH}, \text{BP})$$

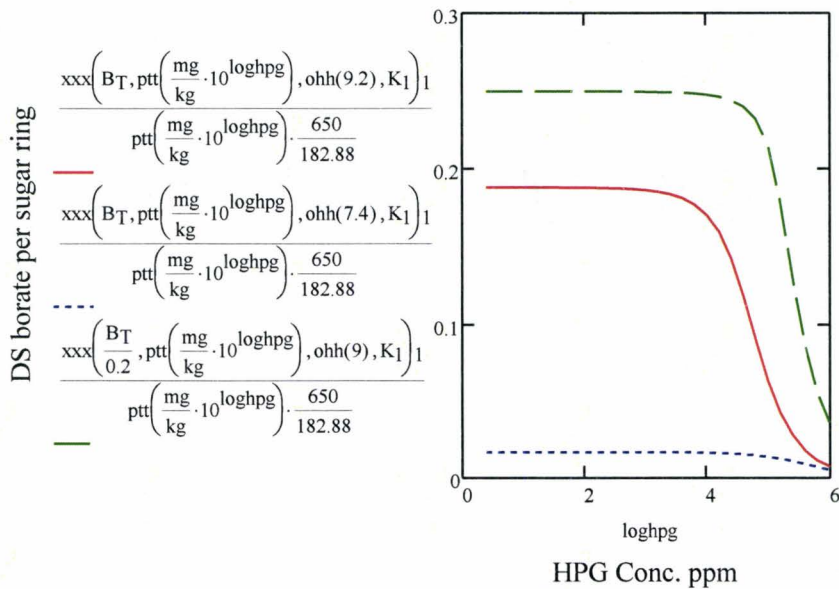
$$\text{xxx}\left(40 \frac{\text{mol}}{\text{m}^3}, \text{P}_T, \text{OH}, K_1\right) = \left(\begin{array}{l} 15.4384 \\ 0.0934 \end{array}\right) \text{m}^{-3} \cdot \text{mol}$$

The first term of xxx is equilibrium conc. of borate, BOH, and the second term is the conc of guar bound borate.

**Variation of HPG-borate degree of substitution (DS) with HPG conc**

$$pH := 9.2 \qquad B_T := 0.04 \frac{\text{mole}}{\text{L}} \qquad \text{ohh}(pH) := \frac{\text{mol}}{\text{L}} \cdot 10^{-(14-pH)}$$

$$\text{ptt}(C_{\text{hpg}}) := \frac{C_{\text{hpg}} \cdot \rho}{EW_{\text{HPG}}} \qquad \text{loghpg} := 0, 0.2 \dots 6$$



$$1\% = 1 \times 10^4 \cdot \text{ppm}$$

$$100\% = 1 \times 10^6 \cdot \text{ppm}$$

From the figure we can see that in HPG concentration lower than 1% (loghpg=4), degree of substitution of borate per sugar ring does not change with HPG concentration at a given pH. At pH 7.4, degree of substitution of borate per sugar ring is 0.017. At pH 9.2, it is 0.19

**Effective salt concentration with the increase of pH gives increasing borate substitution on HPG**

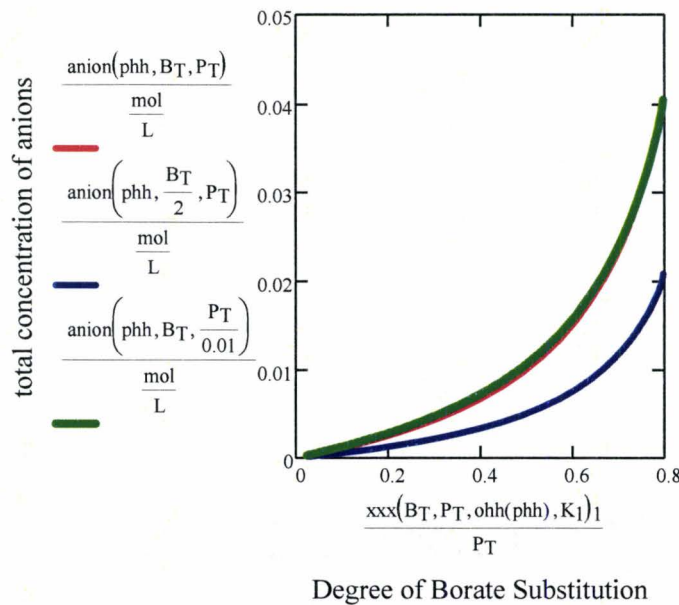
$$P_T := \text{ptt}\left(\frac{10 \cdot \text{mg}}{\text{kg}}\right)$$

$$B_T = 40 \text{ m}^{-3} \cdot \text{mol}$$

$$P_T = 0.0154 \text{ m}^{-3} \cdot \text{mol}$$

$$\text{anion}(\text{pH}, B_T, P_T) := \text{xxx}(B_T, P_T, \text{ohh}(\text{pH}), K_1)_1 + \text{xxx}(B_T, P_T, \text{ohh}(\text{pH}), K_1)_0 + \text{ohh}(\text{pH})$$

$$\text{phh} := 7, 7.1 \dots 11$$



This plot shows how the salt concentration increases with the degree of borate substitution on HPG as we increase pH at constant total boron and HPG.

## Appendix B.6: Calculation of critical salt concentrations on HPG/borate or CMG interaction with lysozyme

The objective of this model is to calculate critical salt concentration for binding of HPG-borate or CMG with lysozyme using Muthukumar model.

Constants

$\epsilon_r := 78$  Relative permmissivity

$\epsilon := \epsilon_r \epsilon_0$

$T := 298\text{K}$  Absolute temperature

$a := 2\text{nm}$  Radius of lysozyme sphere

$\zeta := 6.4 \cdot e_0$  Surface charge of lysozyme

$$\sigma_0 := \frac{\zeta}{4 \cdot \pi \cdot a^2}$$

$\sigma_0 = 0.0204 \text{m}^{-2} \cdot \text{C}$  Surface charge density of lysozyme

$l_0 := 0.54\text{nm}$  We are using two mannose units as the repeat unit, Cheng used one (Cheng et al. Biomacromolecules, 2002).

$C_\omega := 13$  This is the characteristic ratio - Cheng says it is 11 for guar, for charged HPG it should be a bit bigger.

$b := 24\text{nm}$  Kuhn length of HPG

$b_{\text{eff}}(C_\omega) := C_\omega \cdot l_0$  Effective step length of HPG

Apply Muthukumar model, F von Goeler, Journal of chemical physics, 1994

$$T = \frac{12 \cdot \pi \cdot \sigma_0 \cdot q}{\epsilon \cdot \kappa^3 \cdot b_{\text{eff}} \cdot b \cdot k_b} \cdot (1 - \exp(-2\kappa a))$$

$\alpha$  is polyelectrolyte linear charge density,  $q$  is the charge per repeating unit of polyelectrolyte chain

$$\kappa := \frac{1}{10\text{nm}} \quad \text{initial kappa}$$

Rerrange and apply root function

$$\kappa_c(\alpha, C_\omega, a, \sigma_0) := \text{root} \left[ \left[ \frac{12 \cdot \pi \cdot \epsilon_0 \cdot \sigma_0 \cdot \alpha}{\epsilon \cdot \kappa^3 \cdot b_{\text{eff}}(C_\omega) \cdot b \cdot k_b} \cdot (1 - \exp(-2 \cdot a \cdot \kappa)) \right] + T, \kappa \right]$$

$$c_{\text{sc}}(\kappa) := \frac{\kappa^2}{\left( \frac{\epsilon_0^2 \cdot N_{\text{av}}}{\epsilon \cdot k_b \cdot T} \cdot 2 \right)}$$

Critical salt concentration as a function of pH (degree of substitution for HPG-borate) for HPG-borate and CMG

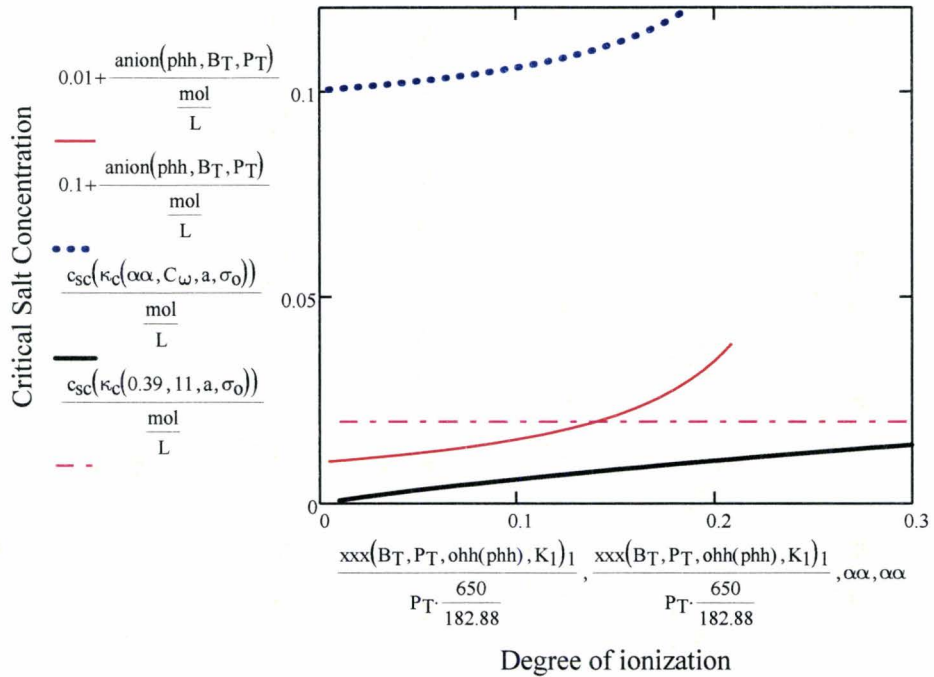
$$\alpha\alpha := 0.01, 0.02 \dots 0.3$$

degree of substitution of borate on HPG

$$\text{phh} := 6.8, 6.9 \dots 9.6$$

pH

see calculation of anion(phh,  $B_T$ ,  $P_T$ ) in appendix B.5-calculation of linear charge density of HPG-borate (borate substitution per sugar ring)



$$\frac{c_{sc}(\kappa_c(0.39, 11, a, \sigma_0))}{\text{mol/L}} = 0.0198$$

The black curve is critical salt concentration for HPG-borate. The dotted pink curve is critical salt concentration for CMG. The red and blue curve are salt concentration as a function of pH with initial salt concentrations of 0.01mol/L and 0.1mol/L respectively.

## Appendix C

### Appendix C.1: Example calculation of HPG viscosity effect on PA liposome mobility

$\epsilon_r := 78$  water permmissivity

$T := 298\text{K}$  Absolute temperature

$c_{\text{NaCl}} := 0.1 \frac{\text{mol}}{\text{L}}$  NaCl concentration

$$\kappa := \left( \frac{\epsilon_0^2 \cdot N_{\text{Av}}}{\epsilon_0 \cdot \epsilon_r \cdot k_{\text{B}} \cdot T} \cdot c_{\text{NaCl}} \right)^{\frac{1}{2}} \quad \kappa = 1.0431 \cdot \text{nm}^{-1} \quad a := 40\text{nm} \quad \text{radius of PA liposome}$$

$\kappa \cdot a = 41.72$   $\kappa a > 1$ , Smoluchowski's model applies

$\zeta := 38\text{mV}$  PA liposome surface potential

$\eta := 0.00091\text{Pa}\cdot\text{s}$  water viscosity at 25°C

$\mu(\eta) := \frac{\epsilon_0 \cdot \epsilon_r \cdot \zeta}{\eta}$  Smoluchowski's model for  $\kappa a > 1$

$\mu(\eta) = 2.88 \times 10^{-8} \cdot \text{m}^2 \text{V}^{-1} \text{s}^{-1}$  PA liposome mobility in water

Assume PA liposome surface potential is constant, mobility is inverse proportional to solution viscosity

$$\eta := \begin{pmatrix} 1.05 \cdot 10^{-3} \\ 1.92 \cdot 10^{-3} \end{pmatrix} \text{Pa}\cdot\text{s} \quad \text{for} \quad c_{\text{HPG}} := \begin{pmatrix} 0.1 \\ 0.5 \end{pmatrix} \frac{\text{gm}}{\text{L}} \quad \text{Chakrabarti 1991} \\ \text{Rheologica Acta}$$

$$\mu(\eta) = \begin{pmatrix} 2.5 \times 10^{-8} \\ 1.37 \times 10^{-8} \end{pmatrix} \cdot \text{m}^2 \text{V}^{-1} \text{s}^{-1}$$

At HPG concentration below 0.1g/L, the solution viscosity are close to that of water. Therefore, the mobility does not change with the increase of HPG concentration. At HPG concentration above 0.1g/L, the solution viscosity sharply increases with the increase of HPG concentration. Therefore, the mobility sharply decreases.

## Appendix C.2: Modeling of depletion flocculation of PA liposomes induced by HPG

The goal of this model is to calculate phosphatidic acid (PA) liposome stability in the presence of HPG

### Constants

$T := 298\text{K}$	absolute temperature
$\epsilon_r := 78$	water permmissivity
$\epsilon := \epsilon_0 \cdot \epsilon_r$	
$a := 40\text{nm}$	radius of PA liposome
$R := 8.314 \frac{\text{joule}}{\text{K}\cdot\text{mole}}$	gas constant
$\text{NaCl} := 0.1 \frac{\text{mole}}{\text{L}}$	sodium chloride concentration
$h := \text{nm}$	surface-surface distance
$\rho := \frac{\text{gm}}{\text{cm}^3}$	density of HPG
$r_g := 128\text{nm}$	radius of gyration of HPG
$\text{Da} := \frac{\text{gm}}{\text{mole}}$	define Dalton
$M_w := 1750000\text{Da}$	HPG molecular weight

$\psi := 38\text{mV}$  Surface potential of PA liposome

$A := 0.7 \cdot 10^{-20}$  joule Hamaker constant of PA

$\phi := 0.0005$  HPG volume fraction

$B_2 := 0.00003 \frac{\text{cm}^3 \cdot \text{mole}}{\text{gm}^2}$  second virial coefficient of HPG

$\kappa(\text{NaCl}) := \left( \frac{\epsilon_0^2 \cdot N_{\text{av}}}{\epsilon_0 \cdot \epsilon_r \cdot k_b \cdot T} \cdot 2 \cdot \text{NaCl} \right)^{0.5}$  calculate kappa

**Theoretical expressions for different potentials (Note: all potentials are normalized by  $k_b T$ )**

**Electrostatic potential**

$$V_{\text{elect}}(a, \text{NaCl}, h, \psi) := \left( 2 \cdot \pi \cdot \epsilon \cdot \psi^2 \cdot a \cdot \ln(1 + \exp(-\kappa(\text{NaCl}) \cdot h)) \right) \cdot \frac{1}{k_b \cdot T}$$

**van der Waals interaction potential**

$$V_{\text{vdw}}(h, A, a) := \frac{-A}{12} \cdot \left( \frac{4 \cdot a^2}{h^2 + 4 \cdot a \cdot h} + \frac{4 \cdot a^2}{h^2 + 4 \cdot a \cdot h + 4 \cdot a^2} + 2 \ln \left( \frac{h^2 + 4 \cdot a \cdot h}{h^2 + 4 \cdot a \cdot h + 4 \cdot a^2} \right) \right) \cdot \frac{1}{k_b \cdot T}$$

**Depletion potential using Fleer & Scheutjens & Vincent's approach (Colloids and Surfaces, 50 (1990) 24)**

$\Delta := 40\text{nm}$  depletion layer thickness

Original equation modified by Seebergh and Berg (Langmuir, Vol. 10, No. 2, 1994)

$$\Delta_t := \text{root} \left[ \frac{N_{\text{av}} \cdot \rho}{2} \cdot \left( \frac{M_w}{N_{\text{av}} \cdot \rho} \right)^{\frac{2}{3}} \cdot \left( \frac{\phi}{M_w} + B_2 \cdot \rho \cdot \phi^2 \right) + \left[ \frac{\Delta}{(1.4 \cdot r_g)^2} - \frac{1}{\Delta} \right], \Delta \right]$$

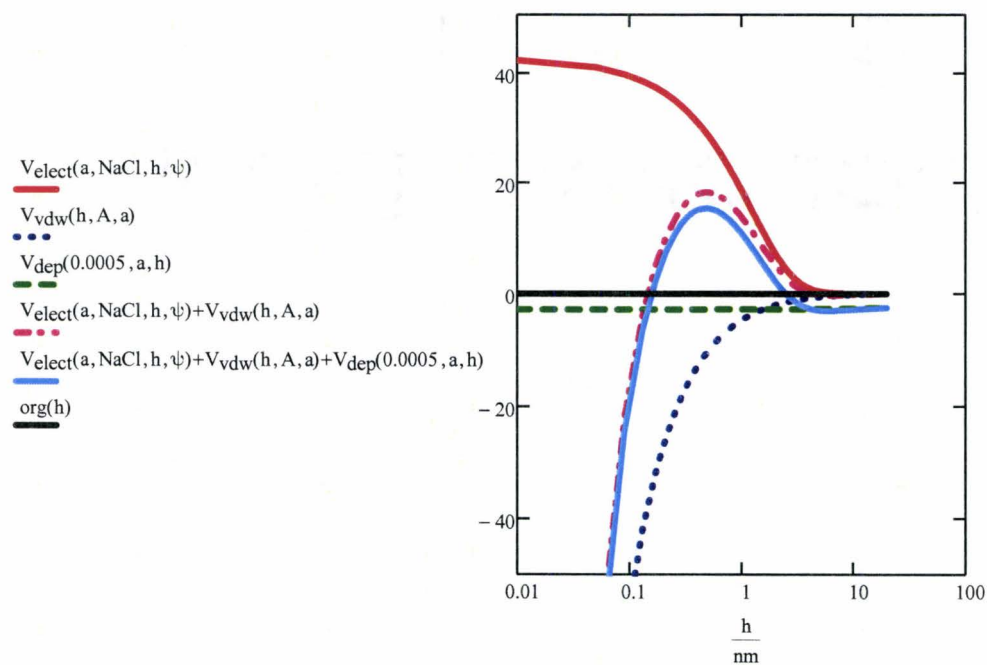
$$V_{\text{dep}}(\phi, a, h) := \frac{-2}{3} \cdot \pi \cdot R \cdot T \cdot \rho \cdot \phi \cdot \left( \frac{1}{M_w} + B_2 \cdot \rho \cdot \phi \right) \cdot \left( \Delta_t - \frac{h}{2} \right)^2 \cdot \left( 3 \cdot a + 2 \cdot \Delta_t + \frac{h}{2} \right) \cdot \frac{1}{k_b \cdot T}$$

$$V_{\text{dep}}(0.0005, a, h) = -2.8346$$

### Potentials as a function of liposomes separation

$h := 0.01 \text{ nm}, 0.05 \text{ nm} \dots 20 \text{ nm}$

$\text{org}(h) := 0$



$$V_{\text{elect}}(a, \text{NaCl}, 6 \text{ nm}, \psi) + V_{\text{vdw}}(6 \text{ nm}, A, a) + V_{\text{dep}}(0.0005, a, 6 \text{ nm}) = -3.0992$$

### Appendix C.3: Estimation of the radius of gyration of HPG, native guar and PHG

This calculation aims to estimate the radius of gyration of HPG, native guar and PHG

#### a. Estimation of the radius of gyration of HPG

$$R_g^2 = \frac{R^2}{6}$$

$R_g$  is radius of gyration of guar,  $R$  is end to end distance of guar.

$$R^2 = C_{inf} \cdot N \cdot l_0^2$$

$C_{inf}$  is characteristic ratio of guar,  $N$  is the number of monomeric unit,  $l_0$  is the length of monomeric unit.

$$N = \frac{M_w \cdot 0.63}{M_m}$$

$M_w$  is the molecular weight of guar molecule,  $M_m$  is the molecular weight of one sugar unit of guar molecule, 0.63 is the mole fraction of mannose main chain sugar unit.

For guar with molecular weight of 1.72 MDa:

$$M_{w\text{guar}} := 1.72 \cdot 10^6 \text{ Da}$$

$$R_{g\text{guar}} := 127 \text{ nm}$$

**Picout Biomacromolecules 2001**

$$M_{m\text{guar}} := 162 \text{ Da}$$

$$l_0 := 0.54 \text{ nm}$$

$$C_{inf\text{guar}} := 11.87$$

**Cheng Biomacromolecules 2002**

For HPG with molecular weight of 1.75 MDa:

$$M_{w\text{HPG}} := 1.75 \cdot 10^6 \text{ Da}$$

$$M_{m\text{HPG}} := 183 \text{ Da}$$

$$l_0 := 0.54 \text{ nm}$$

$$C_{inf\text{HPG}} := 13.02$$

So

$$R_{g\text{HPG}} := 128 \text{ nm}$$

**b. Estimation of the radius of gyration of native guar and PHG**

$$R_g = \alpha \cdot M_w^{0.6} \quad \text{Tunier Food hydrocolloid 2000}$$

$$R_g := 133 \text{ nm} \quad \text{for} \quad M_w := 1.87 \cdot 10^6 \text{ Da}$$

**Picout Biomacromolecules 2001**

$$\alpha := \frac{R_g}{M_w^{0.6}}$$

$$\alpha = 0.0229 \cdot \text{gm}^{-0.6} \cdot \text{mol}^{0.6} \cdot \text{nm}$$

For native guar

$$M_w := 3 \cdot 10^6 \text{ Da}$$

$$R_g := \alpha \cdot M_w^{0.6}$$

$$R_g = 177 \cdot \text{nm}$$

Radius of gyration of native guar is 177nm

For PHG

$$M_w := 1.5 \cdot 10^4 \text{ Da}$$

$$R_g := \alpha \cdot M_w^{0.6}$$

$$R_g = 7.4 \cdot \text{nm}$$

Radius of gyration of PHG is 7.4nm